

**LUMINESCENT TRANSITION METAL COMPLEXES BASED ON
N-HETEROCYCLIC AND N[^]C-CHELATE 4-COORDINATE
ORGANOBORYL LIGANDS**

by

Nan Wang

A thesis submitted to the Department of Chemistry

In conformity with the requirements for

the degree of Doctor of Philosophy

Queen's University

Kingston, Ontario, Canada

(December, 2012)

Copyright ©Nan Wang, 2012

Abstract

The objective of this thesis is to examine the photophysical and structural properties of Ru(II)/Re(I) based bimetallic complexes based on *p*-[*N*-2-(2'-pyridyl)benzimidazolyl]-[*N*-2-(2'-pyridyl)indolyl]-benzene (L1) ligand, as well as the photophysical and photochemical properties of N[^]C-chelate 4-coordinate organoboron compounds that contain a metal acetylide group.

Ligand L1 was synthesized and fully characterized. Due to the incorporation of two distinct chelating sites, an N[^]N-chelate site and an N[^]C-chelate site, L1 has been found to be very effective in selective binding to two different metal ions.

Two new heterobimetallic complexes Ru(II)-Pt(II) and Ru(II)-Pd(II) using L1 as the bridging ligand were prepared and fully characterized. All Ru(II)-containing complexes have been found to be luminescent. The Pt(II) unit appears to enhance phosphorescent efficiency of the Ru(II) unit while the Pd(II) unit has little influence.

Using L1 as the bridging unit, two new Re(I) based heterobimetallic complexes Re(I)-Pt(II) and Re(I)-Pd(II) were also successfully synthesized. Results indicate that there is communication between the two different metal centers. The preliminary results indicated that the mononuclear Re(I) complex based on L1 is a promising candidate for the electrocatalytic CO₂ reduction.

Pd(II) and Pt(II) complexes were synthesized with an atropisomeric bis-pyridyl chelate ligand bis{3,3'-[*N*-Ph-2-(2'-py) indolyl]} (L4). To examine the potential use of the *trans*-chelate L4 ligand in oxidative coupling reactions catalyzed by Pd(II) compounds, acetoxylation of arenes by PhI(OAc)₂ using PhI(OAc)₂/L4 (2:1) as the catalyst was examined and found to accelerate the reaction, but lower the overall yield.

Finally, to examine the impact of metal ions on photochromic properties of N[^]C-chelate organoboron compounds, three metal acetylide compounds that contain a photoactive N[^]C-chelate BMes₂ unit (B(ppy)Mes₂) were prepared and fully characterized. The studies indicated that by taking advantage of different heavy metals the photoisomerization quantum efficiency of the boron chromophores can be readily tuned through the adjustment of ³LC state localized on the chelate backbone or the involvement of MLCT state in the lowest energy electronic transition.

Acknowledgements

It is not only a long but also difficult journey for me to complete this degree. Even though it is impossible to acknowledge all who have been helpful in various ways, several individuals have been especially important in providing guidance and support through the process.

First and most important, I am extremely grateful to my supervisor Prof. Suning Wang. Thank you so much for your academic expertise, unfailing support, diligent supervision and constructive advice. It has been a great fortune to have you as my supervisor. Without your guidance, this work would not have been possible. You will always have a special position in my heart.

My special thanks also go to my committee members, Prof. Anne Petitjean and Prof. Donal H. Macartney for passing on their valuable ideas and knowledge to me. Your insightful feedbacks and comments are invaluable along this journey. Many thanks are extended to Dr Françoise Sauriol and Dr Rui-Yao Wang for their help with instrumentation and helps on X-ray crystallography and NMR spectroscopic analyses.

I wish to express my sincere gratitude to the past and present Wang group members and friends in the department for giving me their valuable help, suggestions, friendship and encouragement in the past four years.

Last but not the least, I would like to give my heartfelt thanks to my parents in China. Your unconditional love and support have shaped my life. You have done your best to better educate me, and have always encouraged me to pursue my goals and assured me that you are just a phone call away. Your caring, giving, patience and understanding helped me through every tough and important moment.

Statement of Originality

I hereby certify that all of the work described within this thesis is the original work of the author carried out under the guidance and supervision of Prof. Suning Wang with the following exceptions. Dr Theresa Michelle McCormick synthesized metal complexes **5.1** and **5.2**, which she also characterized. Ligand L4 and metal complex **3.6** were first synthesized by Dr Theresa Michelle McCormick and the corresponding X-ray structures were also solved by her. X-ray structures of ligand L1 and compound **6.1** were solved by Jiasheng Lu. The DFT and TD-DFT calculations for compounds **5.1** and **6.3** were carried out by Dr Soo-Byung Ko. The DFT and TD-DFT calculations for compound **6.1** were carried out by Leanne Chen. Any published (or unpublished) ideas and/or techniques from the work of others are fully acknowledged in accordance with the standard referencing practices.

(Nan Wang)

(December, 2012)

Table of Contents

Abstract.....	ii
Acknowledgements.....	iv
Statement of Originality.....	v
Table of Contents.....	vi
List of Tables.....	vii
List of Figures.....	viii
List of Abbreviations.....	xiii
Chapter 1 Introduction.....	1
Chapter 2 Synthesis of 2-(2'-Pyridyl)indole and 2-(2'-Pyridyl)benzimidazole Based Ligands....	54
Chapter 3 Heterobimetallic Ru(II) Complexes Based on 2-(2'-Pyridyl)benzimidazolyl and 2-(2'-Pyridyl)indolyl Derivative Ligand.....	68
Chapter 4 Heterobimetallic Re(I) Complexes Based on 2-(2'-Pyridyl)benzimidazolyl and 2-(2'-Pyridyl)indolyl Derivative Ligand.....	92
Chapter 5 Pt(II) and Pd(II) Complexes Based on a <i>trans</i> -Chelating 2-(2'-Pyridyl)indolyl Derivative Ligand.....	125
Chapter 6 Impact of Metal Acetylides on Photoisomerization of an <i>N</i> [^] <i>C</i> -Chelate Organoboron Compound.....	153
Chapter 7 Summary and Perspectives.....	196

List of Tables

Table 2-1 Crystallographic data for compounds L1 and L3.	58
Table 2-2 Selected bond lengths (Å) and angles (°) of compound L1 and L3.	59
Table 2-3. Absorption and luminescence data.	65
Table 3-1. Crystallographic data for complex 3.6.	74
Table 3-2. Selected bond lengths (Å) and angles (°) of complex 3.6.	75
Table 3-3. Electrochemical data of Ru complexes.	81
Table 3-4. Absorption and luminescence data for complexes/ligands studied	87
Table 4-1. Crystallographic data for compounds 4.2 and 4.4.	101
Table 4-2. Selected bond lengths (Å) and angles (°) of compounds 4.2 and 4.4.	102
Table 4-3. Absorption and luminescence data.	108
Table 4-4. Isodensity surface plot of 4.3.	111
Table 4-5. TD-DFT calculation results of 4.3.	112
Table 4-6. Electrochemical data of 4.1, 4.2 and 4.4.	114
Table 5-1. Crystallographic data for complexes 5.1 and 5.2.	131
Table 5-2. Selected bond length (Å) and angles (°) of complexes 5.1 and 5.2.	132
Table 5-3. Absorption and luminescence data.	139
Table 5-4. Isodensity surface plot of 5.1.	140
Table 5-5. Calculated energy levels of the low-lying singlet and triplet states of 5.1.	141
Table 5-6. Reaction conditions and product distributions	144
Table 6-1. Crystallographic data for metal-boron complexes.	164
Table 6-2. Selected bond lengths (Å) and angles (°) of metal containing boron complexes.	165
Table 6-3. Photophysical data for boron compounds.	170
Table 6-4. Activation energy data of the thermal conversion of dark isomer Au-B' to 6.2 using ¹ H NMR.	177
Table 6-5. TD-DFT transition energies (E _{ex}) and oscillator strengths (<i>f</i>) for B1.	185
Table 6-6. TD-DFT transition energies (E _{ex}) and oscillator strengths (<i>f</i>) for PAu1.	186
Table 6-7. TD-DFT transition energies (E _{ex}) and oscillator strengths (<i>f</i>) for PPt1.	187
Table 6-8. TD-DFT transition energies (E _{ex}) and oscillator strengths (<i>f</i>) for 6.1.	188
Table 6-9. TD-DFT transition energies (E _{ex}) and oscillator strengths (<i>f</i>) for 6.2.	188
Table 6-10. TD-DFT transition energies (E _{ex}) and oscillator strengths (<i>f</i>) for TMS-B.	190
Table 6-11. TD-DFT transition energies (E _{ex}) and oscillator strengths (<i>f</i>) for 6.3.	191

List of Figures

Figure 1-1. Structures of ligands: py-im, py-in and L1-L4 presented in this thesis.....	4
Figure 1-2. Fluorescence and phosphorescence pathways.....	5
Figure 1-3. A typical OLED structure.	7
Figure 1-4. Operating principles of a dye-sensitized solar cell.....	9
Figure 1-5. Structure of dye N3.	12
Figure 1-6. Structures of Pt complexes with cyclometalated ligands.	13
Figure 1-7. Structures of triarylboron-functionalized Pt(II) complexes.	14
Figure 1-8. Structures of tridentate cyclometalating Pt complexes.	15
Figure 1-9. Chemical structures of Pt complexes reported by Kavitha.	16
Figure 1-10. Proposed Pd(II)/Pd(IV) catalytic cycle for C-H activation.	17
Figure 1-11. Selectivity of a ligand directed sp^2 C-H functionalization	18
Figure 1-12. Selectivity of a ligand directed sp^3 C-H acetoxylation.....	18
Figure 1-13. Efficient bidentate N^N donor ligand used in Pd-catalyzed naphthalene arylation reaction.....	19
Figure 1-14. Structures of tricarbonyl Re(I) diimine complexes with high quantum yields.	20
Figure 1-15. Structures of various ligands based on py-im.	24
Figure 1-16. Structures of Pt(II) complexes based on py-im ligands.	25
Figure 1-17. Structures of Ru(II) complexes based on py-im ligands.	26
Figure 1-18. Schematic diagram showing the formation of metallo-supramolecular gel-like materials obtained by mixing metal ions with monomer 5.	28
Figure 1-19. Crystal structure of $Zn(py-in)_2(THF)$	30
Figure 1-20. Structures of transition metal complexes prepared by Lorenz et al.	30
Figure 1-21. Structures of py-in based ligand and N^C-chelate Pt(II)/Pd(II) metal complexes. ...	31
Figure 1-22. Energy transfer process in a polynuclear metal complex.	33
Figure 1-23. Structure of Re-Ru polynuclear complex.	33
Figure 1-24. A scheme showing a bimetallic complex serving as a PMD for proton reduction. ..	34
Figure 1-25. Structures of various polynuclear metal complexes used as photochemical molecular devices.	35
Figure 1-26. Structures of 8-Hydroxyquinoline based 4-coordinate organoboron compounds.....	36
Figure 1-27. Chemical structure of N^N chelate organoboron compounds 13-17.	37
Figure 1-28. Chemical structure of boryl-substituted thienylthiazole.	38
Figure 1-29. Diagram showing the pathways of photochromic switching between two isomers..	38

Figure 1-30. Photoisomerization of compound 18 and the influence of pyridine on the isomerization process.....	40
Figure 1-31. Chemical structure of N ^C -chelate boron compounds with different substituted chelation ligands.	41
Figure 1-32. Chemical structures of N ^C -chelate boron compounds that are coordinated with Pt(II).....	42
Figure 2-1. Chemical structures of L1, L2 and L3.....	55
Figure 2-2. Reaction scheme for the synthesis of ligands L1-L3.	60
Figure 2-3. Possible reaction pathways for syntheses of L2 and L3.....	62
Figure 2-4. The crystal structure of L1 with 35% thermal ellipsoids and labeling schemes.	62
Figure 2-5. Top: the crystal structure of L3. Bottom: Parallel structure formed by intermolecular π - π stacking in L3.	63
Figure 2-6. Structure of bis[3,3'-(1,4-bis[2-(2'-pyridyl)indolyl] benzene)] (bbib).	64
Figure 2-7. UV-Vis spectra of $\sim 1 \times 10^{-5}$ M solutions of ligands recorded in CH ₂ Cl ₂ at ambient temperature.	64
Figure 2-8. Emission spectra of $\sim 1 \times 10^{-5}$ M solutions of ligands recorded in CH ₂ Cl ₂ at ambient temperature.	66
Figure 3-1. Reaction scheme for the syntheses of metal complexes.....	76
Figure 3-2. The crystal structures of 3.6 with 35% thermal ellipsoids	77
Figure 3-3. The isomers of 3.4.....	78
Figure 3-4. Variable temperature ¹ H NMR spectra of 3.4 in acetone-d ₆ , showing the inter conversion of the <i>syn</i> and <i>anti</i> isomers depicted in Figure 3-3.....	79
Figure 3-5. The partial COSY spectrum of 3.4 in acetone-d ₆ at 223K.	80
Figure 3-6. Cyclic voltammogram of metal complexes, recorded in DMF, using NBu ₄ PF ₆ as the electrolyte with a scan rate of 100-200 mV/s.	82
Figure 3-7. UV-Vis spectra of $\sim 1 \times 10^{-5}$ M solutions of metal complexes and free ligands recorded in THF at ambient temperature.	83
Figure 3-8. Emission spectra of 3.5 in THF ($\sim 1 \times 10^{-5}$ M) at ambient temperature. Inset: Photographs showing the luminescence color of 3.5 solution under 365 nm irradiation under N ₂ (left) and under air (right).	84
Figure 3-9. Emission spectra of $\sim 1 \times 10^{-5}$ M solutions of metal complexes recorded at 77K in 2-methyl-THF.	85
Figure 3-10. Emission spectra of $\sim 1 \times 10^{-5}$ M solutions of metal complexes recorded in THF at ambient temperature.....	86

Figure 4-1. Chemical structures of L1 and L1 based Re(I) complexes.....	93
Figure 4-2. Chemical structures of Pt(II) and Pd(II) mononuclear compounds.....	95
Figure 4-3. Reaction scheme for the syntheses of metal complexes.....	103
Figure 4-4. Top: the crystal structure of 4.2 with 50% thermal ellipsoids and labeling schemes. Hydrogen atoms are omitted for clarity. Bottom: the packing diagram of 4.2 projected down the b-axis.....	104
Figure 4-5. Top: The crystal structure of 4.4 with 50% thermal ellipsoids and labeling schemes. Hydrogen atoms are omitted for clarity. Bottom: the packing diagram of 4.4 projected down the b-axis.....	105
Figure 4-6. UV-Vis spectra of $\sim 1 \times 10^{-5}$ M solutions of metal complexes recorded in CH_2Cl_2 at ambient temperature.....	107
Figure 4-7. Emission spectra of $\sim 1 \times 10^{-5}$ M solutions of metal complexes recorded in CH_2Cl_2 at ambient temperature. ($\lambda_{\text{ex}} = 400\text{--}430$ nm).....	109
Figure 4-8. CV diagrams of 4.1, 4.2 and 4.4, recorded in acetonitrile, using NBu_4PF_6 as the electrolyte with a scan rate of 150 mV/s.....	114
Figure 4-9. Cyclic voltammogram (oxidation peak) of metal complex (A) 4.1, (B) 4.2 and (C) 4.4 under N_2 . Voltammograms taken at 100mV/s in acetonitrile with 0.1M NBu_4PF_6	115
Figure 4-10. Catalytic comparison of (A) 4.1, (B) 4.2, (C) $\text{Re}(\text{bipy})$ and (D) 4.4 under both nitrogen and carbon dioxide conditions. In (A) also included a blank scan of acetonitrile solution (with no catalyst) with 0.1M NBu_4PF_6 saturated with CO_2/N_2 . Voltammograms taken at 100mV/s in acetonitrile with 0.1M NBu_4PF_6	118
Figure 5-1. Reaction scheme for the syntheses of $\text{Pt}(\text{bpib})\text{Cl}_2$ (5.1) and $\text{Pd}(\text{bpib})\text{Cl}_2$ (5.2).	126
Figure 5-2. The crystal structure of 5.1 with 35% thermal ellipsoids.....	134
Figure 5-3. The crystal structure of 5.2 with 35% thermal ellipsoids.....	134
Figure 5-4. Variable temperature ^1H NMR spectra of 5.1 in CD_2Cl_2 showing the change of the <i>N</i> -phenyl proton chemical shifts with temperature. The assignments of the peaks for the <i>N</i> -phenyl protons are based on COSY NMR data.	136
Figure 5-5. Variable temperature ^1H NMR of 5.2 in CD_2Cl_2 showing the change of the <i>N</i> -phenyl proton chemical shifts with temperature.	137
Figure 5-6. UV-Vis spectra of $\sim 1 \times 10^{-5}$ M solutions of L4, 5.1 and 5.2 recorded in CH_2Cl_2 at ambient temperature.....	138
Figure 5-7. Emission spectrum of complex 5.1 in frozen CH_2Cl_2 at 77K	142
Figure 5-8. Diagrams showing the yields of acetoxylation products with time.	145

Figure 5-9. ^1H NMR spectra showing the change of L4 (bpib) chemical shift after the addition of $\text{Pd}(\text{OAc})_2$ (1:1) in CD_2Cl_2 .	147
Figure 6-1. Reaction scheme for the syntheses of boron complexes.	156
Figure 6-2. Crystal structure of 6.1 with labeling schemes for selected atoms and 50% thermal ellipsoids. Hydrogen atoms are omitted for clarity.	161
Figure 6-3. Crystal structure of 6.2 with labeling schemes for selected atoms and 50% thermal ellipsoids.	161
Figure 6-4. Crystal structure of 6.3 with labeling schemes for selected atoms and 50% thermal ellipsoids. Hydrogen atoms are omitted for clarity.	162
Figure 6-5. A diagram showing the $\text{H}\cdots\text{C}$ interactions ($\sim 2.50 \text{ \AA}$) between CHCl_3 and the alkyne bond in 6.1.	162
Figure 6-6. A diagram showing the relative orientation of the 6.2 molecules and the $\text{H}\cdots\text{C}$ interactions ($\sim 2.90 - 3.0 \text{ \AA}$) in the crystal lattice.	163
Figure 6-7. A diagram showing the π -stacking (the shortest $\text{C}\cdots\text{C}$ separation distance is 3.74 \AA) of 6.3 molecules in the crystal lattice.	163
Figure 6-8. UV-Vis spectra of $\sim 1 \times 10^{-5} \text{ M}$ solutions of boron complexes recorded in CH_2Cl_2 at ambient temperature.	168
Figure 6-9. Emission spectra of $\sim 1 \times 10^{-5} \text{ M}$ solutions of compounds recorded in toluene at ambient temperature under nitrogen.	171
Figure 6-10. Time-resolved phosphorescence spectra of metal complexes and fluorescence spectrum of TIPS-B in 2-methyltetrahydrofuran at 77K.	172
Figure 6-11. Phosphorescent spectral change of 6.1 before and after exposure to O_2 .	172
Figure 6-12. Phosphorescent spectral change of 6.3 before and after exposure to O_2 .	173
Figure 6-13. Time-resolved phosphorescence spectra of metal compounds in toluene at ambient temperature under nitrogen.	173
Figure 6-14. Photoisomerization of 6.2. Inset: Photographs showing the color of the compounds before and after irradiation.	174
Figure 6-15. UV-Vis spectral change of 6.2 in toluene upon irradiation at 365 nm with a hand-held UV lamp.	175
Figure 6-16. Stacked ^{31}P NMR spectra of 6.2 upon UV irradiation, under N_2 , in C_6D_6 .	175
Figure 6-17. Stacked ^1H NMR spectra of 6.2 upon UV irradiation, under N_2 , in C_6D_6 (aromatic region).	176
Figure 6-18. Activation energy of the thermal conversion of Au-B' to 6.2 using Arrhenius plot.	177

Figure 6-19. UV-Vis spectral change of 6.3 in toluene upon irradiation at 390 nm.....	178
Figure 6-20. Stacked ¹ H NMR spectra (aromatic region) of 6.3 upon UV irradiation, under N ₂ , in C ₆ D ₆ . Inset: Photographs showing the color of the compounds before and after irradiation.....	179
Figure 6-21. Stacked ³¹ P NMR spectra showing the conversion of 6.3 to Pt-B' upon UV irradiation with time, under N ₂ , in C ₆ D ₆	180
Figure 6-22. Stacked ¹ H NMR spectra (aromatic region) of 6.1 upon UV irradiation, under N ₂ , in CD ₃ CN.	180
Figure 6-23. UV-Vis spectra of ~1×10 ⁻⁵ M 6.2 and TIPS-B recorded in degassed toluene at ambient temperature used for photoisomerization quantum efficiency comparison measurement.	182
Figure 6-24. UV-Vis spectral change of TIPS-B in toluene upon irradiation at 362 nm.....	182
Figure 6-25. Number of moles of dark isomer produced over time. (top) Ex = 362 nm; (bottom) Ex = 310 nm.....	183
Figure 6-26. Molecular orbitals of B1 with a surface isocontour value of 0.03.	184
Figure 6-27. Molecular orbitals of PAu1 with a surface isocontour value of 0.03.....	185
Figure 6-28. Molecular orbitals of PPt1 with a surface isocontour value of 0.03.	186
Figure 6-29. Molecular orbitals of 6.1 with a surface isocontour value of 0.03.....	187
Figure 6-30. Molecular orbitals of 6.2 with a surface isocontour value of 0.03.....	189
Figure 6-31. Molecular orbitals of TMS-B with a surface isocontour value of 0.03.....	190
Figure 6-32. Molecular orbitals of 6.3 with a surface isocontour value of 0.03.....	191
Figure 7-1. Synthesis of supramolecular Cu(I)-L4 compounds.....	199
Figure 7-2. Structure of possible Ru(II) containing boron complex.....	199
Figure 7-3. Structure of non-conjugated metal containing N ⁺ C-chelate boron compound.	199

List of Abbreviations

o	degrees
$^{\circ}\text{C}$	degrees Celsius
$^1\text{MLCT}$	singlet MLCT state
$^3\text{MLCT}$	triplet MLCT state
ϵ	molar extinction coefficient
λ	absorption/emission maximum
λ_{max}	emission wavelength
λ_{em}	excitation wavelength
μs	microsecond
τ	decay lifetime
Φ	quantum efficiency
\AA	angstrom
acac	acetylacetonate
Alq_3	tris(8-hydroxyquinolate)aluminum(III)
Anal. calcd.	Elemental analysis calculated
Anal	analysis
bipy	2,2'-bipyridine
B3LYP	Becke 3-Parameter Exchange, Lee, Yang and Parr
bpib	bis[3,3'-(2,(2'-pyridyl)indolyl benzene)]
CH_2Cl_2	dichloromethane
COSY	correlation spectroscopy
CT	charge-transfer
CV	cyclic voltammetry
d	doublet
dd	doublet of doublets
dpm	dipivoly methane
DFT	density functional theory
DMF	dimethylsulfoxide

e^-	electron
$E_{1/2}^{\text{ox}}$	half-cell oxidation potential
$E_{1/2}^{\text{red}}$	half-cell reduction potential
EL	electroluminescent
EML	emissive layer
equiv.	equivalents
ETL	electron transport layer
eV	electronvolts
$\text{FeCp}_2^{0/+}$	ferrocene/ferrocenium redox couple
FW	formula weight
g	grams
I	intensity
im	imidazole
in	indole
ISC	intersystem crossing
$h\nu$	light
HOMO	highest occupied molecular orbital
HRMS	high-resolution mass spectrometry
HTL	hole transport layer
Hz	hertz
ITO	indium tin oxide
J	coupling constant
K	Kelvin
kV	kilovolts
LC	ligand-centered
LUMO	lowest unoccupied molecular orbital
M	molar; mass
Me	methyl
MeCN	acetonitrile
Mes	mesityl
mg	milligram

min	minutes
mmol	millimole
mL	milliliter
MLCT	metal-to-ligand charge-transfer
MO	molecular orbital
mol	mole
mV	millivolts
nm	nanometers
NMR	nuclear magnetic resonance
OLED	organic light-emitting diode
Ph	phenyl
1,10-phen	1,10-phenanthroline
pib	2-(2'-pyridyl)indolyl benzene
PL	photoluminescent
PPh ₃	triphenylphosphine
ppy	2-phenylpyridine
py	pyridyl
py-im	2-(2'-pyridyl) benzimidazole
py-in	2-(2'-pyridyl)indole
QY	quantum yield
Reflns	reflections
RT	room temperature
s	second; singlet
S ₀	singlet ground state
S _n , (n>0)	n th singlet excited state
t	triplet; time
td	triplet of doublets
T	temperature
T _n (n>0)	n th triplet excited state
TBAF	tetrabutylammonium fluoride
TBAP	tetrabutylammonium hexafluorophosphate

TD-DFT	time-dependent density functional theory
TON	turn-over number
TFA	trifluoroacetic acid
THF	tetrahydrofuran
UV	ultraviolet light
V	volt; volume
Vis	visible

Chapter 1

Introduction

Luminescent materials have attracted significant research interest due to their various applications, such as emitting materials for organic light emitting diodes (OLEDs),¹ light harvesting materials,² and fluorescent sensors.³ Luminescence can be defined as the emission of light from any substance and occurs from electronically excited states. There are only two pathways for the emissive decay of excited electrons. These emission pathways include fluorescence, which occurs from a singlet excited state, and phosphorescence, which occurs from a triplet excited state. In comparison with fluorescent materials, phosphorescent materials are more desirable, as they have several key advantages over fluorescent materials. Some advantages of phosphorescent materials are that they provide high device efficiency when used for OLEDs, they are highly sensitive to triplet state quenchers, and high color tunability *via* complexation with metal ions. Consequently, much research efforts have been devoted toward the development of phosphorescent materials, especially highly efficient organometallic phosphors, which provide access to the triplet state through the metal centers. Various transition metal complexes have been investigated as efficient phosphorescent emitters, such as Pt(II),⁴ Ir(III),⁵ Ru(II)⁶ and Re(I)⁷ complexes.

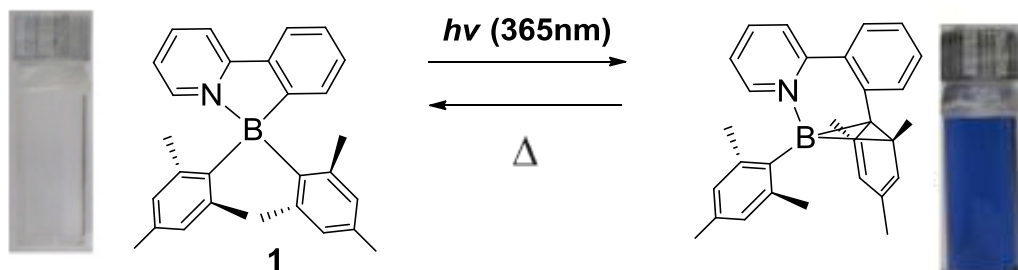
N-heterocyclic compounds and their metal complexes have recently attracted considerable attention due to their various applications in many areas, such as catalysts and light emitting materials.⁸ Previous research in our group on *N*-heterocyclic compounds and their metal complexes has led to successful synthesis of a series of

organic/organometallic compounds, including 7-azaindole,⁹ 2-(2'-pyridyl) benzimidazole (**py-im**),¹⁰ 2-(2'-pyridyl)indole (**py-in**),¹¹ and di-2-pyridylamine¹² derivatives. Some of these compounds have been used to fabricate OLEDs, while others display interesting reactivity toward small molecule activation and thus make them potentially useful in synthesis.^{9e,9f}

In addition to metal-containing *N*-heterocyclic compounds, our group is also active in organoboron-based materials chemistry. Based on the geometry of the boron center, there are two classes of organoboron compounds, including 3-coordinate trigonal planar compounds and 4-coordinate tetrahedral compounds. Because of the empty p_{π} orbital at the boron center, 3-coordinate boron compounds are strong electron acceptors. This vacant p_{π} orbital also allows for conjugation with organic π systems and significant delocalization,¹³ making 3-coordinate boron compounds ideal for applications as emitters, anion sensors, and optoelectronic materials. Since the empty p_{π} orbital on the boron center is readily attacked by nucleophiles, bulky substituents are required to protect the vacant orbital through steric hindrance and thus provide kinetic stability. Substituents such as mesityl (2,4,6-trimethylphenyl, Mes), fluoromesityl (2,4,6-tris(trifluoromethyl)phenyl), and triptyl (2,4,6-triisopropylphenyl) groups are particularly effective for this purpose. These substituents form a propeller-like structure around the boron center, where the ortho-substituents on the aryl ligands form a cage to protect the vacant p_{π} orbital.

Owing to their reactivity, high electron-accepting capabilities and bright luminescence, 4-coordinate boron compounds have also drawn significant attention recently. Numerous N[^]O, N[^]N and N[^]C chelates (where X[^]Y represents a chelate ligand

that coordinates through the X and Y atoms) of 4-coordinate boron complexes have been synthesized.^{11b, 14} In 2008 our group reported an unusual photochromic switch involving tetrahedral N[^]C-chelate boron chromophore (compound **1**). This chromophore undergoes a thermally reversible photoisomerization from a colorless state to a dark colored state upon irradiation at 365 nm, as shown in Scheme 1-1.¹⁵ This discovery significantly broadens the applications of 4-coordinate organoboron compounds in optical memory devices, smart windows and so on.



Scheme 1-1. Isomerization of a N[^]C-chelate boron chromophore.

To continue our research efforts on *N*-heterocyclic metal complexes and organoboron chemistry, the research described in this thesis is focused on the study of *N*-heterocyclic ligands containing **py-im** and/or **py-in** moieties (as shown in Figure 1-1). In addition, this research is also focused on investigating the mono-nuclear and hetero-binuclear transition metal (Ru(II), Pd(II), Pt(II) and Re(I)) complexes of these ligands, and their luminescent and reactivity properties. In addition, 4-coordinate boron-containing transition metal complexes were also studied. In the following sections of this chapter, the background and motivations of this thesis will be briefly presented.

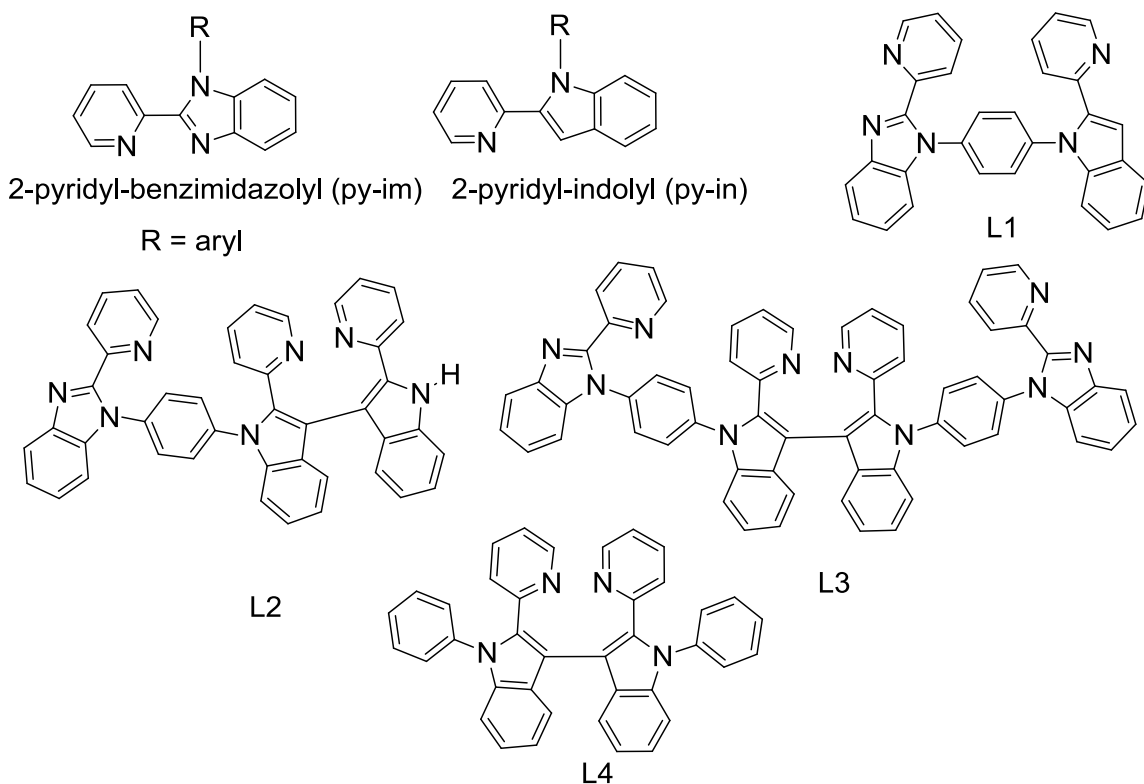


Figure 1-1. Structures of ligands: py-im, py-in and L1-L4 presented in this thesis.

1.1 Basic Principles of Luminescence and Organic Light Emitting Diodes (OLEDs)

As indicated earlier, luminescence is the emission of light from any substance and occurs from electronically excited states. Considering the different ways in which the excitations are generated, there are several types of luminescence. Some examples of luminescence include photoluminescence (PL, which is excited *via* the absorption of light), electroluminescence (EL, which is excited by electrical energy), chemiluminescence (which is excited by chemical energy). In contrast, there are only two pathways for the emissive decay of exciton electrons, fluorescence and phosphorescence.

In the case of fluorescence, the ground state and excited state electrons have the same spin quantum numbers, and as a result, the transition from the excited state to the ground state, ($S_1 \rightarrow S_0$) is spin allowed. Typical fluorescence emission rates and lifetimes are $\sim 10^8$

s^{-1} and 10^{-9} s, respectively. In contrast, in the case of phosphorescence, since the spin quantum number of the excited state and the ground state is different, the $T_1 \rightarrow S_0$ transition is spin forbidden. As a result, the $T_1 \rightarrow S_0$ decay occurs much slowly. Accordingly, phosphorescence has a much longer decay lifetimes ranging from microseconds to seconds.

Organic compounds do not typically exhibit phosphorescent emission. Phosphorescence emission is particularly rare among organic compounds in solution at room temperature, since non-emissive relaxation pathways, such as thermal decay and quenching processes compete effectively with phosphorescence. Therefore, phosphorescence emission of organic compounds is usually very weak and only observed in the solid state or at low temperature, which minimizes the influence of solvent molecules and the thermal decay pathways. When a heavy metal binds with organic ligands, spin-orbit coupling facilitates the mixing of the S_1 and T_1 states and promotes intersystem crossing, thus leading to a significant enhancement of phosphorescence emission and shortening decay lifetimes. Figure 1-2 shows the basic pathways followed during fluorescence and phosphorescence.

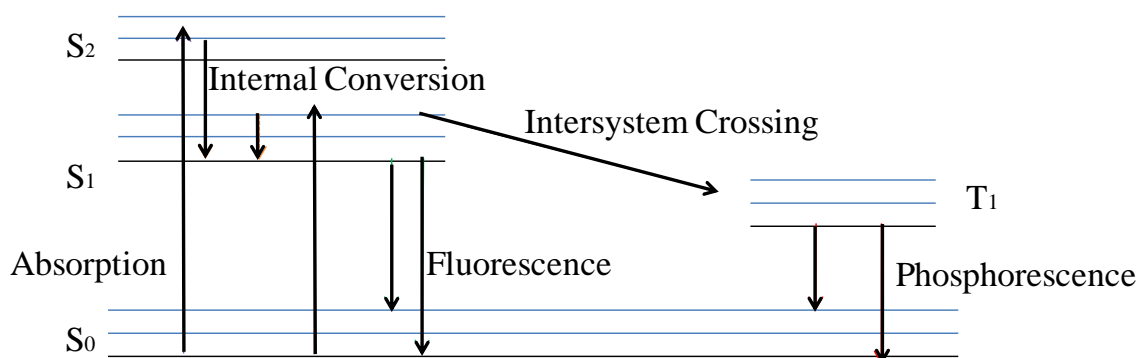


Figure 1-2. Fluorescence and phosphorescence pathways.

The nature of the phosphorescence from metal complexes is mainly determined by the relative energy level of the d orbitals of the metal center and the ligand. If the highest occupied molecular orbital (HOMO) and lowest unoccupied molecular orbital (LUMO) are both ligand based, the phosphorescence is usually ligand-centered (LC) π - π^* transitions.¹⁶ If the HOMO is dominated by the contribution from the metal center and the corresponding LUMO from the ligand, the phosphorescence can be described as transitions of metal-to-ligand charge transfer (MLCT). If the complex has a ligand-based HOMO and a metal-based LUMO, it can show ligand-to-metal charge-transfer (LMCT) transitions.

As a leading technology for the generation of full color flat panel displays, OLEDs have attracted great interest from both academia and industry. This technology is based on the principle of EL.¹⁷ In 1987, the commercial potential of OLEDs was first realized by Tang and van Slyke of Eastman Kodak.¹⁸ They reported the fabrication of a double layer organic light emitting device with low voltages and high luminescence efficiency. Motivated by the enormous potential commercial value of this technology, many researchers have pursued this new field and much progress has been reported since then. Now the luminescence efficiency and device reliability have been greatly improved.¹⁹

Figure 1-3 shows a typical OLED device. The device contains three parts: an anode such as indium tin oxide (ITO) which is composed of 20% SnO₂ and 80% In₂O₃, a metallic cathode which is usually composed of Mg-Ag or LiF-Al, and several thin organic layers sandwiched between the anode and the cathode consisting of a hole transport layer (HTL), an electron transport layer (ETL) and an emitting layer (EML).^{19d}
²⁰To improve the electroluminescence quantum efficiency, exciton blocking layers may

also be included to help confine excitons to the organic emissive layer.^{21,22} When an external voltage is applied to the device, holes from the anode and electrons from the cathode are injected into the hole transport layer and the electron transport layer, respectively. As the holes and the electrons pass through these layers, they eventually form an exciton when they combine with each other in the emitting layer. Relaxation of the exciton from the excited state to the ground state results in the emission of light.

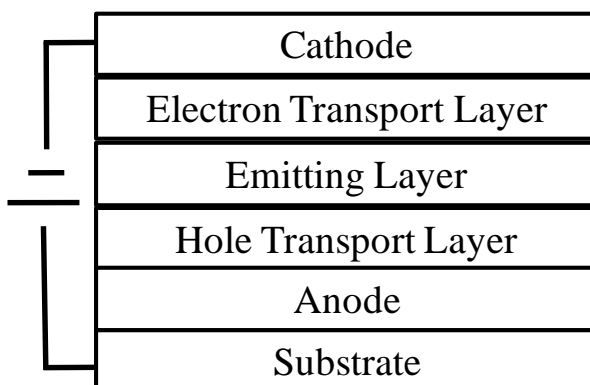


Figure 1-3. A typical OLED structure.

Early OLED devices usually used fluorescent organic compounds as the emissive layer. However, more recent research efforts have been increasingly devoted to the design and synthesis of electro-phosphorescent emitters. The motivation for this research effort has been generated because the quantum efficiency of OLEDs utilizing these emitters can potentially be improved by up to a factor of four.²³ Considering that heavy metal atoms can promote fast and efficient intersystem crossing through strong spin-orbit coupling, transition metal complexes are ideal phosphorescent emitters for OLEDs. Besides the emissive layer, many other issues can also influence the device's performance. These issues are currently being explored by material chemists, engineers,

and device physicists, which can be found in recent literature, and thus will not be presented in this chapter.²⁴

1.2 Polypyridyl Ruthenium(II) Complexes

During the past 50 years, extensive research has been devoted to ruthenium polypyridyl complexes.^{3d, 25} The photophysical and electrochemical properties of these complexes have been comprehensively studied. Due to their low-lying triplet MLCT (³MLCT) state, ruthenium polypyridyl complexes often show phosphorescence in solution at room temperature with quantum yields ranging between 10^{-1} and 10^{-3} . Unfortunately, efforts to change the emission wavelengths of these complexes *via* ligand tuning have generally been unsuccessful, and their emissions are thus restricted to the orange-red region. The investigation of ruthenium polypyridyl complexes grew rapidly in the mid to late 1970s with the realization that the unique excited state and electrochemical properties of ruthenium polypyridyl complexes placed them ideal candidates for the fabrication of dye sensitized solar cells (DSSCs),²⁶ which convert solar energy into electricity. Compared with commercially available silicon-based solar cells, DSSCs have several advantages, such as their low cost, their high flexibility and their light weight. DSSCs are therefore a very promising technology that may eventually replace silicon-based solar panels. In recent years, approximately two or three research articles are typically published daily in this field.

In contrast to silicon-based solar cells, the light absorbance and charge carrier transport processes occur separately in DSSCs. The operation of a DSSC is illustrated in Figure 1-4. The system comprises of a dye which is bound to the surface of an inorganic semiconductor. To maximize the light harvesting, nanocrystalline TiO₂ is usually used

since it provides a large surface area onto which the dye can adsorb. The porous semiconductor layer is interpenetrated by a hole-transport material (HTM), which may be a redox electrolyte in solution or a solid-state or quasi-solid-state material. Photoexcitation of the sensitizer leads to the injection of electrons into the conduction band of the TiO_2 . The oxidized dye is subsequently reduced by the HTM to regenerate the ground state dye. The injected electrons flow through the semiconductor network to arrive at the back contact and then through the external load to the counter electrode. At the counter electrode, the HTM is regenerated through reduction, thus completing the circuit.

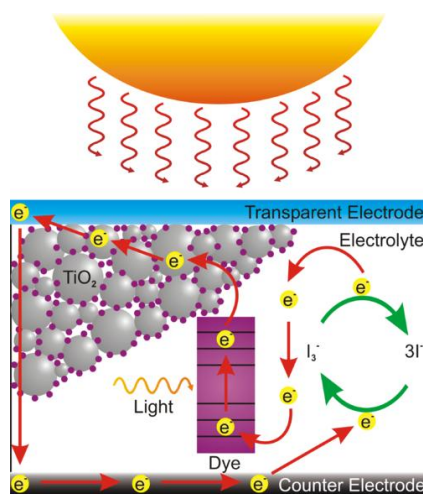


Figure 1-4. Operating principles of a dye-sensitized solar cell.²⁷

The dyes used in DSSCs must fulfill a number of essential design requirements in order to maximize the cell efficiency.²⁸ For example, the photosensitizer should have an intense absorption throughout the entire visible region. Anchoring groups (such as $-\text{COOH}$, $-\text{SO}_3\text{H}$) are also required which make the dyes strongly bind onto the semiconductor surface. In order to provide an efficient electron injection process, the excited state of the dye should be higher in energy than the conduction band edge of a

semiconductor. The photosensitizer must be rapidly regenerated by the mediator layer in order to avoid electron recombination processes. In addition, the photosensitizer should be photochemically, electrochemically and thermally stable. Based on the above considerations, numerous compounds have been studied as photosensitizers, including organic molecules, such as coumarin,²⁹ squaraine,³⁰ indoline,³¹ and hemicyanine,³² and also transition metal complexes. It should be pointed out that transition metal complexes have provided the best performance as photosensitizers so far due to their high thermal and chemical stabilities.³³ Numerous transition metal complex-based dyes have been reported, including those incorporating Ru(II)^{2a}, Os(II),³⁴ Pt(II),^{2c} Re(I),^{2d} Cu(I)^{2e} and Fe(II).^{2f} Among these complexes, Ru(II) complexes have shown the best photovoltaic properties and have undoubtedly been the most widely investigated dye systems. The popularity of the Ru(II) complexes as photosensitizers arises from their broad absorption spectra, suitable excited and ground state energy levels, relatively long excited lifetimes and good electrochemical stability. Several Ru(II) complexes used in DSSCs have provided solar cell efficiencies that exceed 10%.³⁵ The dye N3 shown in Figure 1-5 provides a good example of an ideal photosensitizer, and this Ru(II) complex is considered as a paradigm in the area of dye-sensitized nanocrystalline TiO₂ films. Systematic studies have demonstrated that the presence of carboxylic groups as peripheral substituents significantly increase the sensitization capacity of the dye. In particular, these carboxylic groups help the dye molecules anchor firmly onto the surface of TiO₂ semiconductor film. Additionally, the electronic coupling is also enhanced due to possible overlap of the π^* orbitals of the pyridine ligand with the 3d orbitals of Ti(IV), leading to an ultrafast charge injection. Researchers have also demonstrated that the

positions of the carboxylic groups in the 2,2'-bipyridine ligand is critical for the dye's performance. The theoretical calculations indicate that only in the 4,4'-position the two carboxylic groups have the right orientation for efficient chelation to the TiO₂ surface. As a result, 4,4'-disubstituted 2,2'-bipyridine ligands are more efficient photosensitizers than those bearing two carboxylic groups in the 5,5'- or 6,6'- positions. When an excited electron is injected into the TiO₂, the positive charge density remaining on the dye is distributed over the metal, and also to some extent over the NCS- ligand. This spatial charge separation between the positive charge density on the dye and the injected electrons effectively retards the rate of charge recombination, which is a key loss mechanism.³⁶ In attempts to prepare more efficient photosensitizers, researchers have attempted to prepare derivatives of the N3 dye. For example, phenyl groups have been introduced between the carboxylic groups and the pyridine unit in order to increase the molar absorbance.³⁷ However, after addition of this spacer, the sensitizer performance of the derivative was inferior to that of the parent complex, even though the molar absorbance did increase. The phenyl group reduced the coupling between the electronic excited state of the dye and the semiconductor. Thus, after excitation, the promoted electron would reside mainly within the bipyridine ligand and did not go far into the carboxyl groups, which in turn increases the possibility of undesired charge recombination.

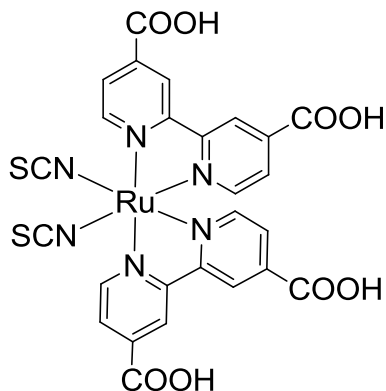


Figure 1-5. Structure of dye N3.

1.3 Platinum(II) and Palladium(II) Complexes

Because of heavy metal effects, the mixing of singlet and triplet states are efficient for platinum(II) complexes, which results in enhanced phosphorescence emission and short decay lifetimes. Investigations into square planar Pt(II) complexes exhibiting room temperature phosphorescence started in the late 1980s. Most of this research has focused on cyclometalated Pt(II) complexes, which could show significant room temperature luminescence.³⁸ Cyclometalation reaction is defined as reactions of transition metal complexes in which organic ligand undergoes intramolecular metalation with formation of a metal-carbon σ bond.³⁹ In comparison with simple mononuclear Pt(II) bipyridine or terpyridine complexes, cyclometalated ligands can increase the brightness of the Pt(II) complexes, which can emit from either the π - π^* or MLCT states. (π - π^* state is the state generated when promotion of an electron from a π -bonding orbital to a higher energy anti-bonding orbital). The strong ligand field of cyclometalated carbon raises the energy of the metal d-d states which diminishes the deactivating effect of non-emissive d-d transition relaxation pathway. In 1984, Pt(N[^]C-ppy)₂ (ppy = phenylpyridine) (Figure 1-6, left) was synthesized by Von Zelewsky as the first example of a homoleptic complex

incorporating phenylpyridine ligands.⁴⁰ Later on, analogues of this complex with 2-thienyl-pyridine (N[^]C-thpy) and its derivatives were also investigated. Due to the more obvious *trans* effect of the cyclometalated carbon, the formation of *cis* isomers are preferred. Investigations involving Pt(N[^]C-thpy)₂ and Pt(N[^]C-thpy-5-SiMe₃)₂ (Figure 1-6, center and right, respectively) have demonstrated that these complexes have high quantum yields in degassed solutions. By using the spin-casting method, which avoids thermal decomposition, these complexes can be successfully used for device fabrication.⁴¹

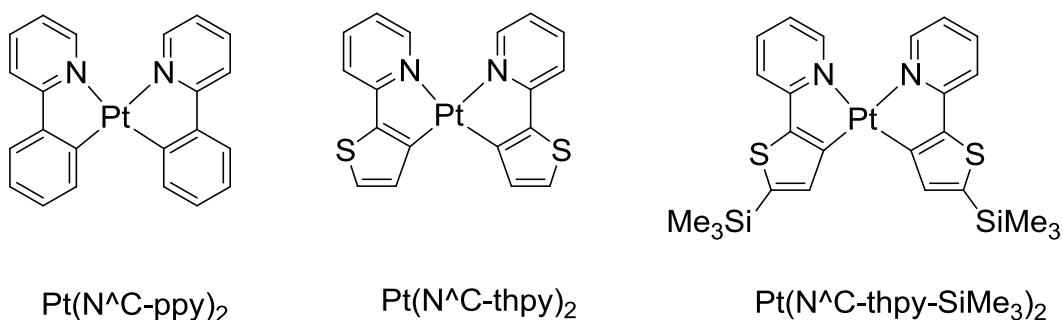


Figure 1-6. Structures of Pt complexes with cyclometalated ligands.

Our group has synthesized a series of triarylboron-functionalized phosphorescent Pt(II) complexes with acetylacetonate (acac) group as the ancillary ligand as shown in Figure 1-7.⁴² One key advantage provided by the acac group is the significant improvement of the stability of the compound in the solution and solid state. Furthermore, the acac ligand has a high triplet state which minimizes its interference with phosphorescent emission from the boron chromophore.⁴³ In addition, the acac group enhances the rigidity of the Pt portion, thus decreasing the loss of energy *via* vibrational radiationless decay. These compounds exhibit bright phosphorescent colors spanning the green to red region in both solution and solid state. Compared with their non-borylated

Pt(II) parent chromophores, the quantum yields of these boron-functionalized Pt(II) complexes significantly enhanced, which can be attributed to the increased participation of the MLCT state in the lowest energy emission pathway that was promoted by the boron moiety. Highly efficient EL devices have also been achieved by using compound Pt-BppyA.

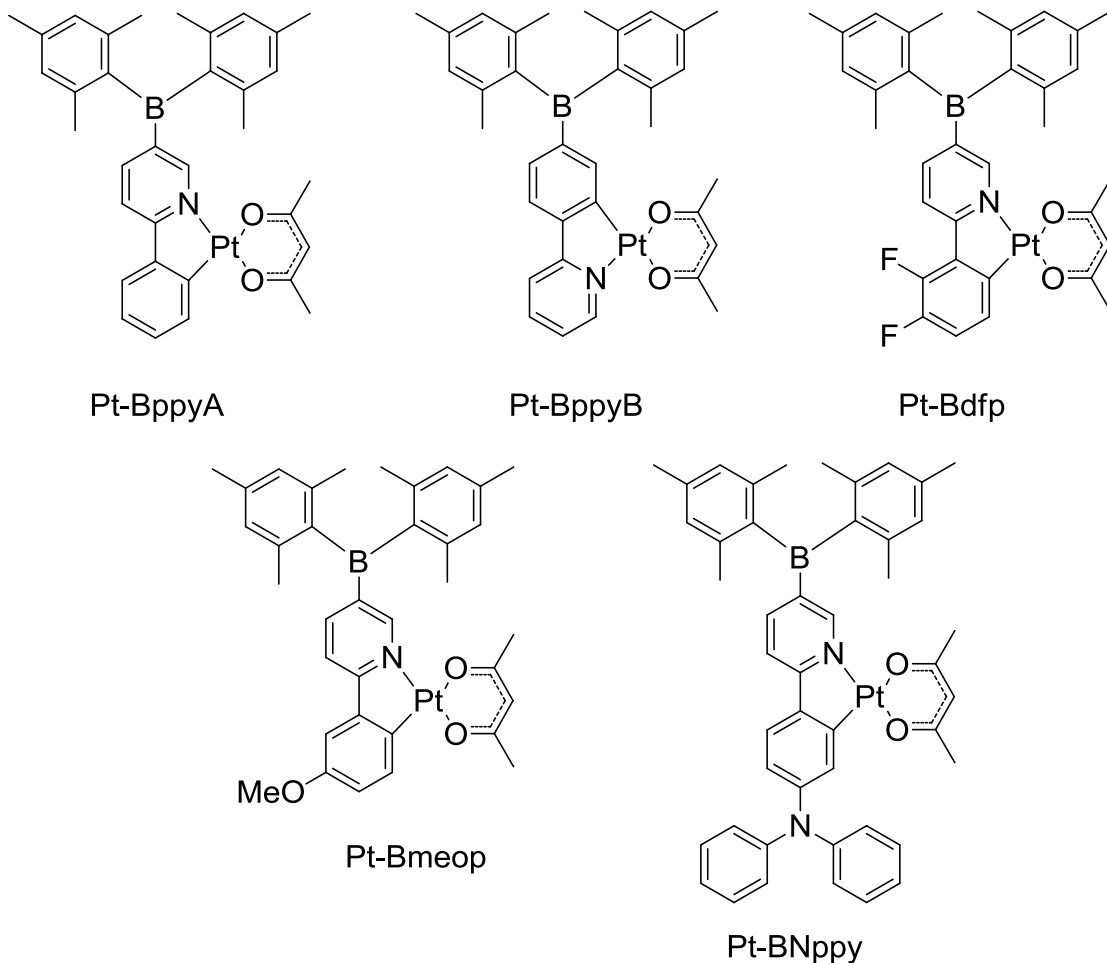


Figure 1-7. Structures of triarylboron-functionalized Pt(II) complexes.

Considering that rigid structures usually favors luminescence over non-radiative decay pathways, tridentate ligands may optimize luminescence efficiency since their geometry offers additional rigidity. A class of tridentate cyclometalating N[^]N[^]C Pt(II) complexes have been investigated by Lu et al., where N[^]N[^]C is aryl-2,2'-bipyridine

(shown in Figure 1-8 left).⁴⁴ By introducing substituents with different electronic properties into the ligands, the colors emitted from these complexes can be tuned from green-yellow to red. Generally, for these N[^]N[^]C Pt(II) compounds the introduction of electron-donating groups at the *para*-position of the central pyridyl ligand resulted in a blue-shift in the emission energy, while placing electron-withdrawing groups at this position resulted in a red-shift. Another class of tridentate ligands is N[^]C[^]N, where the cyclometalating phenyl ring occupies the central position, which results in shorter Pt-C bonds than is encountered among N[^]N[^]C complexes. Important examples of this class of complex include the Pt(II) bipyridyl benzene complexes synthesized by Williams et al., which are shown in Figure 1-8 (right).⁴⁵ In comparison with other cyclometalated Pt(II) complexes, these tridentate complexes show intense green luminescence in solution and much higher quantum yields ($\Phi_p = 0.58-0.68$). These properties can be attributed to $^3\pi-\pi^*$ emission exhibited by these complexes.

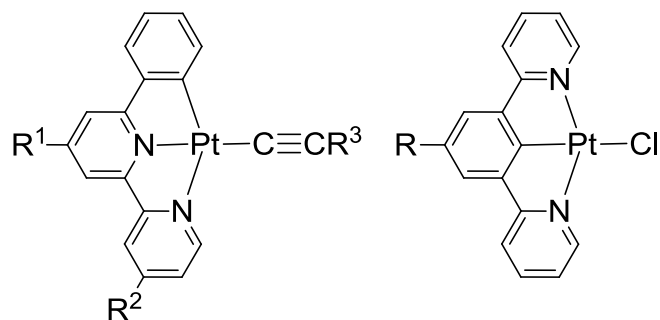


Figure 1-8. Structures of tridentate cyclometalating Pt complexes.

In solution, most of the Pt (II) complexes form excimers at high concentrations owing to their unique planar geometry. An excimer is a dimeric species formed from two molecules, one of which is in its excited state and the other is in its ground state. Consequently, the emission from an excimer is often intense but red-shifted when

compared with that of the corresponding monomer.⁴⁶ Excimer formation can be avoided by proper ligand design. For example, recently Kavitha et al. reported a highly luminescent red light-emitting device that utilized square planar Pt(II) complexes with structures shown in Figure 1-9.⁴⁷ Due to the steric hindrance introduced by the bulky ligands, the stacking effect was diminished. Consequently, excimer formation was avoided, thus leading to remarkable improvements in device performance.

Fortunately, excimer emissions can also be useful for fabricating white OLED devices.⁴⁸ By controlling the levels of doping in the matrix, emissions from both the monomer and the excimer can be realized, thus yielding white electroluminescence with good external quantum efficiency.

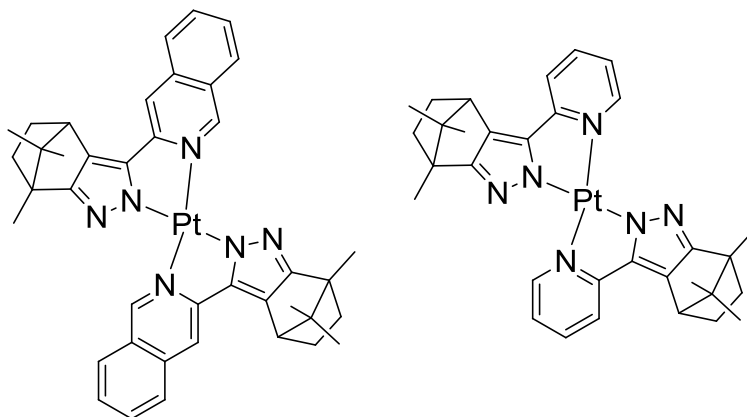


Figure 1-9. Chemical structures of Pt complexes reported by Kavitha.⁴⁷

Unlike the Pt(II) analogous, fewer Pd(II) metal complexes capable of emitting light while in solution or the solid state at room temperature. This limitation is mainly due to the presence of a low lying metal centered d-d transition, which quenches the potentially luminescent MLCT and LC transitions through thermally-activated surface-crossing processes.⁴⁹ Due to this limitation, palladium metal complexes are rarely used as phosphorescent emitters for device fabrication. However, they have been widely used as

highly efficient catalysts in many organic reactions, such as Stille, Negishi, Suzuki-Miyaura and Sonogashira couplings through Pd(0)/Pd(II) cycle.⁵⁰ More recently, C-X (X = C or a heteroatom) bond formation through the Pd(II) /Pd(IV) cycle has also been extensively investigated due to its pronounced advantages, which include higher functional group tolerance and milder reaction conditions.⁵¹ A proposed mechanism for this bond formation reaction is shown in Figure 1-10. The first step of the reaction involves C-H activation at the Pd(II) center, followed by oxidative addition of an R-Pd(IV)-X type compound, thus generating the Pd(IV) species. The subsequent reductive elimination generates the final product and releases Pd(II) back into the cycle.

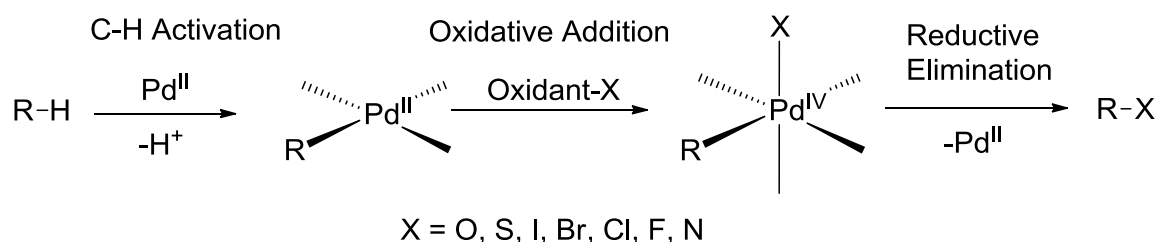


Figure 1-10. Proposed Pd(II)/Pd(IV) catalytic cycle for C-H activation.

However, the above mechanism involved Pd(IV) intermediates in C-H oxidation chemistry is demonstrated to be questionable recently. Through both experimental and computational studies, Ritter and co-workers show that the initial product of oxidation is highly possible to be a binuclear Pd(III) complex instead of mononuclear Pd(IV) complexes.⁵²

During the past few years Sanford,⁵³ Yu,⁵⁴ as well as Daugulis⁵⁵ and their co-workers have made contributions toward palladium catalyzed C-H bond functionalization. A wide variety of C-H functionalization reactions have been developed through the combination of Pd catalysts and oxidants. Sanford and coworkers have demonstrated that by choosing

substrates with appropriate directing groups, using electronically activated substrates, and properly designed catalyst systems, high reaction selectivity can be achieved.^{53c} Some important conclusions have been drawn from their research. During sp^2 C-H functionalization reactions, the favored site for the functional group addition to occur is *ortho* to the directing group at its least hindered side, as shown in Figure 1-11. Meanwhile sp^3 C-H functionalization processes favor the functional group addition to occur at the β position, as is demonstrated in the C-H acetoxylation reaction shown in Figure 1-12.^{53c}

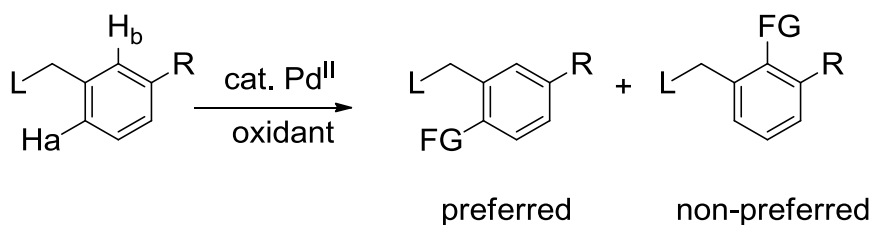


Figure 1-11. Selectivity of a ligand directed sp^2 C-H functionalization .

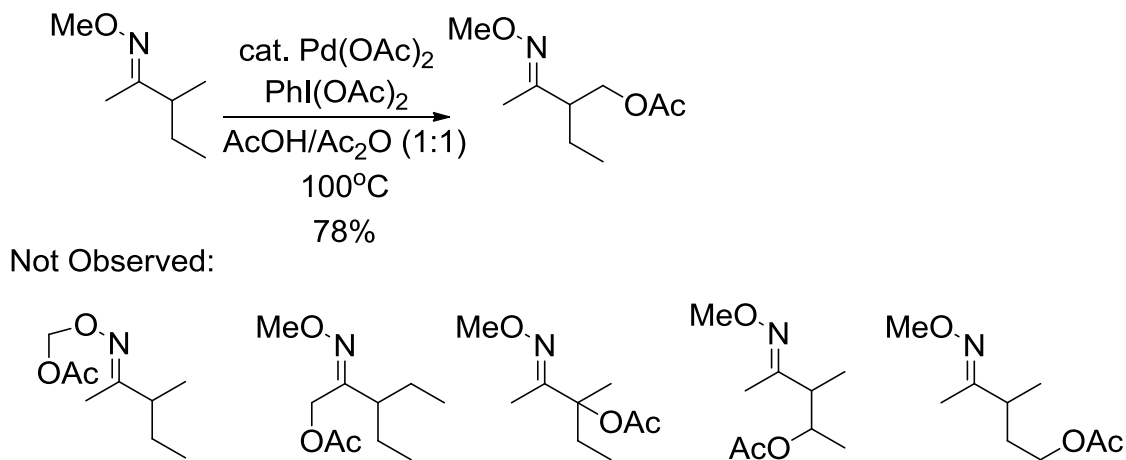


Figure 1-12. Selectivity of a ligand directed sp^3 C-H acetoxylation.

Sanford and co-workers also reported several ligands that significantly enhanced the performance of the Pd catalyst.⁵⁶ For example, they developed a highly efficient bidentate N^N donor ligand which demonstrated high efficiency and selectivity for Pd-catalyzed

naphthalene arylation reactions, as shown in Figure 1-13.^{56a} They also discovered that a simple pyridine ligand could effectively promote Pd-catalyzed arene acetoxylation reactions. Through altering the palladium/pyridine ratio, the rate and site selectivity of this reaction could be adjusted.^{56c}

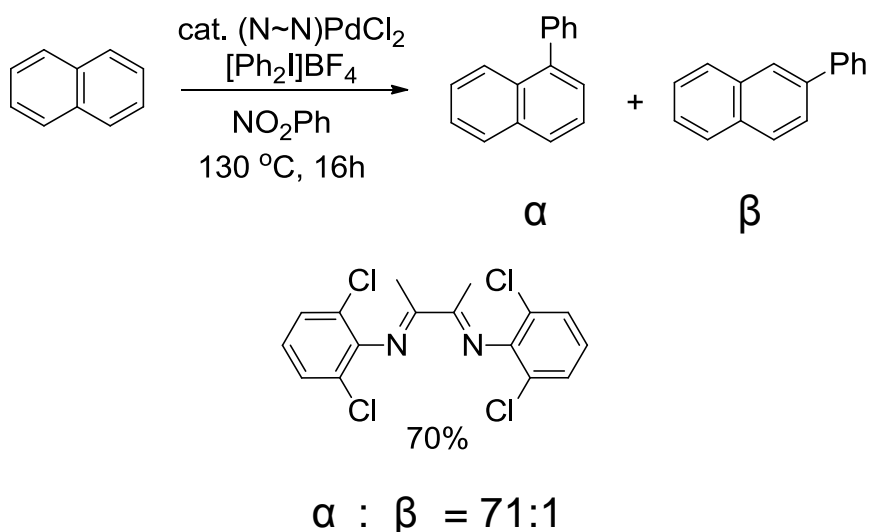


Figure 1-13. Efficient bidentate N^N donor ligand used in Pd-catalyzed naphthalene arylation reaction.

1.4 Tricarbonyl Rhenium(I) Diimine Complexes

The continuous interest in tricarbonyl rhenium(I) diimine complexes (*fac*-[Re(CO)₃(N^N)X], where X is a halogen, an alkyl group or a pyridyl ligand) stems from the fact that these compounds have similar excited state properties as Ru(II) polypyridyl analogues. These compounds have wide-spread applications, including catalysts,⁵⁷ labeling biomolecules,⁵⁸ monitoring polymerizations⁵⁹ and using as optical switching materials.⁶⁰ In 1970, Wrighton and coworkers were the first to investigate the photophysical and photochemical properties of this class of complexes.^{7a,7b,7c} Further studies have focused on the relationship between the nature of the halogen/polypyridyl

ligand and the photophysical properties of these complexes.⁶¹ In general, the lowest excited state of tricarbonyl rhenium(I) diimine complexes involves the low lying MLCT and intraligand (IL) $^3\pi-\pi^*$ excited states.⁶² These low-energy emissions mainly occupy the orange-yellow spectral region, and they occur due to the strong π back-bonding between the carbonyl ligands and rhenium metal center. This back-bonding lowers the energy gap between the metal d orbitals and the π^* ligand orbitals of the carbonyl ligands.

Due to strong spin-orbit coupling, singlet-triplet mixing is enhanced for tricarbonyl rhenium(I) diimine complexes. Consequently, these complexes exhibit phosphorescent emissions with long decay lifetimes that are observed both in the solid state and in solution.⁶³ However, in comparison with other late transition metals, the quantum yields of diimine rhenium complexes are generally low, with typical quantum yields of approximately 10^{-3} .³⁸ Despite this, diimine Re(I) complexes **2** and **3** with high quantum yields ($\Phi_P = 0.39-0.77$) were recently developed by Demas and DeGraff, as shown in Figure 1-14.⁶⁴ Their unusual solution emissions are centered between 450 and 500 nm, which is mainly 3LC in nature.

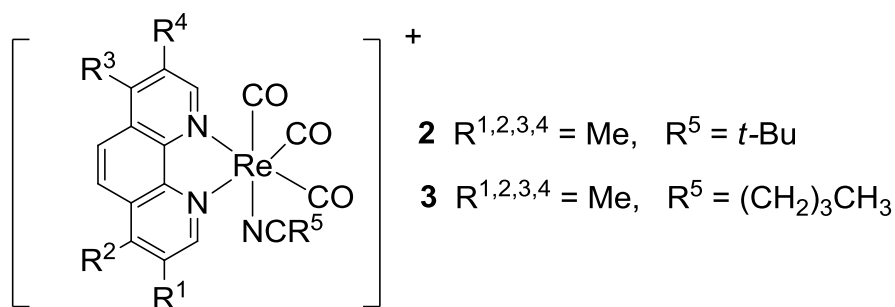
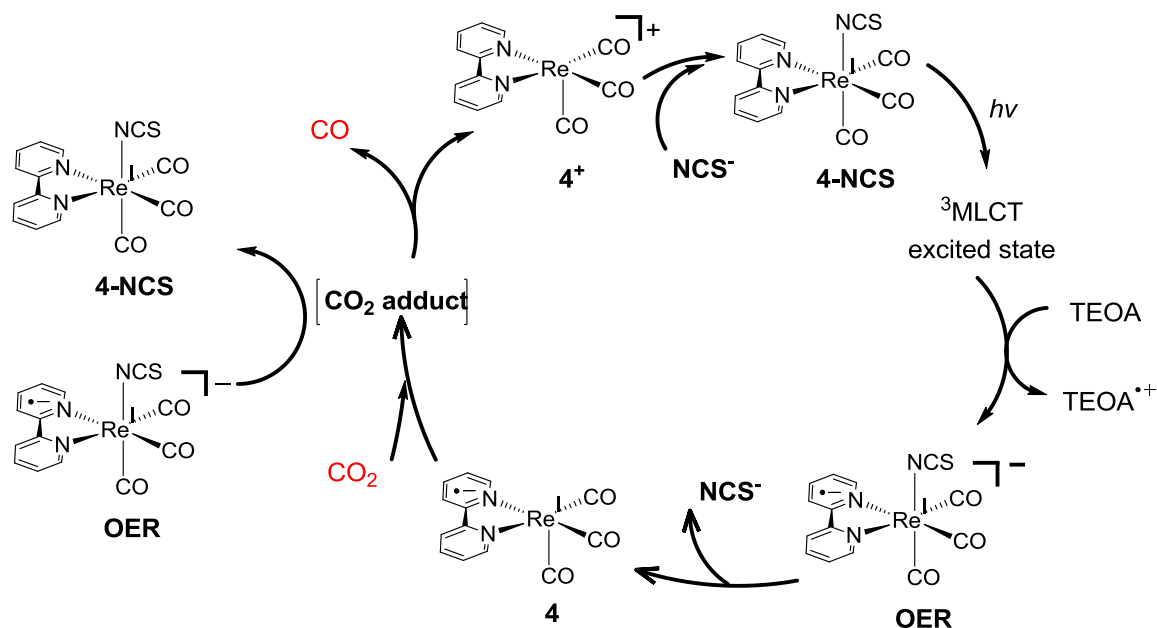


Figure 1-14. Structures of tricarbonyl Re(I) diimine complexes with high quantum yields.

In addition to their luminescent properties, tricarbonyl rhenium(I) complexes have also drawn significant attention because they can facilitate the photochemical⁶⁵ and electrochemical⁶⁶ reduction of CO₂. In 1984 Lehn et al. reported that the compound Re(bipy)(CO)₃Cl catalyzed the reduction of CO₂ to CO on a glassy carbon electrode in a DMF/water mixture.^{66a} Inspired by their work, researchers have investigated many rhenium bipyridine-based catalysts during the last two decades.^{65,66} Ishitani and coworkers developed a series of mononuclear rhenium (I) complexes and rhenium(I)/ruthenium(II)-based supramolecular photocatalytic systems facilitating highly efficient photocatalytic CO₂ reduction.^{67,65c,64d} In 2012, Kubiak et al. reported a light-assisted co-generation of CO and H₂ from CO₂ and water by using Re(^tBu₂bipy)(CO)₃Cl (where ^tBu₂bipy = 4,4'-di-*tert*-butyl-2,2'-bipyridine) and p-Si (*p*-type silicon semiconductor) in a non-aqueous medium.⁶⁸

Much attention has focused on the mechanisms driving the electrocatalytic^{66b} and photocatalytic^{65c,69} CO₂ reduction processes. Despite these efforts, the mechanism behind the latter process still remains unclear and no direct evidence has been observed for the proposed intermediates (such as a CO₂-bridged rhenium dimer and metalcarboxylates). Through a systematic study of three rhenium(I) complexes, *fac*-[Re(bipy)(CO)₃(L)] (L = NCS⁻, Cl⁻, and CN⁻), which have similar photophysical properties, Ishitani and coworkers proposed a reasonable mechanism for photocatalytic CO₂ reduction process, which is shown in Scheme 1-2. In this scheme, the process involving *fac*-[Re(bipy)(CO)₃(NCS)] as a catalyst is shown as an example. Upon irradiation, an electron of the rhenium catalyst is promoted to the ³MLCT excited state. This excited electron is subsequently quenched by a tertiary amine, thus yielding a one-

electron reduced (OER) species. The next key step involves the dissociation of SCN from the OER species, subsequently yielding a “17-electron species” whose proposed structure is $[\text{Re}(\text{bipy}^{\cdot-})(\text{CO})_3]$ (**4**).⁷⁰ This species then reacts with CO_2 to form the CO_2 adduct(s). The product CO is obtained through a two-electron reduction of CO_2 . However, compound **4** has only a single extra electron, and thus the OER species act as a source for the second electron in the catalytic cycle. At the end of the catalytic cycle CO is released as the main product and the eliminated anion SCN^- coordinates to $[\text{Re}(\text{bipy})(\text{CO})_3]^+$ to recover the catalyst *fac*- $[\text{Re}(\text{bipy})(\text{CO})_3(\text{NCS})]$.



Scheme 1-2. A proposed photocatalytic CO_2 reduction mechanism by *fac*- $[\text{Re}(\text{bipy})(\text{CO})_3(\text{NCS})]$.

1.5 *N*-heterocyclic Compounds and Their Transition Metal Complexes

In this part, 2-(2'-pyridyl) benzimidazole, 2-(2'-pyridyl)benzindole, their transition metal complexes, and their derivatives will be discussed. This section will focus mainly

on contributions from our group. However, related work by other research groups will also be discussed.

1.5.1 2-(2'-Pyridyl)benzimidazole and Derivatives

The motivation in preparing 2-(2'-pyridyl)benzimidazole (**py-im**)-based organic ligands stems from the fact that these ligands can bind strongly with transition metal ions. These ligands are especially well-suited for binding with d^8 or d^6 metal ions, which can either enhance ligand-centered phosphorescent emissions or promote MLCT emissions.⁷¹ It has been demonstrated that **py-im** is a promising moiety for the fabrication of luminescent metal complexes due to its rigid geometry. This rigidity can effectively limit energy loss through competing pathways such as vibrational decay, and can thus enhance phosphorescence emission intensities. As shown in Figure 1-15, this family of ligands has two nitrogen atoms that can chelate with metal ions, thus forming a five-membered chelate ring with the metal center. In comparison with a six-membered chelate ring, this five-membered chelate ring is more rigid and more conjugated, providing a more rigid metal complex. Additionally, the empty *NH* site can be further modified. For example, this site may be coupled to the carbon atom of various aryl groups, which may open up new avenues for preparing new classes of diverse ligands and multi-functional materials. Based on these considerations, our group has designed and synthesized a series of **py-im** based ligands as shown in Figure 1-15, and many of these examples incorporate multiple **py-im** subunits.^{10a} A common feature shared between these ligands was that their absorption spectra displayed two absorption bands with λ_{max} at approximately 230 and 300 nm, which result from $\pi \rightarrow \pi^*$ transitions centered on the **py-im** units. Investigations on their extinction coefficients (ϵ) have indicated that ϵ is linearly dependent on the

number of **py-im** units incorporated into the ligand. The emissions of these derivatives at room temperature and at 77K are dominated by the fluorescence emission pathway. These ligands have also been investigated *via* X-ray crystallography, and their crystal structures have revealed that the **py-im** unit has little conjugation with the benzene or the biphenyl groups to which it is directly attached. The **py-im** units are usually arranged in a perpendicular manner to the benzene or the biphenyl linker in order to minimize steric interactions between the *ortho* hydrogen atoms.^{10a}

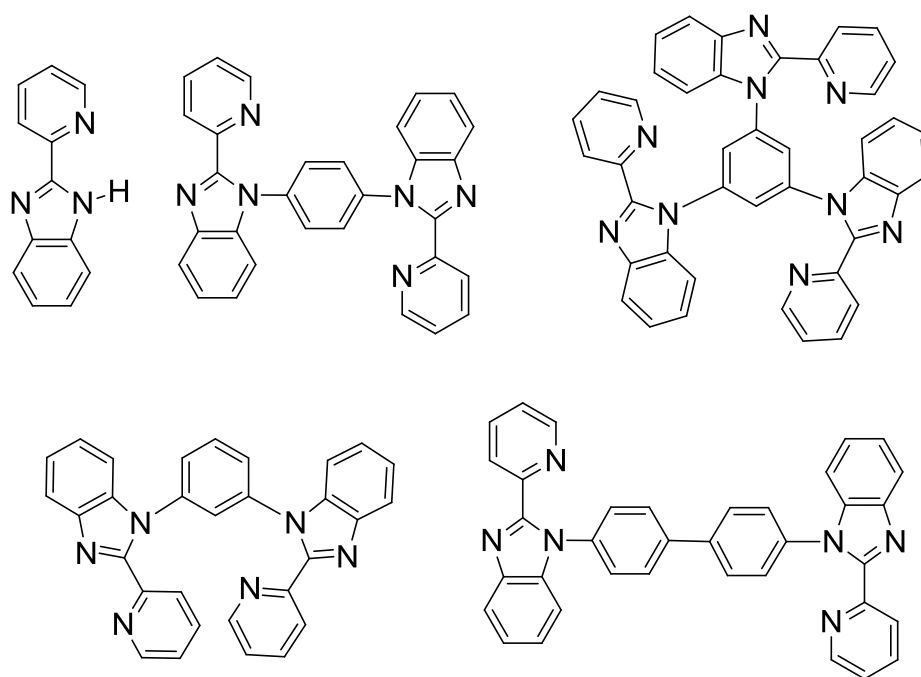


Figure 1-15. Structures of various ligands based on **py-im**.

Following the synthesis of the free ligands, Pt(II) complexes based on this class of ligands were obtained in good yields, and their structures are shown in Figure 1-16.^{10a} These ligands readily bind to the Pt(II) center *via* N^N-chelation. Their absorption spectra have very similar features, and they all show a broad and weak absorption band covering 410-550 nm, which is attributed to MLCT transitions. As is the case among the

free ligands, the ϵ values of these complexes are also linearly dependent on the number of **py-im** units. Unfortunately, solutions of these Pt(II) complexes do not emit at room temperature due to the thermal quenching of the solvent molecules. At 77K, frozen solutions of these complexes emit at 537-601 nm, which originates from a MLCT excited state. The solid state emission covers 582-621 nm at room temperature, thus displaying an orange-red emission.

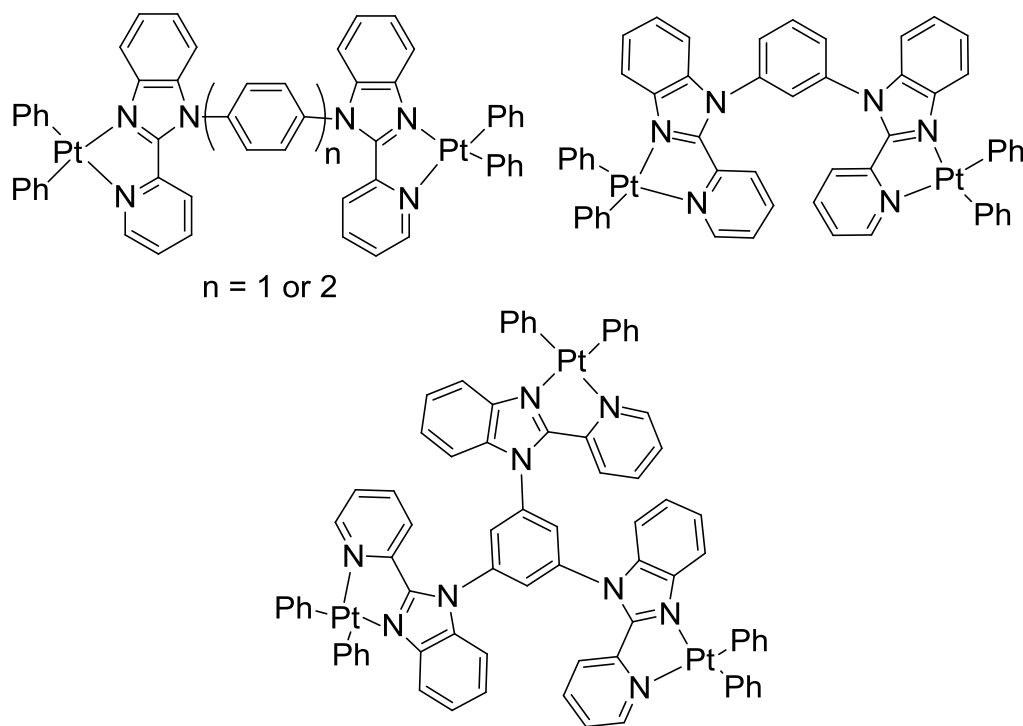


Figure 1-16. Structures of Pt(II) complexes based on **py-im** ligands.

In addition to Pt(II) complexes, Ru(II) complexes based on this **py-im** unit were also developed by our group, as shown in Figure 1-17.^{10b} Upon excitation by light, all of these Ru(II) complexes produce a red emission, which is observed both in solution and in the solid state at room temperature. The emission maximum ranges from 622 to 630 nm in CH₃CN, and from 623 to 629 nm in solid state. In comparison with [Ru(bipy)₃](PF₆)₂ (Φ_p = 6%), all of these complexes exhibit a relatively high emission quantum efficiency (4%

to 17%), which makes them attractive candidates for use in red light-emitting devices. Electrochemical analyses indicate that incorporation of the **py-im** units into the Ru(II) complex causes an increase in the HOMO level and a decrease in the LUMO level, thus decreasing the HOMO-LUMO band gap relative to that of $[\text{Ru}(\text{bpy})_3](\text{PF}_6)_2$.

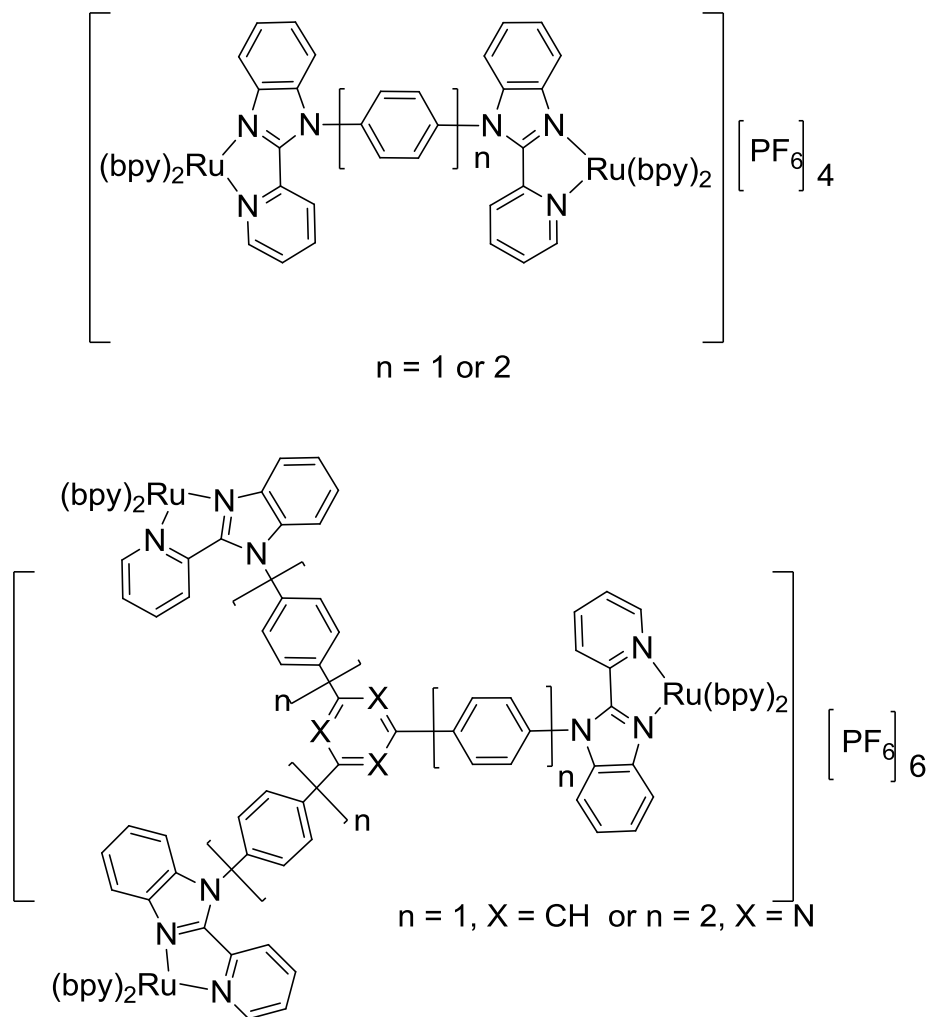


Figure 1-17. Structures of Ru(II) complexes based on **py-im** ligands.

The **py-im** ligand has been used not only to prepare small organometallic complexes, but also been to synthesize metallo-supramolecular polymers by other research groups. Rowan and co-workers successfully prepared a series of multiple-stimuli-responsive metallo-supramolecular polymers based on this benzimidazole moiety using reversible

metal-ligand interactions.^{10c,10d} In this work, they used ligand **5** shown in Figure 1-18 as the monomer. By simply mixing the transition metal ions and lanthanide metal ions with an appropriate functionalized monomer **5**, they obtained metallo-supramolecular gels. Four metallo-supramolecular gel-like materials were prepared by mixing the monomer with either Co(II) or Zn(II) as the transition metal and either La(III) or Eu(III) as the lanthanide metal. Through these combinations, the four metallo-supramolecular gel composition included **5**-Co(II)/La(III), **5**-Zn(II)/La(III), **5**-Co(II)/Eu(III), and **5**-Zn(II)/Eu(III). The metal ions essentially served as junction points connecting the monomer units together via metal-ligand coordination. Within this frame work, the transition metal ions Co(II) or Zn(II) would bind to two different monomer units, and formed junction points connecting monomer units together in a linear fashion as a chain. The lanthanide ions underwent coordination with three monomer units, forming intersections between different chains and thus behaving as crosslinkers. Rowan et al. demonstrated that all four gels responded to thermal and mechanical stimuli. Either heating the gels at high temperature (100 °C) or shaking them resulted in a reversible gel-sol transition. Due to the strong binding affinity between the lanthanides and the carboxylic acids, these lanthanide-containing systems also showed chemoresponsive behavior. For example, addition of a small amount of formic acid caused the **5**-Zn(II)/Eu(III) gel-like complex to breakdown and the Eu(III) emission was also quenched.

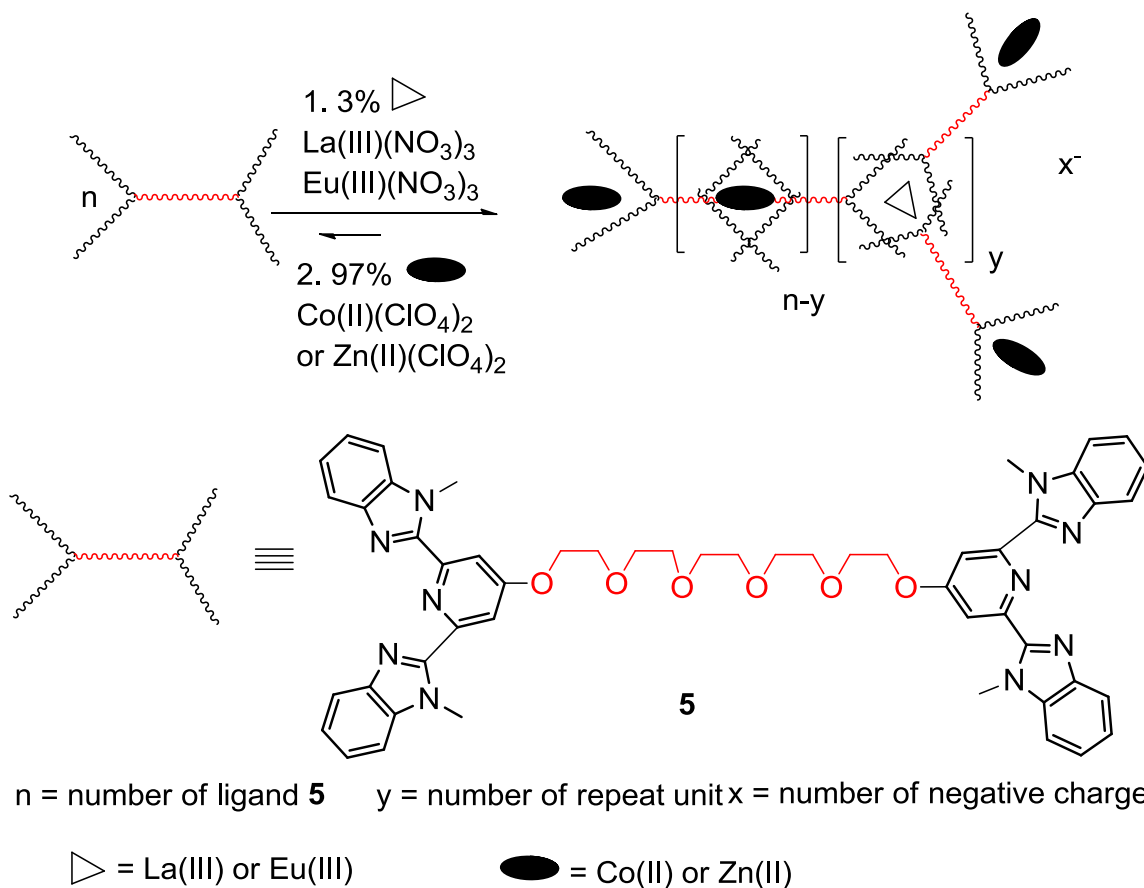


Figure 1-18. Schematic diagram showing the formation of metallo-supramolecular gel-like materials obtained by mixing metal ions with monomer **5**.

1.5.2 2-(2'-Pyridyl)indole and Derivatives

Unlike the **py-im** ligand, **py-in** has a carbon atom located at the 3-position of the indole ring rather than a nitrogen in the benzimidazole (Figure 1-1). After deprotonation, **py-in** can emit blue light since deprotonation of the ligand decreases the $\pi \rightarrow \pi^*$ gap, thus causing a red shift in the emission energy. Additionally, when the indole is deprotonated to generate an anionic ligand, it could bind to the metal center *via* N[^]N chelation.^{11a,11b} For example, our group has synthesized $\text{Zn(py-in)}_2(\text{THF})^{11b}$, by reacting the anionic ligand with ZnCl_2 in THF solution under nitrogen protection. In this reaction, *n*-butyllithium was used to deprotonate the ligand. This reaction involves a simple chelate

binding mode and is thus less complicated than the corresponding reaction involving the 2-(2-pyridyl)-7-azaindole ligand, which involves both the bridging and chelate binding modes. However, the $\text{Zn}(\text{py-in})_2(\text{THF})$ complex is air-sensitive. This air-sensitivity is apparently caused by reactions between the negatively charged **py-in** ligand and moisture, which cause the highly polarized Zn-N(indole) bonds to rupture. X-ray quality crystals were obtained by recrystallizing this complex from $\text{CH}_2\text{Cl}_2/\text{hexane}$, and its crystal structure is shown in Figure 1-19. The crystal structure clearly shows that the Zn(II) center is five coordinate. In particular, the metal center is chelated to two **py-in** ligands and is also coordinated to one THF molecule, which is easily lost when subjected to vacuum. The photophysical properties of this Zn(II) complex were also investigated. In both solution and the solid state, this complex emitted a bright blue-green color upon irradiation by UV light. Its emission maximum was observed at 488 nm and was attributed to a ligand-centered $\pi \rightarrow \pi^*$ transition. This luminescence investigation and the previous literature work^{11d} demonstrated that the central Zn(II) ion stabilizes the negatively charged ligand *via* coordination bond formation. Lorenz and co-workers also synthesized a series of **py-in**-based d^6 transition metal complexes using N[^]N chelation, and the structures of these complexes are shown in Figure 1-20.^{11e} They also reported that even a weak base such as triethylamine could cause deprotonation. However, all of these complexes were air and moisture sensitive, which greatly limited their potential applications.

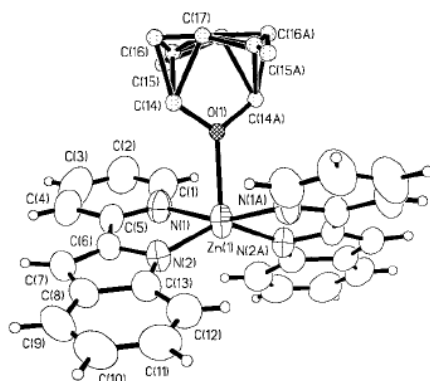


Figure 1-19. Crystal structure of $\text{Zn}(\text{py-in})_2(\text{THF})$.^{11b}

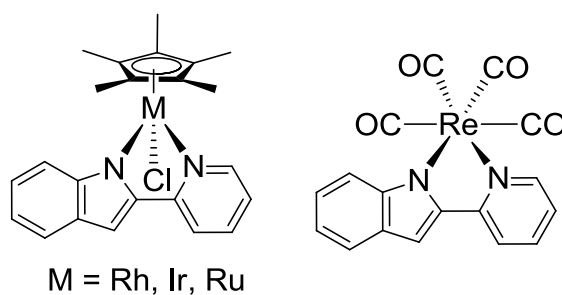


Figure 1-20. Structures of transition metal complexes prepared by Lorenz et al.^{11e}

When a substituent group protects the nitrogen atom on the indole ring from chelation, the C^N chelated metal complexes could be prepared, since the substituent does not deactivate the indole nucleus towards the electrophilic attack by the metal.^{11d} Based on this consideration, a series of 2-(2'-pyridyl)indole derivatives bearing phenyl substituents on the indole nitrogen have been synthesized by our group. In addition, cyclometallated Pd(II) and Pt(II) complexes of these ligands are also under investigation, as shown in Figure 1-21.^{11g}

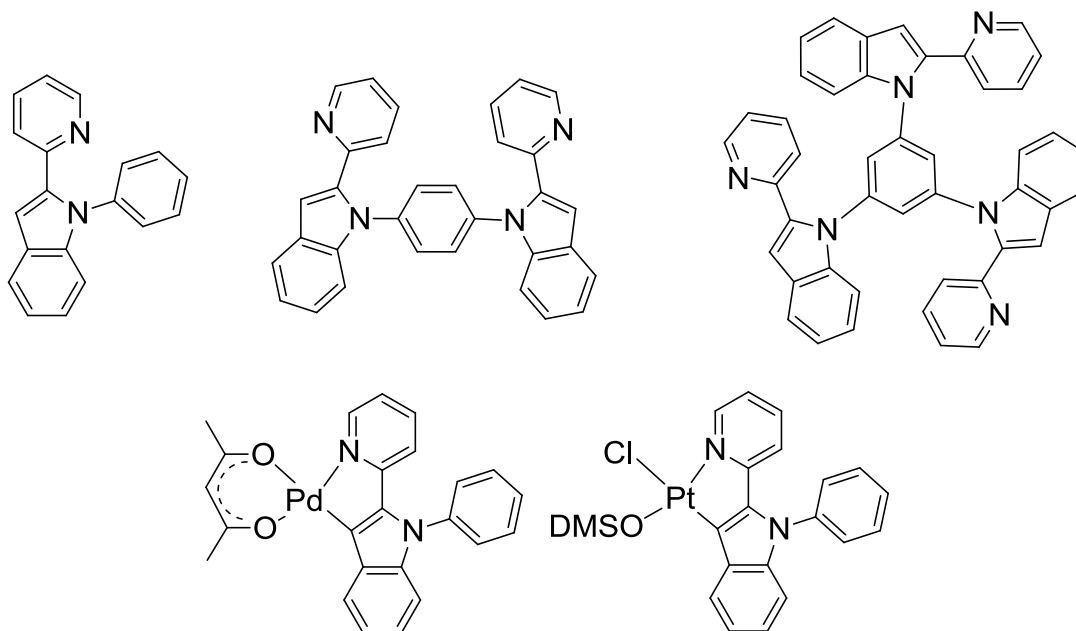


Figure 1-21. Structures of **py-in** based ligand and N[^]C-chelate Pt(II)/Pd(II) metal complexes.

1.6 Polynuclear Metal Complexes

While *N*-heterocyclic compounds have been used to prepare mononuclear metal complexes, they are also widely used to prepare polynuclear metal complexes. Currently, much research attention is devoted to polynuclear metal complexes. This interest is stimulated not only because of the large sizes of these complexes, but also the variety of components that can be incorporated into these supramolecular arrays. The long term goal of these studies is to prepare light harvesting units capable of absorbing the entire solar spectrum and process this light energy into useful chemical energy.⁷² Among the most well-known examples of these systems are solar cells, which convert sunlight into electricity. Research has shown that even though many variables will influence the final performance of solar cells, the design of the dye sensitizers is considered to be the most important factors.³⁷ As discussed above, Ru(II) polypyridyl compounds are considered to

be the most promising photosensitizers. The dye N3 can be considered as an example in this regard, as it has been demonstrated to be an efficient photosensitizer with high stability. Unfortunately, its spectral response decreases rapidly above 700 nm. In order to efficiently harvest sunlight, polynuclear metal complexes have been employed, which consist of several chromophores that are linked together by bridging or spacer units. In such systems, the excitation energy arising from light absorption is transferred from the higher energy chromophores to the lowest energy chromophores, as shown in Figure 1-22. The communication between the constituent units is greatly influenced by the nature of the bridge and the mode of linkage.⁷² If the interactions are weak, the properties of the supramolecular complexes can be considered as simply the sum of their constituent units. However, if strong interactions exist between the metal centers, the properties of the complex will be quite different from those of their monomeric analogs. Significant advances have been made in this field.⁷³ For example, Grätzel and co-workers reported the synthesis of Ru(II)/Re(I) polynuclear complexes utilizing cyanide as the bridging ligand (Figure 1-23).⁷² Their investigations have shown that cyano-bridged Re(I)-Re(I) and Re(I)-Ru(II)-Re(I) complexes are highly emissive. Luminescence and redox properties have been used to assess the intramolecular energy/electron transfer processes between the terminal Re(I)-polypyridyl units and the central Ru(II)-polypyridyl unit. The intervalence transitions and the excitation spectra for the Ru(II)-based emission demonstrate that energy is efficiently transferred from the Re(I) based chromophore to the Ru(II) based unit.

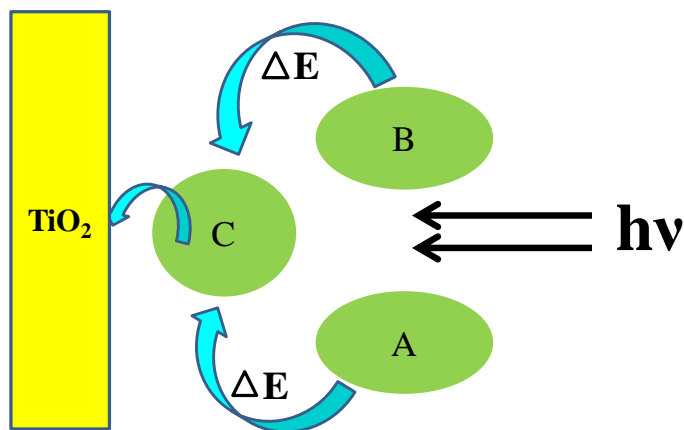


Figure 1-22. Energy transfer process in a polynuclear metal complex.

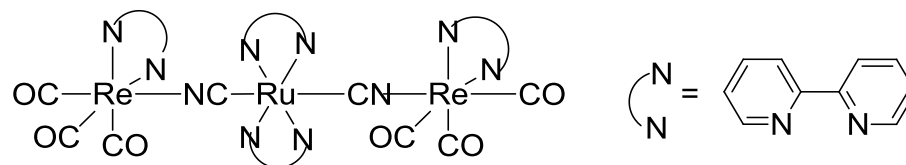


Figure 1-23. Structure of Re-Ru polynuclear complex.

In addition to solar cell applications, the hetero-bimetallic Ru-M (M = Pd, Pt and so on) complexes have also been designed for the visible light splitting of water. This solar energy water splitting process involves two components, the reduction of protons and the oxidation of water. To date, several examples have been reported involving the homogeneous catalysis of individual half reactions. These systems utilized sacrificial agents to provide the required redox equivalents. Photoactive metal complexes play the role of light absorbers, and electrons are transferred from the dye to the catalytic center through an intermolecular process.⁷⁴ The light driven oxidation of water is catalyzed by colloidal particles, and manganese clusters are the most frequently used catalysts for this role.⁷⁵ The light-driven proton reduction can be catalyzed by redox active metals such as platinum or palladium.⁷⁶ Here only the proton reduction half reaction will be discussed. It is difficult to optimize the electron transfer processes through the intermolecular

approach. To address this, much effort has focused on the development of controllable intramolecular electron transfer processes. By manipulating the appropriate molecular components, systems allowing directional light-driven electron transfer from the photo center to the catalytic center can become available. These systems are described as photochemical molecular devices (PMDs), and the general structure of one of these systems is shown in Figure 1-24. A PMDs consists of a photoactive center, a bridging unit and a catalytically active moiety.

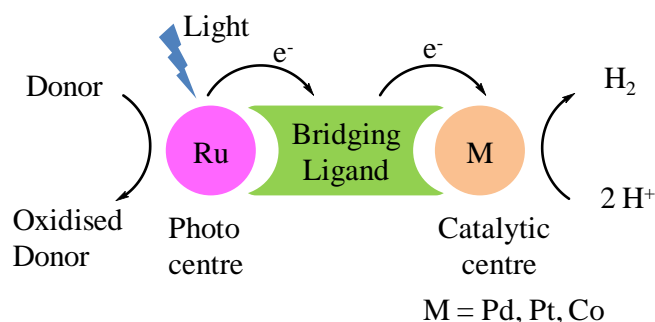


Figure 1-24. A scheme showing a bimetallic complex serving as a PMD for proton reduction.

In 2006, Sakai and coworkers first reported a “photo-hydrogen-evolving molecular device”, which generates H₂ from an aqueous acetate buffer solution in the presence of a sacrificial electron donor upon visible light illumination.^{76a} However, the turn-over-number (TON) of this compound for hydrogen formation was only 2.4. The chemical structure of this compound **6** is shown in Figure 1-25. Following this discovery, much research effort has been given to improve the catalytic performance of these systems. Several polynuclear metal complexes (e.g. compounds **7-10** shown in Figure 1-25) have been investigated as efficient photocatalytic active systems with high TONs.⁷⁷ Further investigations on these complexes have shown that the bridging ligand significantly affects the performance of these systems. In order to obtain active catalysts, the bridging

ligands should have low-lying energy orbitals that can accommodate an electron originating from the photo center.

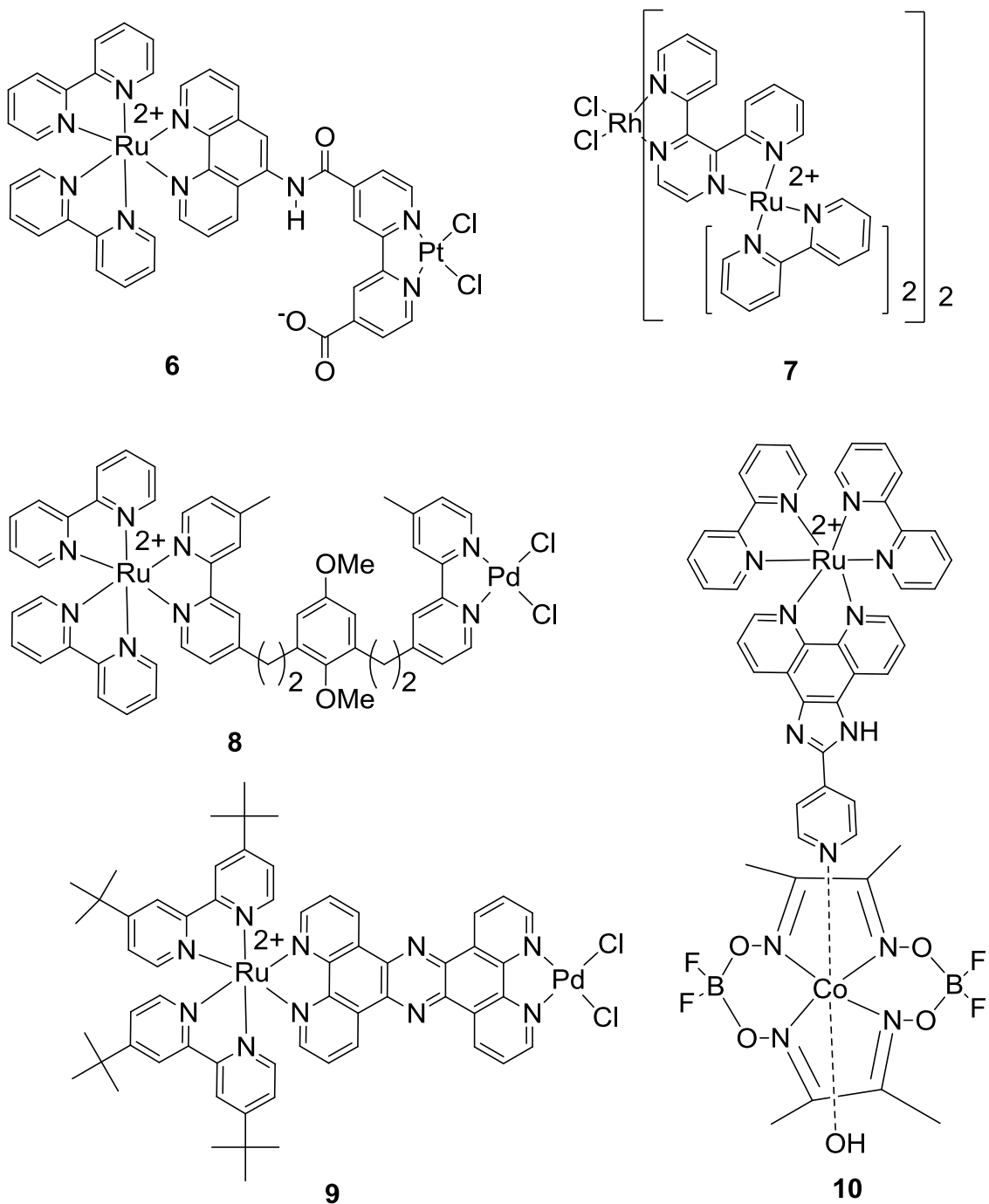


Figure 1-25. Structures of various polynuclear metal complexes used as photochemical molecular devices.

1.7 Organoboron Compounds

1.7.1 Four-coordinate boron compounds

The study of 4-coordinate organoboron compounds stems from the interesting properties exhibited by Alq₃ (q=8-hydroxyquinolate) and its derivatives. In 1987 Tang and Van Slyke first reported an efficient green EL device that prepared from thin films of Alq₃.¹⁸ Since then, this compound and its derivatives have been fully studied and widely used as electron transporting and emissive layers for OLED fabrication. Even though previous studies have achieved OLEDs emitting in green and red regions by doping Alq₃ with different dyes, it is still a big challenge to obtain blue emitters through this method.⁷⁸ This problem was not resolved until the emergence of 4-coordinate boron systems. Our group synthesized 8-hydroxyquinoline based 4-coordinate organoboron compounds, shown as **11** and **12** in Figure 1-26.^{14e} These boron compounds exhibit bright green-blue photoluminescence and have good stability towards air and moisture. This stability can be attributed to the more covalent nature of the boron-ligand bonds, which makes them potentially useful compounds for electroluminescence. Additionally, they also have good electron transport properties, giving them potential applications as electron transport materials.

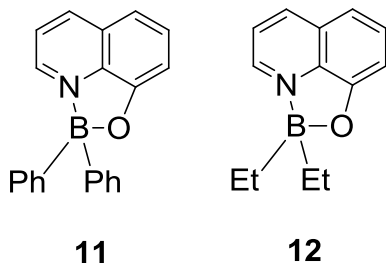


Figure 1-26. Structures of 8-Hydroxyquinoline based 4-coordinate organoboron compounds.

Our group also developed a series of N^N chelated 4-coordinate boron compounds, shown as **13-17** in Figure 1-27.⁷⁹ Those compounds have a general formula of BPh₂(N^N), where N^N represents bidentate chelate ligands containing both neutral and negatively charged nitrogen donor atoms. These compounds display bright luminescence ranging from blue to red, depending on the nature of the chelate ligand. In addition, they can function as both emitters and electron transport materials in EL devices.

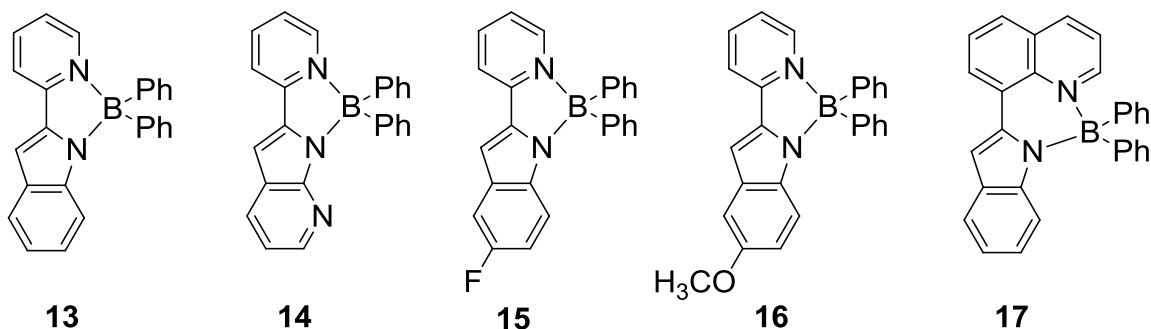


Figure 1-27. Chemical structure of N^N chelate organoboron compounds **13-17**.

In addition to the N^N-chelate, N^C-chelated organoboron compounds are another significant class of molecules used for OLED fabrication. Unlike the widely explored N^C-chelated metal complexes, N^C-chelated boron compounds are still rare. In 2006 Yamaguchi and co-workers designed and synthesized a boryl-substituted thienylthiazole compound, which is shown in Figure 1-28.⁸⁰ The photophysical and electrochemical properties, as well as the solid state structures of this compound were investigated. These investigations revealed that the intramolecular B-N coordination effectively constrains the π -conjugated framework in a planar fashion. Consequently, the electron affinity increases, which in turn lowers the LUMO level. Due to the above properties, these compounds are promising electron transporting materials.

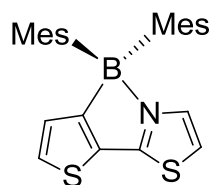


Figure 1-28. Chemical structure of boryl-substituted thienylthiazole.

Recently organoboryl groups have also been shown to exhibit interesting photochromic behaviors^{81,15} which broadens their potential applications in the fabrication of optical memory devices, molecular switches, smart windows and other devices. Photochromism is the light-induced reversible transformation of a chemical species to a new species that has a different absorption spectrum or color.⁸² As shown in Figure 1-29, upon UV irradiation isomer **A** can be converted to the higher energy isomer **B**. The reverse reaction is induced by irradiation at a different wavelength or alternatively by heat to regenerate isomer **A**. Until now, there are only two types of photochromic organoboron compounds, including the azobenzene N[^]C-chelated boron compounds reported by Kawashima⁸¹ and N[^]C-chelated boron compounds reported by our group.¹⁵

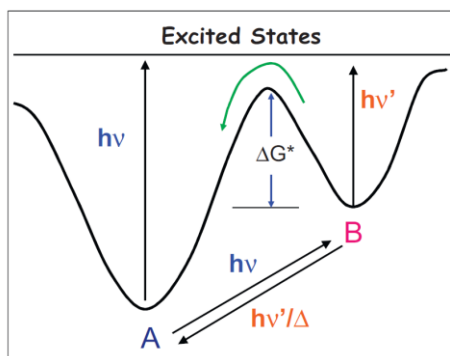


Figure 1-29. Diagram showing the pathways of photochromic switching between two isomers.^{82c}

In 2005 Kawashima and coworkers reported the photoisomerization of a catecholborane ((*E*)-**18**) containing a 2-(phenylazo)phenyl group attached to the boron

through an N-B dative bond, as shown in Figure 1-30.⁸¹ This (*E*)-**18** compound had a maximum absorption at 339 nm, which was assigned as π - π^* transition of the azo group. After irradiation at 360 nm, the absorbance band at 339 nm decreased while a corresponding absorbance increase was observed at 460 nm. This new absorbance maximum at 460 nm was attributed to a n- π^* transition of the azo group in the *cis* isomer. ¹¹B NMR experiments revealed that this isomerization occurs by the dissociation of the B-N bond, which is followed by the azobenzene moiety's *trans* (*E*) to *cis* (*Z*) isomerization. This process is fully reversible, as applying irradiation at 431 nm produces the original isomer. Kawashima and co-workers also discovered that the Lewis acidity of the catecholborane can be switched *via* photoirradiation. Upon transformation from the *trans* isomer to the *cis* isomer, the complexation affinity for pyridine increased by a factor of ~300.

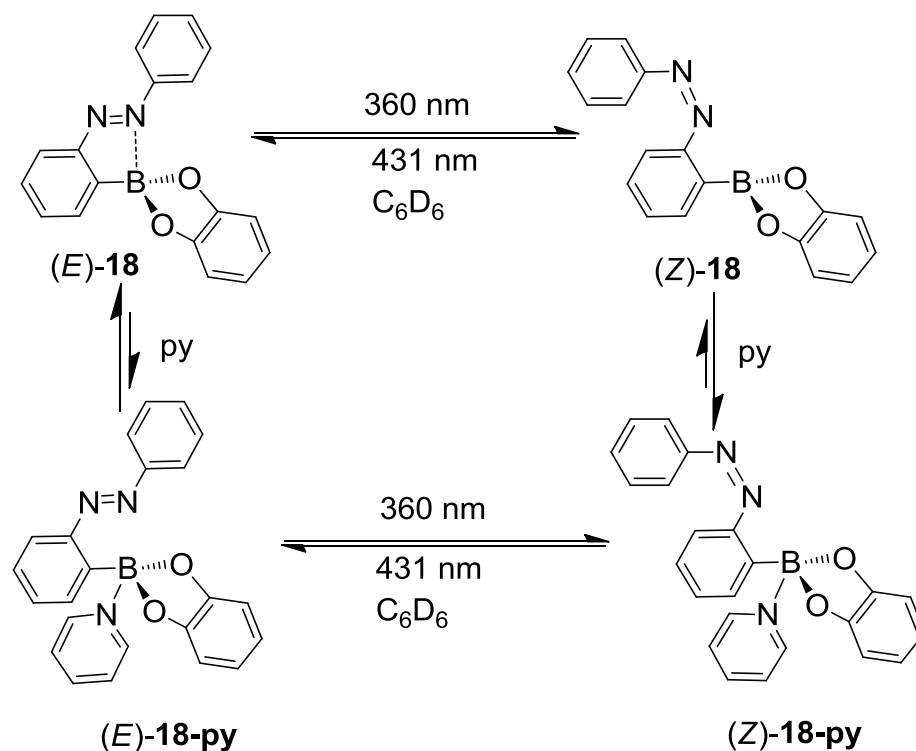


Figure 1-30. Photoisomerization of compound **18** and the influence of pyridine on the isomerization process.

In 2008 our group reported a reversible isomerization process involving a tetrahedral boron center.¹⁵ Unlike the photochromic azobenzene organoboron compounds mentioned above, structural transformation of our N[^]C chelate boron compounds involved the cleavage and subsequent formation of B-C and new C-C bonds, as shown earlier in Scheme 1-1. An example of these compounds is B(ppy)Mes₂, where ppy = 2-phenylpyridine, and Mes = mesityl. Upon irradiation at 365 nm, solutions of these tetrahedral N[^]C-chelated boron compounds rapidly changed from highly fluorescent colorless solutions to non-emissive dark blue solutions. During this process, a new C-C bond was formed between a mesityl and phenyl groups. ¹¹B and ¹H NMR studies confirmed that this process was fully reversible. As part of a systematic investigation of these tetrahedral boron compounds, a series of boron compounds with substituted ppy

chelating ligands were synthesized (Figure 1-31). This investigation was conducted in order to gain a full understanding of the steric and electronic effects which can influence the photochromic behavior and photochemical stability of this class of compounds.⁸³ It was found that the incorporation of electron-withdrawing groups on the chelate backbone increase the mesityl to chelate charge transfer contributions to the lowest excited state, which may lead to enhanced photoisomerization efficiency.

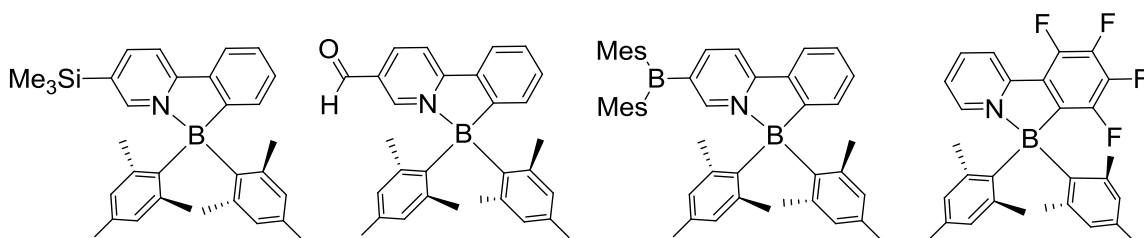


Figure 1-31. Chemical structure of N^C-chelate boron compounds with different substituted chelation ligands.

The impact of metal chelation on the properties of this boron photochromic system has also been investigated by our group, although this research is still at an early stage. Several Pt(II) chelate compounds have been prepared, as shown in Figure 1-32.⁸⁴ At ambient temperature, their toluene solutions all show bright phosphorescent emission, which originate mainly from the ³LC state of the chelate ligand. However, the photoisomerization quantum efficiencies of these complexes are much lower than that of their parent compound **1**. The absorption spectral data and time-dependent density functional theory (TD-DFT) computational results indicate that chelation to the Pt(II) center enhances the ligand-centered singlet to triplet intersystem crossing, resulting in an enhancement of the ³LC state that is localized on the chelate backbone. Consequently, phosphorescence becomes a highly efficient relaxation pathway for energy dissipation

which was not available to the parent B(ppy)Mes₂ chromophore. This new relaxation pathway thus leads to significant photoisomerization quenching.

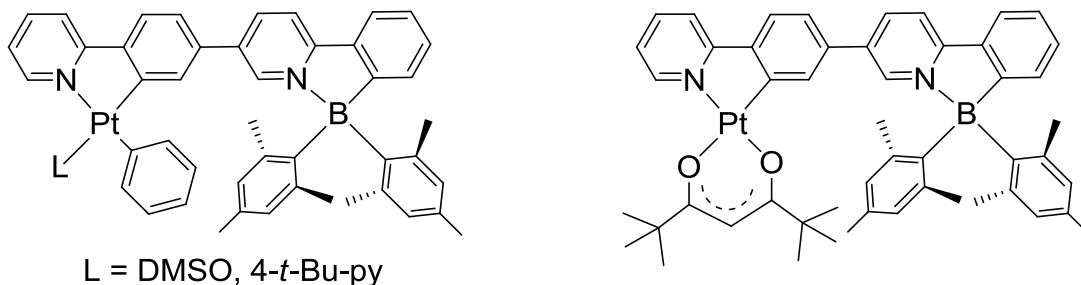


Figure 1-32. Chemical structures of N^C-chelate boron compounds that are coordinated with Pt(II).

1.8 Scope of this Thesis

As shown in the above sections, transition metal complexes and 4-coordinate boron compounds have a wide range of applications in OLEDs, for catalysis, and for various other photochemical devices. This is also apparent, for the transition metal containing 4-coordinate boron compounds, even though research in this area is still in its infancy. Therefore, the goal of this thesis is to investigate the structures and luminescent properties of **py-in** and **py-im**-containing coordination complexes of Ru(II) and Re(I), as well as their corresponding Pd(II) and Pt(II) bimetallic complexes. Additionally, the reactivity of Pd(II) complex incorporating a chiral ligand containing two 3,3'-bis[2-(2'-py)-indolyl] moieties is also examined. The impact of transition metal coordination on the photochromic behavior of N^C-chelate 4-coordinate boron compounds is also discussed.

In Chapter 2 the synthesis of a novel ligand L1 (as shown in Figure 1-1) where a **py-in** and a **py-im** unit are linked together by a phenyl group, is described. In addition, two

C-C bonded polydentate ligands (L2 and L3) were isolated as byproducts which structures are shown in Figure 1-1. Chapter 2 examines the properties of both the monomer and oligomer ligands. In Chapter 3, the synthesis of heterobimetallic Ru(II)-Pt(II) and Ru(II)-Pd(II) complexes based on ligand L1 is discussed. The photophysical and electrochemical properties are also examined. Chapter 4 describes the synthesis of heterobimetallic Re(I)-Pt(II) and Re(I)-Pd(II) complexes based on ligand L1, and also examines their photophysical and electrochemical properties. In addition, preliminary results exploring the electrocatalytic reduction of CO₂ are also presented. In Chapter 5, the synthesis of novel *trans*-chelated Pd(II) and Pt(II) complexes based on chiral ligand bis[3,3'-(2-(2'-pyridyl)indolyl)benzene] (**bpib**, L4) are described. A preliminary investigation on the catalytic activity of the Pd(OAc)₂-L4 system for promoting the arene acetoxylation reaction is also presented. Chapter 6 described the effect of coordination with metals (Au(I), Pt(II), and Re(I)) on the photochromic behavior of 4-coordinate boron compounds. Meanwhile, Chapter 7 provides a general summary of the research described in this thesis along with key conclusions and proposed future work.

1.9 References

1. (a) C. W. Tang, S. A. VanSlyke, C. H. Chen, *J. Appl. Phys.* 1989, **65**, 3611; (b) Y. Shirota, S. Kawami, K. Imai, *Appl. Phys. Lett.* 1994, **65**, 807; (c) Y. Hamada, T. Sana, M. Fujita, T. Fujii, Y. Nishio, K. Shibata, *Jpn. J. Appl. Phys.* 1993, **32**, L514; (d) V. Bulovic, G. Gu, P. E. Burrows, S. R. Forrest, *Nature* 1996, **380**, 29; (e) M. Braun, J. Gmeiner, M. Tzolov, M. Coelle, F. D. Meyer, W. Milius, H. Hillebrecht, O. Wendland, J. U. von Schutz, W. Brutting, *J. Chem. Phys.* 2001, **114**, 9625; (f) H. Schmidaur, J. Lettenbauer, D. L. Wikinson, G. Müller, O. Z. Kumberger, *Naturforsch.* 1991, **46b**, 901.
2. (a) M. K. Nazeeruddin, A. Kay, I. Rodicio, R. Humphry-Baker, E. Müller, P. Liska, N. Vlachopoulos, M. Grätzel, *J. Am. Chem. Soc.* 1993, **115**, 6382; (b) D. Kuciauskas, M. S. Freund, H. B. Gray, J. R. Winkler, N. S. Lewis, *J. Phys. Chem. B* 2001, **105**, 392; (c) E. A. M. Geary, L. J. Yellowlees, L. A. Jack, I. D. H. Oswald, S. Parsons, N. Hirata, J. R. Durrant, N. Robertson, *Inorg. Chem.* 2005, **44**, 242; (d) G. M. Hasselmann, G. J. Meyer, *Z. Phys. Chem.* 1999, **212**, 39; (e) N. Alonso-Vante, J. F. Nierengarten, J. P. Sauvage, *J. Chem. Soc. Dalton Trans.* 1994, 1649; (f) P. M. Jayaweera, S. S. Palayangoda, K. Tennakone, *J. Photochem. Photobiol. A* 2001, **140**, 173.
3. (a) I. A. Hemmilä *Applications of Fluorescence in Immunoassays*, 2nd ed. Wiley, New York, 1991; (b) D. Parker, *Coord. Chem. Rev.* 2000, **205**, 109; (c) L. Prodi, S. Pivari, F. Bolletta, M. Hissler, R. Ziessel, *Eur. J. Inorg. Chem.* 1998, **1959**, 17; (d) A. Juris, V. Balzani, F. Barigelletti, S. Campagna, P. Belser, A. Von Zelewsky, *Coord. Chem. Rev.* 1988, **84**, 85; (e) X. Q. Guo, F. N. Castellano, L. Li, H. Szmecinski, J. R. Lakowicz, *Anal. Biochem.* 1997, **254**, 179; (f) X. Q. Guo, F. N. Castellano, L. Li, J. R. Lakowicz, *Anal. Chem.* 1998, **70**, 632; (g) J. M. Kurner, I. Klimant, C. Krause, H. Preu, W. Kunz, O. S. Wolfbeis, *Bioconjugate Chem.* 2001, **12**, 883.
4. (a) C. She, A. A. Rachford, X. Wang, S. Goeb, A. A. O. El-Ballouli, F. N. Castellano, J. T. Hupp, *Phys. Chem. Chem. Phys.* 2009, **11**, 8586; (b) S.-C. Chan,

- M. C. W. Chan, Y. Wang, C.-M. Che, K.-K. Cheung, N. Zhu, *Chem. Eur. J.* 2001, **7**, 4180.
5. L. Flamigni, A. Barbier, C. Sabatini, B. Ventura, F. Barigelletti, *Top. Curr. Chem.* 2007, **281**, 143.
 6. (a) S. Campagna, F. Puntoriero, F. Nastasi, G. Bergamini, V. Balzani, *Top. Curr. Chem.* 2007, **208**, 117; (b) W.-L. Jia, Y. F. Hu, J. Gao, S. Wang, *Dalton Trans.* 2006, 1721.
 7. (a) M. S. Wrighton, D. L. Morse, *J. Am. Chem. Soc.* 1974, **96**, 998; (b) D. L. Morse, M. S. Wrighton, *J. Am. Chem. Soc.* 1976, **98**, 3931; (c) J. C. Luong, L. Nadjo, M. S. Wrighton, *J. Am. Chem. Soc.* 1978, **100**, 5790; (d) J. C. Luong, R. A. Faltynek, M. S. Wrighton, *J. Am. Chem. Soc.* 1979, **101**, 1597; (e) S. M. Fredericks, J. C. Luong, M. S. Wrighton, *J. Am. Chem. Soc.* 1979, **101**, 7415.
 8. (a) W. A. Herrmann, *Angew. Chem. Int. Ed.* 2002, **41**, 1290; (b) M. Devereux, D. O. Shea, A. Kellett, M. McCann, M. Walsh, D. Egan, C. Deegan, K. Kedziora, G. Rosair, H. Muller-Bunz, *J. Inorg. Biochem.* 2007, **101**, 881; (c) E. Peris, R. H. Crabtree, *Coord. Chem. Rev.* 2004, **248**, 2239.
 9. (a) J. Ashenurst, G. Wu, S. Wang, *J. Am. Chem. Soc.* 2000, **122**, 2541; (b) C. F. Lee, K. F. Chin, S. M. Peng, C. M. Che, *J. Chem. Soc., Dalton Trans.* 1993, 467; (c) Y. G. Ma, H. Y. Chao, Y. Wu, S. T. Lee, W. Y. Yu, C. M. Che, *J. Chem. Soc., Chem. Comm.* 1998, 2491; (d) Q. Wu, J. A. Lavigne, Y. Tao, M. D'Iorio, S. Wang, *Chem. Mater.* 2001, **13**, 71; (e) D. Song, K. Sliwowski, J. Pang, S. Wang, *Organometallics* 2002, **21**, 4978; (f) S.-B. Zhao, S. Wang, *Chem. Soc. Rev.* 2010, **39**, 3142.
 10. (a) Q. D. Liu, W. L. Jia, S. Wang, *Inorg. Chem.* 2005, **44**, 1332; (b) W. L. Jia, Y. F. Hu, J. Gao, S. Wang, *Dalton Trans.* 2006, 1721; (c) P. K. Iyer, J. B. Beck, C. Weder, S. J. Rowan, *Chem. Commun.* 2005, 319; (d) J. B. Beck, S. J. Rowan, *J. Am. Chem. Soc.* 2003, **125**, 13922.
 11. (a) Q. Liu, M. S. Mudadu, H. Schmider, R. Thummel, Y. Tao, S. Wang, *Organometallics* 2002, **21**, 4743; (b) S. F. Liu, Q. Wu, H. L. Schmider, H. Aziz,

- N. Hu, Z. D. Popovic, S. Wang, *J. Am. Chem. Soc.* 2000, **122**, 3671; (c) Q. Wu, M. Esteghamatian, N. X. Hu, Z. D. Popovic, G. Enright, S. R. Breeze, S. Wang, *Angew. Chem., Int. Ed.* 1999, **38**, 985; (d) G. Cravotto, F. Demartin, G. Palmisano, A. Penoni, T. Radice, S. Tollari, *J. Organomet. Chem.* 2005, **690**, 2017; (e) B. Neumann, C. Krinninger, I. P. Lorenz, *Eur. J. Inorg. Chem.* 2007, 472; (f) T. M. McCormick, **2008**. *Luminescent transition metal complexes of 2-(2'-pyridyl)benzimidazolyl and 2-(2'-pyridyl)indolyl based ligands and their applications* Ph.D. Thesis, Queen's University; (g) R. P. Thummel, Y. J. Jahng, *Org. Chem.* 1987, **52**, 73.
12. (a) J. Ashenhurst, L. Brancalion, S. Gao, W. Liu, H. Schmider, S. Wang, G. Wu, Q. G. Wu, *Organometallics* 1998, **17**, 5334; (b) J. Pang, E. J. P. Marcotte, C. Seward, S. Brown, S. Wang, *Angew. Chem. Int. Ed.* 2001, **40**, 4042; (c) C. Seward, W. L. Jia, R. Y. Wang, S. Wang, *Inorg. Chem.* 2004, **43**, 978.
13. Z. Hudson, S. Wang, *Acc. Chem. Res.* 2009, **42**, 1584 and the references cited therein.
14. (a) H. Y. Zhang, C. Huo, K. Q. Ye, P. Zhang, W. J. Tian, Y. Wang, *Inorg. Chem.* 2006, **45**, 2788. (b) Z. L. Zhang, H. Bi, Y. Zhang, D. D. Yao, H. Z. Gao, Y. Fan, H. Y. Zhang, Y. Wang, Y. P. Wang, Z. Y. Chen, D. G. Ma, *Inorg. Chem.* 2009, **48**, 7230; (c) H. Y. Zhang, C. Huo, J. Y. Zhang, P. Zhang, W. J. Tian, Y. Wang, *Chem. Commun.* 2006, 281; (d) Y. Qin, I. Kiburu, S. Shah, F. Jäkle, *Macromolecules* 2006, **39**, 9041; (e) Q. Wu, M. Esteghamatian, N. X. Hu, Z. Popovic, G. Enright, S. Wang, Y. Tao, M. D' Iorio, *Chem. Mater.* 2000, **12**, 79; (f) Y. Cui, Q. D. Liu, D. R. Bai, W. L. Jia, Y. Tao, S. Wang, *Inorg. Chem.* 2005, **44**, 601; (g) H. Y. Chen, Y. Chi, C. S. Liu, J. K. Yu, Y. M. Cheng, K. S. Chen, P. T. Chou, S. M. Peng, G. H. Lee, A. J. Carty, S. J. Yeh, C. T. Chen, *Adv. Funct. Mater.* 2005, **15**, 567.
15. Y. L. Rao, H. Amarne, S. B. Zhao, T. M. McCormick, S. Martić, Y. Sun, R. Y. Wang, S. Wang, *J. Am. Chem. Soc.* 2008, **130**, 12898.

16. J.-P. Collin, I. M. Dixon, J.-P. Sauvage, J. A. G. Williams, F. Barigelletti, L. Flamigni, *J. Am. Chem. Soc.* 1999, **121**, 5009.
17. A. Dodabalapur, *Solid State Commun.* 1997, **102**, 259.
18. C. W. Tang, S. A. Van Slyke, *Appl. Phys. Lett.* 1987, **51**, 913.
19. (a) R. Friend, J. Burroughes, D. Bradley, WO Patent 1990, 90/13148; (b) S. Kappaun, C. Slugovc, E. J. W. List, *Int. J. Mol. Sci.* 2008, **9**, 1527; (c) O. Nuyken, S. Jungermann, V. Wiederhirn, E. Bacher, K. Meerholz, *Monatsh. Chem.* 2006, **137**, 811; (d) M. Ikai, S. Tokito, Y. Sakamoto, T. Suzuki, Y. Taga, *Appl. Phys. Lett.* 2001, **79**, 156.
20. (a) C. Adachi, M. A. Baldo, M. E. Thompson, S. R. Forrest, *J. Appl. Phys.* 2001, **90**, 5048; (b) S. A. VanSlyke, C. H. Chen, C. W. Tang, *Appl. Phys. Lett.* 1996, **69**, 2160.
21. R. C. Kwong, M. R. Nugent, L. Michalski, T. Ngo, K. Rajan, Y.-J. Tung, M. S. Weaver, T. X. Zhou, M. Hack, M. E. Thompson, S. R. Forrest, J. J. Brown, *Appl. Phys. Lett.* 2002, **81**, 162.
22. F. Li, M. Zhang, G. Cheng, J. Feng, Y. Zhao, Y. G. Ma, S. Y. Liu, J. C. Shen, *Appl. Phys. Lett.* 2004, **84**, 148.
23. M. A. Baldo, M. E. Thompson, S. R. Forrest, *Pure Appl. Chem.* 1999, **71**, 2095.
24. Y. Shirota, H. Kageyama, *Chem. Rev.* 2007, **107**, 953 and references therein.
25. (a) S. Z. Shan, Q. Zhao, N. Goswami, D. M. Eichhorn, D. P. Pillema, *Coord. Chem. Rev.* 2001, **211**, 117; (b) S. F. McClanahan, P. F. Dallinger, F. J. Holler, *J. Am. Chem. Soc.* 1985, **107**, 4853.
26. (a) B. O'Regan, M. Grätzel, *Nature* 1991, **335**, 737; (b) A. Hagfeldt, M. Grätzel, *Chem. Rev.*, 1992, **95**, 49; (c) M. Grätzel, *Inorg. Chem.* 2005, **44**, 6841; (d) G. Meyer, *Inorg. Chem.* 2005, **44**, 6852; (e) M. K. Nazeeruddin, P. Pechy, T. Renouard, S. M. Zakeeruddin, R. Humphry-Baker, P. Comte, P. Liska, L. Cevey, E. Costa, V. Shklover, L. Spiccia, G. B. Deacon, C. A. Bignozzi, M. Grätzel, *J. Am. Chem. Soc.* 2001, **123**, 1613.
27. www.energy.com, "know how dye sensitized solar cell", 2009.

28. A. Hagfeldt, G. Boschloo, L. C. Sun, L. Kloo, H. Pettersson, *Chem. Rev.* 2010, **110**, 6595.
29. (a) O. Enea, J. Moser, M. Grätzel, *J. Electroanal. Chem.* 1989, **259**, 59; (b) J. M. Rehm, G. L. McLendon, Y. Nagasawa, K. Yoshihara, J. Moser, M. Grätzel, *J. Phys. Chem.* 1996, **100**, 9577.
30. S. Alex, U. Santhosh, S. Das, *J. Photochem. Photobiol. A* 2005, **172**, 63.
31. T. Horiuchi, H. Miura, K. Sumioka, S. Uchida, *J. Am. Chem. Soc.* 2004, **126**, 12218.
32. Y.-S. Chen, C. Li, Z.-H. Zeng, W.-B. Wang, X.-S. Wang, B.-W. Zhang, *J. Mater. Chem.* 2005, **15**, 1654.
33. K. Kalyanasundaram, M. Grätzel *Coord. Chem. Rev.* 1998, **177**, 347.
34. D. Kuciauskas, M. S. Freund, H. B. Gray, J. R. Winkler, N. S. Lewis *J. Phys. Chem. B* 2001, **105**, 392.
35. (a) N. Sekar, V. Y. Gehlot *Resonance* 2010, 819; (b) M. Grätzel, *Acc. Chem. Res.* 2009, **42**, 1788.
36. N. Robertson, *Angew. Chem. Int. Ed.* 2006, **45**, 2338.
37. M. Grätzel, K. Kalyanasundaram, *Curr. Sci.* 1994, **66**, 706.
38. R. C. Evans, P. Douglas, C. J. Winscom, *Coord. Chem. Rev.* 2006, **250**, 2093.
39. M. I. Bruce, *Angew. Chem. Int. Ed.* 1977, **16**, 73.
40. L. Chassot, E. Müller, A. von Zelewsky, *Inorg. Chem.* 1984, **23**, 4249.
41. M. Cocchi, D. Virgili, C. Sabatini, V. Fattori, P. D. Marco, M. Maestri, J. Kalinowski, *Synthetic Metals* 2004, **147**, 253.
42. Z. M. Hudson, C. Sun, M. G. Helander, H. Amarné, Z.-H. Lu, S. Wang, *Adv. Funct. Mater.* 2010, **20**, 3426.
43. (a) Y. You, S. Y. Park, *Dalton Trans.* 2009, 1267; (b) Y. Chi, P. T. Chou, *Chem. Soc. Rev.* 2010, **39**, 638 and reference therein.
44. W. Lu, B.-X. Mi, M. C. W. Chan, Z. Hui, C.-M. Che, N. Zhu, S.-T. Lee, *J. Am. Chem. Soc.* 2004, **126**, 4958.

45. J. A. G. Williams, A. Beeby, S. Davies, J. A. Weinstein, C. Wilson, *Inorg. Chem.* 2003, **42**, 8609.
46. F. C. DeSchryver, P. Collart, J. Vandendriessche, R. Goedeweck, A. Swinnen, M. Van der Auweraer, *Acc. Chem. Res.* 1987, **20**, 159.
47. J. Kavitha, S. Y. Chang, Y. Chi, J. K. Yu, Y. H. Hu, P. T. Chou, S. M. Peng, G. H. Lee, Y. T. Tao, C. H. Chien, A. J. Carty, *Adv. Funct. Mater.* 2005, **15**, 223.
48. J. Brooks, Y. Babayan, S. Lamansky, P. Djurovich, I. Tsyba, R. Bau, M. E. Thompson, *Inorg. Chem.* 2002, **41**, 3055.
49. (a) C. Bronner, A. S. Baudron, M. W. Hosseini, C. A. Strassert, A. Guene, L. D. Cola, *Dalton Trans.* 2010, **39**, 180; (b) D. V. Aleksanyan, V. A. Kozlov, Y. V. Nelyubina, K. A. Lyssenko, L. N. Puntus, E. I. Gutsul, N. E. Shepel, A. A. Vasil'ev, P. V. Petrovskii, I. L. Odinets, *Dalton Trans.* 2011, **40**, 1535.
50. (a) N. Miyaura, *Adv. Met.-Org. Chem.* 1998, **6**, 187 and references therein; (b) A. J. Suzuki, *Organomet. Chem.* 1999, **576**, 147 and references therein; (c) G. P. McGlacken, I. J. S. Fairlamb, *Eur. J. Org. Chem.* 2009, 4011 and references therein; (d) J. Hartwig, *Organotransition Metal Chemistry : From Bonding to Catalysis*; University Science Books: Sausalito, CA, 2010.
51. (a) I. V. Seregin, V. Gevorgyan, *Chem. Soc. Rev.* 2007, **36**, 1173; (b) E. M. Beck, M. J. Gaunt, *Top. Curr. Chem.* 2009, **292**, 85.
52. D. C. Power, E. L. Lee, A. Afriafard, M. S. Sanford, B. F. Yates, A. J. Canty, T. Ritter, *J. Am. Chem. Soc.* 2012, **134**, 12002.
53. (a) D. Kalyani, N. R. Deprez, L. V. Desai, M. S. Sanford, *J. Am. Chem. Soc.* 2005, **127**, 7330; (b) K. L. Hull, E. L. Lanni, M. S. Sanford, *J. Am. Chem. Soc.* 2006, **128**, 14047; (c) S. R. Neufeldt, M. S. Sanford, *Acc. Chem. Res.* 2012, **45**, 936.
54. (a) R. Giri, X. Chen, J. -Q. Yu, *Angew. Chem., Int. Ed.* 2005, **44**, 2112; (b) R. Giri, J. Liang, J.-G. Lei, J.-J. Li, D.-H. Wang, X. Chen, I. C. Naggarr, C. Guo, B. M. Foxman, J.-Q. Yu, *Angew. Chem., Int. Ed.* 2005, **44**, 7420.
55. (a) V. G. Zaitsev, O. Daugulis, *J. Am. Chem. Soc.* 2005, **127**, 4156; (b) D. Shabashov, O. Daugulis, *Org. Lett.* 2005, **7**, 3657. (c) O. Daugulis, V. G. Zaitsev,

- Angew. Chem., Int. Ed.* 2005, **44**, 4046; (d) V. G. Zaitsev, D. Shabashov, O. Daugulis, *J. Am. Chem. Soc.* 2005, **127**, 13154; (e) O. Daugulis, V. G. Zaitsev, D. Shabashov, Q.-N. Pham, A. Lazareva, *Synlett.* 2006, 3382.
56. (a) A. J. Hickman, M. S. Sanford, *ACS Catal.* 2011, **1**, 170; (b) M. H. Emmert, J. B. Gary, J. M. Villalobos, M. S. Sanford, *Angew. Chem. Int. Ed.* 2010, **49**, 5884; (c) M. H. Emmert, A. K. Cook, Y. J. Xie, M. S. Sanford, *Angew. Chem. Int. Ed.* 2011, **50**, 9409.
57. S. Chardon-Noblat, A. Deronzier, F. Hartl, J. van Slageren, T. Mahabiersing, *Eur. J. Inorg. Chem.* 2001, 613.
58. (a) K. K.-W. Lo, W.-K. Hui, C.-K. Chung, K. H.-K. Tsang, D. C.-M. Ng, N. Zhu, K.-K. Cheung, *Coord. Chem. Rev.* 2005, **249**, 1434; (b) M.-J. Li, X. Liu, M.-J. Nie, Z.-Z. Wu, C.-Q. Yi, G.-N. Chen, V. W.-W. Yam, *Organometallics* 2012, **31**, 4459; (c) D. I. Yoon, C. A. Berg-Brennan, H. Lu, J. T. Hupp, *Inorg. Chem.* 1992, **31**, 3192.
59. T. G. Kotch, A. J. Lees, S. J. Fuerniss, K. Papatomas, I. R. W. Snyder, *Inorg. Chem.* 1993, **32**, 2570.
60. V. W.-W. Yam, V. C. Y. Lau, K. K. Cheung, *J. Chem. Soc. Chem. Commun.* 1995, 259.
61. (a) J. V. Casper, T. J. Meyer, *J. Phys. Chem.* 1983, **87**, 952; (b) L. A. Worl, R. Duesing, P. Chen, L. D. Ciana, T. J. Meyer, *J. Chem. Soc., Dalton Trans.* 1991, 849.
62. A. Coleman, C. Brennan, J. G. Vos, M. T. Pryce, *Coord. Chem. Rev.* 2008, **252**, 2585.
63. (a) K. Kalyanasundaram *Photochemistry of polypyridine and porphyrin complexes*, Chap 10. Academic, New York, **1992**, p 321; (b) S. Ranjan, S.-Y. Lin, K.-C. Hwang, Y. Chi, W.-L. Ching, C.-S. Liu, Y.-T. Tao, C.-H. Chien, S.-M. Peng, G.-H. Lee, *Inorg. Chem.* 2003, **42**, 1248.
64. L. Sacksteder, M. Lee, J. N. Demas, B. A. DeGraff, *J. Am. Chem. Soc.* 1993, **115**, 8230.

65. (a) H. Hori, F. P. A. Johnson, K. Koike, O. Ishitani, T. Ibusuki, *J. Photochem. Photobiol. A: Chem.* 1996, **96**, 171; (b) P. Kurz, B. Probst, B. Spingler, R. Alberto, *Eur. J. Inorg. Chem.* 2006, 2966; (c) H. Takeda, O. Ishitani, *Coord. Chem. Rev.* 2010, **254**, 346; (d) Y. Tamaki, K. Watanabe, K. Koike, H. Inoue, T. Morimoto, O. Ishitani, *Faraday Discuss.* 2012, **155**, 115.
66. (a) J. Hawecker, J. M. Lehn, R. Ziessel, *J. Chem. Soc., Chem. Commun.* 1984, 328; (b) B. P. Sullivan, C. M. Bolinger, D. Conrad, W. J. Vining, T. J. Meyer, *J. Chem. Soc., Chem. Commun.* 1985, 1414; (c) J. M. Smieja, C. P. Kubiak, *Inorg. Chem.* 2010, **49**, 9283; (e) J. Hawecker, J.-M. Lehn, R. Ziessel, *Helv. Chim. Acta* 1986, **69**, 1990.
67. (a) B. Gholamkhash, H. Mametsuka, K. Koike, T. Tanabe, M. Furue, O. Ishitani, *Inorg. Chem.* 2005, **44**, 2326; (b) K. Koike, S. Naito, S. Sato, Y. Tamaki, O. Ishitani, *J. Photochem. Photobiol. A: Chem.* 2009, **207**, 109.
68. B. Kumar, J. M. Smieja, A. F. Sasayama, C. P. Kubiak, *Chem. Commun.* 2012, **48**, 272.
69. H. Takeda, K. Koike, H. Inoue, O. Ishitani, *J. Am. Chem. Soc.* 2008, **130**, 2023.
70. (a) Y. Hayashi, S. Kita, B. S. Brunshwig, E. Fujita, *J. Am. Chem. Soc.* 2003, **125**, 11976; (b) K. Shinozaki, Y. Hayashi, B. S. Brunshwig, E. Fujita, *Res. Chem. Intermed.* 2007, **33**, 27.
71. (a) M. A. Baldo, S. Lamansky, P. Burrows, M. E. Thompson, S. R. Forrest, *Appl. Phys. Lett.* 1999, **75**, 5; (b) R. C. Kwong, S. Sibley, T. Dubovoy, M. Baldo, S. R. Forrest, M. E. Thompson, *Chem. Mater.* 1999, **11**, 3709; (c) C. Adaci, M. A. Baldo, S. R. Forrest, M. E. Thompson, *Appl. Phys. Lett.* 2000, **77**, 904; (d) S. Lamansky, P. Djurovich, D. Murphy, F. Abdel-Razzaq, H. E. Lee, C. Adachi, P. E. Burrows, S. R. Forrest, M. E. Thompson, *J. Am. Chem. Soc.* 2001, **123**, 4304; (e) Q. D. Liu, L. Thorne, I. Kozin, D. Song, C. Seward, M. D'Iorio, Y. Tao, S. Wang, *J. Chem. Soc., Dalton Trans.* 2002, 3234; (f) W. Lu, B. X. Mi, M. C. W. Chan, Z. Hui, N. Zhu, S. T. Lee, C. M. Che, *Chem. Commun.* 2002, 206.

72. K. Kalyanasundaram, M. Gräzel, M. K. Nazeeruddin, *Inorg. Chem.* 1992, **31**, 5243.
73. (a) C. H. Brauenstein, A. D. Baker, T. D. Streckas, H. D. Gafney, *J. Am. Chem. Soc.* 1984, **23**, 857; (b) Y. Fuchs, S. Lofters, T. Dieter, W. Shi, R. Morgan, T. C. Streckas, H. D. Gafney, *J. Am. Chem. Soc.* 1987, **109**, 269; (c) M. Furue, M. Naiki, Y. Kanematsu, T. Kushida, M. Kamachi, *Coord. Chem. Rev.* 1991, **111**, 221.
74. P. Du, J. Schneider, F. Li, W. Zhao, U. Patel, F. N. Castellano, R. Eisenberg, *J. Am. Chem. Soc.* 2008, **130**, 5056.
75. R. Brimblecombe, G. F. Swiegers, G. C. Dismukes, L. Spiccia, *Angew. Chem., Int. Ed.* 2008, **47**, 7335.
76. (a) H. Ozawa, M. Haga, K. Sakai, *J. Am. Chem. Soc.* 2006, **128**, 4926; (b) M. Schwalbe, M. Karnahl, H. Górls, D. Chartrand, F. Laverdiere, G. S. Hanan, S. Tschierlei, B. Dietzek, M. Schmitt, J. Popp, J. G. Vos, S. Rau, *J. Chem. Soc., Dalton Trans.* 2009, 4012.
77. (a) S. Rau, B. Schafer, D. Gleich, E. Anders, M. Rudolph, M. Friedrich, H. Górls, W. Herny, J. G. Vos, *Angew. Chem., Int. Ed.* 2006, **45**, 6215; (b) M. Elvington, J. Brown, S. M. Arachchige, K. J. Brewer, *J. Am. Chem. Soc.* 2007, **129**, 10644; (c) A. Fihri, V. Artero, M. Razavet, C. Baffert, W. Leibl, M. Fontecave, *Angew. Chem., Int. Ed.* 2008, **47**, 564; (d) A. Fihri, V. Artero, A. Pereirab, M. Fontecave, *Dalton Trans.* 2008, 5567.
78. C. D. Entwistle, T. B. Marder, *Angew. Chem. Int. Ed.* 2002, **41**, 2927.
79. Q. D. Liu, M. S. Mudadu, R. Thummel, Y. Tao, S. Wang, *Adv. Funct. Mater.* 2005, **15**, 143.
80. A. Wakamiya, T. Taniguchi, S. Yamaguchi, *Angew. Chem., Int. Ed.* 2006, **45**, 3170.
81. (a) N. Kano, J. Yoshino, T. Kawashima, *Org. Lett.* 2005, **7**, 3909; (b) J. Yoshino, N. Kano, T. Kawashima, *Tetrahedron* 2008, **64**, 7774.

82. (a) H. Bouas-Laurent, H. Durr, *Pure Appl. Chem.* 2001, **73**, 639; (b) N. Tamai, H. Miyasaka, *Chem. Rev.* 2000, **100**, 1875; (c) Y. L. Rao, H. Amarne, S. Wang, *Coord. Chem. Rev.* 2012, **256**, 759.
83. H. Amarne, C. Baik, S. K. Murphy, S. Wang, *Chem. Eur. J.* 2010, **16**, 4750.
84. Y. L. Rao, S. Wang, *Organometallics* 2011, **30**, 4453.

Chapter 2

Synthesis of 2-(2'-Pyridyl)indole and 2-(2'-Pyridyl)benzimidazole Based Ligands

2.1 Introduction

As discussed in Chapter 1, 2-(2'-pyridyl)benzimidazole (**py-im**) ligand can strongly bind with transition metal ions. These ligands are especially well-suited for binding with d^8 or d^6 metal,¹ which can either enhance ligand-centered phosphorescent emissions or promoted MLCT emissions. Due to its rigid geometry, **py-im** is a promising moiety for fabricating luminescent metal complexes. Previously our group has reported a series of polydentate ligands that have multiple **py-im** binding sites and can chelate readily to metal ions, producing luminescent dinuclear and trinuclear Ru(II), Pt(II) and Cu(I) compounds.² In contrast to the N^N-chelate **py-im** chromophore, the 2-(2'-pyridyl)indolyl (**py-in**) chromophore may bind to metal ions either as a terminal ligand or an N^C-chelate ligand *via* cyclometalation.³ Because of the different binding modes and different reactivity of **py-im** and **py-in** toward metal ions, ligand systems that contain both **py-im** and **py-in** binding sites would allow the attachment of two different metal centers, thus achieving heterobimetallic compounds. Based on this consideration, a new ligand L1 was designed and synthesized where a **py-in** and a **py-im** unit are linked together by a phenyl group, as shown in Figure 2-1.

During the synthesis of ligand L1, a new class of ligands L2 and L3 were isolated as byproducts, as shown in Figure 2-1. These two ligands can be considered as the corresponding 3,3'-C-C coupled products whose mechanism of formation has been

reported previously.⁴ This chapter will examine the syntheses and characterization of these ligands.

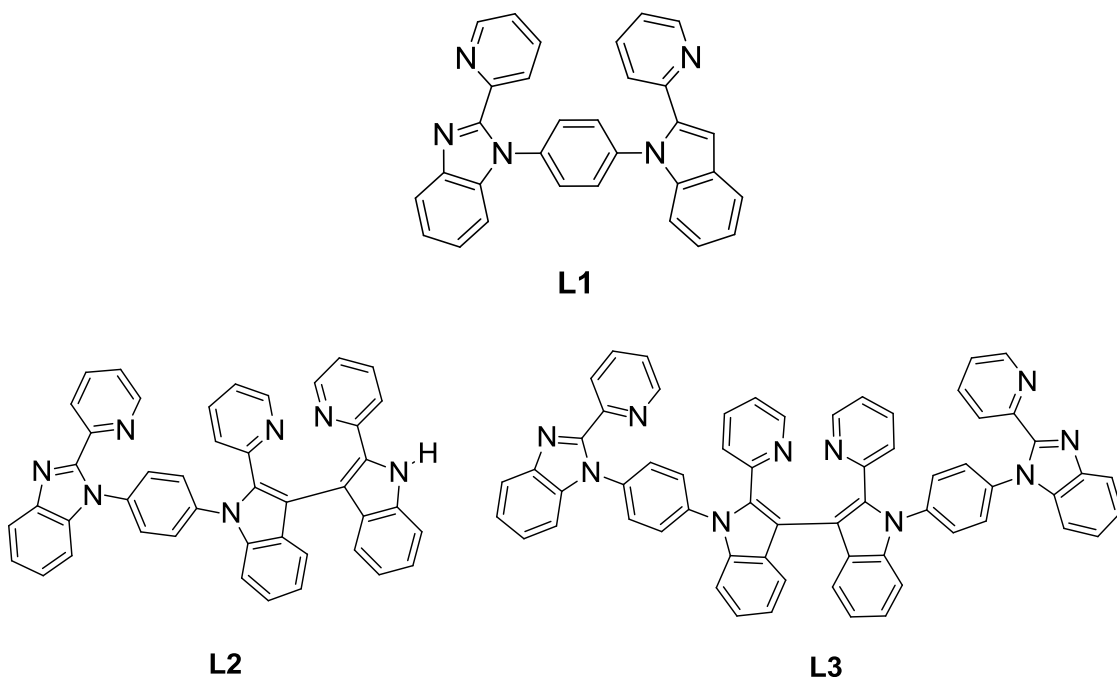


Figure 2-1.Chemical structures of L1, L2 and L3.

2.2 Experimental

2.2.1 General Considerations

All reactions were performed under dry N_2 with standard Schlenk techniques unless otherwise noted. All starting materials were purchased from Aldrich Chemical Co. and used without further purification. Solvents were freshly distilled over appropriate drying reagents under N_2 atmosphere. NMR spectra were recorded on a Bruker Avance 400 or 500 MHz spectrometer as stated. Excitation and emission spectra were recorded on a Photon Technologies International QuantaMaster Model C-60 spectrometer. UV-Vis spectra were recorded on a Varian Cary 50Bio UV-Vis spectrophotometer. The syntheses

of 2-(2'-pyridyl)indole⁴ and 1-bromo-4-[2-(2'-pyridyl)-benzimidazolyl]benzene (Brmb)^{2a} were achieved by methods described in the literature.

2.2.2 Synthesis of Ligand L1

A mixture of Brmb (0.374 g, 1.07 mmol), 2-(2'-pyridyl)indole (0.207 g, 1.07 mmol), CuSO₄•5H₂O (0.027 g, 0.107 mmol), Cs₂CO₃ (0.707 g, 2.17 mmol) was suspended in 2.5 mL of dodecane. The mixture was refluxed for 12 h and then cooled to room temperature. The resulting residue was extracted with CH₂Cl₂ (50 mL × 4), and the organic extracts were combined, dried over MgSO₄, and purified by column chromatography (1:1 THF/hexane) to obtain the product as white powder. Recrystallization of the crude product in CH₂Cl₂-hexane afforded L1 as white crystals (yield 30%, m. p. 218.0 °C-219.0 °C). ¹H NMR (400 MHz, CD₂Cl₂, 298.0 K, δ, ppm): 8.57 (d, J = 4.6 Hz, 1H), 8.42 (d, J = 4.6 Hz, 1H), 8.30 (d, J = 7.9 Hz, 1H), 7.90 (d, J = 5.8 Hz, 1H), 7.86 (td, J = 7.7, 1.8 Hz, 1H), 7.79 (d, J = 7.7 Hz, 1H), 7.68 (td, J = 7.7, 1.8 Hz, 1H), 7.46-7.30 (m, 11H), 7.29-7.20 (m, 3H); ¹³C{¹H} NMR (100 MHz, CD₂Cl₂, δ, ppm): 151.5, 150.9, 149.8, 149.6, 148.8, 143.2, 139.9, 139.1, 138.1, 137.1, 136.9, 136.2, 128.8, 128.5, 128.4, 124.9, 124.2, 124.1, 123.6, 123.6, 123.4, 122.1, 121.5, 121.3, 120.3, 111.1, 110.9, 106.2. HRMS calcd for C₃₁H₂₁N₅[M]⁺: m/z 463.1797, found: 463.1792.

2.2.3 Synthesis of Ligand L2

This compound was isolated as a byproduct from the reaction mixture for L1 in 10% yield after recrystallization from CH₂Cl₂ and hexanes. (m. p. 187.1 °C-188.6 °C) ¹H NMR (500 MHz, CD₂Cl₂, 298.0 K, δ, ppm): 9.88 (s, 1H), 8.54 (d, J = 5.1 Hz, 1H), 8.39 (d, J = 4.9 Hz, 1H), 8.32 (d, J = 4.9 Hz, 1H), 8.24 (d, J = 7.5 Hz, 1H), 7.87 (d, J = 7.5 Hz, 1H), 7.82 (t, J = 6.4 Hz, 1H), 7.58 (d, J = 8.4 Hz, 1H), 7.48 (t, J = 8.4 Hz, 4H), 7.42-7.20 (m,

13H), 7.13 (t, J = 7.5 Hz, 1H), 7.06 (t, J = 6.4 Hz, 1H), 6.98-6.92 (m, 2H). HRMS calcd for $C_{44}H_{29}N_7[M]^+$: m/z 655.2484, found: 655.2471. The ^{13}C NMR spectrum could not be obtained due to poor solubility.

2.2.4 Synthesis of Ligand L3

This compound was isolated as a byproduct from the reaction mixture for L1 in 7% yield after recrystallization from CH_2Cl_2 and hexanes. It decomposes at $T > 300$ °C. 1H NMR (500 MHz, CD_2Cl_2 , 298.0 K, δ , ppm): 8.35 (d, J = 4.2 Hz, 2H), 8.24-8.21 (m, 4H), 7.86 (d, J = 7.8 Hz, 2H), 7.81 (t, J = 7.8 Hz, 2H), 7.59 (d, J = 7.8, Hz, 2H), 7.53 (d, J = 8.2 Hz, 2H), 7.38-7.26 (m, 20H), 7.19 (t, J = 7.8 Hz, 2H), 7.10 (d, J = 7.2 Hz, 2H), 6.97-6.95 (m, 2H). HRMS calcd for $C_{62}H_{40}N_{10}[M]^+$: m/z 924.3437, found: 924.3463. The ^{13}C NMR spectrum could not be obtained due to poor solubility.

2.2.5 X-ray Diffraction Analyses

Single crystals of L1 and L3 were mounted on glass fibers and were collected on a Bruker Apex II single-crystal X-ray diffractometer with graphite-monochromated $M_o K_\alpha$ radiation, operating at 50 kV and 30 mA and at 180 K. Data were processed on a PC with the aid of the Bruker SHELXTL software package (version 5.10)⁵ and corrected for absorption effects. All non-hydrogen atoms were refined anisotropically. The crystal data of L1 has been deposited at Cambridge Crystallographic Data Center (CCDC No. 860141). The crystal data of L1 and L3 are reported in Table 2-1. Their selected bond lengths and angles are given in Table 2-2.

Table 2-1 Crystallographic data for compounds L1 and L3.

	L1	L3
Empirical formula	C31 H21 N5	C62 H40 N10
Formula weight	463.53	925.04
Space group	P2 ₁ 2 ₁ 2 ₁	P4 ₂
a, Å	7.578(4)	18.178(1)
b, Å	10.822(5)	18.178(1)
c, Å	28.380(14)	18.065(1)
α, deg	90	90
β, deg	90	90
γ, deg	90	90
V, Å ³	2327(2)	5969(9)
Z	4	4
Density (calculated), gcm ⁻³	1.323	1.029
μ, mm ⁻¹	0.080	0.06
2θ _{max} , deg	49.98	51.98
Reflns meads	20451	59315
Reflns used	4078	11753
(R _{int})	(0.1040)	(0.2171)
Final R[I > 2σ(I)]		
R1 ^a	0.0858	0.0998
wR2 ^b	0.2113	0.2048
R(all data)		
R1 ^a	0.0991	0.2493
wR2 ^b	0.220	0.2617
GOF on F ²	1.147	0.860

^a R1 = Σ[|F_o| - |F_c|]/Σ|F_o|. ^b wR2 = {Σ[w(F_o² - F_c²)]/ Σ(wF_o²)}^{1/2}. ω = 1/[σ²(F_o²) + (0.075P)²], where P = [max.(F_o²,0) + 2F_c²]/3.

Table 2-2 Selected bond lengths (Å) and angles (°) of compound L1 and L3.

L1			
N(1)-C(1)	1.380(6)	C(1)-N(1)-C(8)	107.3(4)
N(1)-C(8)	1.394(6)	C(1)-N(1)-C(14)	125.6(4)
N(1)-C(14)	1.409(6)	C(8)-N(1)-C(14)	127.2(4)
N(2)-C(9)	1.330(6)	C(9)-N(2)-C(13)	117.6(4)
N(2)-C(13)	1.348(6)	C(20)-N(3)-C(26)	105.3(4)
N(3)-C(20)	1.393(6)	C(20)-N(3)-C(17)	123.7(4)
N(3)-C(26)	1.393(6)	C(26)-N(4)-C(25)	105.4(4)
N(3)-C(17)	1.414(6)	C(27)-N(5)-C(31)	116.9(4)
N(4)-C(26)	1.293(6)	N(1)-C(1)-C(6)	108.7(4)
N(5)-C(27)	1.327(6)	N(1)-C(1)-C(2)	130.1(4)
N(5)-C(31)	1.336(6)	N(4)-C(26)-N(3)	113.4(4)
C(1)-C(6)	1.400(7)	N(4)-C(26)-C(27)	121.5(4)
C(1)-C(2)	1.408(7)	N(5)-C(27)-C(28)	123.3(5)
L3			
N(1)-C(1)	1.325(9)	N(1)-C(1)-C(2)	130.8(8)
N(1)-C(7)	1.355(11)	N(1)-C(1)-C(6)	106.3(7)
N(1)-C(13)	1.380(9)	N(2)-C(6)-C(5)	134.6(9)
N(2)-C(6)	1.314(11)	N(2)-C(6)-C(1)	109.1(8)
N(2)-C(7)	1.380(10)	N(3)-C(8)-C(9)	123.3(9)
N(3)-C(8)	1.240(9)	N(4)-C(19)-C(24)	108.0(7)
N(3)-C(12)	1.431(10)	N(4)-C(19)-C(20)	125.3(9)
N(4)-C(19)	1.299(9)	N(4)-C(26)-C(27)	120.7(6)
N(4)-C(26)	1.440(9)	N(5)-C(27)-C(26)	107.2(7)
N(4)-C(16)	1.572(10)	N(6)-C(38)-C(33)	109.0(7)
N(6)-C(38)	1.340(10)	C(32)-C(39)-N(6)	129.3(6)
N(6)-C(39)	1.378(8)		
N(6)-C(45)	1.436(9)		
N(8)-C(51)	1.299(10)		

2.3 Results and Discussion

2.3.1 Synthesis and Structures

Ligand L1 was obtained through a two-step Ullmann condensation reaction using 1,4-dibromobenzene, 2-(2'-pyridyl)benzimidazole and 2-(2'-pyridyl)indole as the starting materials, as shown in Figure 2-2. In the first step, one of the bromine atoms in 1,4-dibromobenzene is replaced by a **py-im** group to produce the monosubstituted compound. In the second step, the remaining bromine atom is replaced by a **py-in** group. L1 is fully characterized by NMR and HRMS analyses.

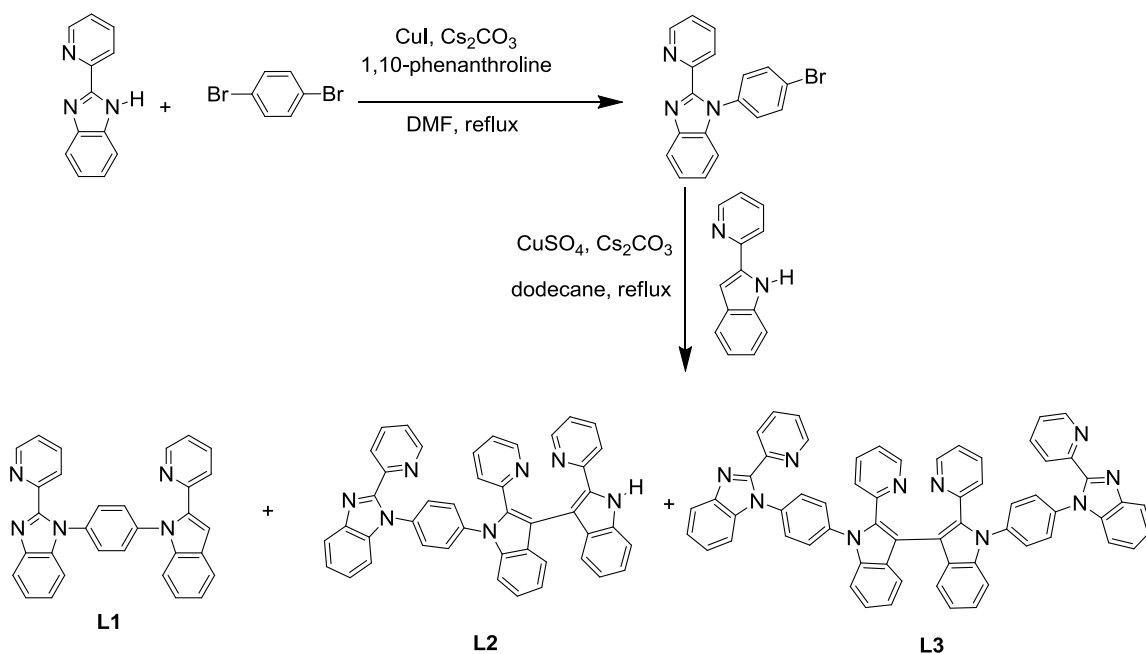


Figure 2-2. Reaction scheme for the synthesis of ligands L1-L3.

Ligand L2 and L3 were isolated as byproducts from the reaction with the intended target being L1 as shown in Figure 2-2. In this copper catalyzed Ullmann condensation reaction, both C-N and C-C bonds were formed at the same time which was already observed previously by our group.⁴ The isolated yields of L2 and L3 are normal (10% and 7%, respectively) for these larger oligomers due to their poor solubility and possible

decomposition under the harsh reaction condition employed. ($T = \sim 210\text{ }^{\circ}\text{C}$). Two possible reaction pathways have been proposed to explain the formation of L2 and L3, which are shown in Figure 2-3. One is direct C-C coupling at the three position of indolyl first, following with the C-N bond formation. The other is the formation of L1 as precursor first, which then undergoes direct C-C coupling at the three position of indolyl. Mechanism of this unusual copper catalyzed C-C coupling reaction has been explored by our group which can be found in literature ^{4,6} and thus will not be presented in this chapter. Even though the exact mechanism is still unclear, considering the relatively easy C-N bond formation compared to C-C coupling on sp^2 carbons under this copper catalyzed reaction condition and the higher yield of ligand L1, we believe that the second pathway is more possible and reasonable. Both L2 and L3 were characterized by ^1H NMR and HRMS analyses.

The crystal structures of L1 and L3 were determined by X-ray diffraction and shown in Figure 2-4 and Figure 2-5. For L1, the crystal structure confirms the non-coplanarity of the two chelate units with the central benzene ring.

It was found that L3 crystallized in the tetragonal space group $P4_2$. The dihedral angle between the indolyl rings is 122.1° . The crystal structure also confirms significant π - π interactions between the central pyridyl ring and central indolyl ring with the atomic separation distances being $3.50\text{ \AA} - 4.50\text{ \AA}$. Additionally, each **py-im** group of L3 nearly anti-parallel with another **py-im** group of an adjacent molecule, hence forming a π - π stacking structure (shown in Figure 2-5 bottom). The distance between the stacked planes is about 3.54 \AA . Previously our group reported bis[3,3'-(1,4-bis[2-(2'-pyridyl)indolyl]benzene)] (**bbib**) (as shown in Figure 2-6).⁶ The only difference between this compound

and ligand L3 is that the ending group in **bbib** is **py-in**, while in ligand L3 is **py-im**. Interestingly, unlike L3 where the central **py-in** groups are in the opposite direction, in **bbib** the central **py-in** units are in the same direction.

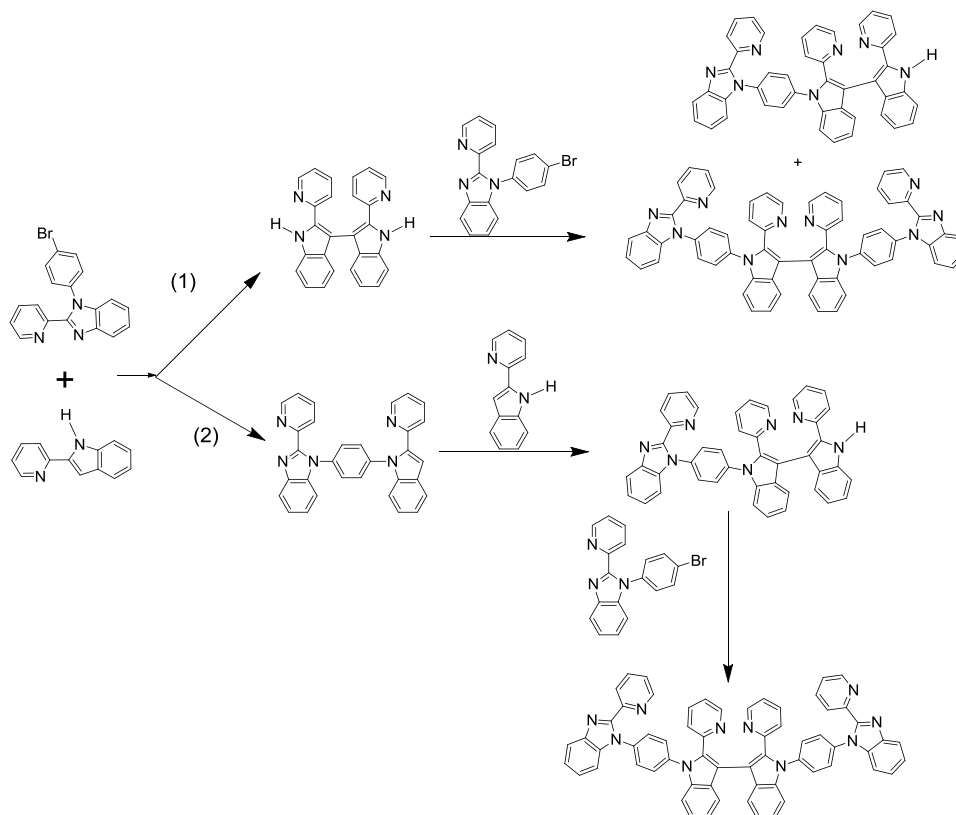


Figure 2-3. Possible reaction pathways for syntheses of L2 and L3.

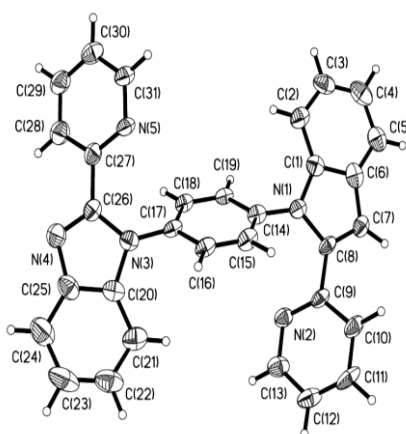


Figure 2-4. The crystal structure of L1 with 35% thermal ellipsoids and labeling schemes.

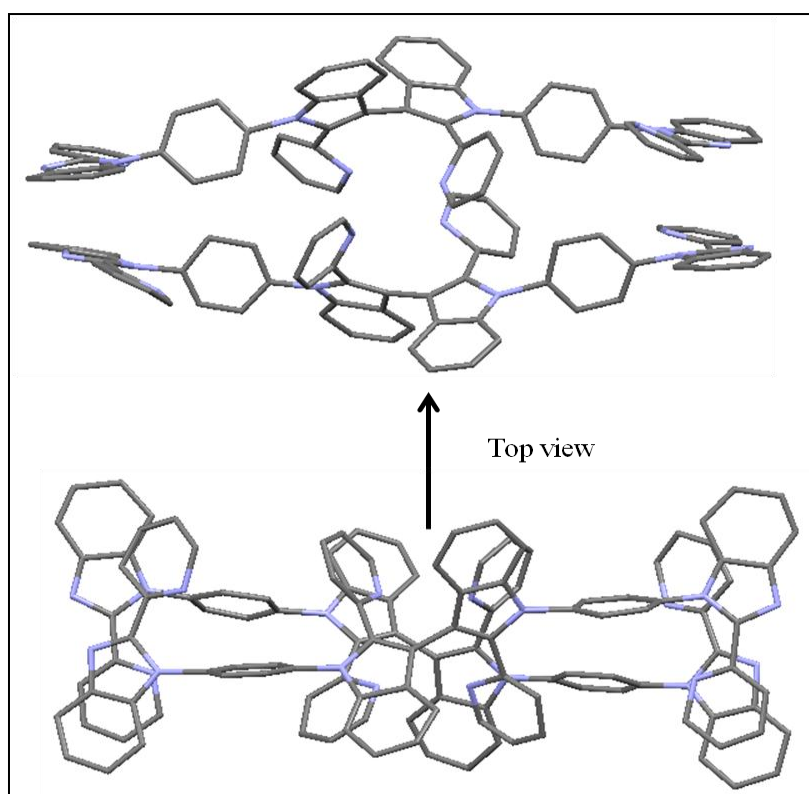
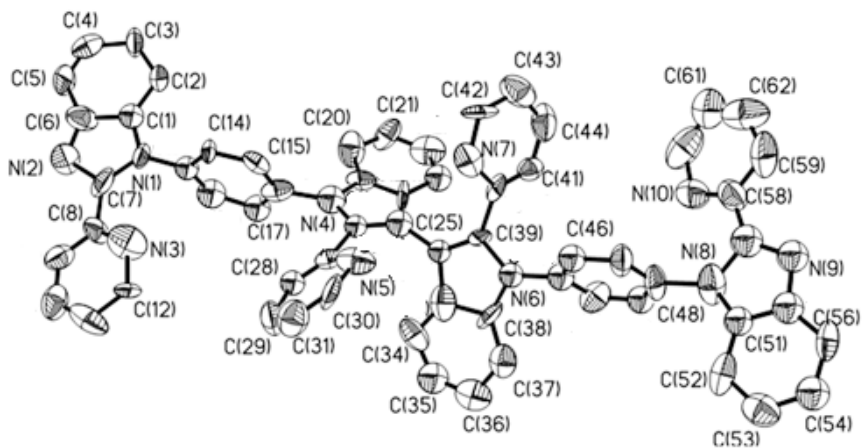


Figure 2-5. Top: the crystal structure of L3. Bottom: Parallel structure formed by intermolecular π - π stacking in L3.

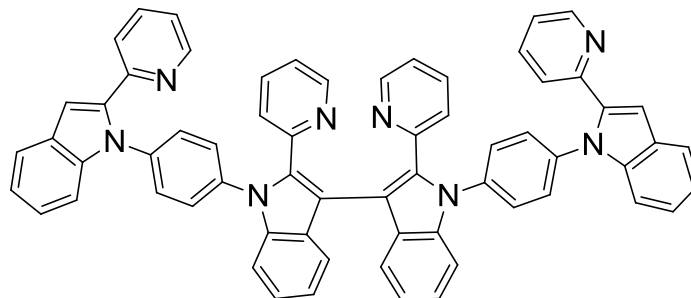


Figure 2-6. Structure of bis[3,3'-(1,4-bis[2-(2'-pyridyl)indolyl] benzene)] (**bbib**).

2.3.2 UV-Vis Absorption Spectra

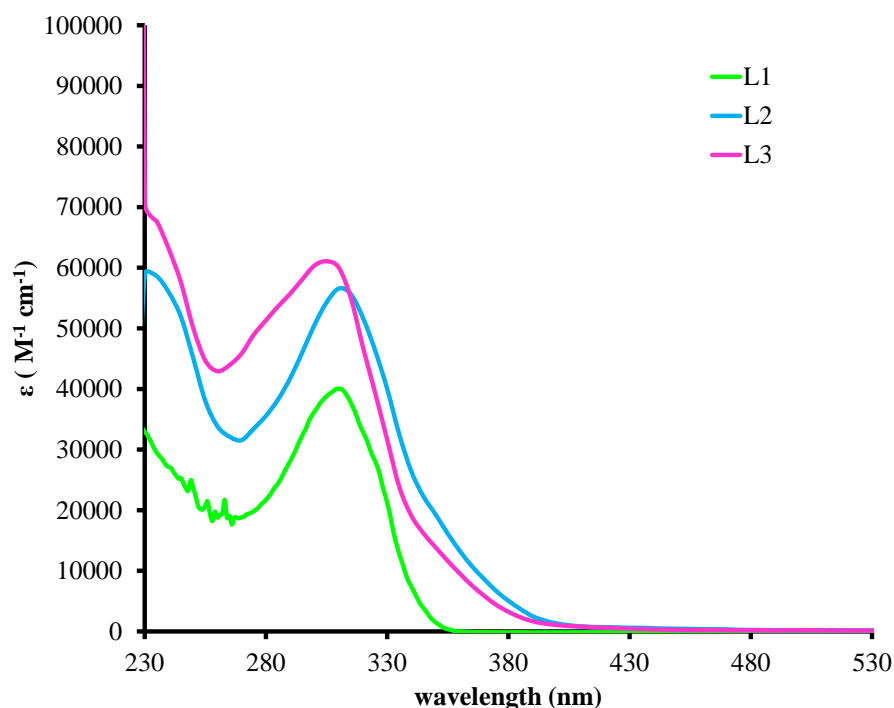


Figure 2-7. UV-Vis spectra of $\sim 1 \times 10^{-5}$ M solutions of ligands recorded in CH_2Cl_2 at ambient temperature.

All photophysical property measurements were done in CH_2Cl_2 at room temperature. Absorption spectra are shown in Figure 2-7 and the data are summarized in Table 2-3. The UV-Vis absorption spectra of ligands are all similar in shape, with the molar absorptivity increasing with the number of **py-im** or **py-in** unit. The absorption bands shown at around ~ 310 nm are attributed to the $\pi \rightarrow \pi^*$ transition of **py-im** or **py-in** units.

Compared to L1, both L2 and L3 have a shoulder band at ~370 nm in the UV-Vis spectra, which most likely originates from π - π interactions of the two central pyridyl and indolyl rings, as revealed by the crystal structure of L3. A similar phenomenon was also observed in the **bbib** molecule in which π - π interactions between the two central indolyl units also produce a distinct shoulder absorption band.⁶

Table 2-3. Absorption and luminescence data.

Compound	Absorption, λ_{\max}/nm ($\epsilon/\text{M}^{-1}\text{cm}^{-1}$)	Emission, λ_{\max}/nm (Φ_{phos}^a)
L1	312 (39700)	384 (0.05)
L2	310 (56600)	440 (0.26)
L3	305 (61100)	448 (0.21)

Conditions: All the spectra of $\sim 1 \times 10^{-5}$ M solutions of free ligands were recorded in degassed CH_2Cl_2 at ambient temperature. ^a Determined using 9,10-diphenylanthracene as the standard.⁷

2.3.3 Luminescence Spectra

All ligands are emissive in solution at ambient temperature. As shown in Figure 2-8, L1 emits in the UV region with $\lambda_{\max} = 384$ nm. In contrast, both L2 and L3 emit in the UV region with $\lambda_{\max} = 440$ nm and 448 nm, respectively. This dramatic spectral red shift between L1 and L2/L3 can be attributed to the intramolecular excimer formation between the central pyridyl ring and indolyl ring in L2 and L3. The similar phenomenon involving two **py-in** groups in **bbib**⁶ or two pyrene rings in a sterically constrained environment⁸ is also observed. It is believed that the restricted rotation around the 3,3'-C-C bond in L2 and L3 assist the excimer formation.

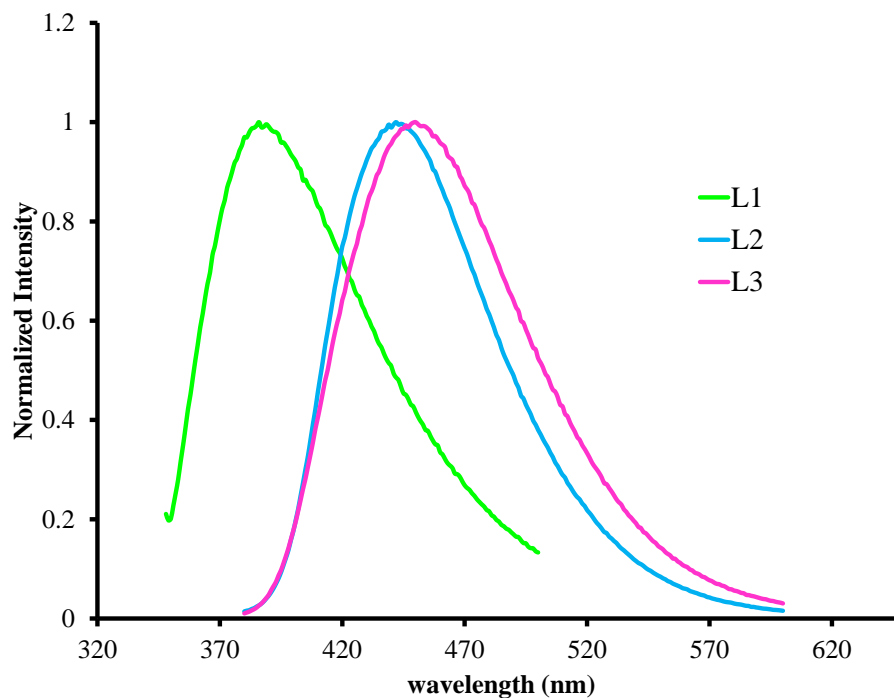


Figure 2-8. Emission spectra of $\sim 1 \times 10^{-5}$ M solutions of ligands recorded in CH_2Cl_2 at ambient temperature.

2.4 Conclusion

New ligands L1, L2 and L3 based on **py-in** and **py-im** units have been synthesized and isolated in a one pot reaction catalyzed by copper ions. The intramolecular excimer emission has been observed for L2 and L3 due to the restricted rotation around the 3,3'-C-C bond. Because of the different binding modes and reactivity, all of these ligands will show different affinity toward metal ions, which may find applications in synthesis of heterometallic complexes and supramolecular architectures.

2.5 References

1. (a) M. A. Baldo, S. Lamansky, P. Burrows, M. E. Thompson, S. R. Forrest, *Appl. Phys. Lett.* 1999, **75**, 5; (b) R. C. Kwong, S. Sibley, T. Dubovoy, M. Baldo, S. R. Forrest, M. E. Thompson, *Chem. Mater.* 1999, **11**, 3709; (c) C. Adaci, M. A. Baldo, S. R. Forrest, M. E. Thompson, *Appl. Phys. Lett.* 2000, **77**, 904; (d) S. Lamansky, P. Djurovich, D. Murphy, F. Abdel-Razzaq, H. E. Lee, C. Adachi, P. E. Burrows, S. R. Forrest, M. E. Thompson, *J. Am. Chem. Soc.* 2001, **123**, 4304; (e) Q. D. Liu, L. Thorne, I. Kozin, D. Song, C. Seward, M. D'Iorio, Y. Tao, S. Wang, *J. Chem. Soc., Dalton Trans.* 2002, 3234; (f) W. Lu, B. X. Mi, M. C. W. Chan, Z. Hui, N. Zhu, S. T. Lee, C. M. Che, *Chem. Commun.* 2002, 206.
2. (a) Q. D. Liu, W. L. Jia, S. Wang, *Inorg. Chem.* 2005, **44**, 1332; (b) W. L. Jia, T. M. McCormick, Y. Tao, J. P. Lu, S. Wang, *Inorg. Chem.* 2005, **44**, 5706.
3. (a) S. Tollari, S. Cenini, A. Penoni, G. Granata, G. Palmisano, F. Demartin, *J. Organomet. Chem.* 2000, **608**, 34; (b) G. Cravotto, F. Demartin, G. Palmisano, A. Penoni, T. Radice, S. Tollari, *J. Organomet. Chem.* 2005, **690**, 2017.
4. T. M. McCormick, Q. Liu, S. Wang, *Org. Lett.* 2007, **9**, 4087.
5. SHELXTL Version 6.14, Bruker AXS, 2000-2003.
6. T. M. McCormick, **2008**. *Luminescent transition metal complexes of 2-(2'-pyridyl)benzimidazolyl and 2-(2'-pyridyl)indolyl based ligands and their applications* Ph.D. Thesis, Queen's University.
7. N. J. Demas, G. A. Crosby, *J. Am. Chem. Soc.* 1970, **92**, 7262.
8. (a) A. C. Benniston, A. Harriman, S. L. Howell, C. A. Sams, Y. G. Zhi, *Chem. Eur. J.* 2007, **13**, 4665; (b) C. Lodeiro, J. C. Lima, A. J. Parola, J. S. Seixas de Melo, J. L. Capelo, B. Covelo, A. Tamayo, B. Pedra, *Sensors and Actuators B* 2006, **115**, 276.

Chapter 3

Heterobimetallic Ru(II) Complexes Based on 2-(2'-Pyridyl)benzimidazolyl and 2-(2'-Pyridyl)indolyl Derivative Ligand

3.1 Introduction

Luminescent transition metal complexes have attracted much research attention due to their broad applications, such as triplet emitters for organic light emitting diodes (OLEDs),¹ light harvesting materials,² and fluorescent sensors.³ Ru(II) polypyridyl and derivative compounds are a class of extensively investigated molecules because of their unique redox properties, interesting excited state/photo-catalytic reactivity, and luminescence.⁴ It has been shown by several research teams that the introduction of a 2nd metal center to a Ru(II) bipy chromophore can significantly alter or enhance the photophysical and photochemical properties of the compounds.⁵ To promote electronic communications between two metal centers, the use of an appropriate bridging ligand is necessary and is in fact a commonly used strategy in homo- or heterobimetallic compounds involving Ru(II).⁶ Many heterobimetallic systems that contain a Ru(bipy)₂ unit such as Ru-Pd and Ru-Pt compounds have been shown to be much better catalysts than the individual mononuclear components for photo-catalytic reduction of water.⁷ A number of Ru(bipy)₂-containing heterobimetallic compounds have also been shown to be effective sensors for a number of analytes.⁸

In chapter 2, we have reported the synthesis of ligand L1 which containing a 2-(2'-pyridyl)benzimidazolyl (**py-im**) and a 2-(2'-pyridyl)indolyl (**py-in**) moiety that are linked together by a phenyl group. As discussed in Chapter 1 and 2, **py-im** chromophore usually

prefers N^N chelate binding mode, while **py-in** chromophore may bind to metal ions either as terminal ligand or an N^C-chelate ligand *via* cyclometalation.⁹ Due to the different binding modes and different reactivity of **py-im** and **py-in** toward metal ions, ligand L1 would allow the attachment of two different metal centers, thus achieving heterobimetallic compounds. We have found that L1 is a very effective ligand for achieving bimetallic **Ru-Pt (3.3)** and **Ru-Pd (3.4)** compounds. The synthetic details and photophysical properties of new metal compounds based on L1 are presented in this chapter.

3.2 Experimental

3.2.1 General Considerations

All reactions were performed under dry N₂ with standard Schlenk techniques unless otherwise noted. All starting materials were purchased from Aldrich Chemical Co. and used without further purification. Solvents were freshly distilled over appropriate drying reagents under N₂ atmosphere. NMR spectra were recorded on a Bruker Avance 400 or 500 MHz spectrometer as stated. Excitation and emission spectra were recorded on a Photon Technologies International QuantaMaster Model C-60 spectrometer. UV-Vis spectra were recorded on a Varian Cary 50Bio UV-Vis spectrophotometer. Phosphorescent lifetimes were measured on a Photon Technologies International (PTI) phosphorimeter (Time-Master C-631F) that was equipped with a xenon flash lamp and a digital emission photon multiplier tube, using a band pathway of 5 nm for excitation and 2 nm for emission. Fluorescent lifetime was measured on a PTI spectrofluorometer with LED excitation. Cyclic voltammetry (CV) was performed using a BAS CV-50W analyzer, with a scan rate of 100 mV/s to 350 mV/s and a typical concentration of 5 mg of the

compound in 2 mL of DMF, at room temperature using 0.10 M NBu_4PF_6 as the supporting electrolyte. The ferrocenium/ferrocene couple was used as the internal standard ($E_0 = 0.54$ V). The electrolytic cell used was a conventional three-compartment cell, in which a Pt working electrode, a Pt auxiliary electrode, and an Ag/AgCl reference electrode were employed. Elemental analyses were performed at Elemental Analysis Service, Department of chemistry, University of Montreal (Montreal, Quebec, Canada). The syntheses of ligand *N*-phenyl-2-(2'-pyridyl)indole (**pib**),¹⁰ *cis*-dichlorobis(4,4'-di-*tert*-butyl-2,2'-bipyridyl)ruthenium(II) ($\text{Ru}(\text{tbbipy})_2\text{Cl}_2$),¹¹ and *cis*- $[\text{PtPh}_2(\text{DMSO})_2]$ ¹² were achieved by methods described in the literature.

3.2.2 Synthesis of $[\text{Ru}(t\text{-Bu}_2\text{-bipy})_2(\text{L1})][\text{PF}_6]_2$ (**3.1**).

A mixture of $\text{Ru}(\text{tbbipy})_2\text{Cl}_2$ (0.142 g, 0.20 mmol), L1 (0.093 g, 0.20 mmol) and ethylene glycol (4 mL) was heated to reflux for 4 h then cooled to room temperature. Water (20 mL) was added to the mixture. An aqueous solution (5 mL) of NH_4PF_6 (0.500 g) was added to precipitate the complex, which was subsequently filtered off, and rinsed with water (2×10 mL) and cold THF (2×10 mL). Recrystallization from CH_2Cl_2 -hexane afforded **3.1** as a red solid in 78% yield. ^1H NMR (400 MHz, CD_2Cl_2 , 298.0 K, δ , ppm): 8.48 (d, $J = 4.2$ Hz, 1H), 8.35-8.33 (m, 3H), 8.26 (d, $J = 1.9$ Hz, 1H), 7.86-7.70 (m, 11H), 7.65 (d, $J = 6.1$ Hz, 1H), 7.62-7.55 (m, 3H), 7.53-7.47 (m, 6H), 7.38-7.34 (m, 2H), 7.30-7.24 (m, 2H), 7.20 (s, 1H), 7.17 (t, $J = 7.6$ Hz, 1H), 5.89 (d, $J = 8.3$ Hz, 1H), 1.52 (s, 9H), 1.47 (s, 9H), 1.45 (s, 9H), 1.44 (s, 9H). Anal calcd for $\text{C}_{67}\text{H}_{69}\text{F}_{12}\text{N}_9\text{P}_2\text{Ru}$: C, 57.84; H, 5.00; N, 9.06. Found: C, 58.22; H, 4.99; N, 8.69. The ^{13}C NMR spectrum could not be obtained due to poor solubility.

3.2.3 Synthesis of [Ru(bipy)₂(L1)][PF₆]₂ (3.2)

Mononuclear complex [Ru(bipy)₂(L1)][PF₆]₂ (**3.2**) was obtained using the same method as that applied for **3.1**. Yield 72%. ¹H NMR (400 MHz, CD₂Cl₂, 298.0 K, δ, ppm): 8.52-8.48 (m, 4H), 8.43 (d, J = 8.2 Hz, 1H), 8.19 (td, J = 8.2 Hz, 1.5 Hz, 1H), 8.14-8.05 (m, 3H), 8.00 (d, J = 6.5 Hz, 1H), 7.96 (d, J = 6.5 Hz, 1H), 7.88-7.70 (m, 10H), 7.61-7.46 (m, 9H), 7.39-7.33 (m, 2H), 7.31-7.20 (m, 4H), 5.96 (d, J = 8.5 Hz, 1H). Anal calcd for C₅₁H₃₇F₁₂N₉P₂Ru: C, 52.49; H, 3.20; N, 10.80. Found: C, 52.20; H, 3.11; N, 10.47. The ¹³C NMR spectrum could not be obtained due to poor solubility.

3.2.4 Synthesis of [Ru(t-Bu₂-bipy)₂(L1)Pt(DMSO)(Ph)][PF₆]₂ (3.3)

A mixture of **3.1** (0.060 g, 0.04 mmol) and *cis*-[PtPh₂(DMSO)₂] (0.033 g, 0.06 mmol) was dissolved in 30 mL THF. The mixture was stirred at 50 °C for 6 h, and the solvent was removed under reduced pressure. Recrystallization from CH₂Cl₂-hexane afforded **3.3** as an orange-red solid in 56% yield. ¹H NMR (400 MHz, acetone-d₆, 298.0 K, δ, ppm): 9.69 (d, J = 5.1 Hz, 1H), 8.95 (d, J = 1.9 Hz, 1H), 8.91 (d, J = 2.0 Hz, 1H), 8.90 (d, J = 2.0 Hz, 1H), 8.86 (d, J = 1.9 Hz, 1H), 8.20 (d, J = 6.0 Hz, 1H), 8.15-8.12 (m, 2H), 8.08-8.02 (m, 3H), 7.94-7.92 (m, 2H), 7.88 (d, J = 6.0 Hz, 1H), 7.83-7.71 (br, 2H), 7.68-7.51 (m, 10H), 7.22-7.18 (m, 2H), 7.11-7.07 (m, 4H), 7.0 (t, J = 7.2 Hz, 1H), 6.91-6.85 (br, 1H), 6.59 (t, J = 7.9 Hz, 1H), 5.94 (d, J = 8.3 Hz, 1H), 5.90 (d, J = 8.0 Hz, 1H), 2.96 (s, 6H), 1.48 (s, 9H), 1.40 (s, 9H), 1.39 (s, 9H), 1.38 (s, 9H). Anal calcd for C₇₅H₇₉F₁₂N₉OP₂RuPtS: C, 51.75; H, 4.57; N, 7.24. Found: C, 52.28; H, 4.90; N, 6.69. The ¹³C NMR spectrum could not be obtained due to poor solubility.

3.2.5 Synthesis of [Ru(t-Bu₂-bipy)₂(L1)Pd(acac)][PF₆]₂ (3.4)

A mixture of **3.1** (0.060 g, 0.04 mmol) and Pd(acac)₂ (0.032 g, 0.08 mmol) was suspended in 30 mL methanol. The mixture was refluxed for 2 days, and the solvent was removed under reduced pressure. The residue was washed by diethyl ether (3 × 10 mL). Recrystallization from CH₂Cl₂-diethyl ether afforded **3.4** as a red solid in 38% yield. ¹H NMR (400 MHz, CD₂Cl₂, 298.0 K, δ, ppm): 8.85 (d, J = 4.9 Hz, 1H), 8.35-8.27 (m, 5H), 7.96 (d, J = 7.9 Hz, 1H), 7.91-7.78 (m, 8H), 7.72-7.43 (m, 10H), 7.32-7.31 (m, 2H), 7.22-7.18 (m, 2H), 7.07 (t, J = 6.0 Hz, 1H), 6.82 (br, 1H), 5.91 (d, J = 8.3 Hz, 1H), 5.56 (s, 1H), 2.23 (s, 3H), 2.15 (s, 3H), 1.53 (s, 9H), 1.48 (s, 9H), 1.47 (s, 9H), 1.45 (s, 9H). Anal calcd for C₇₂H₇₅F₁₂N₉P₂O₂RuPd: C, 54.19; H, 4.74; N, 7.90. Found: C, 53.35; H, 4.69; N, 7.49. The ¹³C NMR spectrum could not be obtained due to poor solubility.

3.2.6 Synthesis of Pt(pib)(DMSO)(Ph) (3.5)

Mononuclear complex **3.5** was obtained using the same method as that applied for **3.3** using pib and PtPh₂(DMSO)₂ as the starting materials. Recrystallization of the crude product in CH₂Cl₂-hexane afforded **3.5** as yellow crystals (yield 62%). ¹H NMR (400 MHz, CD₂Cl₂, 298.0 K, δ, ppm): 9.61 (d, J = 5.5 Hz, 1H), 7.65-7.55 (m, 5H), 7.48 (td, J = 8.2 Hz, J = 1.6 Hz, 1H), 7.42-7.40 (m, 2H), 7.15-7.10 (m, 3H), 7.07-7.04 (m, 1H), 6.99-6.96 (m, 1H), 6.87 (d, J = 8.2 Hz, 1H), 6.59 (td, J = 7.1 Hz, J = 1 Hz, 1H), 6.50 (d, J = 8.2 Hz, 1H), 5.77 (d, J = 8.2 Hz, 1H), 2.95 (s, 6H). Anal calcd for C₂₇H₂₄N₂O₂PS: C, 52.34; H, 3.90; N, 4.52. Found: C, 52.25; H, 3.94; N, 5.37. The ¹³C NMR spectrum could not be obtained due to poor solubility.

3.2.7 Synthesis of Pd(pib)(acac) (3.6)

Mononuclear complex **3.6** was obtained using the same method as that applied for **3.4** using pib and Pd(acac)₂ as the starting materials. Recrystallization of the crude product in CH₂Cl₂-hexane afforded **3.6** as orange crystals (yield 40%). ¹H NMR (400 MHz, CDCl₃, 298.0 K, δ, ppm): 8.72 (d, J = 4.8 Hz, 1H), 8.29 (d, J = 7.9 Hz, 1H), 7.55-7.53 (m, 2H), 7.50 (d, J = 7.3 Hz, 1H), 7.40-7.37 (m, 3H), 7.17-7.14 (m, 1H), 7.10-7.07 (m, 1H), 6.99 (d, J = 8.2 Hz, 1H), 6.86 (dd, J = 6.1 Hz, J = 6.0 Hz, 1H); 6.37 (d, J = 8.2 Hz, 1H), 5.45 (s, 1H), 2.18 (s, 3H), 2.08 (s, 3H); ¹³C{¹H} NMR (100 MHz, CDCl₃, δ, ppm): 187.6, 186.3, 157.7, 148.7, 140.9, 139.2, 138.4, 138.2, 132.5, 129.6, 129.5, 128.2, 128.1, 124.1, 123.4, 120.2, 118.7, 117.4, 109.9, 100.4, 28.0, 26.7; Anal calcd for C₂₄H₂₀N₂O₂Pd: C, 60.71; H, 4.25; N, 5.90. Found: C, 60.66; H, 4.21; N, 5.80.

3.2.8 X-Ray Diffraction Analysis

Single crystals of complex **3.6** was mounted on glass fibers and was collected on a Bruker Apex II single-crystal X-ray diffractometer with graphite-monochromated Mo K_α radiation, operating at 50 kV and 30 mA and at 180 K. Data were processed on a PC with the aid of the Bruker SHELXTL software package (version 5.10)¹³ and corrected for absorption effects. All non-hydrogen atoms were refined anisotropically. The crystal data of **3.6** have been deposited at Cambridge Crystallographic Data Center (CCDC No. 860142) and reported in Table 3-1. The selected bond lengths and angles are given in Table 3-2.

Table 3-1. Crystallographic data for complex **3.6**.

3.6	
Empirical formula	C ₂₄ H ₂₀ N ₂ O ₂ Pd
Formula weight	474.82
Space group	P2(1)2(1)2(1)
a, Å	12.1096(18)
b, Å	12.2832(18)
c, Å	13.777(2)
α, deg	90
β, deg	90
γ, deg	90
V, Å ³	2049.2(5)
Z	4
Density (calculated), gcm ⁻³	1.539
μ, mm ⁻¹	0.928
2θ _{max} , deg	52.00
Reflns meads	10916
Reflns used	4022
(R _{int})	(0.0534)
Final R[I > 2σ(I)]	
R1 ^a	0.0497
wR2 ^b	0.1159
R(all data)	
R1 ^a	0.0720
wR2 ^b	0.1316
GOF on F ²	1.074

^a $R1 = \Sigma[|F_o| - |F_c|]/\Sigma|F_o|$. ^b $wR2 = \{\Sigma[w(F_o^2 - F_c^2)]/\Sigma(wF_o^2)\}^{1/2}$. $\omega = 1/[\sigma^2(F_o^2) + (0.075P)^2]$, where $P = [\max.(F_o^2, 0) + 2F_c^2]/3$.

Table 3-2. Selected bond lengths (Å) and angles (°) of complex **3.6**.

3.6			
Pd(1)-C(2)	1.968(7)	C(2)-Pd(1)-O(2)	93.2(2)
Pd(1)-O(2)	1.997(5)	C(2)-Pd(1)-N(2)	80.8(3)
Pd(1)-N(2)	2.045(6)	O(2)-Pd(1)-N(2)	173.7(2)
Pd(1)-O(1)	2.066(5)	C(2)-Pd(1)-O(1)	173.3(2)
O(1)-C(21)	1.292(8)	N(2)-Pd(1)-O(1)	92.8(2)
N(1)-C(8)	1.388(9)	C(8)-N(1)-C(1)	107.4(5)
N(1)-C(1)	1.394(8)	C(8)-N(1)-C(14)	124.0(5)
N(1)-C(14)	1.440(8)	C(13)-N(2)-Pd(1)	123.9(5)
N(2)-C(13)	1.331(9)	C(9)-N(2)-Pd(1)	116.3(5)
N(2)-C(9)	1.372(9)	C(3)-C(2)-Pd(1)	139.8(5)
C(1)-C(2)	1.371(9)	N(1)-C(8)-C(7)	130.1(6)
C(1)-C(9)	1.453(10)	N(2)-C(9)-C(1)	109.7(6)
C(2)-C(3)	1.418(10)		
C(3)-C(4)	1.412(10)		

3.3 Results and Discussion

3.3.1 Syntheses and Structures

The mononuclear Ru(II) complex [Ru(bipy)₂(L1)][PF₆]₂ (**3.2**) was synthesized according to Figure 3-1, using modified procedures reported previously for polynuclear Ru(II) compounds that contain Ru(bipy)₂(**py-im**) units.¹⁴ However, due to its poor solubility, this molecule cannot be used for the formation of bimetallic compounds. Thus, bis-*t*-butyl-bipy ligand is then used to replace the simple bipy ligand to synthesize the **3.1**. Using a similar procedure as shown in Figure 3-1, **3.1** was obtained in high yield as a red solid with adequate solubility for further modification.

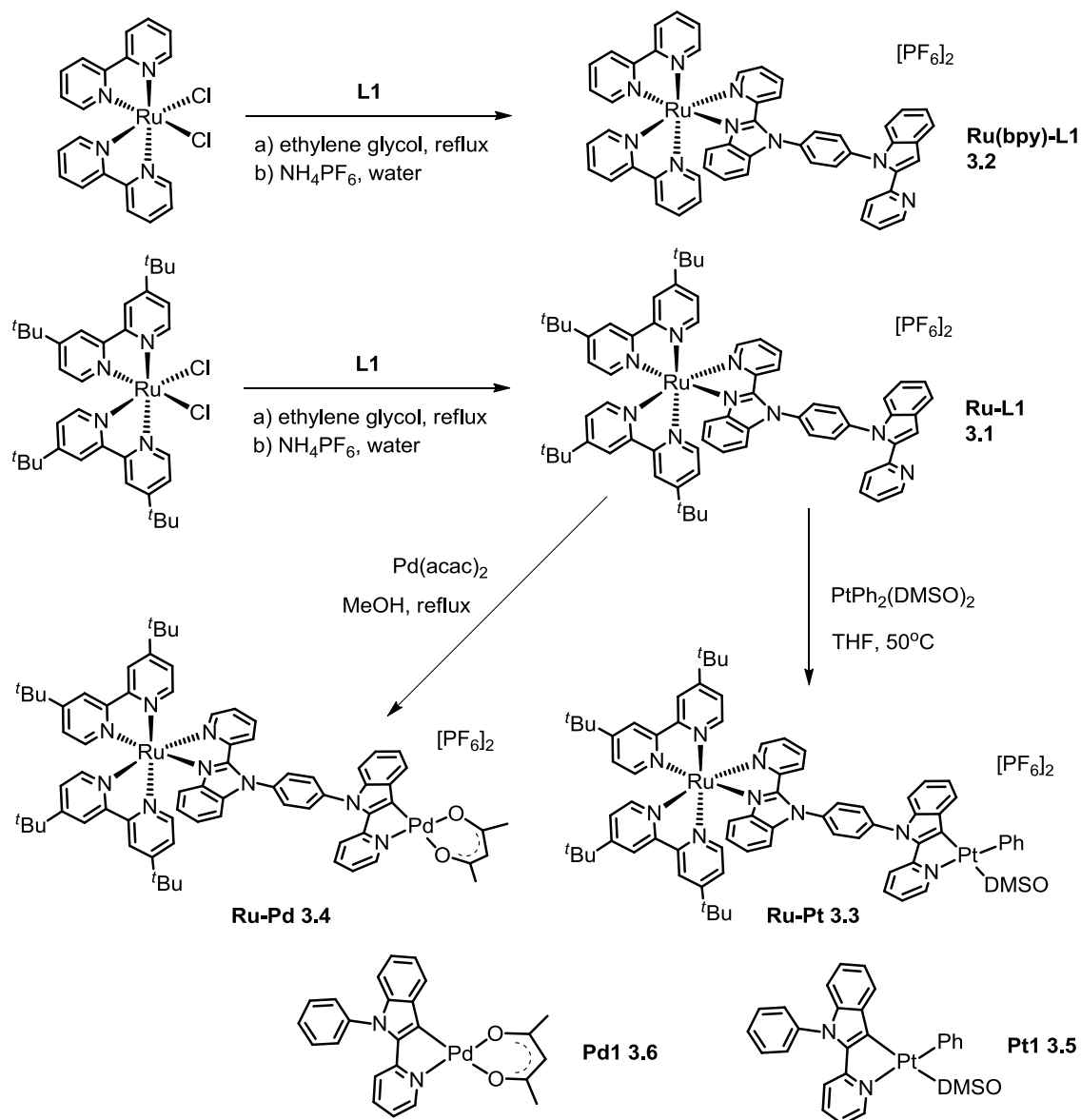


Figure 3-1. Reaction scheme for the syntheses of metal complexes.

To synthesize the bimetallic complexes, Pd(acac)₂ and Pt(DMSO)₂Ph₂ were used as the second metal sources, respectively. The bimetallic compound **3.4** was obtained by refluxing **3.1** with Pd(acac)₂ in methanol for 2 days, while **3.3** was prepared by the reaction of **3.1** with PtPh₂(DMSO)₂ in THF at 50°C for 6 hours (Figure 3-1). As control compounds for understanding the photophysical properties of the bimetallic compounds,

the N[^]C-chelate mononuclear compounds **3.6** and **3.5** were also synthesized by the reaction of **pib** with Pd(acac)₂ and Pt(DMSO)₂Ph₂, respectively. All new metal complexes were characterized by ¹H NMR and elemental analyses. Attempts to obtain single crystals suitable for X-ray diffraction analyses of the bimetallic compounds were unsuccessful. The crystal structure of **3.6** was determined by X-ray diffraction and shown in Figure 3-2. For **3.6**, it has a typical square planar geometry around the Pd(II) center. The most important feature shown by the crystal structure is that the *N*-phenyl ring is nearly perpendicular to the indolyl to minimize steric interactions between the *ortho*-hydrogen atoms.

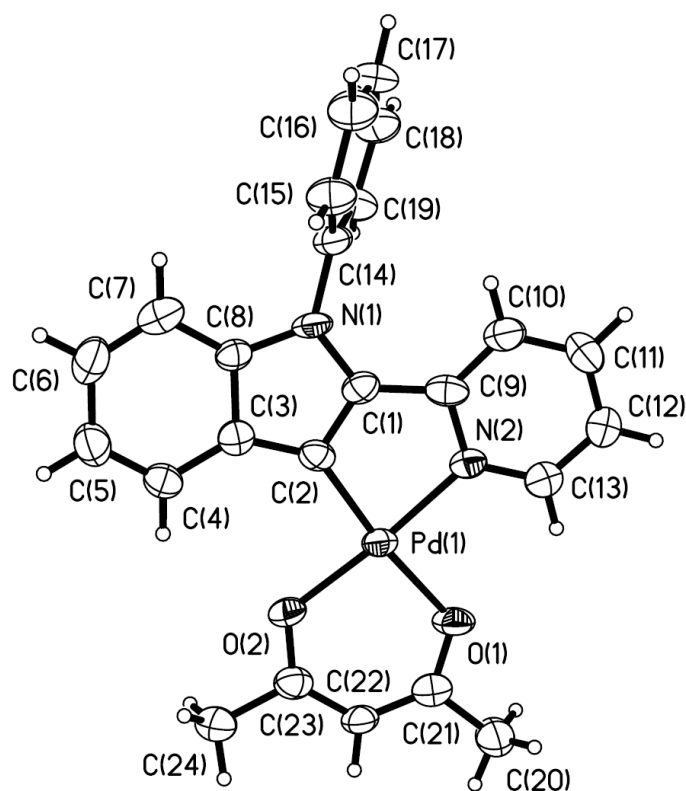


Figure 3-2. The crystal structures of **3.6** with 35% thermal ellipsoids

3.3.2 Variable Temperature NMR

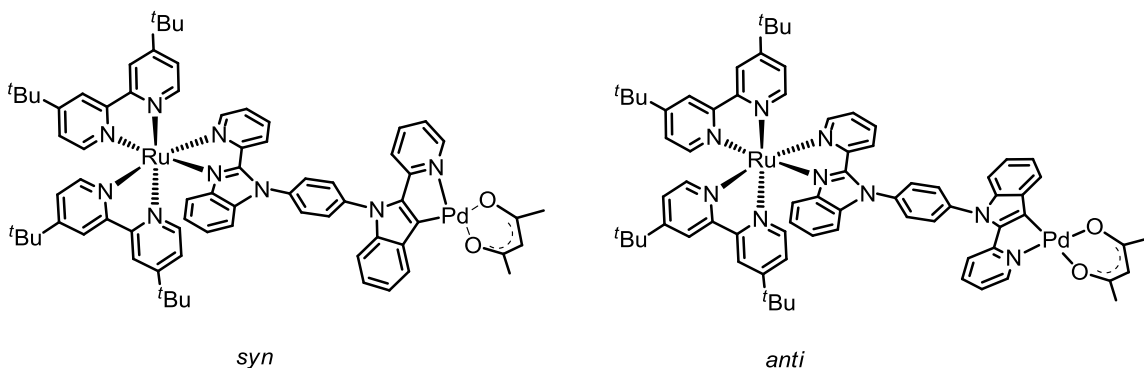


Figure 3-3. The isomers of **3.4**.

Variable-temperature ^1H (Figure 3-4) and 2D NMR (Figure 3-5) are employed to study the behavior of **3.4** in solution. At room temperature, broad peaks are observed for the pyridyl protons which become sharp with decreasing temperature. At 253 K, two distinct sets of well resolved peaks in ~1:1 ratio corresponding to two different groups of 2-(2'-pyridyl)benzimidazolyl were observed, indicating the coexistence of the *anti* and *syn* isomers in solution as shown in Figure 3-3. With the variable-temperature ^1H NMR spectral data, the activation energy for the exchange process of *anti* and *syn* structures was estimated to be ~56 kJ/mol.¹⁵ This energy barrier is attributed to the hindered rotation of the 2-(2'-pyridyl)benzimidazolyl and 2-(2'-pyridyl)indolyl group with respect to the central benzene ring, caused by the *ortho* hydrogen steric interaction as shown by the structure of **3.6** and the chelation of the two chromophores to the Pd/Ru atoms. Similar restricted rotation involving two 2-(2'-pyridyl)benzimidazolyl groups in $\text{Pt}_2(1,4\text{-bmb})\text{Ph}_4$ (1,4-bmb = 1,4-bis[2-(2'-pyridyl)benzimidazolyl]benzene) compounds has been observed previously.¹⁶

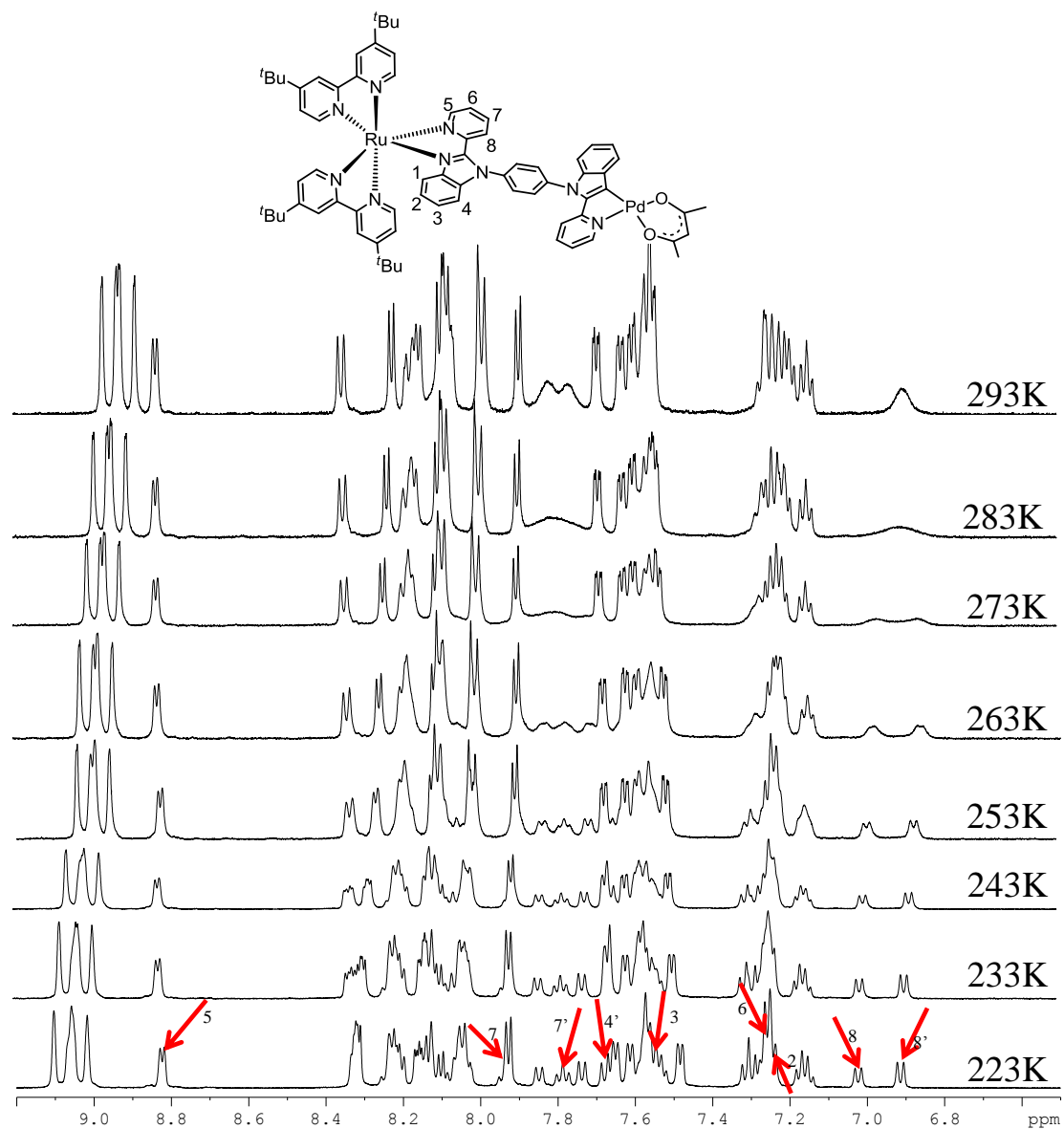


Figure 3-4. Variable temperature ^1H NMR spectra of **3.4** in acetone- d_6 , showing the interconversion of the *syn* and *anti* isomers depicted in Figure 3-3.

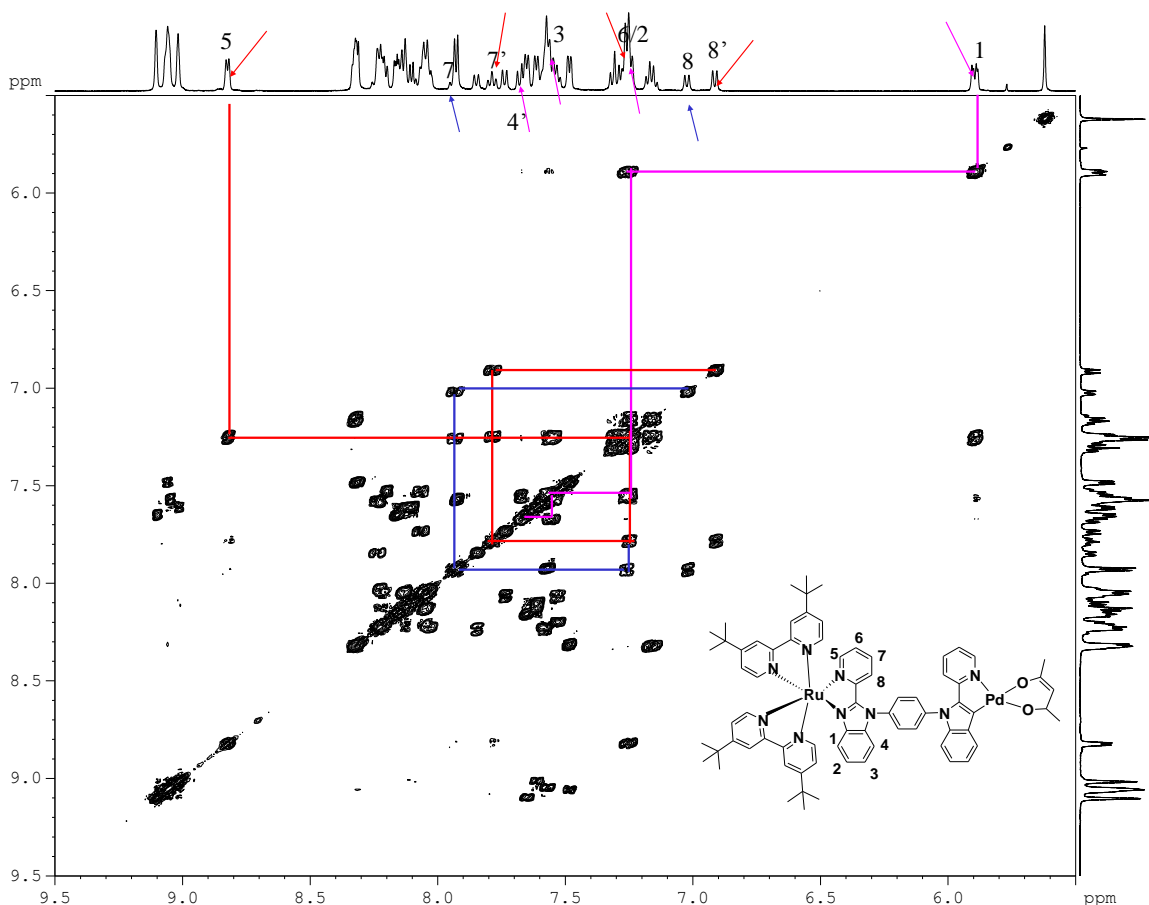


Figure 3-5. The partial COSY spectrum of **3.4** in acetone- d_6 at 223K.

3.3.3 Electrochemical Properties

The CV diagrams of complexes **3.1**, **3.3** and **3.4** display one reversible oxidation peak in DMF with a nearly identical oxidation potential (0.61 V, 0.59 V and 0.60 V respectively, relative to that of $\text{FeCp}_2^{+/0}$, as shown in Figure 3-6) that can be assigned to oxidation of Ru(II) to Ru(III). The similarity of this oxidation potential for all three compounds suggests that there is little electronic communication between the Ru(II) and Pd(II)/Pt(II) centers in the bimetallic complexes. The oxidation potential of **3.2** is significantly more positive (0.70 V) than those of **3.1**, **3.3**, and **3.4**, indicating that the HOMO levels of **3.1**, **3.3**, and **3.4** are higher than that of **3.2**. The electron donating *t*-butyl groups thus seem to significantly raise the HOMO energy level of **3.1**, **3.3**, and **3.4**

by putting more electron density on the Ru(II) center, compared to **3.2**. The weak electronic communication between the metal centers in these complexes is clearly caused by the non-coplanarity of the chelate units with the benzene linker and is in agreement with our earlier observations in homonuclear bimetallic complexes based on the **bmb** and related ligands.¹⁴ The **3.1**, **3.2**, **3.3** and **3.4** complexes display similar and well resolved multi-reduction peaks, which can be attributed to the reduction of the 2-(2'-pyridyl)benzimidazolyl and bipy ligands in the complex. The fact that the first reduction potentials for all these compounds are nearly identical and similar to that of [Ru(bipy)₃][PF₆]₂ supports that LUMO levels for these compounds are localized on the Ru(II) unit. Hence, based on the CV data, we suggest that the lowest electronic transition in these compounds is localized on the Ru(II) unit. The electrochemical data for **3.1**, **3.2**, **3.3**, **3.4** and [Ru(bipy)₃][PF₆]₂ are summarized in Table 3-3.

Table 3-3. Electrochemical data of Ru complexes.

	$E_{1/2}^{\text{red1}}$ (V)	$E_{1/2}^{\text{red2}}$ (V)	$E_{1/2}^{\text{red3}}$ (V)	$E_{1/2}^{\text{ox}}$ (V)	Electrochemical energy gap (V)
3.1	-1.81	-2.08	-2.37	0.61	2.42
3.2	-1.81	-2.02	-2.31	0.70	2.51
3.3	-1.81	-2.07	-2.33	0.59	2.40
3.4	-1.80	-2.07	-2.34	0.60	2.40
[Ru(bipy) ₃][PF ₆] ₂	-1.81	-1.99	-2.27	0.75	2.56

All potentials are relative to FeCp₂^{0/+}, measured in DMF, using NBu₄PF₆ as the electrolyte with a scan rate of 100 - 200 mV/s

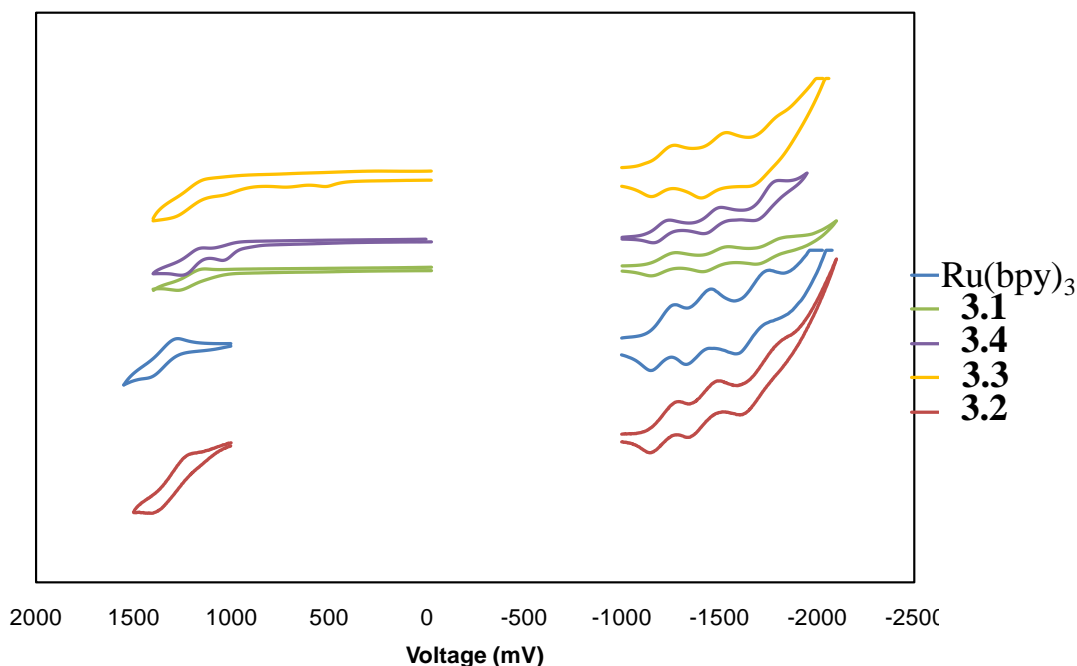


Figure 3-6. Cyclic voltammogram of metal complexes, recorded in DMF, using NBu_4PF_6 as the electrolyte with a scan rate of 100-200 mV/s.

3.3.4 UV-Vis Absorption Spectra

All photophysical property measurements were done in the degassed THF at room temperature. The results are summarized in Table 3-4. Both free ligand **L1** and **pib** show an absorption band at around 310 nm, which is attributed to the $\pi \rightarrow \pi^*$ transition of the 2-(2'-pyridyl)benzimidazolyl or 2-(2'-pyridyl)indole units. Compared with ligand **pib**, ligand **L1** has nearly twice the molar absorptivity since it contains two similar chromophores. The four Ru(II) complexes, **3.1**, **3.2**, **3.3** and **3.4**, show similar absorption spectra as shown in Figure 3-7. Besides the 310 nm absorption band, another high energy absorption at ~290 nm is observed, which can be assigned to the $\pi \rightarrow \pi^*$ transition introduced by the bipy and (*t*-butyl)₂-bipy moieties. The lowest energy absorption in **3.1** is a broad metal-to-ligand-charge-transfer (MLCT) band, from ~410 nm to ~510 nm. Compared with **3.1**, the MLCT band of **3.2** is a few nanometers blue shifted, which is in

agreement with the relatively low HOMO level of **3.2**, as revealed by the CV data, that increases the MLCT energy. In order to understand the role of the second metal center in the bimetallic complexes, the spectra of **3.5** and **3.6** are also recorded and compared to those of complexes **3.3** and **3.4**. Both **3.5** and **3.6** display a weak but distinct MLCT band that is about 30 nm blue shifted, compared to that of the bimetallic compounds. Thus, the MLCT bands of the bimetallic compounds are predominately from transitions involving the Ru(II) center.

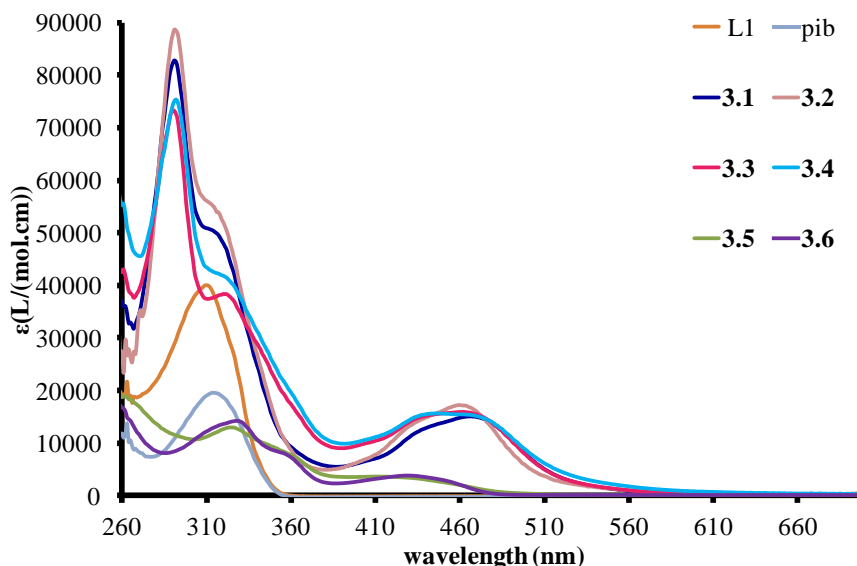


Figure 3-7. UV-Vis spectra of $\sim 1 \times 10^{-5}$ M solutions of metal complexes and free ligands recorded in THF at ambient temperature.

3.3.5 Luminescence Spectra

The luminescent properties of all the complexes are studied at both room temperature and frozen state. The data are summarized in Table 3-4.

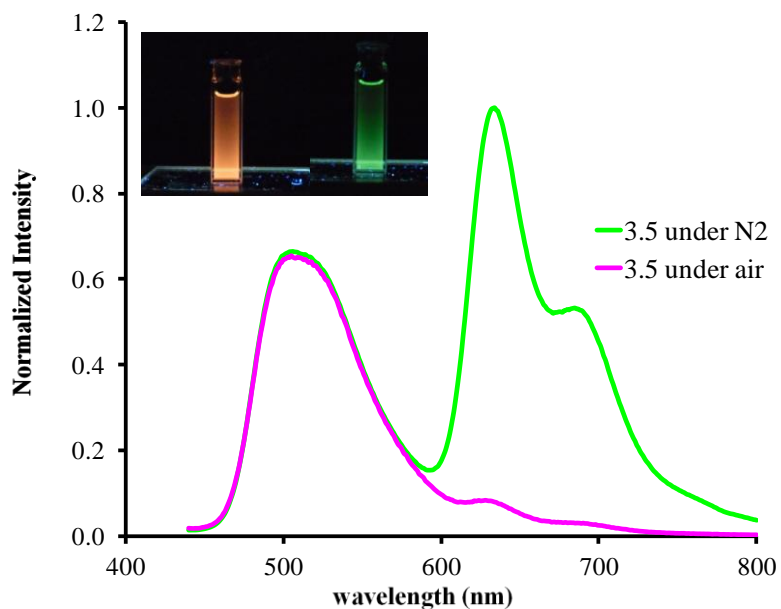


Figure 3-8. Emission spectra of **3.5** in THF ($\sim 1 \times 10^{-5}$ M) at ambient temperature. Inset: Photographs showing the luminescence color of **3.5** solution under 365 nm irradiation under N₂ (left) and under air (right).

At ambient temperature **3.5** shows interesting dual emission with two peaks at 507 nm and 633 nm, respectively. The excitation spectra monitored for these two peaks are identical, indicating that the dual emission originates from the same molecule. Based on its long decay lifetime and the sensitivity toward oxygen, the emission band at 633 nm is assigned to phosphorescence. The high energy emission band is insensitive to oxygen, thus attributed to ligand-centered fluorescence. The relative intensity of the two emission bands can be modulated reversibly by using nitrogen and oxygen as shown in Figure 3-8. The presence of well-resolved vibrational fine features in the 633 nm peak of **3.5** indicates that this phosphorescent peak likely has significant contributions from both ³MLCT and ³LC states, in agreement with related N[^]C-chelate Pt(II) compounds reported previously.¹⁷ The **3.6** complex is not emissive at room temperature. At 77 K, the frozen

solution of **3.6** shows an emission band at 608 nm with a decay lifetime of $\sim 70 \mu\text{s}$, which is attributed to phosphorescent emission, as shown in Figure 3-9.

The Ru complexes **3.1**, **3.2**, **3.3** and **3.4** are all luminescent in solution at ambient temperature as shown in Figure 3-10. The mononuclear ruthenium complex **3.2** has a much lower luminescence quantum yield (627 nm, $\Phi = 0.83\%$), compared to that of $[\text{Ru}(\text{bipy})_3][\text{PF}_6]_2$ ($\Phi = 6.1\%$), indicating that bipy is more efficient in promoting Ru(II) MLCT phosphorescence than L1. In the frozen state (77 K), the emission of **3.2** is blue-shifted to 600 nm with a decay lifetime of $4.13 \mu\text{s}$ which is a typical phosphorescent emission. This blue shift phenomenon can be attributed to the increase rigidity of the environment at frozen state, which has been usually described as “luminescence rigidochromism”.¹⁸ Like the absorption spectra, the emission peak of **3.2** is blue shifted, compared to that of **3.1** by $\sim 13 \text{ nm}$ at ambient temperature, in agreement with the trend of the MLCT absorption energy.

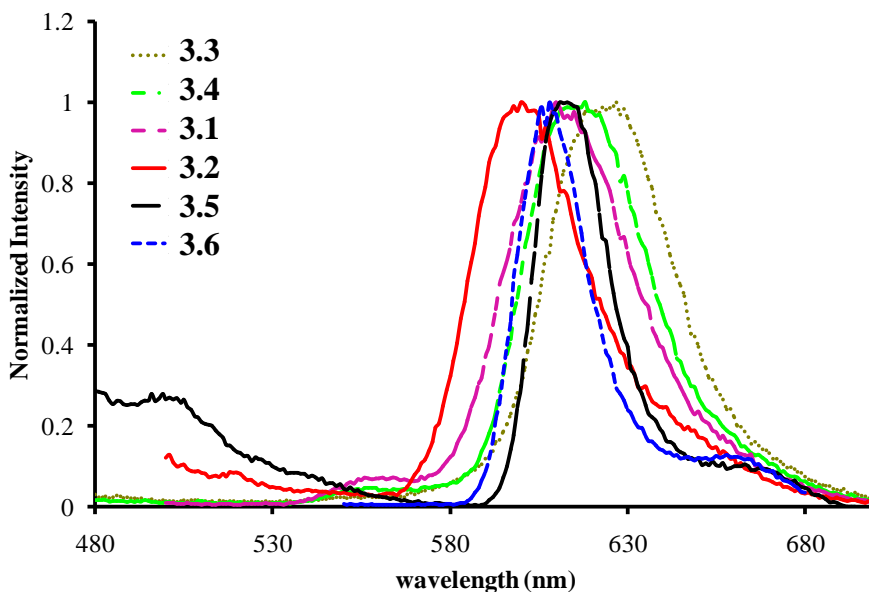


Figure 3-9. Emission spectra of $\sim 1 \times 10^{-5} \text{ M}$ solutions of metal complexes recorded at 77K in 2-methyl-THF.

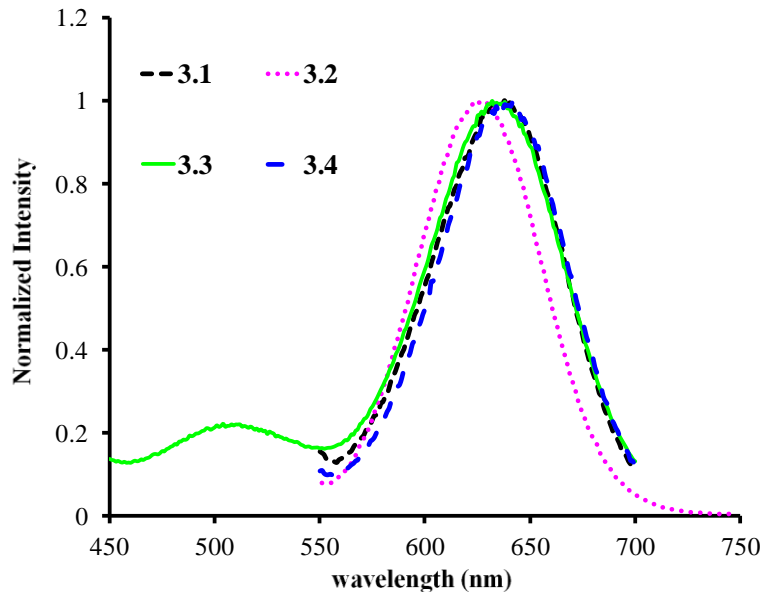


Figure 3-10. Emission spectra of $\sim 1 \times 10^{-5}$ M solutions of metal complexes recorded in THF at ambient temperature.

The emission spectra of **3.1**, **3.3** and **3.4** are all featureless and resemble each other with similar decay lifetimes at ambient temperature, and experience considerable reduction in intensity upon exposure to air. Thus, the luminescence of these compounds can be attributed to phosphorescence, originating most likely from the MLCT transition of the Ru(II) unit. The weak peak at ~ 507 nm in the emission spectrum of **3.3** is believed to be fluorescent and originate from the Pt(II) unit, as observed in **3.5**. It is noteworthy that the emission quantum efficiency of **3.3** is about twice that of **3.1**. Chelation to the Pt center and energy transfer from the Pt(II) unit to the Ru(II) unit may be responsible for the enhanced phosphorescent efficiency of **3.3**. In contrast, the Pd(II) unit appears to have little influence on the emission efficiency of the Ru(II) unit at ambient temperature. This difference may be attributed to the fact that the Pt(II) unit is emissive and its emission energy is close to that of the Ru(II) unit, thus effective in facilitating energy transfer to the Ru(II) unit.

Table 3-4. Absorption and luminescence data for complexes/ligands studied

Compound	Absorption λ_{\max}/nm ($\epsilon/\text{M}^{-1}\text{cm}^{-1}$) ^a	Emission		τ (μs) ^d	
		$\lambda_{\max}/\text{nm}, \Phi_{\text{phos}}^{\text{c}}$		298 K ^a	77 K ^b
		298 K ^a	77 K ^b		
3.1	292 (82600)	640	610	<1	3.93(3)
	317 sh (49700)	(0.44%)			
	471 (14900)				
3.2	292(88600)	627	600	< 1	4.13(3)
	318 sh (53500)	(0.83%)			
	464 (17200)				
3.3	289 (72900)	634	627	<1	3.35(1)
	325 sh (37500)	(1.02%)			
	459 (15500)				
3.4	293 (74900)	641	618	<1	10.77(6)
	324 sh (40800)	(0.43%)			
	447 (15600)				
3.5	327 (12900)	507	611	0.00087(2)	6.03(2)
	364 sh (8260)	633		5.75(4)	
	431 (3340)	685sh		3.83(6)	
		(1.0%)			
3.6	331 (13900)		608		70.98(3)
	360 sh (7240)				
	434 (3660)				
L1	312 (39700)	377			
pib	318 (19200)	377			

Conditions: ^a All the spectra of $\sim 1 \times 10^{-5}$ M solutions of free ligands and metal complexes were recorded in degassed THF at ambient temperature. ^b All the spectra of $\sim 1 \times 10^{-5}$ M solutions of metal complexes were recorded in 2-methyltetrahydrofuran at 77K. ^c Degassed $[\text{Ru}(\text{bipy})_3](\text{PF}_6)_2$ in CH_3CN ($\Phi = 6.1\%$) was used as a reference for quantum efficiency measurements. ^d The decay lifetimes were obtained by fitting the decay curve with a single exponential function.

3.4 Conclusions

A new ligand L1 that have two distinct chelating sites for the formation of heterobimetallic compounds has been achieved. Its use in the synthesis of bimetallic **3.3** and **3.4** compounds has been demonstrated. The electronic and photophysical properties of the heterobimetallic compounds were investigated and compared to those of the corresponding monometallic compounds. Our investigation revealed that there is little electronic communication between the two different metal centers bridged by L1, due to the lack of conjugation of the two chelating units with the central benzene ring. The Pt(II) unit is found to enhance phosphorescence efficiency of the Ru(II) unit via intramolecular energy transfer.

3.5 References

1. (a) C. W. Tang, S. A. Van Slyke, C. H. Chen, *J. Appl. Phys.* 1989, **65**, 3611; (b) Y. Shirota, S. Kawami, K. Imai, *Appl. Phys. Lett.* 1994, **65**, 807; (c) Y. Hamada, T. Sana, M. Fujita, T. Fujii, Y. Nishio, K. Shibata, *Jpn. J. Appl. Phys.* 1993, **32**, L514; (d) V. Bulovic, G. Gu, P. E. Burrows, S. R. Forrest, *Nature* 1996, **380**, 29; (e) M. Braun, J. Gmeiner, M. Tzolov, M. Coelle, F. D. Meyer, W. Milius, H. Hillebrecht, O. Wendland, J. U. von Schutz, W. Brutting, *J. Chem. Phys.* 2001, **114**, 9625; (f) H. Schmidaur, J. Lettenbauer, D. L. Wikinson, G. Müller, O. Z. Kumberger, *Naturforsch.* 1991, **46b**, 901.
2. (a) M. K. Nazeeruddin, A. Kay, I. Rodicio, R. Humphry-Baker, E. Müller, P. Liska, N. Vlachopoulos, M. Grätzel, *J. Am. Chem. Soc.* 1993, **115**, 6382; (b) D. Kuciauskas, M. S. Freund, H. B. Gray, J. R. Winkler, N. S. Lewis, *J. Phys. Chem. B* 2001, **105**, 392; (c) E. A. M. Geary, L. J. Yellowlees, L. A. Jack, I. D. H. Oswald, S. Parsons, N. Hirata, J. R. Durrant, N. Robertson, *Inorg. Chem.* 2005, **44**, 242; (d) G. M. Hasselmann, G. J. Meyer, *Z. Phys. Chem.* 1999, **212**, 39; (e) N. Alonso-Vante, J. F. Nierengarten, J. P. Sauvage, *J. Chem. Soc. Dalton Trans.* 1994, 1649; (f) P. M. Jayaweera, S. S. Palayangoda, K. Tennakone, *J. Photochem. Photobiol. A* 2001, **140**, 173.
3. (a) I. A. Hemmilä *Applications of Fluorescence in Immunoassays*, 2nd ed. Wiley, New York, 1991; (b) D. Parker, *Coord. Chem. Rev.* 2000, **205**, 109; (c) L. Prodi, S. Pivari, F. Bolletta, M. Hissler, R. Ziessel, *Eur. J. Inorg. Chem.* 1998, **1959**, 17; (d) A. Juris, V. Balzani, F. Barigelletti, S. Campagna, P. Belser, A. Von Zelewsky, *Coord. Chem. Rev.* 1988, **84**, 85; (e) X. Q. Guo, F. N. Castellano, L. Li, H. Szmecinski, J. R. Lakowicz, *Anal. Biochem.* 1997, **254**, 179; (f) X. Q. Guo, F. N. Castellano, L. Li, J. R. Lakowicz, *Anal. Chem.* 1998, **70**, 632; (g) J. M. Kurner, I. Klimant, C. Krause, H. Preu, W. Kunz, O. S. Wolfbeis, *Bioconjugate Chem.* 2001, **12**, 883.
4. (a) M. Grätzel, K. Kalyanasundaram, *Curr. Sci.* 1994, **66**, 706; (b) P. Wang, C. Klein, R. Humphry-Baker, S. M. Zakeeruddin, M. Grätzel, *J. Am. Chem. Soc.*

- 2005, **127**, 808; (c) V. Fernández-Moreira, F. L. Thorp-Greenwood, M. P. Coogan, *Chem. Commun.* 2010, **46**, 186; (d) A. Hagfeldt, G. Boschloo, L. Sun, L. Kloo, H. Pettersson, *Chem. Rev.* 2010, **110**, 6595; (5) V. Friese, S. Nag, J. Wang, M.-P. Santoni, A. Rodrigues-Witchel, G. S. Hanan, F. Schaper, *Eur. J. Inorg. Chem.* 2011, 39.
5. (a) S.-H. Wu, S. E. Burkhardt, J. Yao, Y.-W. Zhong, H. D. Abruña, *Inorg. Chem.* 2011, **50**, 3959; (b) A. Magnuson, M. Anderlund, O. Johansson, P. Lindblad, R. Lomoth, T. Polivka, S. Ott, K. Stensjö, S. Styring, V. Sundström, L. Hammarström, *Acc. Chem. Res.* 2009, **42**, 1899; (c) S. Rau, B. Schäfer, D. Gleich, E. Anders, M. Rudolph, M. Friedrich, H. Görlos, W. Henry, J. G. Vos, *Angew. Chem. Int. Ed.* 2006, **45**, 6215; (d) S. M. Arachchige, J. R. Brown, E. Chang, A. Jain, D. F. Zigler, K. Rangan, K. Brewer, *Inorg. Chem.* 2009, **48**, 1989; (e) A. Fihri, V. Artero, M. Razavet, C. Baffert, W. Leibl, M. Fontecave, *Angew. Chem. Int. Ed.* 2008, **47**, 564.
6. (a) M. D. Ward, J. A. McCleverty, *J. Chem. Soc., Dalton Trans.* 2002, 275; (b) J. L. Chen, Y. Chi, K. Chen, Y. M. Cheng, M. W. Chung, Y. C. Yu, G. H. Lee, P. T. Chou, C. F. Shu, *Inorg. Chem.* 2010, **49**, 823; (c) J. A. Treadway, G. F. Strouse, R. R. Ruminski, T. J. Meyer, *Inorg. Chem.* 2001, **40**, 4508.
7. (a) H. Ozawa, M. Haga, K. Sakai, *J. Am. Chem. Soc.* 2006, **128**, 4926; (b) M. Schwalbe, M. Karnahl, H. Górls, D. Chartrand, F. Laverdiere, G. S. Hanan, S. Tschierlei, B. Dietzek, M. Schmitt, J. Popp, J. G. Vos, S. Rau, *J. Chem. Soc., Dalton Trans.* 2009, 4012; (c) S. Rau, B. Schafer, D. Gleich, E. Anders, M. Rudolph, M. Friedrich, H. Górls, W. Henry, J. G. Vos, *Angew. Chem., Int. Ed.* 2006, **45**, 6215; (d) M. Elvington, J. Brown, S. M. Arachchige, K. J. Brewer, *J. Am. Chem. Soc.* 2007, **129**, 10644; (e) A. Fihri, V. Artero, M. Razavet, C. Baffert, W. Leibl, M. Fontecave, *Angew. Chem., Int. Ed.* 2008, **47**, 564; (f) A. Fihri, V. Artero, A. Pereirab, M. Fontecave, *Dalton Trans.* 2008, 5567.
8. (a) R. Zhang, X. Yu, Y. Yin, Z. Ye, G. Wang, J. Yuan, *Anal. Chim. Acta* 2011, **691**, 83; (b) D. Saha, S. Das, D. Maity, S. Dutta, S. Baitalik, *Inorg. Chem.* 2011,

- 50**, 46; (c) C. F. Chow, B. K. W. Chiu, M. H. W. Lam, W. Y. Wong, *J. Am. Chem. Soc.* 2003, **125**, 7802; (d) P. D. Beer, F. Szemes, V. Balzani, C. M. Salà M. G. B. Drew, S. W. Dent, M. Maestri, *J. Am. Chem. Soc.* 1997, **119**, 11864; (e) F. Szemes, D. Heseck, Z. Chen, S. W. Dent, M. G. B. Drew, A. J. Goulden, A. R. Graydon, A. Grieve, R. J. Mortimer, T. J. Wear, J. S. Weightman, P. D. Beer, *Inorg. Chem.* 1996, **35**, 5868.
9. (a) S. Tollari, S. Cenini, A. Penoni, G. Granata, G. Palmisano, F. Demartin, *J. Organomet. Chem.* 2000, **608**, 34. (b) G. Cravotto, F. Demartin, G. Palmisano, A. Penoni, T. Radice, S. Tollari, *J. Organomet. Chem.* 2005, **690**, 2017.
 10. T. M. McCormick, Q. D. Liu, S. Wang, *Org. Lett.* 2007, **9**, 4087.
 11. S. Rau, M. Ruben, T. Büttner, C. Temme, S. Dautz, H. Görls, M. Rudolph, D. Walther, A. Brodkorb, M. Duati, C. O'Connor, J. G. Vos, *J. Chem. Soc., Dalton Trans.* 2000, 3649.
 12. A. Klein, T. Schurr, A. Knodler, D. Gudat, K. W. K. Klinkhammer, V. Jain, S. Zalis, W. Kaim, *Organometallics* 2005, **17**, 4125.
 13. SHELXTL Version 6.14, Bruker AXS, 2000-2003.
 14. W. L. Jia, Y. F. Hu, J. Gao, S. Wang, *Dalton Trans.* 2006, 1721.
 15. D. H. Williams, I. Fleming, *Spectroscopic Methods in Organic Chemistry*, 4th ed.; McGraw-Hill Co. Ltd.: London, 1987; Chapter 3.
 16. Q. D. Liu, W. L. Jia, S. Wang, *Inorg. Chem.* 2005, **44**, 1332.
 17. (a) J. Brooks, Y. Babayan, S. Lamansky, P. I. Djurovich, I. Tsyba, R. Bau, M. E. Thompson, *Inorg. Chem.* 2002, **41**, 3055; (b) Y. L. Rao, S. Wang, *Inorg. Chem.* 2009, **48**, 7698.
 18. (a) S. Wang, G. Garzön, C. King, J. C. Wang, J. P. Fackler, *Inorg. Chem.* 1989, **28**, 4623; (b) A. J. Lees, *Chem. Rev.* 1987, **87**, 711; (c) G. J. Ferraudi, *Elements of Inorganic Photochemistry*, John Wiley & Sons, New York, 1988.

Chapter 4

Heterobimetallic Re(I) Complexes Based on 2-(2'-Pyridyl)benzimidazolyl and 2-(2'-Pyridyl)indolyl Derivative Ligand

4.1 Introduction

Bimetallic transition metal compounds that contain redox active and photoactive units have attracted considerable research attention.¹ These research interests stem from the fact that the multicomponent systems often have better performance than single component systems in various processes and applications including solar energy conversion,² light harvesting,³ catalysis,⁴ sensing,⁵ light emitting diode devices⁶ and so forth. Re(I) complexes are good candidates for incorporation into functional bimetallic or multimetallic systems because of their good stability and interesting photophysical/photochemical properties. Particularly, Re(I) carbonyl diimine complexes are a class of extensively investigated molecules for facilitating photochemical⁷ and electrochemical⁸ reduction of CO₂, labeling biomolecules,⁹ monitoring polymerizations,¹⁰ and using as optical switching materials.¹¹

Several bimetallic Ru(II)-Re(I) polypyridyl complexes where the metal ions are connected by various bridging ligands have been reported recently and demonstrated to have potential applications as efficient photocatalysts for CO₂ fixation.^{7c,7d, 12} In comparison, bimetallic compounds that contain a Re(I) unit and other metal ions such as Pt(II) and Pd(II) have not been extensively investigated with only a few examples known in the literature.¹³

As discussed in Chapter 2 and Chapter 3, ligand L1 has two different binding units, 2-(2'-pyridyl)benzimidazolyl (**py-im**) and 2-(2'-pyridyl)indolyl (**py-in**) unit linked together by a benzene ring.¹⁴ We have shown that L1 can selectively bind with two different metal centers such as Ru(II) and Pt(II) or Ru(II) and Pd(II) by taking advantage of the different binding modes and reactivity of the two binding sites toward metal ions. To further investigate the utility of ligand L1 in achieving new bimetallic compounds, we have extended our investigation to Re-Pt and Re-Pd systems. The synthesis, electrochemical and photophysical properties of new bimetallic Re(I)-Pt(II) and Re(I)-Pd(II) compounds (Figure 4-1) based on ligand L1 are presented herein.

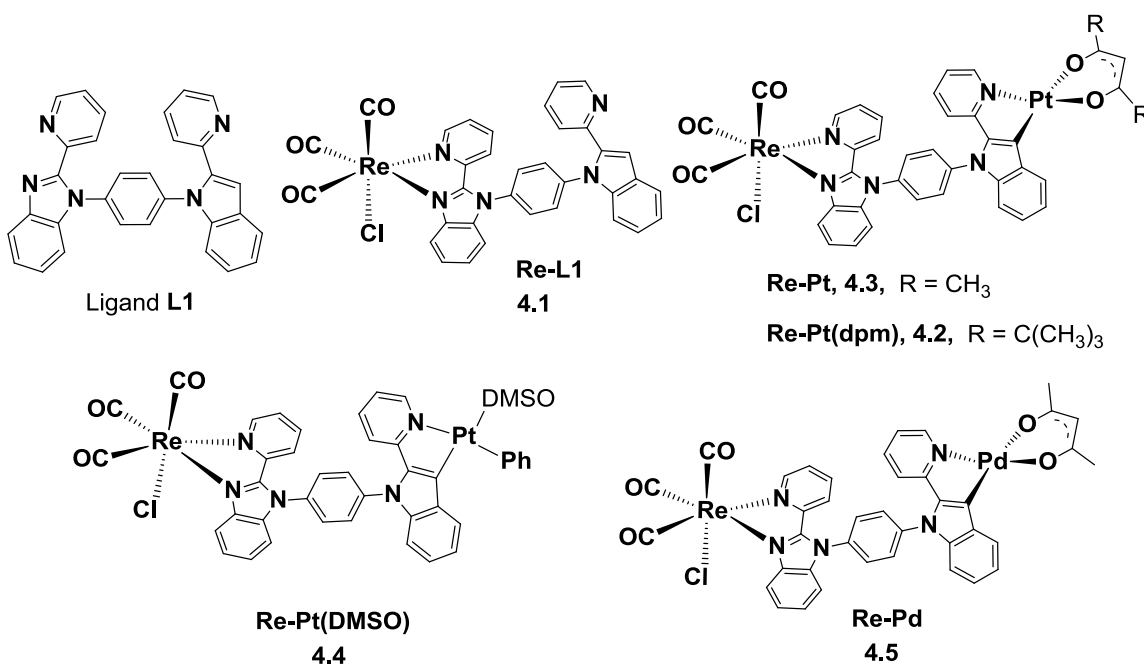


Figure 4-1. Chemical structures of L1 and L1 based Re(I) complexes.

4.2 Experimental

4.2.1 General Considerations

All reactions were performed under dry N₂ with standard Schlenk techniques unless otherwise noted. All starting materials were purchased from Aldrich Chemical Co. and

used without further purification. Solvents were freshly distilled over appropriate drying reagents under N₂ atmosphere. NMR spectra were recorded on a Bruker Avance 400 or 500 MHz spectrometer as stated. Excitation and emission spectra were recorded on a Photon Technologies International QuantaMaster Model C-60 spectrometer. UV-Vis spectra were recorded on a Varian Cary 50 UV-Vis spectrophotometer. Phosphorescent lifetimes were measured on a Photon Technologies International (PTI) phosphorimeter (Time-Master C-631F) that was equipped with a xenon flash lamp and a digital emission photon multiplier tube, using a band pathway of 5 nm for excitation and 2 nm for emission.

Cyclic voltammetry (CV) was performed using a BAS CV-50W analyzer, with a scan rate of 100 or 150 mV/s. The electrochemical experiments were performed with 0.10 M NBu₄PF₆ as the electrolyte, and solutions were purged with nitrogen or CO₂ before CV diagrams were recorded. The metal complex concentration is 6.5 mM in 1 mL of acetonitrile. The ferrocenium/ferrocene couple was used as the internal standard ($E_0 = 0.45$ V). The CV cell used was a conventional three-compartment cell, in which a Pt working electrode, a Pt auxiliary electrode, and an Ag/AgCl reference electrode were employed.

Elemental analyses were performed at Elemental Analysis Service, Department of chemistry, University of Montreal (Montreal, Quebec, Canada). The syntheses of ligand [PtMe₂(SMe₂)₂],¹⁵ complexes Pt(**pib**)(acac) (**4.6**)¹⁶ and Pt(**pib**)(dpm) (**4.7**)¹⁶ were achieved by methods described in the literature. The chemical structures of **4.6** and **4.7** are shown in Figure 4-2.

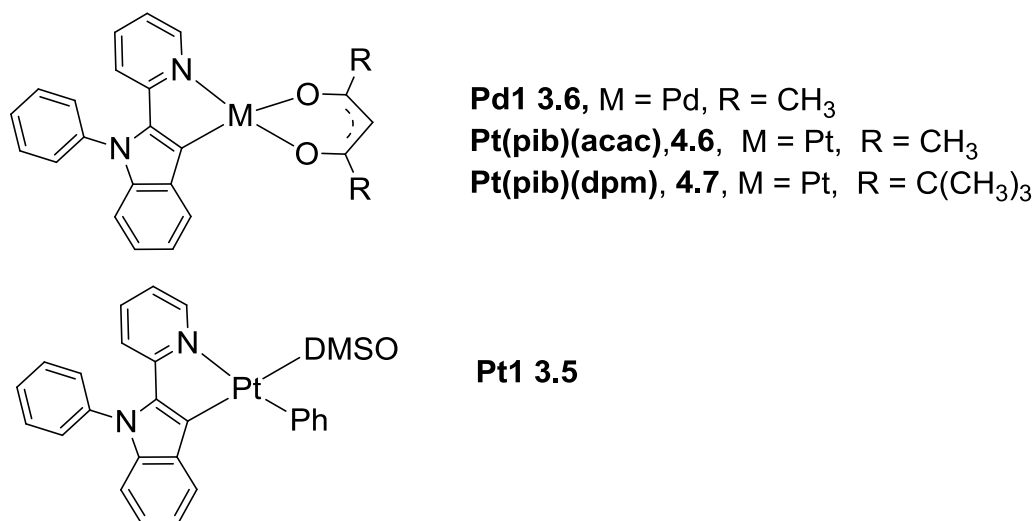


Figure 4-2. Chemical structures of Pt(II) and Pd(II) mononuclear compounds.

4.2.2 Molecular Calculation

The computational calculations were performed using Gaussian09, revision B.01¹⁷ software package and the High Performance Computing Virtual Laboratory (HPCVL) at Queen's University. The ground-state geometries were fully optimized at the B3LYP¹⁸ level using LANL2DZ basis set for platinum and rhenium as well as 6-31G(d) basis set for all other atoms.¹⁹ The initial geometric parameters in the calculations were employed from crystal structure data for geometry optimization. Time-dependent density function theory (TD-DFT) calculations were performed to obtain the vertical singlet and triplet excitation energies.

4.2.3 Synthesis of Re-L1 (4.1)

Re(CO)₅Cl (155 mg, 0.43 mmol) and ligand L1 (200 mg, 0.43 mmol) were dissolved in 40 mL toluene. The reaction mixture was stirred with reflux for 4 h. After cooling to room temperature, the yellow powder was filtered and washed with cold toluene and diethyl ether. A yield of 62% was obtained for this reaction. ¹H NMR (600 MHz, CD₂Cl₂,

298.0 K, δ , ppm): 9.16 (d, 1H, J = 5.2 Hz), 8.44 (d, 1H, J = 4.2 Hz), 8.14 (d, 1H, J = 8.2 Hz), 7.88 (td, 1H, J = 8.2 Hz, 1.3 Hz), 7.79-7.72 (m, 3H), 7.70-7.54 (m, 7H), 7.49 (d, 1H, J = 8.2 Hz), 7.35-7.32 (m, 3H), 7.27 (t, 1H, J = 7.1 Hz), 7.21 (td, 1H, J = 6.0 Hz, 1.1 Hz), 7.18 (s, 1H); $^{13}\text{C}\{^1\text{H}\}$ NMR (100 MHz, CD_2Cl_2 , δ , ppm): 198.3, 198.1, 189.4, 155.1, 152.5, 151.7, 149.4, 147.7, 142.9, 140.8, 139.9, 139.7, 139.4, 137.9, 137.1, 132.7, 131.1, 130.8, 129.3, 128.9, 128.8, 127.8, 127.7, 126.8, 124.6, 124.4, 124.1, 122.7, 122.1, 122.0, 120.1, 112.3, 110.9, 107.2. Anal. for $\text{C}_{34}\text{H}_{21}\text{N}_5\text{O}_3\text{ReCl}$: found C 53.50, H 3.20, N 8.51, calcd C 53.09, H 2.75, N 9.10.

4.2.4 Synthesis of Re-Pt(dpm) (4.2)

This bimetallic compound was synthesized by methods described in the literature.¹⁶ To a 20 mL screw-cap vial with a stir bar are added one equivalent of **4.1** (0.13 mmol, 100 mg), $[\text{PtMe}_2(\text{SMe}_2)]_2$ (37 mg, 0.065 mmol) and 3 mL of THF. The reaction is allowed to stir 1 hour at room temperature. Then a solution of HOTf (trifluoromethanesulfonic acid, 0.4 mL, 0.35 M in THF) is added dropwise. The mixture is stirred for 30 minutes, then a solution of Na(dipivalylmethane) (Na(dpm), 0.30 mmol in 2 mL MeOH) is added. The mixture is stirred for 1.5 hour, and then partitioned between water and CH_2Cl_2 . The organic layer is washed with brine, dried over MgSO_4 , filtered, and concentrated. The residue is then purified by column chromatography using THF- CH_2Cl_2 (1:60) as eluent to give analytically pure material. Recrystallization of the yellow product in CHCl_3 -hexane afforded **4.2** as orange-yellow crystals (yield 25%). ^1H NMR (600 MHz, CDCl_3 , 298.0 K, δ , ppm): 9.23 (d, 1H, J = 5.7 Hz), 9.12 (d, 1H, J = 5.7 Hz), 8.54 (d, 1H, J = 7.7 Hz), 8.23 (d, 1H, J = 8.1 Hz), 7.85-7.78 (m, 5H), 7.66 (t, 1H, J = 7.7 Hz), 7.59 (t, 1H, J = 7.4 Hz), 7.54-7.51 (m, 2H), 7.35 (t, 1H, J = 7.0 Hz), 7.32-7.24 (m,

4H), 6.94 (t, 1H, J = 6.3 Hz), 6.63 (d, 1H, J = 8.1 Hz), 5.94 (s, 1H), 1.40 (s, 9H), 1.33 (s, 9H); $^{13}\text{C}\{^1\text{H}\}$ NMR (100 MHz, CD_2Cl_2 , δ , ppm): 197.1, 196.9, 194.6, 193.6, 188.7, 159.2, 154.8, 151.8, 148.3, 147.2, 142.2, 141.9, 141.7, 140.4, 138.5, 138.0, 137.1, 133.6, 132.4, 130.1, 129.8, 129.5, 128.8, 127.5, 127.1, 126.5, 125.1, 124.6, 123.6, 121.7, 121.3, 120.2, 118.7, 116.9, 111.3, 109.5, 93.6, 41.9, 41.5, 28.9, 28.3. Anal. for $\text{C}_{45}\text{H}_{39}\text{N}_5\text{O}_5\text{RePtCl}$: found C 46.67, H 3.29, N 5.89, calcd C 47.14, H 3.43, N 6.11.

4.2.5 Synthesis of Re-Pt (4.3)

Compound **4.3** was obtained using the same method as that for **4.2**. Yield 28%. ^1H NMR (400 MHz, CD_2Cl_2 , 298.0 K, δ , ppm): 9.19 (d, 1H, J = 6.0 Hz), 9.03 (d, 1H, J = 5.3 Hz), 8.33 (d, 1H, J = 8.1 Hz), 8.18 (d, 1H, J = 8.1 Hz), 7.90-7.79 (m, 5H), 7.68 (td, 1H, J = 7.3 Hz, 1.0 Hz), 7.62 (td, 1H, J = 7.3 Hz, 1.0 Hz), 7.58-7.54 (m, 2H), 7.40 (d, 1H, J = 8.1 Hz), 7.34-7.28 (m, 3H), 7.20 (td, 1H, J = 6.6 Hz, 1.4 Hz), 6.95 (td, 1H, J = 6.1 Hz, 1.4 Hz), 6.69 (d, 1H, J = 8.1 Hz), 5.61 (s, 1H), 2.10 (s, 3H), 2.05 (s, 3H). Anal. for $\text{C}_{39}\text{H}_{27}\text{N}_5\text{O}_5\text{RePtCl}$: found C 43.32, H 2.36, N 6.29, calcd C 44.09, H 2.56, N 6.59. The ^{13}C NMR spectrum could not be obtained due to poor solubility.

4.2.6 Synthesis of Re-Pt(DMSO) (4.4)

A mixture of **4.1** (0.060 g, 0.08 mmol) and *cis*-PtPh₂(DMSO)₂ (0.039 g, 0.08 mmol) was dissolved in 30 mL of THF. The mixture was stirred at 50 °C for 6 hrs, and the solvent was removed under reduced pressure. Recrystallization from CH_2Cl_2 -hexane afforded **4.4** as a yellow solid in 57% yield. ^1H NMR (400 MHz, CD_2Cl_2 , 298.0 K, δ , ppm): 9.68 (d, J = 5.5 Hz, 1H), 9.19 (d, J = 5.5 Hz, 1H), 8.18 (d, J = 7.9 Hz, 1H), 7.88 (td, J = 6.7 Hz, 1.3 Hz, 1H), 7.83-7.78 (m, 4H), 7.70-7.54 (m, 6H), 7.38 (d, J = 8.1 Hz, 1H), 7.34-7.28 (br, 1H), 7.16-7.10 (m, 6H), 6.72-6.66 (m, 2H), 5.81 (d, J = 8.1 Hz, 1H), 2.94

(s, 6H). Anal calcd for $C_{42}H_{31}N_5O_4PtReSCl$: C, 45.10; H, 2.79; N, 6.26. Found: C, 44.39; H, 2.65; N, 5.99. The ^{13}C NMR spectrum could not be obtained due to poor solubility.

4.2.7 Synthesis of Re-Pd (4.5)

A mixture of **4.1** (60 mg, 0.08 mmol) and $Pd(acac)_2$ (35 mg, 0.15 mmol) was suspended in 30 mL methanol. The mixture was refluxed for 2 days, and the solvent was removed under reduced pressure. The residue was washed by diethyl ether (3×10 mL). Recrystallization from THF-diethyl ether afforded **4.5** as a dark green solid in 92% yield. 1H NMR (400 MHz, CD_2Cl_2 , 298.0 K, δ , ppm): 9.19 (d, 1H, $J = 6.2$ Hz), 8.84 (d, 1H, $J = 6.2$ Hz), 8.33 (d, 1H, $J = 7.6$ Hz), 8.18 (d, 1H, $J = 7.6$ Hz), 7.89-7.80 (m, 5H), 7.69-7.55 (m, 4H), 7.39 (d, 1H, $J = 8.3$ Hz), 7.33-7.25 (m, 3H), 7.19 (t, 1H, $J = 5.9$ Hz), 7.03 (t, 1H, $J = 5.9$ Hz), 6.69 (d, 1H, $J = 8.3$ Hz), 5.53 (s, 1H), 2.21 (s, 3H), 2.12 (s, 3H). Anal. for $C_{39}H_{27}N_5O_5RePdCl$: found C 48.00, H 2.78, N 7.13, calcd C 48.10, H 2.79, N 7.19. The ^{13}C NMR spectrum could not be obtained due to poor solubility.

4.2.8 X-Ray Diffraction Analysis

Single crystals of **4.2** and **4.4** were obtained and used for structural determination by X-ray diffraction method. The crystals were mounted on glass fibers and the data were collected on a Bruker Apex II single-crystal X-ray diffractometer with graphite-monochromated $M_o K_{\alpha}$ radiation, operating at 50 kV and 30 mA, and at 180 K. Data were processed on a PC with the aid of the Bruker SHELXTL software package (version 5.10)^{20a} and corrected for absorption effects. Crystals of **4.2** belong to the chiral orthorhombic space group $Pna2_1$ while those of **4.4** belong to the monoclinic space group $P2_1/c$. The data quality for both crystals is poor due to mostly un-resolved twinning of the crystals. Disordering of the pyridyl ring bound to the Re atom in **4.4** was partially

resolved. Some degree of disordering of ligands around the Pt(II) unit in **4.2** is also present. However, we could not model it due to the limitation of data. The very long a-axis (43.4528(12) Å) of **4.2** may also be a contributing factor to the poor diffraction quality of the crystal. As a consequence, it was necessary to apply constraints on some of the bond lengths and angles for both crystals. For compound **4.4**, disordered solvent molecules are present in the crystal lattice and were removed by the Platon Squeeze routine.^{20b,20c} In addition, not all non-hydrogen atoms could be refined anisotropically. The crystal data of **4.2** has been deposited at the Cambridge Crystallographic Data Centre (CCDC 898415) and reported with **4.4** in Table 4-1. Their selected bond lengths and angles are given in Table 4-2.

4.3 Results and Discussions

4.3.1 Syntheses and Structures

To synthesize the bimetallic compounds, we first synthesized the Re(I) compound **4.1** by the reaction of ligand L1 with Re(CO)₅Cl in refluxing toluene, as shown in Figure 4-3. Compound **4.1** was isolated in 62% yield. The reaction of **4.1** with PtPh₂(DMSO)₂ in THF at 50°C for 6 hours led to the isolation of the bimetallic compound **4.4** in 57% yield. To examine the impact of ancillary ligands on photophysical properties of the bimetallic compound, two other Re(I)/Pt(II) compounds **4.3** and **4.2** were also synthesized, where the phenyl and the DMSO ligand in **4.4** are replaced by an acetylacetonato (acac) and its derivative, dipivolylmethane (dpm), respectively. One key advantage provided by the acac group is the significant improvement of the stability of the compound in the solution and solid state. Furthermore, the acac ligand has a high triplet state which minimizes its interference with phosphorescent emission. In addition, the acac group enhances the

rigidity of the Pt portion, thus decreasing the loss of energy *via* vibrational radiationless decay. Compound **4.3** was prepared by a one spot procedure developed recently by our group for N[^]C-chelate Pt(II) acac compounds.¹⁶ In this procedure, **4.1** was reacted first with 0.5 eq. [Pt(CH₃)₂(SMe₂)₂] in THF to attach the PtMe(SMe₂) unit to the N[^]C-chelate site, followed by the addition of HOTf to remove the methyl group, and the subsequent addition of Na(acac) in methanol to add the acac ligand, resulting in the formation and isolation of **4.3**, as shown in Figure 4-3. Because the solubility of **4.3** is poor, we synthesized **4.2** using the same procedure as that for **4.3**. The **4.2** compound shows good solubility in common organic solvents. Compound **4.5** was prepared by the reaction of **4.1** with Pd(acac)₂ in methanol in 92% yield. As control compounds for understanding the photophysical properties of the bimetallic complexes, the N[^]C-chelate mononuclear compounds **3.5**, **3.6**, **4.6** and **4.7** shown in Figure 4-2 were also synthesized using ligand *N*-phenyl-2(2'-py)indole (**pib**) and the appropriate Pt(II) and Pd(II) precursor compounds. All new metal compounds were characterized by ¹H NMR and elemental analyses.

Table 4-1. Crystallographic data for compounds **4.2** and **4.4**.

	4.2	4.4
Empirical formula	C45H39ClN5O5PtRe	C42H31ClN5O4PtReS
Formula weight	1146.55	1118.52
Space group	Pna2(1)	P2(1)/c
a, Å	43.4528(12)	19.0195(5)
b, Å	11.8801(3)	8.0623(2)
c, Å	8.1619(2)	27.8363(8)
α , deg	90	90
β , deg	90	95.642(2)
γ , deg	90	90
V, Å ³	4213.37(19)	4247.8(2)
Z	4	4
Density (calculated), gcm ⁻³	1.807	1.749
μ , mm ⁻¹	6.302	6.294
2 θ_{\max} , deg	53.00	52.00
Reflns meads	20645	36370
Reflns used	8183	8313
(R_{int})	(0.0962)	(0.0795)
Final $R[I > 2\sigma(I)]$		
R1 ^a	0.0747	0.1109
wR2 ^b	0.1463	0.2899
R(all data)		
R1 ^a	0.1346	0.1452
wR2 ^b	0.1713	0.3118
GOF on F^2	1.035	1.074

^a $R1 = \Sigma[|F_o| - |F_c|]/\Sigma|F_o|$. ^b $wR2 = \{\Sigma[w(F_o^2 - F_c^2)]/\Sigma(wF_o^2)\}^{1/2}$. $\omega = 1/[\sigma^2(F_o^2) + (0.075P)^2]$, where $P = [\max.(F_o^2, 0) + 2F_c^2]/3$.

Table 4-2. Selected bond lengths (Å) and angles (°) of compounds **4.2** and **4.4**.

4.2			
Pt(1)-C(22)	1.93(2)	O(4)-Pt(1)-N(4)	174.6(6)
Pt(1)-O(4)	2.015(13)	C(22)-Pt(1)-O(5)	171.4(8)
Pt(1)-N(4)	2.008(16)	C(2)-Re(1)-N(1)	170.6(7)
Pt(1)-O(5)	2.066(14)	C(1)-Re(1)-N(2)	172.5(7)
Re(1)-C(1)	1.92(2)	C(3)-Re(1)-Cl(1)	176.7(6)
Re(1)-C(2)	1.88(3)		
Re(1)-C(3)	1.96(2)		
Re(1)-N(1)	2.157(18)		
Re(1)-N(2)	2.212(14)		
Re(1)-Cl(1)	2.455(6)		
4.4			
Re(1)-C(41)	1.86(5)	C(41)-Re(1)-C(40)	86.6(17)
Re(1)-C(40)	1.92(4)	C(41)-Re(1)-C(42)	90.1(16)
Re(1)-C(42)	1.927(17)	C(40)-Re(1)-C(42)	88.4(15)
Re(1)-N(1A)	2.14(5)	C(41)-Re(1)-N(1A)	94(2)
Re(1)-N(2)	2.15(2)	C(40)-Re(1)-N(1A)	96.2(18)
Re(1)-N(1)	2.37(3)	C(42)-Re(1)-N(1A)	174.2(17)
Re(1)-Cl(1)	2.454(7)	C(41)-Re(1)-N(2)	94.7(15)
Pt(1)-C(25)	2.02(2)	C(25)-Pt(1)-C(32)	92.8(8)
Pt(1)-C(32)	2.028(12)	C(25)-Pt(1)-N(4)	77.5(8)
Pt(1)-N(4)	2.144(15)	C(32)-Pt(1)-N(4)	169.7(7)
Pt(1)-S(1)	2.282(5)	C(25)-Pt(1)-S(1)	177.2(7)

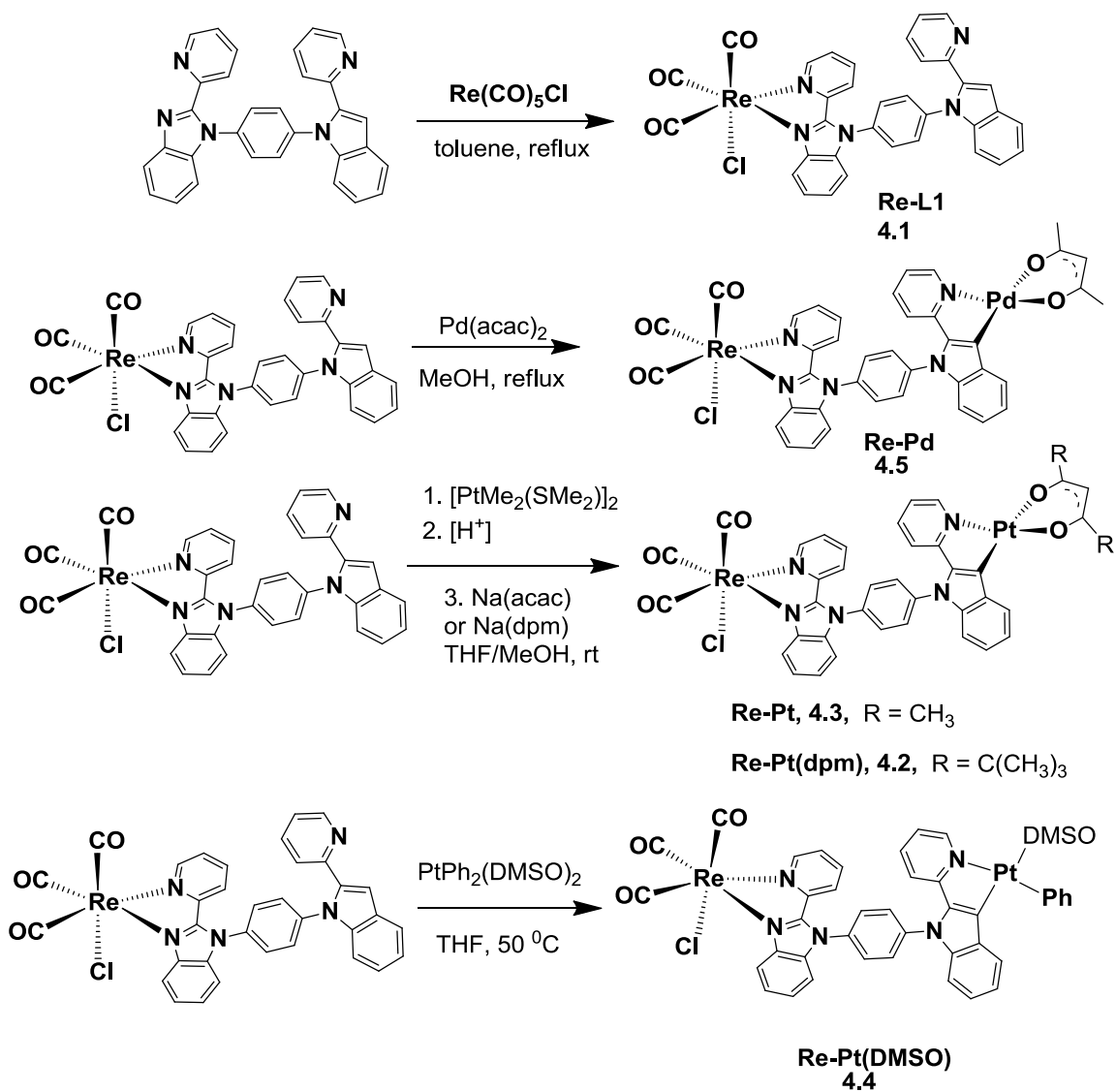


Figure 4-3. Reaction scheme for the syntheses of metal complexes.

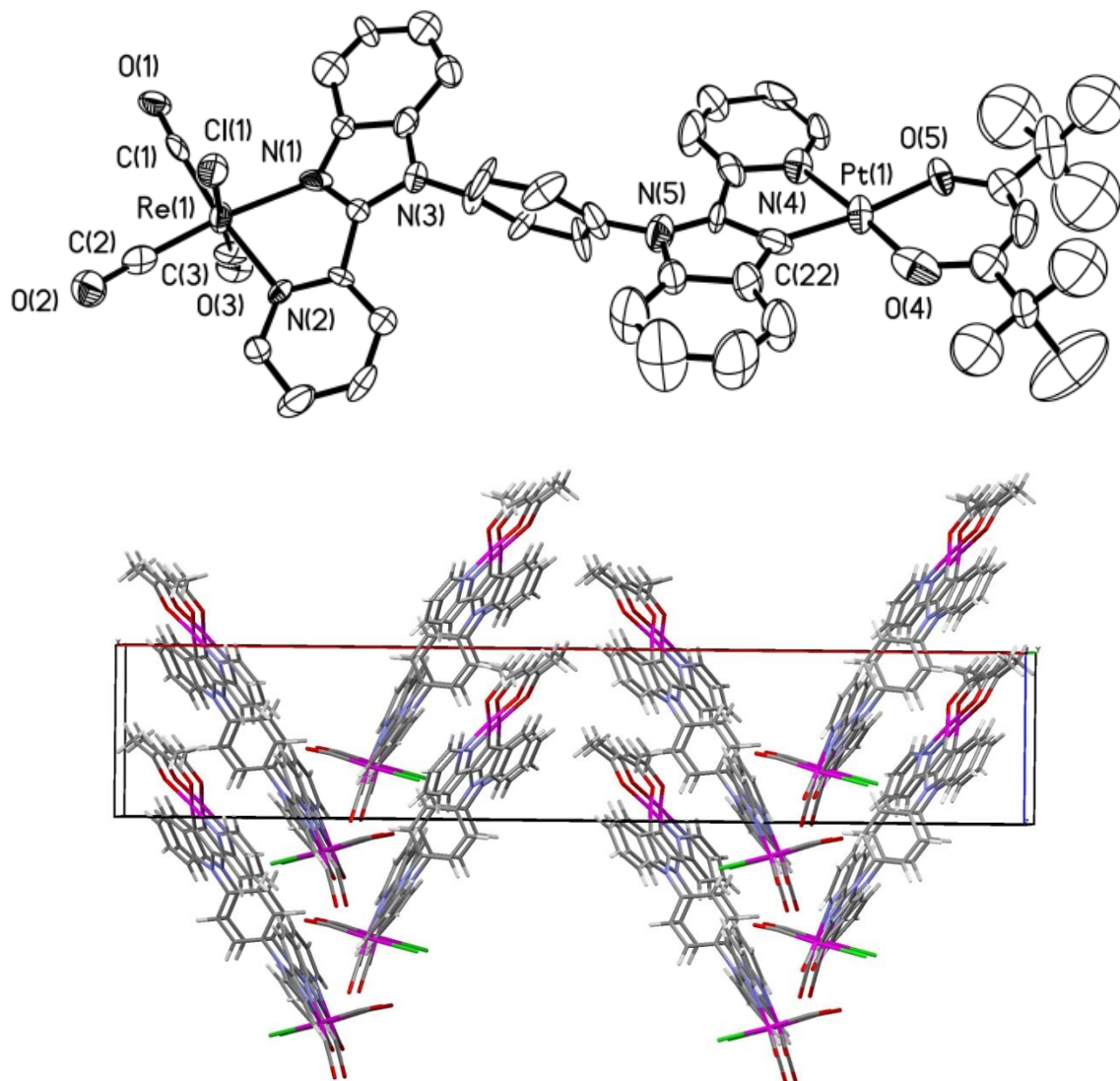


Figure 4-4. Top: the crystal structure of **4.2** with 50% thermal ellipsoids and labeling schemes. Hydrogen atoms are omitted for clarity. Bottom: the packing diagram of **4.2** projected down the b-axis.

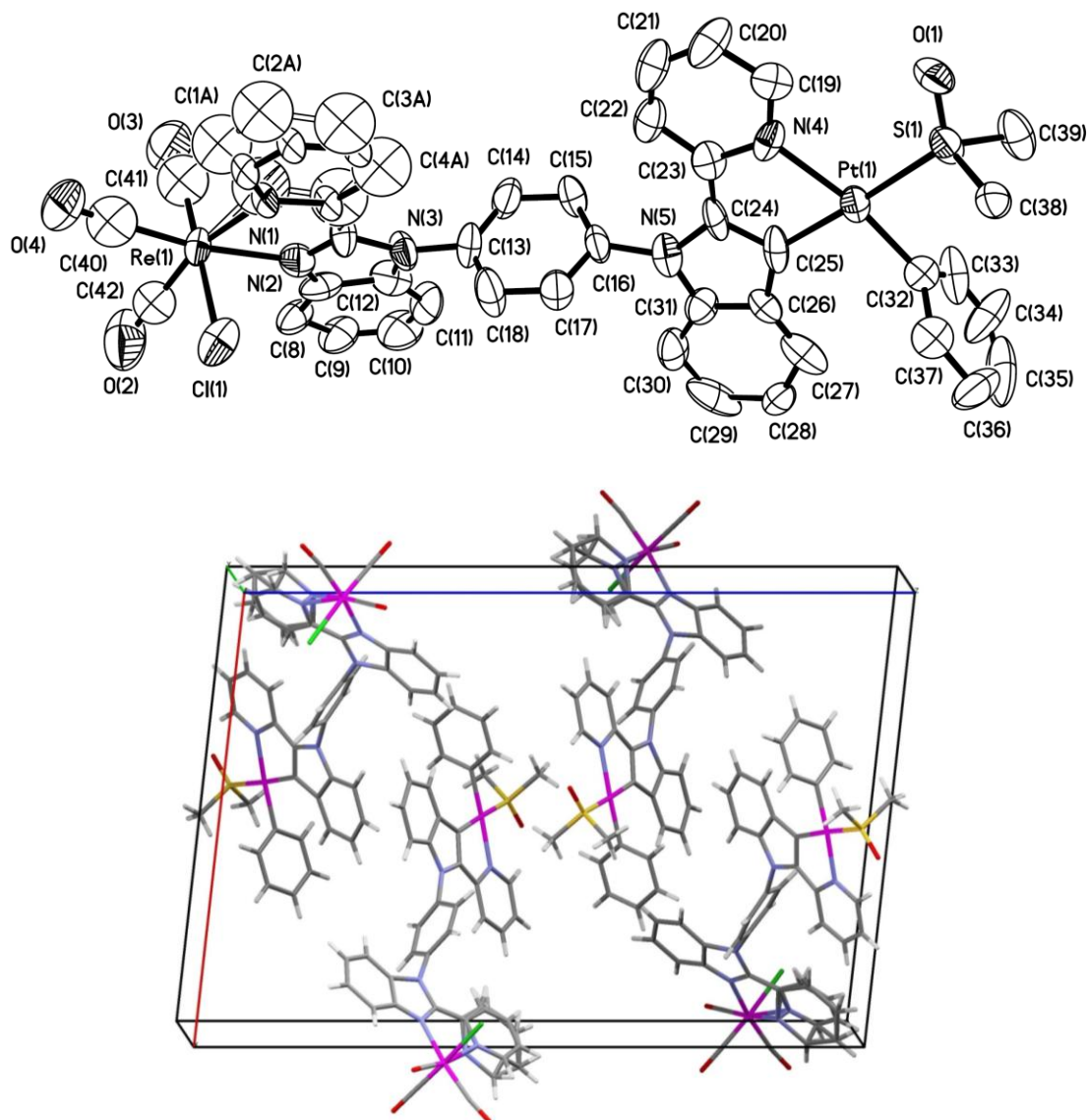


Figure 4-5. Top: The crystal structure of **4.4** with 50% thermal ellipsoids and labeling schemes. Hydrogen atoms are omitted for clarity. Bottom: the packing diagram of **4.4** projected down the b-axis.

The structures of **4.2** and **4.4** were determined by X-ray diffraction analyses. The crystal quality of both compounds is poor. Both crystals display some degree of twinning and disordering, which could not be fully resolved. As a result, the crystal data for both compounds are not of high quality. Nonetheless, the crystal structural data confirmed the connectivity and geometry of both compounds. The crystal data of **4.2** and **4.4** are shown

in Figure 4-4 and Figure 4-5, respectively. As shown in Figure 4-4, the Re and Pt units have the typical octahedral and square-planar geometry, respectively. However, the **py-in** and **py-im** chelate groups for the two metal ions are not coplanar with the central benzene ring. The dihedral angles between the central benzene ring, the **py-in** and the **py-im** ring are 62° and 96°, respectively. This lack of co-planarity is characteristic of the L1 ligand and can be attributed to the interactions of *ortho*-hydrogen atoms between the chelate units and the central benzene ring. Interestingly molecules of **4.2** crystallize in a chiral space group, Pna2₁ and pack in the crystal lattice in a head-to-head and tail-to-tail manner, forming “stacked badminton balls” structure, as shown by the packing diagram showing in Figure 4-4, bottom. The basic structural features of **4.4** are similar to those of **4.2** except that molecules of **4.4** crystallize in a centric space group P2₁/c, and are packed in a center-symmetric manner as shown in Figure 4-5, bottom.

4.3.2 UV-Vis Absorption spectra

The absorption spectral data are shown in Figure 4-6 and Table 4-3. For comparison purpose, the spectra of the corresponding mononuclear metal compounds **4.1**, **4.6**, **3.5** and **3.6** were all recorded. Because the dpm and acac ligands are similar and have a similar impact on the photophysical properties of the Pt(II) compound,²¹ the spectrum of **4.7** was not recorded. The absorption bands of the metal complexes in the UV region (< 390 nm) are assigned to the ligand based $\pi \rightarrow \pi^*$ transition. All mononuclear metal complexes display a distinct weak low energy band in the region of 390 nm to 520 nm, which can be assigned to MLCT transitions. The bimetallic **4.2**, **4.3**, **4.4**, and **4.5** all display weak and broad absorption bands in the same region as their corresponding mononuclear components, which may be attributed to MLCT transitions with contributions from both

metal centers. The impact of the 2nd metal center on the absorption spectra of the bimetallic compounds can be illustrated by using **4.2** as an example. Compared with the mononuclear **4.1**, the incorporation of a Pt metal center shifts the maximum of the ligand based $\pi \rightarrow \pi^*$ transition from ~315 nm to ~335 nm, due to the chelation of the ligand to the **4.7** moiety. The $\pi \rightarrow \pi^*$ transition band at $\lambda_{\max} = 335$ nm of **4.2** has nearly twice the molar absorptivity as that of **4.6** due to the contribution from the **4.1** portion. The MLCT band of **4.2** covers ~390 nm to 480 nm region, which can be considered as the sum of their **4.1** and **4.6** mononuclear precursors. Thus, the MLCT bands of the bimetallic compounds involve both metal centers. The same conclusion can also be made for the other three bimetallic compounds.

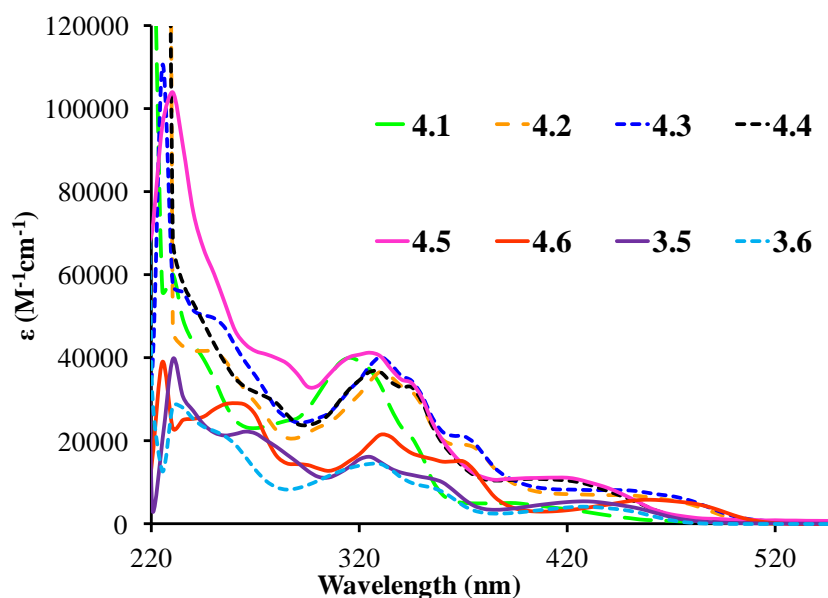


Figure 4-6. UV-Vis spectra of $\sim 1 \times 10^{-5}$ M solutions of metal complexes recorded in CH_2Cl_2 at ambient temperature.

Table 4-3. Absorption and luminescence data.

Compound	Absorption λ_{\max}/nm ($\epsilon/\text{M}^{-1}\text{cm}^{-1}$) ^a	Emission	τ (μs) ^d
		$\lambda_{\max}/\text{nm}, \Phi_{\text{phos}}$ ^c	
		298 K ^a	298 K ^a
4.1	230 (60200), 320 (40000), 395 (5040)	625 (0.20%)	< 1
4.2	250 (41600), 335 (35500), 345 sh (32100), 375 (18500) 455 (6780)	650 (0.73%)	2.47(2)
4.3	250 (49600), 330 (40200), 345 sh (34500), 375 (19600) 455 (7760)	650 (0.78%)	2.45(2)
4.4	330 (31700), 345 (28600), 420 (9065)	627 (0.23%)	< 1
4.5	230 (103950), 285 (38650), 325 (41240), 345 sh (33960) 425 (10750)	N/A	N/A
4.6	265 (28700), 295 (14200), 330 (21500), 370 (15100), 465 (5720)	657 (0.58%)	2.00(1)
3.5	327 (16300), 360 sh (10100), 430 (3340)	512 633 (0.60%)	4.17(3)
3.6	230 (28360), 255 sh (21190), 330 (14450), 355 (8700), 435 (3990)	77K ^b , 616	77K ^b , 74.39(5)

Conditions:^a All the spectra of $\sim 1 \times 10^{-5}$ M solutions of metal complexes were recorded in degassed CH_2Cl_2 at ambient temperature. ^b All the spectra of $\sim 1 \times 10^{-5}$ M solutions of metal complexes were recorded in 2-methyltetrahydrofuran at 77 K. ^c Degassed $[\text{Ru}(\text{bipy})_3][(\text{PF}_6)_2]$ in CH_3CN ($\Phi = 6.1\%$) was used as a reference for quantum efficiency

measurements.^d The decay lifetimes were obtained by fitting the decay curve with a single exponential function.

4.3.3 Luminescence Spectra

The phosphorescence spectra of all compounds were recorded under nitrogen in CH₂Cl₂ and the data are provided in Figure 4-7 and Table 4-3. None of the Pd(II) compounds are phosphorescent at ambient temperature.

It is known that in a polynuclear system, if the components behave as isolated and separate identities, they would relax from the excited state in a similar manner as the corresponding mononuclear precursors. However, if there are interactions or electronic communications between the components, energy transfer/charge transfer would be expected to occur according to well-known mechanisms.²² To understand the luminescence properties of our bimetallic compounds, we examined all relevant mononuclear compounds.

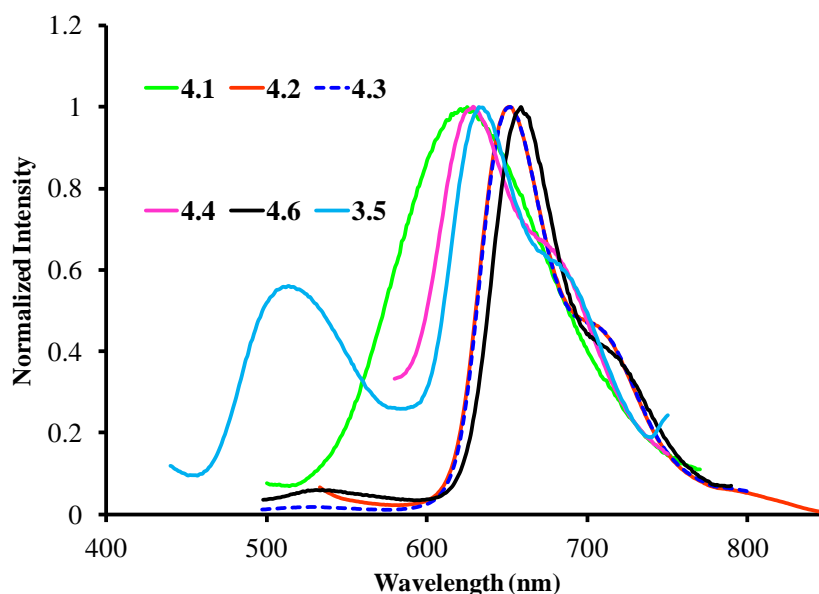


Figure 4-7. Emission spectra of $\sim 1 \times 10^{-5}$ M solutions of metal complexes recorded in CH₂Cl₂ at ambient temperature. ($\lambda_{\text{ex}} = 400\sim 430$ nm).

In CH₂Cl₂ and at ambient temperature, compound **4.1** exhibits a weak and broad luminescent band at 625 nm with a quantum yield of 0.20%, while **4.6** displays a peak at 657 nm with well resolved vibrational features and a quantum yield of 0.58%. The bimetallic compounds **4.3** and **4.2** have an emission band at 650 nm with quantum yields of 0.78% and 0.73%, respectively. The emission spectra of the bimetallic Re(I)-Pt(II) compounds closely resemble that of **4.6** as shown in Figure 4-7, thus can be assigned to the Pt(**py-im**)(acac) chelate unit. This observation indicates that the MLCT excited state of the Re(**py-im**) chelate unit in the bimetallic compound is fully quenched by the Pt unit via energy transfer. Perhaps because of the efficient energy transfer from the Re(I) unit to the Pt(II) unit, the emission quantum efficiency of the bimetallic compounds **4.2** and **4.3** is substantially enhanced, compared to the monomer **4.6**. The phosphorescent spectra of **3.5** and **4.4** are very similar except that **3.5** has a distinct fluorescence band at 512 nm. Thus the emission of **4.4** is also from the Pt portion of the molecule. The lack of luminescence in **4.5** can be attributed to the low-lying d-d state of the Pd(II) center that results in the Pd(II) chelate unit to be non-emissive. Intramolecular energy transfer from the Re(I) unit to the non-emissive Pd(II) unit leads to effective quenching of the emission of the Re(I) unit.

4.3.4 Theoretical Calculations

Density functional theory calculations were performed on **4.3** to better understand the electronic structure of this bimetallic compound. TD-DFT data show that the LUMO and HOMO of **4.3** reside at the Pt and the Re unit, respectively, as shown in Table 4-4, and the singlet HOMO→LUMO has a very low oscillator strength (0.0030). TD-DFT data indicate that the first triplet state is in fact dominated by HOMO→LUMO+1 transition

(91%) with LUMO+1 being localized on the Pt-chelate portion. The TD-DFT data support that the observed phosphorescence of the **4.3** compound is indeed from the Pt chelate unit. The details of the TD-DFT data are shown in Table 4-4 and Table 4-5.

Table 4-4. Isodensity surface plot of **4.3**

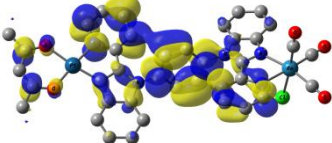
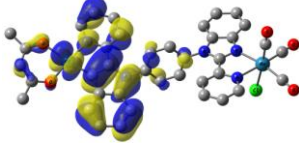
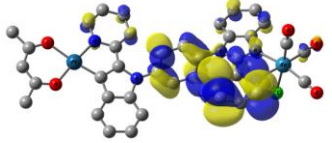
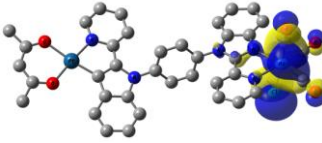
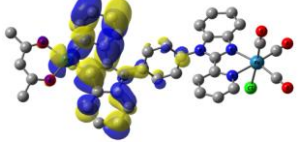
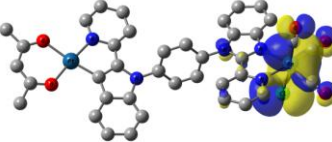
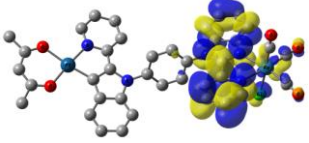
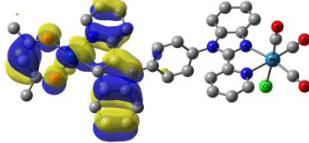
4.3	
<p>LUMO+3</p>  <p>-1.50 eV</p>	<p>HOMO</p>  <p>-5.31 eV (Pt d orbital contribution = 16%)</p>
<p>LUMO+2</p>  <p>-1.68 eV</p>	<p>HOMO-1</p>  <p>-5.45 eV (Re d orbital contribution = 38%)</p>
<p>LUMO+1</p>  <p>-2.00 eV</p>	<p>HOMO-2</p>  <p>-5.56 eV (Re d orbital contribution = 35%)</p>
<p>LUMO</p>  <p>-2.55 eV</p>	<p>HOMO-3</p>  <p>-6.05 eV (Pt d orbital contribution = 20%)</p>

Table 4-5. TD-DFT calculation results of **4.3**.

Complex	Spin state	Transition configurations	Excitation energy (nm, eV)	Oscillator strength
4.3	S ₁	HOMO-1 → LUMO (99%)	577.4 (2.15)	0.0004
	S ₂	HOMO-2 → LUMO (98%)	526.4 (2.36)	0.0539
	S ₃	HOMO → LUMO (99%)	510.9 (2.43)	0.0030
	S ₄	HOMO → LUMO+1 (91%) HOMO → LUMO+3 (3%)	453.0 (2.74)	0.0721
	S ₅	HOMO-4 → LUMO (99%)	432.0 (2.87)	0.0021
	S ₆	HOMO-2 → LUMO+2 (90%) HOMO-2 → LUMO+3 (5%)	399.1 (3.11)	0.0031
	S ₇	HOMO → LUMO+1 (2%) HOMO → LUMO+2 (55%) HOMO → LUMO+3 (37%)	393.0 (3.16)	0.1110
	S ₈	HOMO-1 → LUMO+1 (99%)	388.3 (3.19)	0.0000
	S ₉	HOMO-5 → LUMO (8%) HOMO-3 → LUMO (89%)	387.1 (3.20)	0.0059
	S ₁₀	HOMO-7 → LUMO (4%) HOMO-2 → LUMO+2 (86%) HOMO-2 → LUMO+3 (4%)	386.1 (3.211)	0.0023
T ₁	HOMO-3 → LUMO+1 (2%) HOMO → LUMO+1 (91%)	623.4 (1.99)	-	

4.3.5 Electrochemical Properties

The electrochemical redox properties of the Re(I)-containing complexes were investigated by cyclic voltammetry (CV) in dry acetonitrile under N₂ and are shown in Figure 4-8 and Table 4-6. Due to the poor solubility, CV diagrams for **4.3** and **4.5** were not recorded. The binuclear complex **4.2** displays three reduction waves at -1.73V, -2.42V and -2.18 V respectively. The two reversible/pseudo-reversible reduction waves are assigned to the reduction of 2-(2'-pyridyl)benzimidazolyl and 2-(2'-pyridyl)indole moiety chelated to two metal centers, while the irreversible wave is a Re(I)-based reduction, according to previous reports on related bipy-Re(I) compounds.^{8b} The reduction wave of mononuclear **4.1** is also shown for comparison which displays one ligand based reversible wave and one Re(I) based irreversible wave. The introduction of the Pt(II) center shifts the irreversible wave potential shift from -2.25 V to -2.18 V, increasing the electron affinity of the Re(I) center. Compound **4.4** displays one reversible reduction wave at -1.73 V which is similar to that of **4.1** and **4.2** and thus can be assigned to the reduction of 2-(2'-pyridyl)benzimidazolyl chelating ligand. The Re(I)-based reduction wave is not obvious at about -2.21 V. The 3rd reduction wave for **4.4** is not resolved. All three compounds display an oxidation wave at about 1.00 V, which can be attributed to the oxidation of the Re(I) center.²³ The oxidation peaks are shown in Figure 4-9.

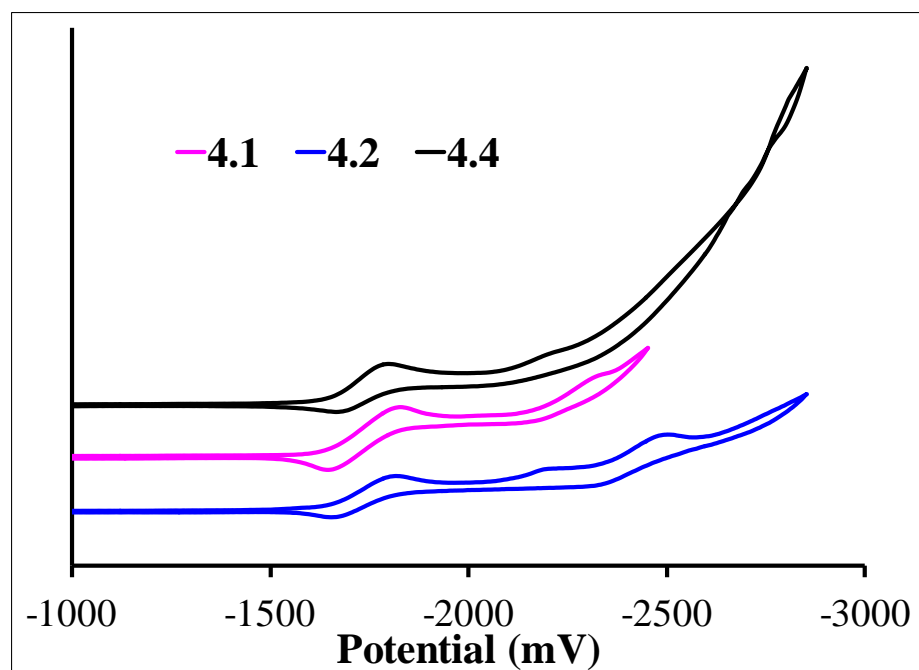


Figure 4-8. CV diagrams of **4.1**, **4.2** and **4.4**, recorded in acetonitrile, using NBu_4PF_6 as the electrolyte with a scan rate of 150 mV/s.

Table 4-6. Electrochemical data of **4.1**, **4.2** and **4.4**.

Complex	$E_{1/2}^{\text{red1}}$ (V)	E^{red} (V)	$E_{1/2}^{\text{red2}}$ (V)	$E_{1/2}^{\text{ox}}$ (V)	Electrochemical energy gap (V)
4.1	-1.73	-2.25		1.02	2.75
4.2	-1.73	-2.18	-2.42	0.97	2.70
4.4	-1.73	-2.21		1.03	2.76

All potentials are relative to $\text{FeCp}_2^{0/+}$, measured in acetonitrile, using NBu_4PF_6 as the electrolyte with a scan rate of 150 mV s^{-1} .

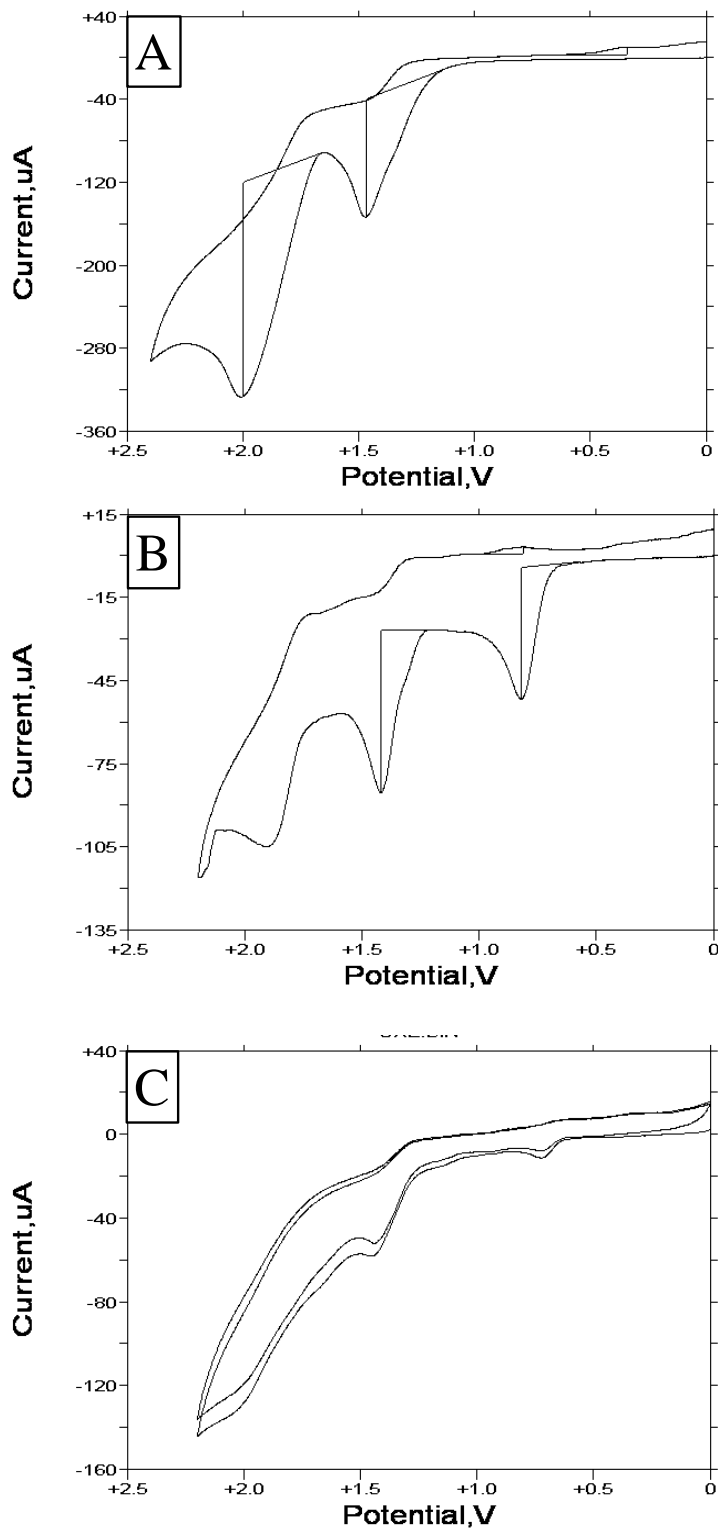
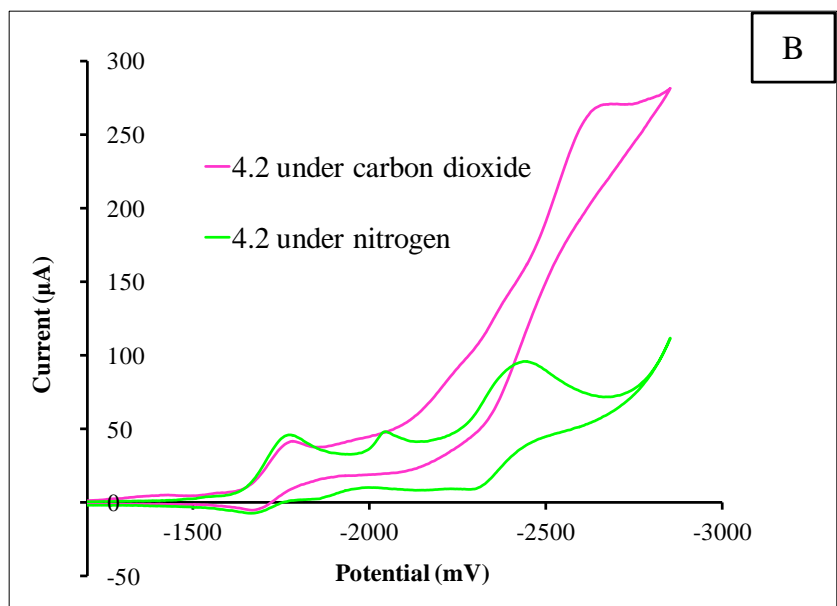
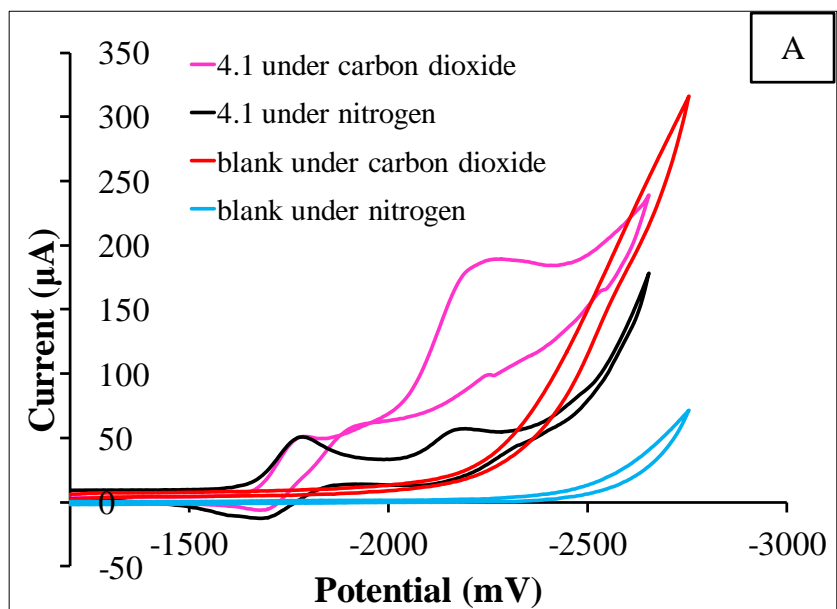


Figure 4-9. Cyclic voltammogram (oxidation peak) of metal complex (A) **4.1**, (B) **4.2** and (C) **4.4** under N_2 . Voltammograms taken at 100mV/s in acetonitrile with 0.1M NBu_4PF_6 .

One important application of tricarbonylhalorhenium(I) complexes of diimines is catalytically reduction of CO₂. In 1984 Lehn et al. reported that compound Re(bipy)(CO)₃Cl can effectively catalyze the reduction of CO₂ to CO on a glassy carbon electrode in a DMF/water mixture.^{8a} Inspired by their work, many rhenium bipyridine based systems have been extensively investigated for either electrochemical or photochemical reduction of CO₂ in the last two decades.^{7,8} To determine if our compounds have any utilities in catalytic electrochemical CO₂ reduction, we carried out a preliminary study on CO₂ reduction using our mononuclear and bimetallic rhenium complexes as the catalysts using conditions and procedures similar to those reported for Re-bipy systems^{8a, 8b, 8c} and the results are shown in Figure 4-10.

These tests were conducted in dry acetonitrile solution of the metal complexes with 0.10 M NBu₄PF₆ as electrolyte. The CV diagrams under N₂ and CO₂ were recorded and compared. As shown in Figure 4-10, when the acetonitrile solutions of the metal compounds are saturated with CO₂, a drastic change of the 2nd reduction wave was observed. Compound **4.1** shows about 3-fold increase in peak current at 100 mV/s from nitrogen to CO₂ at -2.25 V. By subtracting the contribution from the blank solution under CO₂, the net increase in peak current of **4.1** is about 2-fold. Under the same conditions, the net increase in peak current for Re(bipy-tBu)(CO)₃Cl (bipy-tBu = 4,4'-di-tert-butyl-2,2'-bipyridine) (Re(bipy)), a well known catalyst in electrochemical reduction of CO₂ is 0.36-fold. Thus, under the conditions we used, the performance of the new compound **4.1** appears to be better than Re(bipy).



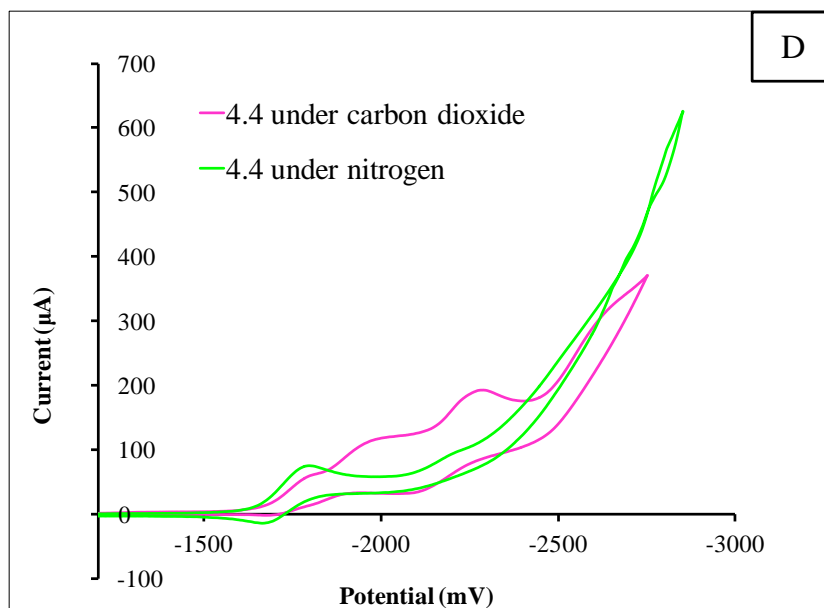
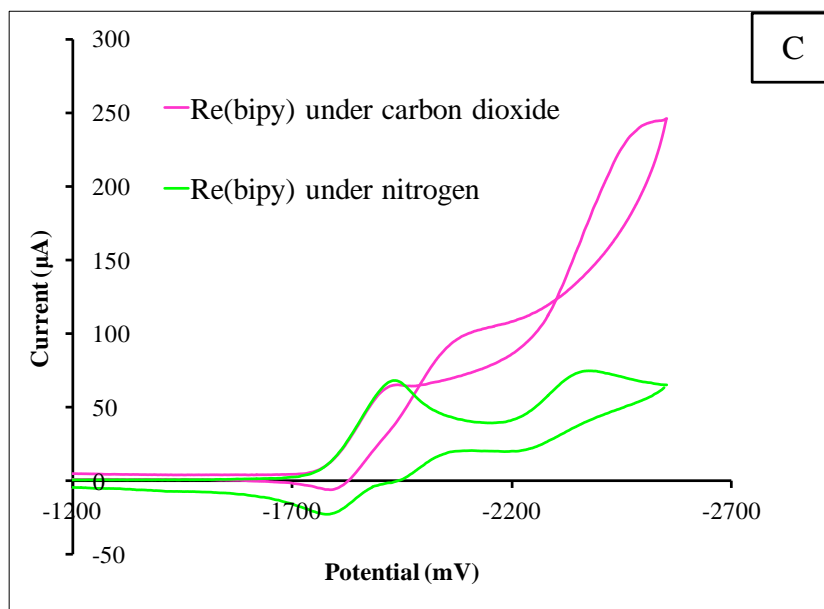


Figure 4-10. Catalytic comparison of (A) **4.1**, (B) **4.2**, (C) Re(bipy) and (D) **4.4** under both nitrogen and carbon dioxide conditions. In (A) also included a blank scan of acetonitrile solution (with no catalyst) with 0.1M NBu₄PF₆ saturated with CO₂/N₂. Voltammograms taken at 100mV/s in acetonitrile with 0.1M NBu₄PF₆

The bimetallic compounds **4.2** and **4.4** display a 0.20-fold and 0.46-fold net catalytic current increase at -2.25 V, which are similar to that of Re(bipy). The reason compound

4.1 works better than Re(bipy) may be because the more electron rich 2-(2'-pyridyl)benzimidazolyl chelating ligand makes the Re(I) center more nucleophilic toward CO₂ reduction than the simple bipyridyl moiety. For **4.2**, the introduction of the Pt center shifts the reduction potential of the Re(I) center to more positive, thus the Re(I) center becomes less electron-rich for reduction of CO₂. Over all these preliminary results indicate the ligand L1-based Re(I) complexes have the potential for use in the CO₂ reduction process.

4.4 Conclusions

Bimetallic compoexes **4.2**, **4.3**, **4.4** and **4.5** have been achieved based on ligand L1 which has two distinct chelating sites. The electronic and photophysical properties of these heterobimetallic compounds were investigated and compared with the monometallic parent compounds. Our investigation indicates that there is communication between the two different metal centers. At room temperature, the Re(I) unit is found to enhance phosphorescence efficiency of Pt(II) unit *via* efficient intramolecular energy transfer. The preliminary electrochemistry study also shows that the **4.1** is promising candidate for the electrocatalytic CO₂ reduction.

4.5 References

- (a) H. Ringsdorf, B. Schlarb, J. Venzmer, *Angew. Chem., Int. Ed.* 1988, **27**, 113; (b) J.-M. Lehn, *Angew. Chem., Int. Ed.* 1988, **27**, 89; (c) W. R. Browne, N. M. O'Boyle, J. Mc.Garvey, J. G. Vos, *Chem. Soc. Rev.* 2005, **34**, 641; (d) H. Hofmeier, U. S. Schubert, *Chem. Soc. Rev.* 2004, **33**, 373; (e) F. Würthner, C. You, C. R. Saha-Möller, *Chem. Soc. Rev.* 2004, **33**, 133; (f) M. Beley, S. Chodorowski, J.-P. Collin, J.-P. Sauvage, L. Flamigni, F. Barigelletti, *Inorg. Chem.* 1994, **33**, 2543; (g) K. J. Brewer, L. M. Vogler, *Inorg. Chem.* 1996, **35**, 818; (h) C. Chiorboli, S. Fracasso, M. Ravaglia, F. Scandola, S. Campagna, K. L. Wouters, R. Konduri, F. M. MacDonnell, *Inorg. Chem.* 2005, **44**, 8368; (i) S. Serroni, S. Campagna, R. S. Nascone, G. S. Hanan, G. J. E. Davidson, J.-M. Lehn, *Chem. Eur. J.* 1999, **5**, 3523; (j) A. Juris, L. Prodi, A. Harriman, R. Ziessel, M. Hissler, A. El-ghayoury, F. Wu, E. C. Riesgo, R. P. Thummel, *Inorg. Chem.* 2000, **39**, 3590; (k) F. Weldon, L. Hammarström, E. Mukhtar, R. Hage, E. Gunneweg, J. G. Haasnoot, J. Reedijk, W. R. Browne, A. L. Guckian, J. G. Vos, *Inorg. Chem.* 2004, **43**, 4471; (l) M. I. J. Polson, F. Loiseau, S. Campagna, G. S. Hanan, *Chem. Commun.* 2006, 1301; (m) M. Venturi, F. Marchioni, V. Balzani, D. M. Opris, O. Henze, A. D. Schluter, *Eur. J. Org. Chem.* 2003, 4227.
- (a) G. T. Higgins, B. V. Bergeron, G. M. Hasselmann, F. Farzad, T. J. Meyer, *J. Phys. Chem. B* 2006, **110**, 2598; (b) F. Farzad, D. W. Thompson, C. A. Kelly, G. J. Meyer, *J. Am. Chem. Soc.* 1999, **121**, 5577; (c) S. A. Trammell, T. J. Meyer, *J. Phys. Chem. B* 1999, **103**, 104; (d) S. A. Trammell, J. Yang, M. Sykora, C. N. Fleming, F. Odobel, T. J. Meyer, *J. Phys. Chem. B* 2001, **105**, 8895; (e) K. Westermark, H. Rensmo, A. C. Lees, J. G. Vos, H. Slegbahn, *J. Phys. Chem. B* 2002, **106**, 10108; (f) P. G. Hoertz, A. Staniszewski, A. Marton, G. T. Higgins, C. D. Incavito, A. L. Rheingold, G. J. Meyer, *J. Am. Chem. Soc.* 2006, **128**, 8234; (g) T. W. Hamann, F. Gstrein, B. S. Brunschwig, N. S. Lewis, *J. Am. Chem. Soc.* 2005, **127**, 13949; (h) F. Odobel, D. Massiot, B. S. Harrison, K. S. Schanze,

- Langmuir* 2003, **19**, 30; (i) A. C. Lees, C. J. Kleverlaan, C. A. Bignozzi, J. G. Vos, *Inorg. Chem.* 2001, **40**, 5343.
3. (a) B. O'Regan, M. Grätzel, *Nature* 1991, **353**, 737; (b) A. Hagfeldt, M. Grätzel, *Chem. Rev.* 1995, **95**, 49; (c) J. N. Demas, E. W. Harris, C. M. Flynn Jr., D. Diemente, *J. Am. Chem. Soc.* 1975, **97**, 3838; (d) H. Zabri, F. Odobel, S. Altobello, S. Caramori, C. A. Bignozzi, *J. Photochem. Photobiol. A* 2004, **166**, 99; (e) P. G. Hoertz, T. E. Mallouk, *Inorg. Chem.* 2005, **44**, 6828; (f) C. G. Garcia, J. F. de Lima, N. Y. M. Iha, *Coord. Chem. Rev.* 2000, **196**, 219; (g) N. Sabbatini, M. Guardigli, J.-M. Lehn, *Coord. Chem. Rev.* 1993, **123**, 201; (h) C. Devadoss, P. Bharathi, J. S. Moore, *J. Am. Chem. Soc.* 1996, **118**, 9635; (i) L. M. Dupray, M. Devenney, D. R. Striplin, T. J. Meyer, *J. Am. Chem. Soc.* 1997, **119**, 10243; (j) P. G. van Patten, A. P. Shreve, J. S. Lindsey, R. J. Donohoe, *J. Phys. Chem. B*, 1998, **102**, 4209; (k) V. Balzani, S. Campagna, G. Denti, A. Juris, S. Serroni, M. Venturi, *Acc. Chem. Soc. Res.* 1998, **31**, 26.
4. S. Chardon-Noblat, A. Deronzier, F. Hartl, J. van Slageren, T. Mahabiersing, *Eur. J. Inorg. Chem.* 2001, 613.
5. (a) Y. Nakabayashi, A. Omayu, S. Yagi, K. Nakamura, J. Motonaka, *Anal. Sci.* 2001, **17**, 945; (b) C. Xue, F.-T. Luo, J. Chen, H. Liu, *Anal. Chim. Acta* 2006, **569**, 27; (c) C. Zhang, T. Haruyama, E. Kobatake, M. Aizawa, *Anal. Chim. Acta* 2000, **408**, 225; (d) M. V. del Pozo, A. F. Pariente, E. Lorenzo *Anal. Chem.* 2005, **77**, 2550; (e) W. Xu, K. A. Kneas, J. N. Demas, B. A. DeGraff, *Anal. Chem.* 1996, **68**, 2605; (f) M. C. Jung, N. Munro, G. Shi, A. C. Michael, S. G. Wener, *Anal. Chem.* 2006, **78**, 1761; (g) M. K. Itokazu, A. S. Polo, N. Y. M. Iha, *J. Photochem. Photobiol. A: Chem.* 2003, **160**, 27.
6. (a) B. Carlson, G. D. Phelan, W. Kaminsky, L. Dalton, X. Jiang, S. Liu, A. K.-Y. Jen, *J. Am. Chem. Soc.* 2002, **124**, 14162; (b) P. Chou, Y. Chi, *Eur. J. Inorg. Chem.* 2006, 3319; (c) T. Albrecht, A. Guckian, J. Ulstrup, J. G. Vos, *Nano Lett.* 2005, **5**, 1451; (d) R. C. Evans, P. Douglas, C. J. Winscam, *Coord. Chem. Rev.* 2006, **250**, 2093; (e) B. Li, M. Li, Z. Hong, W. Li, T. Yu, H. Wei, *Appl. Phys. Lett.*

- 2004, **85**, 4786; (f) H. L. Wong, L. S. M. Lam, K. W. Cheng, K. Y. K. Man, W. K. Chan, C. Y. Kwong, A. B. Djuricic, *Appl. Phys. Lett.* 2004, **84**, 2557.
7. (a) H. Hori, F. P. A. Johnson, K. Koike, O. Ishitani, T. Ibusuki, *J. Photochem. Photobiol. A: Chem.* 1996, **96**, 171; (b) P. Kurz, B. Probst, B. Spingler, R. Alberto, *Eur. J. Inorg. Chem.* 2006, 2966; (c) H. Takeda, O. Ishitani, *Coord. Chem. Rev.* 2010, **254**, 346; (d) Y. Tamaki, K. Watanabe, K. Koike, H. Inoue, T. Morimoto, O. Ishitani, *Faraday Discuss.* 2012, **155**, 115.
 8. (a) J. Hawecker, J. M. Lehn, R. Ziessel, *J. Chem. Soc., Chem. Commun.* 1984, 328; (b) B. P. Sullivan, C. M. Bolinger, D. Conrad, W. J. Vining, T. J. Meyer, *J. Chem. Soc., Chem. Commun.* 1985, 1414; (c) J. M. Smieja, C. P. Kubiak, *Inorg. Chem.* 2010, **49**, 9283; (d) J. Hawecker, J.-M. Lehn, R. Ziessel, *Helv. Chim. Acta* 1986, **69**, 1990.
 9. (a) K. K.-W. Lo, W.-K. Hui, C.-K. Chung, K. H.-K. Tsang, D. C.-M. Ng, N. Zhu, K.-K. Cheung, *Coord. Chem. Rev.* 2005, **249**, 1434; (b) M.-J. Li, X. Liu, M.-J. Nie, Z.-Z. Wu, C.-Q. Yi, G.-N. Chen, V. W.-W. Yam, *Organometallics* 2012, **31**, 4459; (c) D. I. Yoon, C. A. Berg-Brennan, H. Lu, J. T. Hupp, *Inorg. Chem.* 1992, **31**, 3192.
 10. T. G. Kotch, A. J. Lees, S. J. Fuerniss, K. Papatomas, I. R. W. Snyder, *Inorg. Chem.* 1993, **32**, 2570.
 11. V. W.-W. Yam, V. C. Y. Lau, K. K. Cheung, *J. Chem. Soc. Chem. Commun.* 1995, 259.
 12. (a) R. L. Cleary, K. J. Byrom, D. A. Bardwell, J. C. Jeffery, M. D. Ward, G. Calogero, N. Armaraoli, L. Flamigini, F. Barigelletti, *Inorg. Chem.* 1997, **36**, 2601; (b) T. L. Easun, W. Z. Alsindi, M. Towrie, K. L. Ronayne, X.-Z. Sun, M. D. Ward, M. W. George, *Inorg. Chem.* 2008, **47**, 5; (c) T. Lazarides, A. Barbieri, C. Sabatini, F. Barigelletti, H. Adams, M. D. Ward, *Inorg. Chim. Acta*, 2007, **360**, 814; (d) M. Furue, M. Naiki, Y. Kanematsu, T. Kushida, M. Kamachi, *Coord. Chem. Rev.* 1991, **111**, 221; (e) S. V. Wallendael, D. P. Rillema *Coord. Chem. Rev.* 1991, **111**, 297.

13. (a) S.-S. Sun, J. A. Anspach, A. Lees, *Inorg. Chem.* 2002, **41**, 1862; (b) K. D. Benkstein, J. T. Hupp, C. L. Stern, *Angew Chemie Int Ed* 2002, **39**, 2891; (c) K. D. Benkstein, C. L. Stern, K. E. Splan, R. C. Johnson, K. A. Walters, F. W. M. Vanhelmont, J. T. Hupp, *Eur. J. Inorg. Chem.* 2002, 2818; (d) Y. Fan, L.-Y. Zhang, F.-R. Dai, L.-X. Shi, Z.-N. Chen, *Inorg. Chem.* 2008, **47**, 2811.
14. N. Wang, J.-S. Lu, T. M. McCormick, S. Wang, *Dalton Trans.* 2012, 5553.
15. G. S. Hill, M. J. Irwin, C. J. Levy, L. M. Rendina, R. J. Puddephatt, *Inorg. Synth.* 1998, **32**, 149.
16. Z. M. Hudson, B. A. Blight, S. Wang, *Org. Lett.* 2012, **14**, 1700.
17. M. J. Frisch, G. W. Trucks, H. B. Schlegel, G. E. Scuseria, M. A. Robb, J. R. Cheeseman, G. Scalmani, V. Barone, B. Mennucci, G. A. Petersson, H. Nakatsuji, M. Caricato, X. Li, H. P. Hratchian, A. F. Izmaylov, J. Bloino, G. Zheng, J. L. Sonnenberg, M. Hada, M. Ehara, K. Toyota, R. Fukuda, J. Hasegawa, M. Ishida, T. Nakajima, Y. Honda, O. Kitao, H. Nakai, T. Vreven, J. A. Montgomery, Jr., J. E. Peralta, F. Ogliaro, M. Bearpark, J. J. Heyd, E. Brothers, K. N. Kudin, V. N. Staroverov, T. Keith, R. Kobayashi, J. Normand, K. Raghavachari, A. Rendell, J. C. Burant, S. S. Iyengar, J. Tomasi, M. Cossi, N. Rega, J. M. Millam, M. Klene, J. E. Knox, J. B. Cross, V. Bakken, C. Adamo, J. Jaramillo, R. Gomperts, R. E. Stratmann, O. Yazyev, A. J. Austin, R. Cammi, C. Pomelli, J. W. Ochterski, R. L. Martin, K. Morokuma, V. G. Zakrzewski, G. A. Voth, P. Salvador, J. J. Dannenberg, S. Dapprich, A. D. Daniels, O. Farkas, J. B. Foresman, J. V. Ortiz, J. Cioslowski, and D. J. Fox, Gaussian, Inc., Wallingford CT, 2010.
18. (a) A. D. Becke, *J. Chem. Phys.* 1993, **98**, 5648; (b) C. Lee, C. W. Yang, R. G. Parr, *Phys. Rev. B* 1988, **37**, 785.
19. P. J. Hay, *J. Phys. Chem. A* 2002, **106**, 1634.
20. (a) SHELXTL Version 6.14, Bruker AXS, 2000–2003; (b) A. L. Spek, *Acta Cryst.* 2009, D65, 148; (c) Platon – A Multipurpose Crystallographic Tool, Utrecht University, Utrecht, The Netherlands, A. L. Spek, 2011.

21. J. Brooks, Y. Babayan, S. Lamansky, P. I. Djurovich, I. Tsyba, R. Bau, M. E. Thompson, *Inorg. Chem.* 2002, **41**, 3055.
22. A. Gillbert, J. Baggott, *Essentials of Molecular Photochemistry*; Blackwell: Oxford, U.K., 1991.
23. A. Klein, C. Vogler, W. Kaim, *Organometallics* 1996, **15**, 236.

Chapter 5

Pt(II) and Pd(II) Complexes Based on a *trans*-Chelating 2-(2'-Pyridyl)indolyl Derivative Ligand

5.1 Introduction

Due to the broad applications in organic synthesis,¹ catalytic processes,² biological and pharmacological usage,³ Pt(II) and Pd(II) complexes have attracted considerable research efforts. For bis-chelate Pd(II) and Pt(II) compounds, the most commonly observed binding mode is *cis*-geometry.⁴ Examples of N[^]N-*cis*-chelating Pt(II) and Pd(II) complexes with bipyridyl based ligands are well known^{5,6,7} and their use in C-H activation and catalysis have also been investigated extensively previously. In contrast, Pd(II) and Pt(II) compounds that contain a *trans*-chelating ligand are still relatively rare but interesting since they often display unusual properties,⁸ and have found use in asymmetric catalysis.⁹ During the past few decades, many *trans*-diphosphine ligands and their corresponding d⁸ metal complexes have been reported and investigated.¹⁰ Diphosphine ligands that have an intermediate or large bite angle have been found to have a significant impact on reactivity of their metal complexes.^{10o, 10p, 10q} In contrast, Pt(II) or Pd(II) compounds with *trans*-N[^]N-chelate ligands remain scarce. To our best knowledge, the only examples of *trans*-chelating bipyridyl ligands are 1,2-bis(2-pyridylethynyl)benzene and its derivatives reported previously by Bosch and others.¹¹ The use of the *trans*-PdCl₂ compound with this type of ligands in Heck coupling reactions has been investigated by several research groups.¹²

Recently we reported a class of interesting antipisomeric ligands that can readily chelate to a Cu(I) or a Zn(II) center, forming chiral coordination compounds.¹³ One of these ligands, bpib (L4), is shown in Figure 5-1, which contains two 3,3'-bis[2-(2'-py)-indolyl] binding sites. Compared to phosphine ligands, polypyridyl ligands such as L4 are much harder donors, which in turn may enhance the stability of their metal complexes toward oxidation, in addition to the possible introduction of rich photophysical/photochemical properties. Based on these considerations, our group has already synthesized and investigated the L4 based Pd(II) and Pt(II) complexes.¹⁴ We have found that both Pd(II) and Pt(II) compounds adapt an unusual *trans*-chelate geometry. In this chapter, the preliminary study on the catalytic activity of the Pd(OAc)₂-L4 (2:1) system in the acetoxylation reaction of benzene, chlorobenzene and toluene with PhI(OAc)₂ will be presented, which is a well known direct C-H bond functionalization process.¹⁵

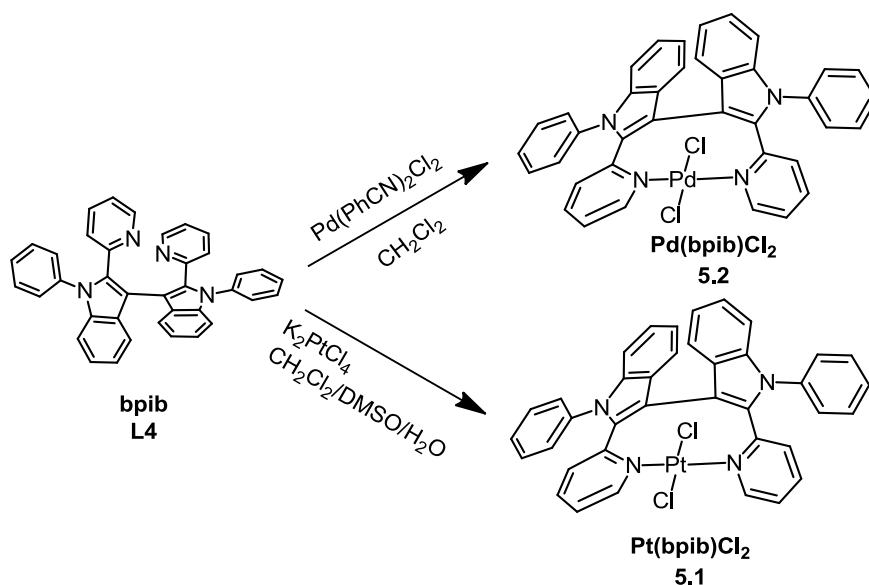


Figure 5-1. Reaction scheme for the syntheses of Pt(bpib)Cl₂ (**5.1**) and Pd(bpib)Cl₂ (**5.2**).

5.2 Experimental

5.2.1 General Considerations

All reactions were performed under dry N₂ with standard Schlenk techniques unless otherwise noted. All starting materials were purchased from Aldrich Chemical Co. and used without further purification. Solvents were freshly distilled over appropriate drying reagents under N₂ atmosphere. NMR spectra were recorded on a Bruker Avance 500 MHz spectrometer as stated. Excitation and emission spectra were recorded on a Photon Technologies International QuantaMaster Model C-60 spectrometer. UV-Vis spectra were recorded on an Ocean Optics ISS-UV-Vis spectrophotometer. Emission lifetimes were measured on a Photon Technologies International phosphorimeter (Time-Master C-631F) that was equipped with a xenon flash lamp and a digital emission photon multiplier tube, using a band pathway of 5 nm for excitation and 2 nm for emission. GC analyses were performed on an HP 6850 network FID-GC with automatic injector. The column used was an HP-5 of 30 m in length with an internal diameter of 0.32 mm. The inlet conditions were 250 °C, 25 psi and a flow rate of 28.9 mL/min using a splitless injector with helium as the carrier gas. The method used had an initial temperature of 70 °C with an immediate increase to 240 °C using a 6 °/min ramp. GC yield was determined with hexamethylbenzene acting as internal standard. Raw data for catalytic study were analyzed using GraphPad Prism version 5.00 for windows, GraphPad Software, San Diego California USA, choosing one phase association equation. Elemental analyses were performed at Canadian Microanalytical Service, Ltd. (Delta, British Columbia, Canada). Ligand L4 was prepared using methods reported previously.¹³

5.2.2 Synthesis of Pt(bpib)Cl₂ (5.1)

K₂PtCl₄ (85 mg, 206 μmol) was dissolved in DMSO/H₂O/CH₂Cl₂ (1 mL/5 mL/5 mL) mixture solvent. After stirring 30 minutes, a solution of L4 (100 mg, 187 μmol) in 3 mL CH₂Cl₂ was slowly added. The mixture was refluxed at 80°C for 6 hours. The organic layer was extracted and washed three times with water. Then solvent was removed under vacuum and the residual was re-dissolved in CH₂Cl₂. The un-dissolved Pt(DMSO)₂Cl₂ was removed out through filtration. The resulting yellow solution was allowed to slowly evaporate to afford orange powders of **5.1** with an overall yield of ~50%. This compound can be recrystallized from CH₂Cl₂. ¹H NMR in CD₂Cl₂, 500MHz (δ, ppm, 263 K): 8.77 (d, *J* = 5.6 Hz, 1H), 8.14 (d, *J* = 7.7 Hz, 1H), 7.87 (d, *J* = 7.7 Hz, 1H), 7.52-7.49 (m, 2H), 7.47 (d, *J* = 8 Hz, 1H), 7.39 (dd, *J* = 7.5 Hz, *J* = 7.5 Hz, 1H), 7.35 (dd, *J* = 7 Hz, *J* = 7 Hz, 1H), 7.27 (d, *J* = 7.5 Hz, 1H), 7.12 (dd, *J* = 7.5 Hz, *J* = 7.5 Hz, 1H), 6.98-6.95 (m, 2H), 6.73 (d, *J* = 9 Hz, 1H). Due to the poor solubility, the ¹³C NMR spectrum was not obtained. Anal calcd for C₃₈H₂₆N₄PtCl₂ • CH₂Cl₂: C, 52.66; H, 3.17; N, 6.30; found: C, 52.03; H, 3.24; N, 6.33.

5.2.3 Synthesis of Pd(bpib)Cl₂ (5.2)

A solution of 150 mg (280 μmol) of L4 in THF was layered with a solution of 108 mg of bis(phenylacetonitrile) palladium(II) dichloride (280 μmol) in ethyl acetate to give a red precipitate. The crude product was then purified by recrystallization in CH₂Cl₂. Red crystals of **5.2** were obtained in 62% yield. ¹H NMR in CD₂Cl₂, 500 MHz (δ, ppm, 263 K): 8.43 (d, *J* = 5 Hz, 1H), 7.83 (d, *J* = 10 Hz, 1H), 7.62 (dd, *J* = 7.5 Hz, *J* = 7.5 Hz, 1H), 7.54 (dd, *J* = 7.5 Hz, *J* = 7.5 Hz, 1H), 7.41 (d, *J* = 5 Hz, 2H), 7.38 (d, *J* = 5 Hz, 1H), 7.30 (d, *J* = 10 Hz, 1H), 7.26-7.18 (m, 4H), 7.10 (dd, *J* = 7.5 Hz, *J* = 7.5 Hz, 1H). Anal calcd

for $C_{38}H_{26}N_4PdCl_2 \cdot 0.25CH_2Cl_2$: C, 62.32; H, 3.62; N, 7.60; found: C, 62.32; H, 3.47; N, 7.51. Due to the poor solubility, ^{13}C NMR spectra were not obtained.

5.2.4 Pd Catalyzed Acetoxylation of Benzene-Pd(OAc)₂/2,2'-bipyridine

To a mixture of $PhI(OAc)_2$ (361 mg, 1.12 mmol), $Pd(OAc)_2$ (5.0 mg, 22.4 μ mol, 2.0 mol %) and 0.50 mL (11.2 μ mol, 1.0 mol %) of a stock solution of 2,2'-bipyridine (bipy) (35.0 mg, 224 μ mol) in 10 mL AcOH, glacial acetic acid (0.40 mL) and acetic anhydride (0.10 mL) were added. The suspension was stirred at ambient temperature for 1 min, before benzene (1.00 mL, 875 mg, 11.2 mmol, 10.0 equiv) was added. The tube was sealed and heated to 100 °C using a preheated hotplate. At the end of the reaction, the tube was cooled to ambient temperature and 1 mL EtOAc solution containing hexamethylbenzene (8.11 mg, 0.05 mmol) was added as an internal standard for quantitative GC analysis. The mixture was diluted with EtOAc (2 mL) and filtered through a plug of celite. The filtrate was extracted with a saturated aqueous solution of K_2CO_3 (9 M in H_2O , 2 \times 2 mL) to quench and separate the acid. The organic layer was carefully separated and diluted with additional EtOAc to a total volume of 25 mL. The resulting solution was analyzed by GC. This same procedure was also used for chlorobenzene and toluene acetoxylation reactions.

5.2.5 Pd Catalyzed Acetoxylation of Benzene-Pd(OAc)₂/L4

The procedure is identical to the bipy system described above. $PhI(OAc)_2$ (361 mg, 1.12 mmol), $Pd(OAc)_2$ (5.0 mg, 22.4 μ mol, 2.0 mol %), L4 (6 mg, 11.2 μ mol, 1.0 mol %), AcOH (0.90 mL), acetic anhydride (0.10 mL) and benzene (1.00 mL, 875 mg, 11.2 mmol) were reacted at 100 °C. For chlorobenzene and toluene substrates, the same procedure was used.

5.2.6 X-Ray Diffraction Analysis

Single crystals of **5.1** and **5.2** were mounted on glass fibers for data collection. Data were collected on a Bruker Apex II single-crystal X-ray diffractometer with graphite-monochromated Mo K α radiation, operating at 50 kV and 30 mA and at 180 K. Data were processed on a PC with the aid of the Bruker SHELXTL software package (version 5.10) and corrected for absorption effects. All structures were solved by direct methods. Both compounds co-crystallize with CH₂Cl₂ solvent molecules (two CH₂Cl₂ per molecule), which were modeled and refined successfully. The complete crystal structural data have been deposited at the Cambridge Crystallographic Data Center (CCDC 879680 & 879681) and reported in Table 5-1. Their selected bond lengths and angles are given in Table 5-2.

5.2.7 Theoretical Calculations

The computational calculations were performed using Gaussian09, revision B.01¹⁶ software package and the High Performance Computing Virtual Laboratory (HPCVL) at Queen's University. The ground-state geometries were fully optimized at the B3LYP¹⁷ level using LANL2DZ basis set for platinum and 6-31G(d) basis set for all other atoms.¹⁸ The initial geometric parameters in the calculations were employed from crystal structure data for geometry optimization. Time-dependent density function theory (TD-DFT) calculations were performed to obtain the vertical singlet and triplet excitation energies.

Table 5-1. Crystallographic data for complexes **5.1** and **5.2**.

	5.1	5.2
Empirical formula	C ₃₈ H ₂₆ Cl ₂ N ₄ Pt/2CH ₂ Cl ₂	C ₁₅₂ H ₁₀₄ Cl ₈ N ₁₆ Pd ₄ /8CH ₂ Cl ₂
Formula weight	974.47	3543.20
Space group	C2/c	C2/c
a, Å	17.8594(2)	17.8880(11)
b, Å	12.3237(2)	12.3483(8)
c, Å	17.4634(2)	17.3962(11)
α, deg	90	90
β, deg	103.1340(10)	102.9640(10)
γ, deg	90	90
V, Å ³	3743.04(9)	3744.6(4)
Z	4	1
Density (calculated), gcm ⁻³	1.729	1.571
μ, mm ⁻¹	4.213	0.960
2θ _{max} , deg	54.20	54.98
Reflns meads	12925	20469
Reflns used	4117	4255
(<i>R</i> _{int})	(0.0203)	(0.0184)
Final <i>R</i> [<i>I</i> > 2σ(<i>I</i>)]		
<i>R</i> 1 ^a	0.0206	0.0255
w <i>R</i> 2 ^b	0.0468	0.0654
<i>R</i> (all data)		
<i>R</i> 1 ^a	0.0230	0.0267
w <i>R</i> 2 ^b	0.0477	0.0663
GOF on <i>F</i> ²	1.061	1.069

^a $R1 = \Sigma[|F_o| - |F_c|]/\Sigma|F_o|$. ^b $wR2 = \{\Sigma[w(F_o^2 - F_c^2)]/\Sigma(wF_o^2)\}^{1/2}$. $\omega = 1/[\sigma^2(F_o^2) + (0.075P)^2]$, where $P = [\max.(F_o^2, 0) + 2F_c^2]/3$.

Table 5-2. Selected bond length (Å) and angles (°) of complexes **5.1** and **5.2**.

5.1			
Pt(1)-N(1)	2.019(2)	N(1)-Pt(1)-N(1')	164.81(12)
Pt(1)-N(1')	2.019(2)	N(1)-Pt(1)-Cl(1')	88.12(6)
Pt(1)-Cl(1')	2.3061(6)	C(19)-C(14)-N(2)	119.5(2)
Pt(1)-Cl(1)	2.3061(6)	N(1')-Pt(1)-Cl(1')	93.23(6)
N(1)-C(1)	1.350(3)	N(1)-Pt(1)-Cl(1)	93.23(6)
C(7)-C(7')	1.476(5)	N(1')-Pt(1)-Cl(1)	88.12(6)
C(8)-C(9)	1.399(4)	Cl(1')-Pt(1)-Cl(1)	169.78(4)
C(8)-C(13)	1.406(4)	C(1)-N(1)-C(5)	119.5(2)
C(14)-C(15)	1.387(4)	C(1)-N(1)-Pt(1)	123.63(18)
		C(5)-N(1)-Pt(1)	116.21(17)
5.2			
Pd(1)-N(1)	2.0205(14)	N(1)-Pd(1)-N(1')	165.08(8)
Pd(1)-Cl(1)	2.3092(4)	N(1)-Pd(1)-Cl(1)	93.22(4)
N(1)-C(5)	1.347(2)	N(1')-Pd(1)-Cl(1)	88.70(4)
N(2)-C(6)	1.400(2)	Cl(1)-Pd(1)-Cl(1')	165.23(3)
N(2)-C(14)	1.436(2)	C(5)-N(1)-C(1)	119.60(16)
C(1)-C(2)	1.385(3)	C(5)-N(1)-Pd(1)	123.97(12)
C(7)-C(7')	1.478(3)	C(1)-N(1)-Pd(1)	115.97(12)
C(8)-C(9)	1.401(3)	C(13)-N(2)-C(14)	123.91(15)
C(8)-C(13)	1.408(3)		

5.3 Results and Discussion

5.3.1 Synthesis and Structures

The ligand L4 was synthesized by our previously reported procedure.¹³ The syntheses of Pt(II) and Pd(II) complexes **5.1** and **5.2** were accomplished by the reactions shown in

Figure 5-1. The Pt(II) compound was obtained by refluxing K_2PtCl_4 and L4 in a solvent mixture of $H_2O/DMSO/CH_2Cl_2$ in a 5:1:5 ratio at 80 °C for 6 hours. The DMSO solvent molecules likely reacted with K_2PtCl_4 first to generate $Pt(DMSO)_2Cl_2$, which subsequently reacted with the L4 ligand to produce the chelate complex **5.1** which was isolated as orange crystals. Complex **5.2** was synthesized by layering an ethyl acetate solution of stoichiometric amount of $Pd(PhCN)_2Cl_2$ with a THF solution of L4 at ambient temperature. Through slow diffusion of these two layers, the chelating ligand L4 displaced the labile benzonitrile ligands to generate **5.2**, which precipitated out as a red powder. Both compounds were fully characterized by NMR and CHN analysis. Single-crystals suitable for X-ray diffraction analyses for both compounds were obtained by recrystallization of the compounds in CH_2Cl_2 .

The crystal structures of both complexes are shown in Figures 5-2 and Figure 5-3. Both molecules belong to the $C2/c$ space group with similar unit cell dimensions. Both molecules are chiral with a crystallographically imposed C_2 axis, although both enantiomers coexist in the crystal lattice. The most important feature revealed by the crystal structures is that ligand L4 is chelated to Pd(II) and Pt(II) in a rare *trans* geometry, forming a large 9-membered chelate ring. Both compounds show a considerable distortion from an ideal square-planar geometry with the $N(1) - M - N(1')$ and $Cl(1) - M - Cl(1')$ angles being $\sim 165^\circ$ to $\sim 169^\circ$. This distortion can be attributed to the strain imposed by the bis-*N*-Ph-indolyl linker on the chelate ligand, as commonly observed in many previously known *trans*-chelate complexes.^{10a, 10b, 10c} The ligand L4 has a large natural bite angle that spans a considerable range. For example, when bound to Cu(I) and Zn(II) ions,¹³ it forms distorted tetrahedral geometry with a bite angle of observed to be

137° to 141°. Thus, the *trans*-geometry of the Pt(II) and Pd(II) compounds is a consequence of the ligand's large bite angle. The Pd(1)-N(2) bond length in **5.2** is 2.0205(14) Å, which is similar to that¹¹ of *trans*-Pd[1,2-bis-(2-pyridylethynyl)benzene]Cl₂. The dihedral angle between the two indolyl rings is 103.9° for **5.1** and 104.5° for **5.2**.

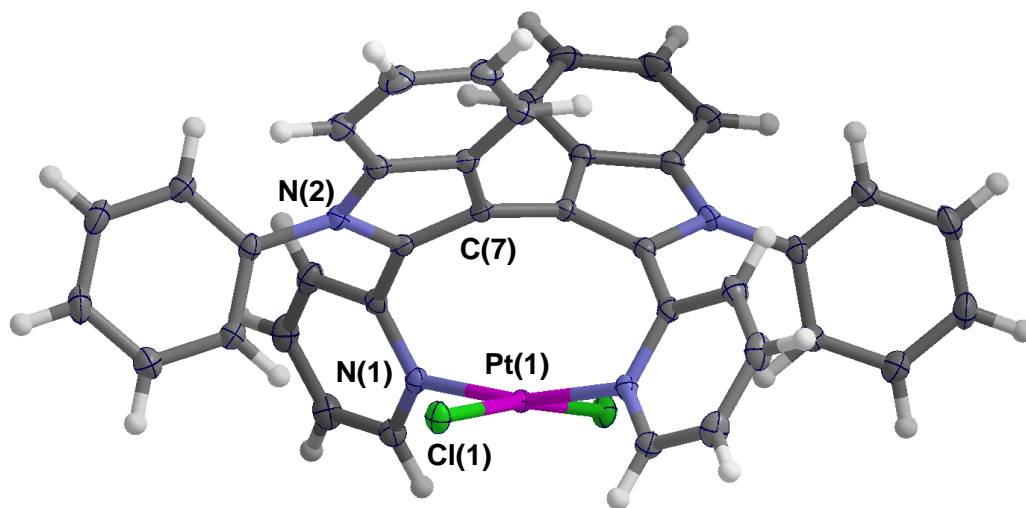


Figure 5-2. The crystal structure of **5.1** with 35% thermal ellipsoids.

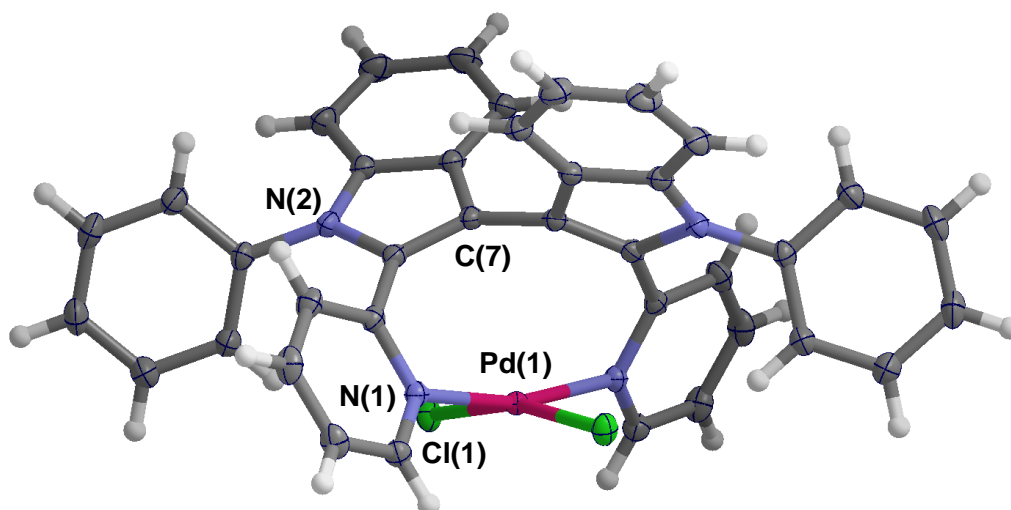


Figure 5-3. The crystal structure of **5.2** with 35% thermal ellipsoids.

5.3.2 Variable Temperature NMR

Compared to the previously known *trans*-chelating ligand, 1,2-bis(2-pyridylethynyl)benzene that has an extended conjugation and a highly rigid structure to reinforce the *trans*-geometry,¹¹ the L4 ligand has much rotational freedom, albeit having a high rotation barrier around the C(7)-C(7') bond.¹³ Previously, using DFT computational methods, we have established^{13a} that the rotation barrier of L4 around the C(7)-C(7') bond is ~92 kJ mol⁻¹. Our efforts to resolve the enantiomers of L4 were not successful.^{13a} Variable-temperature ¹H NMR spectra of **5.1** show that this complex retains its structure with no evidence of *trans-cis* isomerisation in solution. The *N*-phenyl groups show a restricted rotation in solution, caused by the *ortho*-hydrogen atom interactions between the phenyl and the pyridyl ring, as shown by the VT NMR spectra in Figure 5-4. The activation energy for the restricted rotation of the *N*-phenyl ring was estimated to be ~62 kJ mol⁻¹ using an Eyring equation (5-1),¹⁹ where T_c is coalescence temperature and Δν is the frequency separation of the initially sharp lines reading from proton NMR. The **5.2** displays a similar solution dynamics as established by VT ¹H NMR as shown in Figure 5-5, and its activation energy for the restricted rotation of *N*-phenyl ring was estimated to be ~61 kJ mol⁻¹. A similar restricted rotation of the *N*-phenyl groups was also observed in the Cu(I) and Zn(II) L4 compounds reported previously.¹³

$$\Delta G = RT_c [2.3 + \ln(T_c/\Delta\nu)] \quad (\text{Equation 5-1})$$

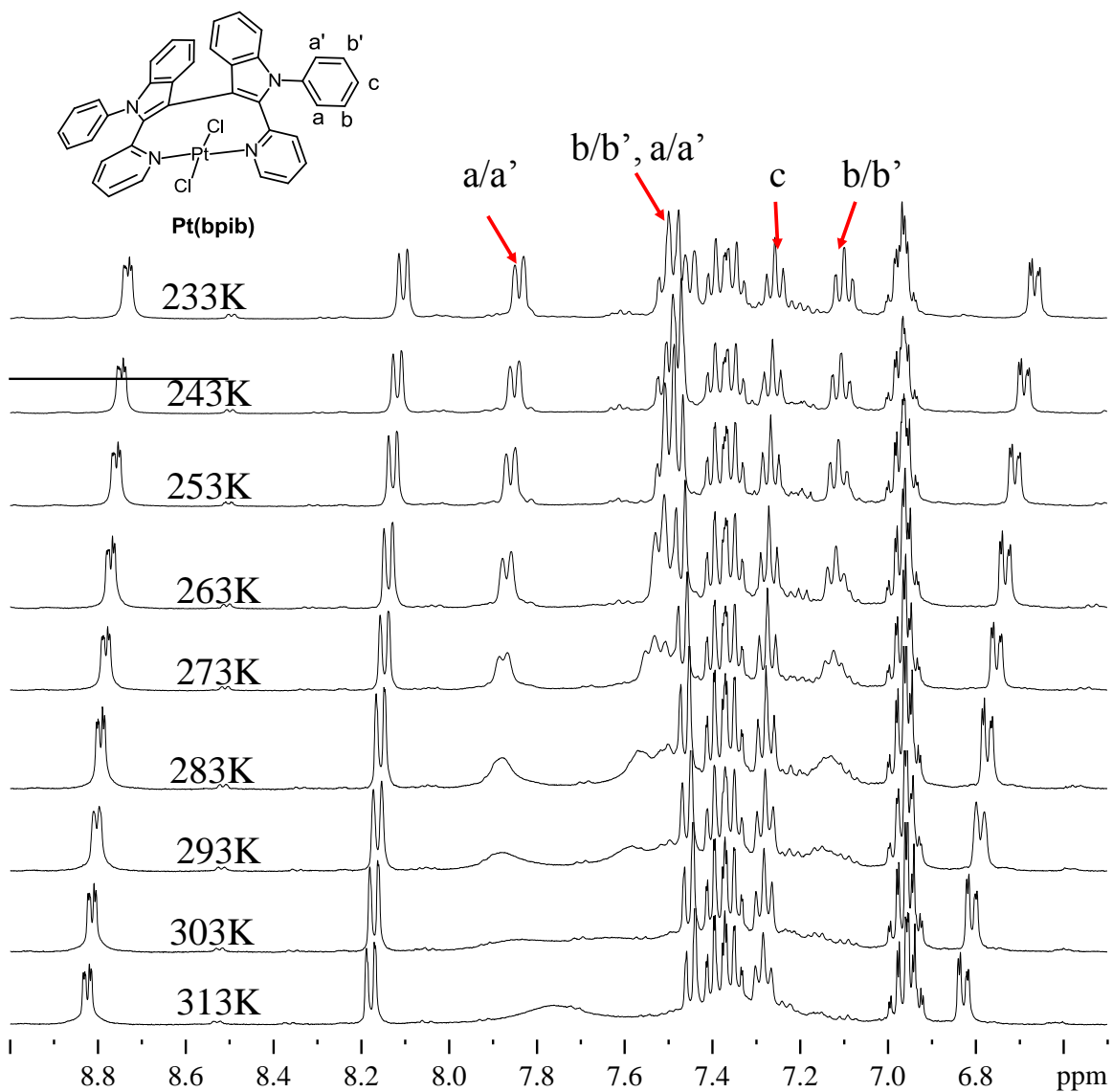


Figure 5-4. Variable temperature ^1H NMR spectra of **5.1** in CD_2Cl_2 showing the change of the *N*-phenyl proton chemical shifts with temperature. The assignments of the peaks for the *N*-phenyl protons are based on COSY NMR data.

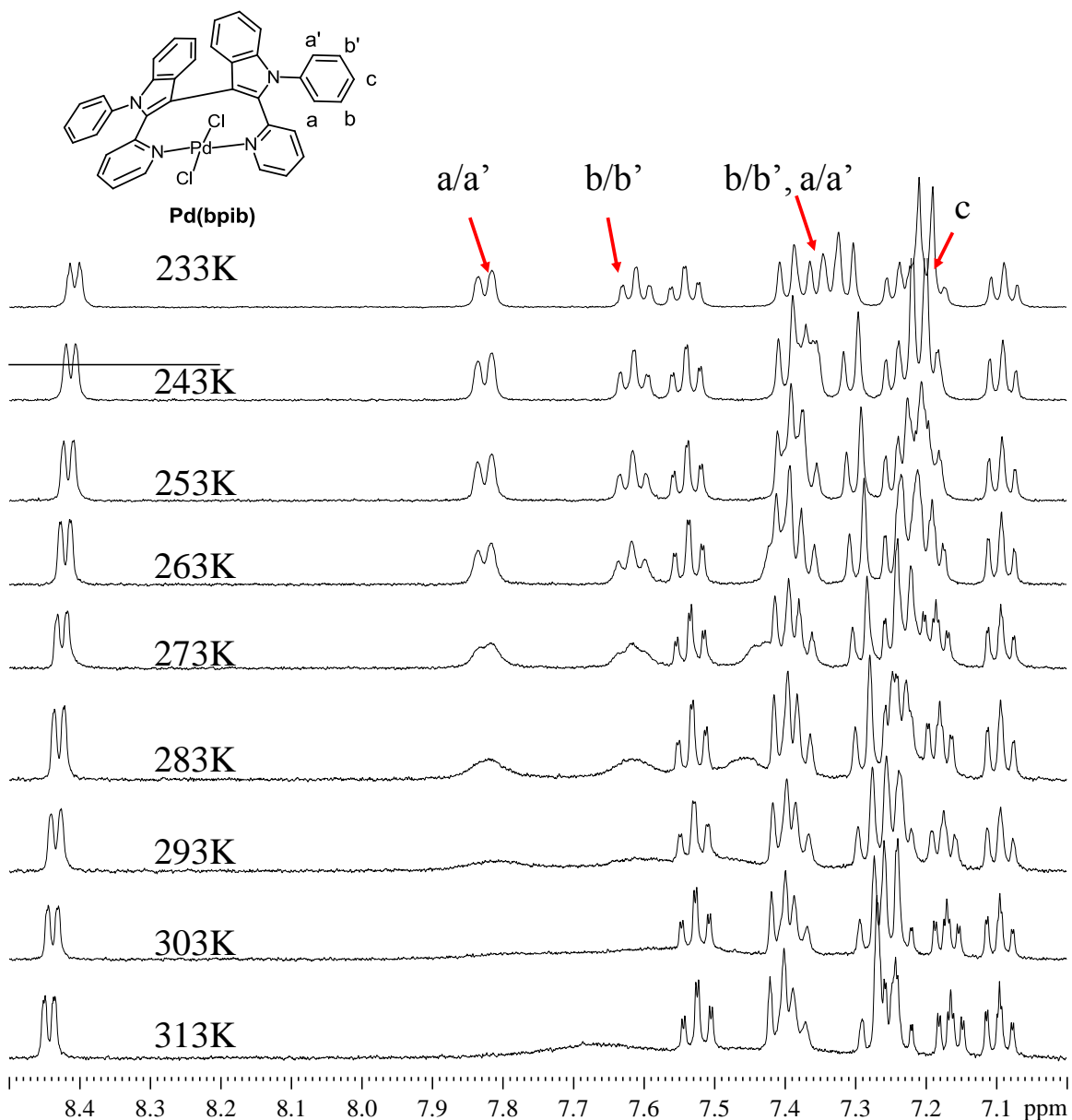


Figure 5-5. Variable temperature ^1H NMR of **5.2** in CD_2Cl_2 showing the change of the *N*-phenyl proton chemical shifts with temperature. The assignments of the peaks for the *N*-phenyl protons are based on COSY NMR data.

5.3.3 UV-Vis Absorption Spectra

The absorption spectra of L4 and the two complexes are shown in Figure 5-6 and the photophysical data are given in Table 5-3. In the absorption spectra there are intense bands at 234 nm and 310 nm for ligand L4 which were attributed to $\pi \rightarrow \pi^*$ transition. In

addition, a broad shoulder band at 340 nm is also observed which was attributed to π - π interactions of the two central pyridyl rings, based on our earlier investigation on the photophysical properties of this free ligand.¹³ The absorption spectra of **5.1** and **5.2** are similar to that of the free L4 except the presence of a well-resolved metal-to-ligand-charge-transfer (MLCT) band with a moderate intensity at ~360 nm for the Pt(II) compound and ~380 nm for the Pd(II) compound. The assignment of the MLCT band is in agreement with TD-DFT data, which shows that the first three singlet transitions all have significant MLCT contributions as shown in Table 5-4 and Table 5-5.

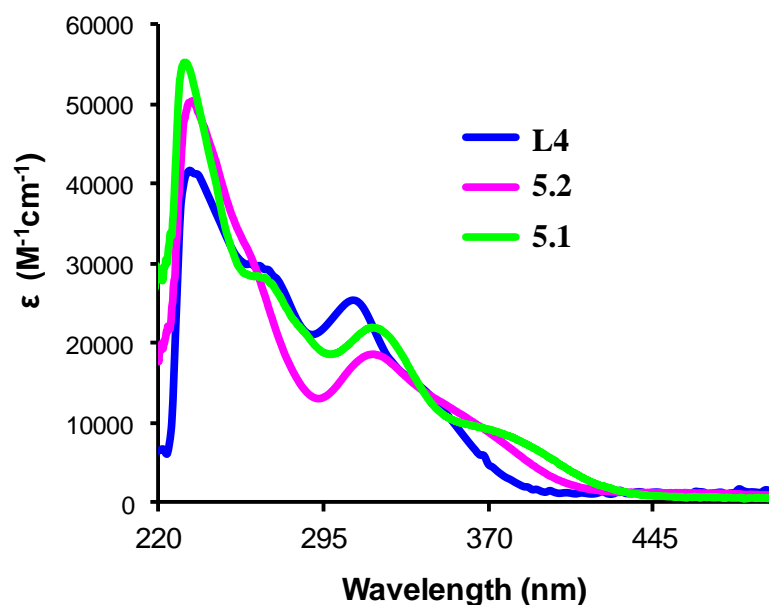


Figure 5-6. UV-Vis spectra of $\sim 1 \times 10^{-5}$ M solutions of L4, **5.1** and **5.2** recorded in CH_2Cl_2 at ambient temperature.

Table 5-3. Absorption and luminescence data.

Compound	Absorption, ^a λ_{\max}/nm ($\epsilon/ \text{M}^{-1}\text{cm}^{-1}$)	Emission, λ_{\max}/nm (quantum yield)	τ (μs)
L4	234 (41600) 268 sh (29200) 310 (25200) 340 sh (11400)	441 ^a (0.22) ^b	
5.1	233 (54600) 270 sh (27800) 319 (21900) 383 (7920)	595 ^c	231.8 \pm 2.14 ^c
5.2	237 (49500) 320 (18400) 362 (10100)		

^a in CH_2Cl_2 at 298 K, ^b determined using 9,10-diphenylanthracene as the standard, ^c at 77 K in CH_2Cl_2 with 150 μs delay.

5.3.4 Luminescence Spectrum

The free ligand L4 is blue fluorescent. Complex **5.1** does not display any luminescence in solution at ambient temperature. However, in a frozen solution of CH_2Cl_2 at 77 K, it does emit an orange color with $\lambda_{\max} = 595$ nm with a long decay lifetime, 231(2) μs , (as shown in Figure 5-7) which is attributed to a mixed ³LC and ³MLCT transition with significant d-d transition contributions, based on TD-DFT data. The unusually long decay lifetime is attributed to the involvement of the d-d transition in the first triplet state, and is responsible for the lack of ambient temperature phosphorescence in solution, due to collisional quenching by solvent molecules.^{20a, 20b} Not surprisingly, complex **5.2** shows no luminescence at either ambient temperature or at

77 K, which is common for Pd(II) complexes due to quenching by low lying d-d states.^{20c,20d}

Table 5-4. Isodensity surface plot of **5.1**

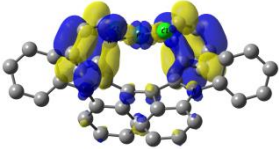
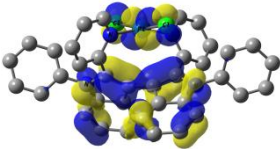
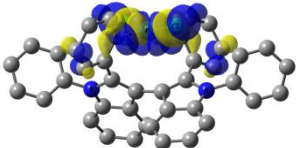
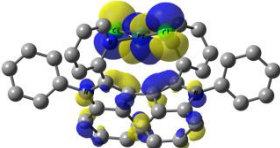
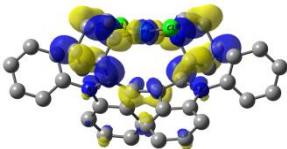
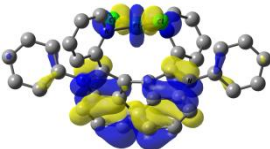
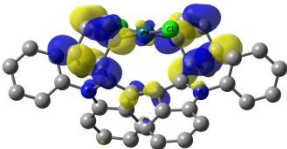
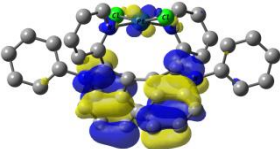
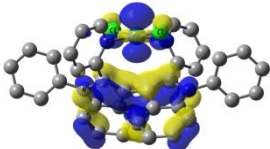
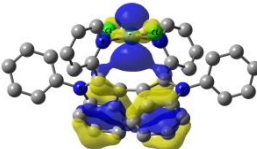
5.1	
LUMO+3	HOMO-1
	
-1.03 eV	-5.23 eV (Pt d orbital contribution = 18%)
LUMO+2	HOMO-2
	
-1.27 eV (Pt d orbital contribution = 40%, Cl p orbital contribution = 13%)	-5.57 eV (Pt d orbital contribution = 30%)
LUMO+1	HOMO-3
	
-1.58 eV	-5.83 eV
LUMO	HOMO-4
	
-1.69 eV	-5.84 eV
HOMO	HOMO-6
	
-5.19 eV (Pt d orbital contribution = 24%)	-6.29 eV

Table 5-5. Calculated energy levels of the low-lying singlet and triplet states of **5.1**.

Spin state	Transition configurations	Excitation energy (nm, eV)	Oscillator strength
S ₁	HOMO-6 → LUMO+1 (2%)	458.1 (2.71)	0.0009
	HOMO-6 → LUMO+2 (8%)		
	HOMO → LUMO+1 (31%)		
	HOMO → LUMO+2 (48%)		
	HOMO → LUMO+3 (3%)		
S ₂	HOMO-2 → LUMO+1 (8%)	453.3 (2.74)	0.0045
	HOMO-2 → LUMO+2 (25%)		
	HOMO-1 → LUMO+1 (25%)		
	HOMO-1 → LUMO+2 (32%)		
	HOMO-1 → LUMO+3 (2%)		
	HOMO → LUMO (3%)		
S ₃	HOMO → LUMO (94%)	442.5 (2.80)	0.0185
S ₄	HOMO-2 → LUMO (7%)	431.2 (2.87)	0.0051
	HOMO-1 → LUMO (90%)		
S ₅	HOMO-6 → LUMO+2 (3%)	413.3 (3.00)	0.0304
	HOMO → LUMO+1 (64%)		
	HOMO → LUMO+2 (30%)		
T ₁	HOMO-2 → LUMO+1 (7%)	606.4 (2.04)	--
	HOMO-2 → LUMO+2 (41%)		
	HOMO-2 → LUMO+3 (4%)		
	HOMO-1 → LUMO+1 (7%)		
	HOMO-1 → LUMO+2 (34%)		
	HOMO-1 → LUMO+3 (3%)		

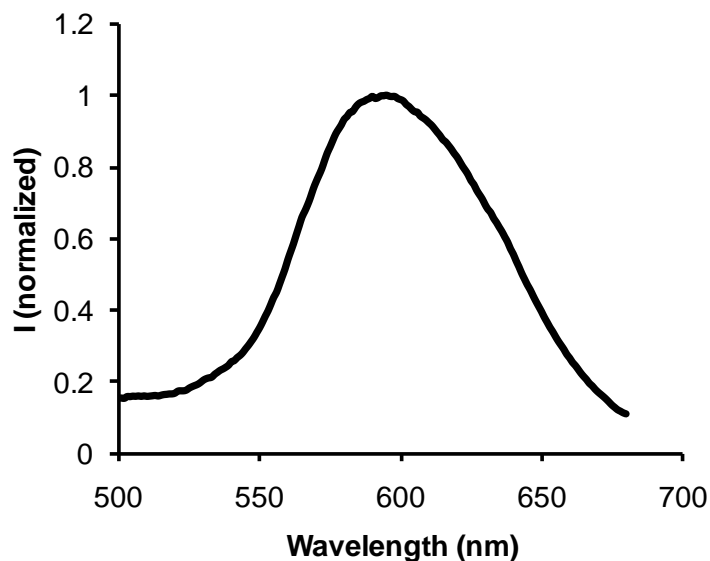


Figure 5-7. Emission spectrum of complex **5.1** in frozen CH_2Cl_2 at 77K

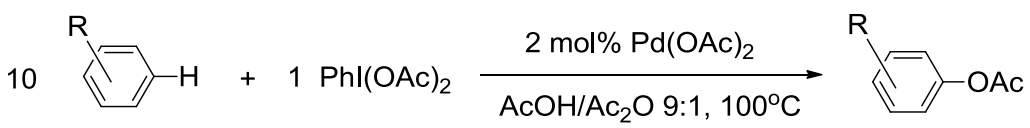
5.3.5 Reactivity of Pd(II)/L4 in Acetoxylation

To examine the impact of the *trans*-chelating ligand L4 on catalytic properties of Pd(II) compounds, we compared the catalytic activity of L4/Pd(OAc)₂ with that of 2,2'-bipy/Pd(OAc)₂ in acetoxylation of arenes using PhI(OAc)₂ as a reagent, where a C-H bond is directly functionalized by an acetoxy group.^{15,21} The choice of using Pd(OAc)₂ as the Pd reagent is based on the fact that it is commonly used in C-H bond functionalization in previous studies,^{15,21} thus providing a convenient platform for us to examine the impact of L4 on Pd catalysis. The mechanistic aspects of benzene acetoxylation using PhI(OAc)₂ as the oxidant and Pd(OAc)₂ as the catalyst have been well established previously.^{15,21} The first step of the reaction involves C-H activation at the Pd(II) center, followed by oxidation of the Pd(II) complex to high valent Pd complexes (probably binuclear Pd(III) complexes) by the oxidant. The subsequent reductive elimination generates the final product. The selection of PhI(OAc)₂ as the oxidant is based on the fact that it is a common oxidant used in previous studies,¹⁵ which

would allow us to follow the well established procedure to compare the reactivity difference of bpid with the standard bipy ligand in Pd(II) catalyzed arene acetoxylation.

Standard reaction conditions used in previously reported Pd(II) catalytic systems^{15c} were employed for our study. Previous studies have shown that the 1:2 ratio of *N*[^]*N*-chelate ligand/Pd(OAc)₂ is the best for arene acetoxylation and that the catalytic system based on Pd(OAc)₂ only is much less effective.^{15c,15e} We therefore adopt the 1:2 ratio of ligand/Pd(OAc)₂ for our study. 2,2'-bipy/Pd(OAc)₂ was used as the standard system. The reaction was carried out at 100°C for three substrates, benzene, toluene and chlorobenzene and the results are shown in Figure 5-8 and Table 5-6. The active catalyst L4-Pd(OAc)₂ is generated in situ, following previous established procedures. ¹H NMR studies show that the L4 ligand rapidly reacts with Pd(OAc)₂ to generate the L4-Pd complex as shown in Figure 5-9. Attempts were not made to fully characterize this complex.

Table 5-6. Reaction conditions and product distributions



R = H, CH₃, Cl

R	bipy	L4
	<i>ortho/metal/para</i>	<i>ortho/metal/para</i>
CH ₃	32% : 31% : 37%	25% : 34% : 41%
Cl	32% : 32% : 36%	22% : 37% : 41%

As illustrated in Figure 5-8, the use of ligand L4 for the acetoxylation of benzene appears to significantly accelerate the reaction in the first 6 hours, compared to the standard catalyst bipy/Pd(OAc)₂, and the maximum yield (~60%, calculated based on PhI(OAc)₂) is achieved after ~6 hours. This moderate yield could be attributed to the side reactions and the formation of by-products such as biphenyl, IC₆H₄OAc and C₆H₄(OAc)₂ identified by GC-MS analysis. The same phenomenon was observed in previously reported bipy/Pd(II) systems.^{15c} Black Pd(0) precipitates were also observed after about 2 hours heating, which may be responsible for side reactions such as C-C coupling reactions involving Ph(OAc), thus lowering the overall yield of acetoxylation.

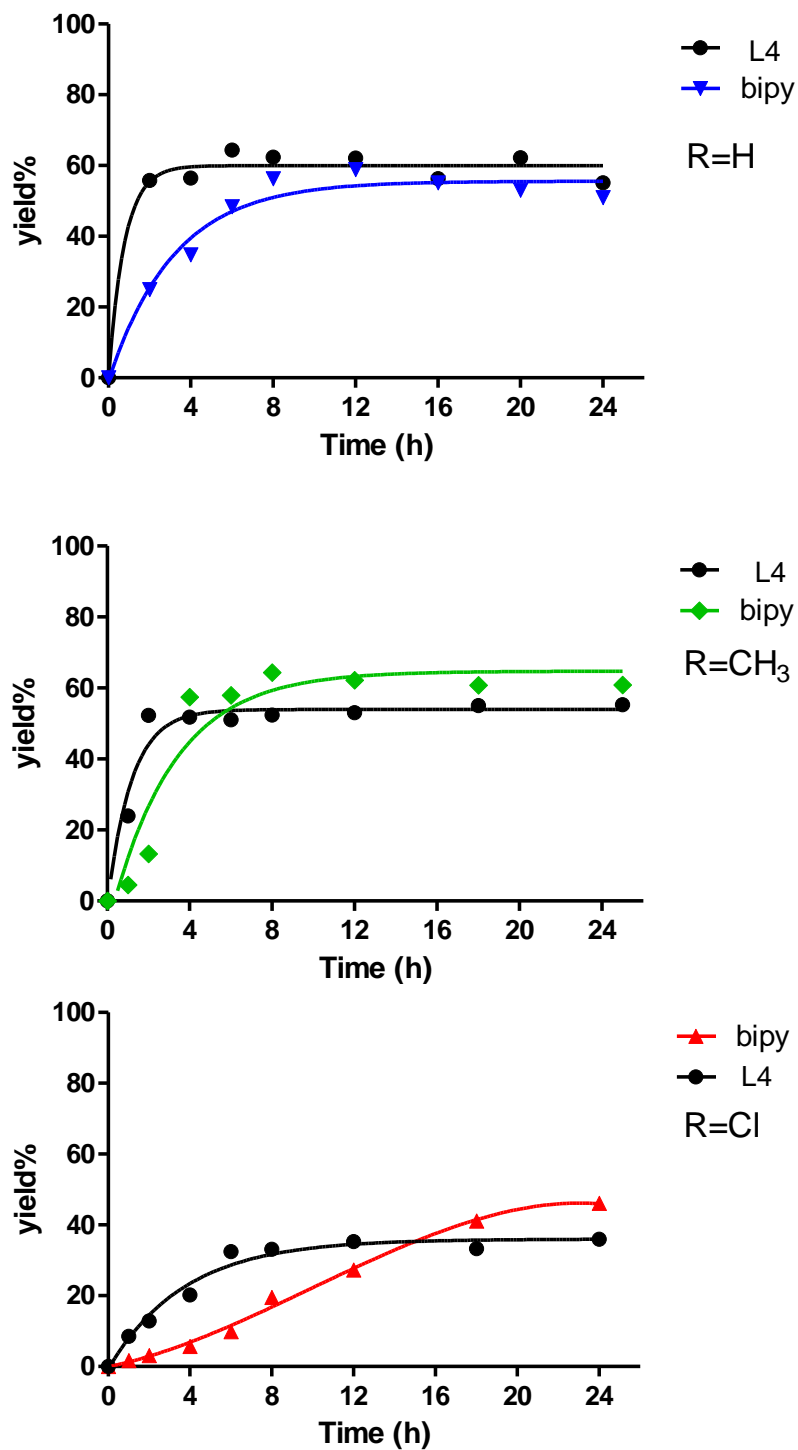


Figure 5-8. Diagrams showing the yields of acetoxylation products with time. Top: benzene substrate; Middle: toluene substrate; Bottom: chlorobenzene substrate. Catalysts: (●) Pd(OAc)₂/L4 2:1; (▼, ◆, ▲) Pd(OAc)₂/bipy 2:1. The yields are calculated based on PhI(OAc)₂, the limiting reagent.

Similar acceleration effects were also observed in the acetoxylation of toluene and chlorobenzene as shown in Figure 5-8, middle and bottom, although the overall yields obtained by the Pd(OAc)₂/L4 catalyst are again lower than the control Pd(OAc)₂/bipy catalyst for these two substrates. The product distribution study for the Pd(OAc)₂/L4 system indicated that the *p*-isomer is somewhat favored (41% for both toluene and chlorobenzene substrates), compared to the *o*-isomer (25% for toluene and 22% for chlorobenzene) and the *m*-isomer (34% for toluene and 37% for chlorobenzene). For Pd(OAc)₂/bipy system, the *p*-isomer is also slightly favored, but the yields of *o*- and the *m*-isomers are now similar.

This preliminary study shows that the new *trans*-chelating L4 ligand does have different behavior, compared to the bipy ligand in Pd(II) catalysis. For the acetoxylation reactions we examined, the L4/Pd(II) system appear to accelerate the reaction rate for the three substrates we examined, compared to the 2,2'-bipy ligand, which may be attributed to the relatively facile binding mode change of the L4 ligand from chelating to terminal facilitated by the large bite angle, thus allowing easy access of the substrate to the Pd(II) center in the C-H activation step. The low yields of the acetoxylation reactions for the substituted benzenes using L4/Pd(II), compared to 2,2'-bipy/Pd(II), may be attributed to the relatively low stability of the *trans*-L4-Pd complex, causing irreversible decomposition of the catalyst and side reactions under the reaction conditions employed.

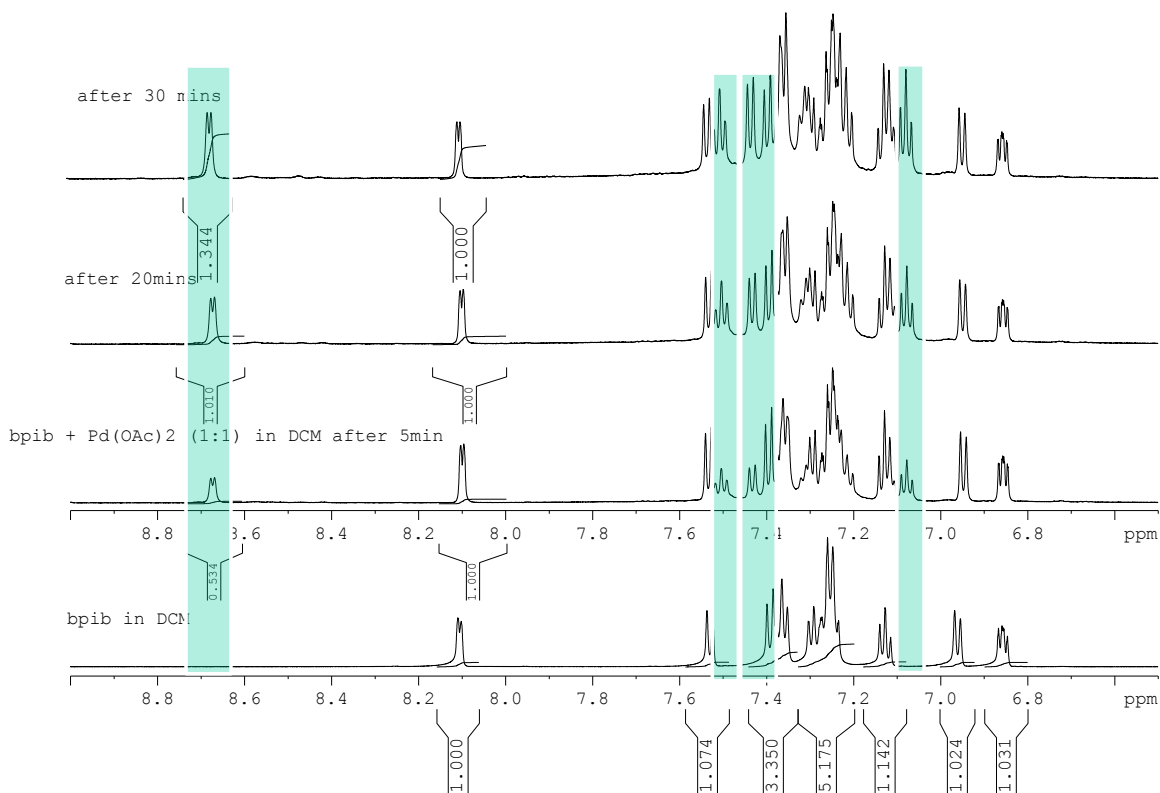


Figure 5-9. ^1H NMR spectra showing the change of L4 (bpib) chemical shift after the addition of $\text{Pd}(\text{OAc})_2$ (1:1) in CD_2Cl_2 . The peaks from the complex of L4- $\text{Pd}(\text{OAc})_2$ are highlighted in blue.

5.4 Conclusions

In summary, the L4 ligand has been found to be very effective in forming chiral *trans*-chelate Pd(II) and Pt(II) complexes. When combined with $\text{Pd}(\text{OAc})_2$ in a 2:1 ratio (Pd:L4), it accelerates the acetoxylation of benzene, toluene and chlorobenzene by $\text{PhI}(\text{OAc})_2$, but the yield is low for some of the substrates, compared to the bipy- $\text{Pd}(\text{OAc})_2$ system. If the enantiomers of the complexes can be resolved, the *trans*-L4 chelate Pd(II)/Pt(II) compounds may find applications in asymmetric catalysis, which warrants further investigation.

5.5 References

1. J. Tsuji, *Synthesis with Palladium Compounds*; Springer: Berlin, Heidelberg, New York, 1980.
2. P. M. Maitlis, *The Organic Chemistry of Palladium*, Academic Press, New York, 1971.
3. (a) B. Rosenberg, *Platinum Met. Rev.* 1971, **15**, 42; (b) M. J. Cleare, *Coord. Chem. Rev.* 1974, **12**, 349.
4. (a) P. Barbaro, C. Bianchini, G. Giambastiani, S. L. Parisel, *Coord. Chem. Rev.* 2004, **248**, 2131; (b) C. J. Elsevier, J. Reedijk, P. H. Walton, M. D. Ward, *Dalton Trans.* 2003, 1869; (c) P. E. Goudriaan, P. W. N. M. van Leeuwen, M.-N. Birkholz, J. N. H. Reek, *Eur. J. Inorg. Chem.* 2008, 2939.
5. (a) Y. Sun, N. Ross, S. B. Zhao, K. Huszarik, W.-L. Jia, R.-Y. Wang, D. Macartney, S. Wang, *J. Am. Chem. Soc.* 2007, **129**, 7510; (b) Q. Liu, R.-Y. Wang, S. Wang, *Dalton Trans.* 2004, 2073; (c) S.-W. Lai, Y. Chen, W.-M. Kwok, X.-J. Zhao, W.-P. To, W.-F. Fu, C.-M. Che, *Chem-Asian J.* 2010, **5**, 60; (d) T. Lazarides, T. M. McCormick, K. C. Wilson, S. Lee, D. W. McCamant, R. Eisenberg, *J. Am. Chem. Soc.* 2011, **133**, 350; (e) J. A. Zuleta, M. S. Burberry, R. Eisenberg, *Coord. Chem. Rev.* 1990, **97**, 47; (f) M. Hissler, W. B. Connick, D. K. Geiger, J. E. McGarrah, D. Lipa, R. J. Lachicotte, R. Eisenberg, *Inorg. Chem.* 2000, **39**, 447; (g) J. Ni, X. Zhang, N. Qiu, Y.-H. Wu, L.-Y. Zhang, J. Zhang, Z.-N. Chen, *Inorg. Chem.* 2011, **50**, 9090.
6. (a) C. M. Ong, T. J. Burchell, R. J. Puddephatt, *Organometallics* 2004, **23**, 1493; (b) F. Zhang, C. W. Kirby, D. W. Hairsine, M. C. Jennings, R. J. Puddephatt, *J. Am. Chem. Soc.* 2005, **127**, 14196; (c) F. Zhang, E. M. Prokopchuk, M. E. Broczkowski, M. C. Jennings, R. J. Puddephatt, *Organometallics* 2006, **25**, 1583; (d) F. Zhang, M. E. Broczkowski, M. C. Jennings, R. J. Puddephatt, *Can. J. Chem.* 2005, **83**, 595; (e) S. B. Zhao, G. H. Liu, D. T. Song, S. Wang, *Dalton Trans.* 2008, 6953.

7. (a) C. Bolm, M. Zehnder, D. Bur, *Angew. Chem., Int. Ed.* 1990, **29**, 205; (b) C. Bolm, M. Ewald, M. Felder, G. Schlingloff, *Chem. Ber.* 1992, **125**, 1169; (c) W.-S. Lee, H.-L. Kwong, H.-L. Chan, W.-W. Choi, L.-Y. Ng, *Tetrahedron: Asymmetry* 2001, **12**, 1007; (d) H. L. Wong, Y. Tian, K. S. Chan, *Tetrahedron Lett.* 2000, **41**, 7723; (e) G. Chelucci, G. A. Pinna, A. Saba, *Tetrahedron: Asymmetry* 1998, **9**, 531; (f) G. Chelucci, A. Saba, G. Sanna, F. Soccolini, *Tetrahedron: Asymmetry* 2000, **11**, 3427; (g) G. Chelucci, S. Chessa, G. Orrù, *J. Mol. Catal.* 2004, **220**, 145.
8. (a) I. J. S. Fairlamb, S. Tommasi, B. E. Moulton, W. Zheng, Z. Lin, A. C. Whitwood, *Eur. J. Inorg. Chem.* 2007, 3173; (b) J. Kuehnert, M. Dusek, J. Demel, H. Lang, P. Stepnicka, *Dalton Trans.* 2007, 2802; (c) B. P. Morgan, R. C. Smith, *J. Organomet. Chem.* 2008, **693**, 11; (d) L. Poorters, M. Lejeune, D. Armspach, D. Matt, *Actual. Chim.* 2009, **326**, 15; (e) Z. Freixa, M. S. Beentjes, G. D. Batema, C. B. Dieleman, G. P. F. van Strijdonck, J. N. H. Reek, P. C. J. Kamer, J. Fraanje, K. Goubitz, P. W. N. M. van Leeuwen, *Angew. Chem., Int. Ed.* 2003, **42**, 1284.
9. (a) G. Bringmann, A. J. Price Mortimer, P. A. Keller, M. J. Gresser, J. Garner, M. Breuning, *Angew. Chem., Int. Ed.* 2005, **44**, 5384; (b) C. D. Wu, W. Lin, *Angew. Chem., Int. Ed.* 2007, **46**, 1076; (c) C. D. Wu, L. Zhang, W. Lin, *Inorg. Chem.* 2006, **45**, 7278; (d) H. Shimizu, I. Nagasaki, T. Saito, *Tetrahedron* 2005, **61**, 5404; (e) M. McCarthy, P. J. Guiry, *Tetrahedron* 2001, **57**, 3809.
10. (a) R. Kuwano, T. Uemura, M. Saitoh, Y. Ito, *Bull. Chem. Soc. Jpn.* 1997, **70**, 2807; (b) J. Yin, S. L. Buchwald, *J. Am. Chem. Soc.* 2002, **124**, 6043; (c) M. R. Eberhard, K. M. Heslop, A. G. Orpen, P. G. Pringle, *Organometallics* 2005, **24**, 335; (d) L. Kaganovsky, D. Gelman, K. Rueck-Braun, *J. Organomet. Chem.* 2010, **695**, 260; (e) Z. Freixa, P. W. N. M. van Leeuwen, *Coord. Chem. Rev.* 2008, **252**, 1755; (f) N. Nasser, D. J. Eisler, R. J. Puddephatt, *Chem. Commun.* 2010, **46**, 1953; (g) Y. Canac, N. Debono, C. Lepetit, C. Duhayon, R. Chauvin, *Inorg. Chem.* 2011, **50**, 10810; (h) T. Benincori, E. Brenna, F. Sannicolò, L. Trimarco, P. Antognazza, E. Cesarotti, F. Demartin, T. Pilati, G. Zotti, *J. Organomet. Chem.*

- 1997, **529**, 445; (i) P. Antognazza, T. Benincori, S. Mazzoli, F. Sannicolo, T. Pilati, *Phosphorus Sulfur Silicon Relat. Elem.* 1999, **144**, 405; (j) T. T.-L. Au-Yeung, A. S. C. Chan, *Coord.Chem. Rev.* 2004, **248**, 2151; (k) N. Debono, Y. Canac. C. Duhayon, R. Chauvin, *Eur. J. Inorg. Chem.* 2008, 2991; (l) I. Abdellah, N. Debono, Y. Canac, L. Vendier, R. Chauvin, *Chem. Asian J.* 2010, **5**, 1225; (m) I. Abdellah, M. Boggio-Pasqua, Y. Canac, C. Lepetit, C. Duhayon, R. Chauvin, *Chem. Eur. J.* 2011, **17**, 5110; (n) R. Zhang, J. Liu, S. Wang, J. Niu, C. Xia, W. Sun, *Chem. Cat. Chem.* 2011, **3**, 149; (o) P. W. N. M. van Leeuwen, P. C. J. Kamer, J. N. H. Reek, P. Dierkes, *Chem. Rev.* 2000, **100**, 2741; (p) P. C. J. Kamer, P. W. N. M. van Leeuwen, J. N. H. Reek, *Acc. Chem. Res.* 2001, **34**, 895; (q) Z. Freixa, P. W. N. M. van Leeuwen, *Dalton Trans.* 2003, 1890.
11. (a) E. Bosch, C. L. Barnes, *Inorg. Chem.* 2001, **40**, 3097; (b) Y. Z. Hu, C. Chamchoumis, J. S. Grebowicz, R. P. Thummel, *Inorg. Chem.* 2002, **41**, 2296; (c) E. Bosch, C. L. Barnes, N. L. Brennan, G. L. Eakins, B. E. Breyfogle, *J. Org. Chem.* 2008, **73**, 3931; (c) Q. Ren, C. G. Reedy, E. A. Terrell, J. M. Wieting, R. W. Wagie, J. P. Asplin, L. M. Doyle, S. J. Long, M. T. Everard, J. S. Sauer, C. E. Baumgart, J. S. D'Acchioli, N. P. Bowling, *J. Org. Chem.* 2012, **77**, 2571.
12. (a) T. Kawano, T. Shinomauru, U. Ikuo, *Org. Lett.* 2002, **4**, 2545; (b) Y. Suzuki, K. Shimada, E. Chihara, T. Saito, Y. Tsuchido, K. Osakada, *Org. Lett.* 2011, **13**, 3774.
13. (a) T. M. McCormick, Q. Liu, S. Wang, *Org. Lett.* 2007, **9**, 4087; (b) T. M. McCormick, S. Wang, *Inorg. Chem.* 2008, **47**, 10017.
14. T. M. McCormick, **2008**. *Luminescent transition metal complexes of 2-(2'-pyridyl)benzimidazolyl and 2-(2'-pyridyl)indolyl based ligands and their applications* Ph.D. Thesis, Queen's University.
15. (a) T. Yoneyama, R. H. Crabtree, *J. Mol. Catal. A* 1996, **108**, 35; (b) L. Eberson, L. Jönsson, *J. Chem. Soc. Chem. Commun.* 1974, 885; (c) M. H. Emmert, J. B. Gary, J. M. Villalobos, M. S. Sanford, *Angew. Chem. Int. Ed.* 2010, **49**, 5884; (d) D. Kruis, B. A. Markies, A. J. Canty, J. Boersma, G. van Koten, *J. Organomet.*

- Chem.* 1997, **532**, 235; (e) M. H. Emmert, A. K. Cook, Y. J. Xie, M. S. Sanford, *Angew. Chem. Int. Ed.* 2011, **50**, 9409.
16. M. J. Frisch, G. W. Trucks, H. B. Schlegel, G. E. Scuseria, M. A. Robb, J. R. Cheeseman, G. Scalmani, V. Barone, B. Mennucci, G. A. Petersson, H. Nakatsuji, M. Caricato, X. Li, H. P. Hratchian, A. F. Izmaylov, J. Bloino, G. Zheng, J. L. Sonnenberg, M. Hada, M. Ehara, K. Toyota, R. Fukuda, J. Hasegawa, M. Ishida, T. Nakajima, Y. Honda, O. Kitao, H. Nakai, T. Vreven, J. A. Montgomery, Jr., J. E. Peralta, F. Ogliaro, M. Bearpark, J. J. Heyd, E. Brothers, K. N. Kudin, V. N. Staroverov, T. Keith, R. Kobayashi, J. Normand, K. Raghavachari, A. Rendell, J. C. Burant, S. S. Iyengar, J. Tomasi, M. Cossi, N. Rega, J. M. Millam, M. Klene, J. E. Knox, J. B. Cross, V. Bakken, C. Adamo, J. Jaramillo, R. Gomperts, R. E. Stratmann, O. Yazyev, A. J. Austin, R. Cammi, C. Pomelli, J. W. Ochterski, R. L. Martin, K. Morokuma, V. G. Zakrzewski, G. A. Voth, P. Salvador, J. J. Dannenberg, S. Dapprich, A. D. Daniels, O. Farkas, J. B. Foresman, J. V. Ortiz, J. Cioslowski, and D. J. Fox, Gaussian, Inc., Wallingford CT, 2010.
17. (a) A. D. Becke, *J. Chem. Phys.* 1993, **98**, 5648; (b) C. Lee, C. W. Yang, R. G. Parr, *Phys. Rev. B* 1988, **37**, 785.
18. P. J. Hay, *J. Phys. Chem. A* 2002, **106**, 1634.
19. J. Sandström, *Dynamic NMR Spectroscopy*, Academic Press, London 1982.
20. (a) J. D. Ingle, S. R. Crouch, *Spectrochemical Analysis*; Prentice Hall, New Jersey, 1988. J.; (b) R. Lakowicz, *Principles of Fluorescence Spectroscopy, 2nd edn*; Kluwer Academic: New York, 1999; (c) C. Bronner, A. S. Baudron, M. W. Hosseini, C. A. Strassert, A. Guene, L. De Cola, *Dalton Trans.* 2010, **39**, 180; (d) D. V. Aleksanyan, V. A. Kozlov, Y. V. Nelyubina, K. A. Lyssenko, L. N. Puntus, E. I. Gutsul, N. E. Shepel, A. A. Vasil'ev, P. V. Petrovskii, I. L. Odinet, *Dalton Trans.* 2011, 1535.
21. (a) L. Ebersson, E. Jonsson, *Acta Chem. Scand. B* 1974, **28**, 771; (b) P. M. Henry, *J. Org. Chem.* 1971, **36**, 1886; (c) A. J. Canty, M. C. Denney, G. van Koten, B. W. Skelton, A. H. White, *Organometallics* 2004, **23**, 5432; (d) E. Benazzi, C. J.

Cameron, H. Mimoun, *J. Mol. Catal.* 1991, **69**, 299; (e) N. R. Deprez, M. S. Sanford, *Inorg. Chem.* 2007, **46**, 1924.

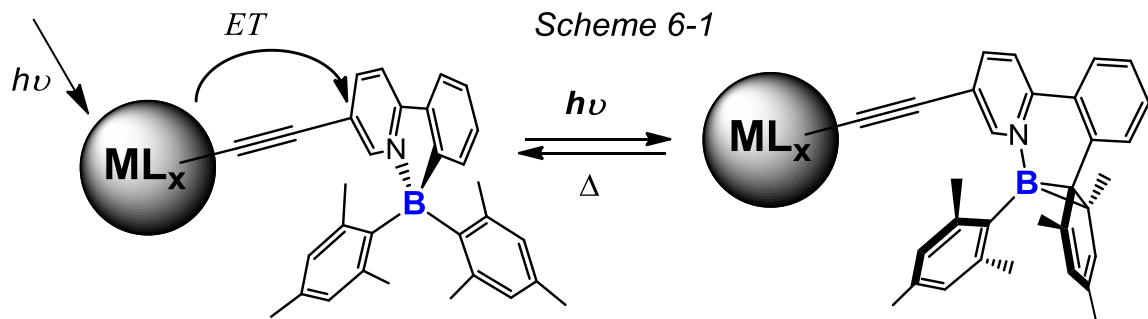
Chapter 6

Impact of Metal Acetylides on Photoisomerization of an *N*[^]C-Chelate Organoboron Compound

6.1 Introduction

N[^]C-chelate organoboranes such as B(ppy)Mes₂ (ppy = 2-phenylpyridine, Mes = mesityl) have been found recently to display thermally reversible photoisomerization, changing colors from colorless or light yellow to deep blue or green, on excitation by light.¹ This leads to new opportunities in organoboron-based photochromic materials. We have shown that by varying the *N*[^]C-chelate ligands and substituents, the colors of the dark isomers and the photoisomerization quantum efficiency of this class of boron compounds can be tuned.² The key factors that have been found to have a great impact on photoisomerization of the boron compounds are charge transfer (CT) transition from the mesityl to the chelate backbone and the steric congestions imposed by the mesityls. In order for the photoisomerization to proceed efficiently, the lowest excited state must be dominated by the CT transition. As a result, extended π -conjugation of the chelate backbone that leads to a low-lying $\pi \rightarrow \pi^*$ transition state must be avoided. The sterically bulky aryl groups such as mesityl around the boron center are necessary to enable the photoisomerization with moderate to high quantum efficiencies. We have also shown that the attachment of a Pt(II) chelate unit to the backbone can also greatly inhibit the photoisomerization owing to the introduction of a low-lying and highly emissive triplet state that effectively quenches the isomerization process.³ Nonetheless, the role of triplet states in the photoisomerization of *N*[^]C-chelate BMes₂ compounds was not understood

until a recent report from our group, in which we demonstrated the possible involvement of a photoactive triplet state in the isomerization process.⁴ By examining the impact of triplet acceptors with varying triplet energies covalently attached to a N[^]C-chelate BMes₂ chromophore *via* a non-conjugated linker on photoisomerization quantum efficiencies, we have shown that the photoisomerization of this class of boron compounds proceeds mostly likely through a triplet state. A number of well established photochromic chromophores such as diarylethenes and spiropyrans are known to isomerize through photoactive triplet states.⁵ The attachment of a transition metal unit as a triplet sensitizer in such systems has been extensively used as an effective approach to modulate the isomerization efficiency. To further understand the role of triplet states and to determine if transition metal ions can be used as triplet sensitizers for the isomerization of N[^]C-chelate BMes₂ compounds, we initiated the investigation on the influence of Re(I) ([Re(CO)₃(t-Bu₂-bipy)]⁺), Au(I) ([Au(PPh₃)]⁺) and Pt(II) ([Pt(PPh₃)₂]²⁺) metal ions on B(ppy)Mes₂ isomerization using the general system shown in Scheme 6-1. These three metal units were chosen because of their distinct triplet energies and coordination geometries. We have found that these metal ions have a distinct impact on this system and the details are presented herein.



6.2 Experimental

6.2.1 General Considerations

All reactions were performed under dry N_2 with standard Schlenk techniques unless otherwise noted. All starting materials were purchased from Aldrich Chemical Co. and used without further purification. Solvents were freshly distilled over appropriate drying reagents under N_2 atmosphere. NMR spectra were recorded on a Bruker Avance 400 MHz spectrometer as stated. Excitation and emission spectra were recorded on a Photon Technologies International QuantaMaster Model C-60 spectrometer. UV-vis spectra were recorded on a Varian Cary 50Bio UV-vis spectrophotometer. Phosphorescent lifetimes were measured on a Photon Technologies International (PTI) phosphorimeter (Time-Master C-631F) that was equipped with a xenon flash lamp and a digital emission photon multiplier tube, using a band pathway of 5 nm for excitation and 2 nm for emission.

Molecular orbital and molecular geometry calculations were performed using the Gaussian 03 program suite using crystal structure as the starting point for geometry optimizations where possible. Calculations were performed at the B3LYP level of theory using LAN2LDZ as the basis set for metal atoms, and 6-31G* for all other atoms.

Elemental analyses were performed at Elemental Analysis Service, Department of chemistry, University of Montreal (Montreal, Quebec, Canada). The syntheses of the

starting material **B1**⁶ (shown in Figure 6-1) and $[\text{Re}(\text{t-Bu}_2\text{bipy})(\text{CO})_3\text{Cl}]$ ^{7 a} were accomplished by methods previously described in the literature.

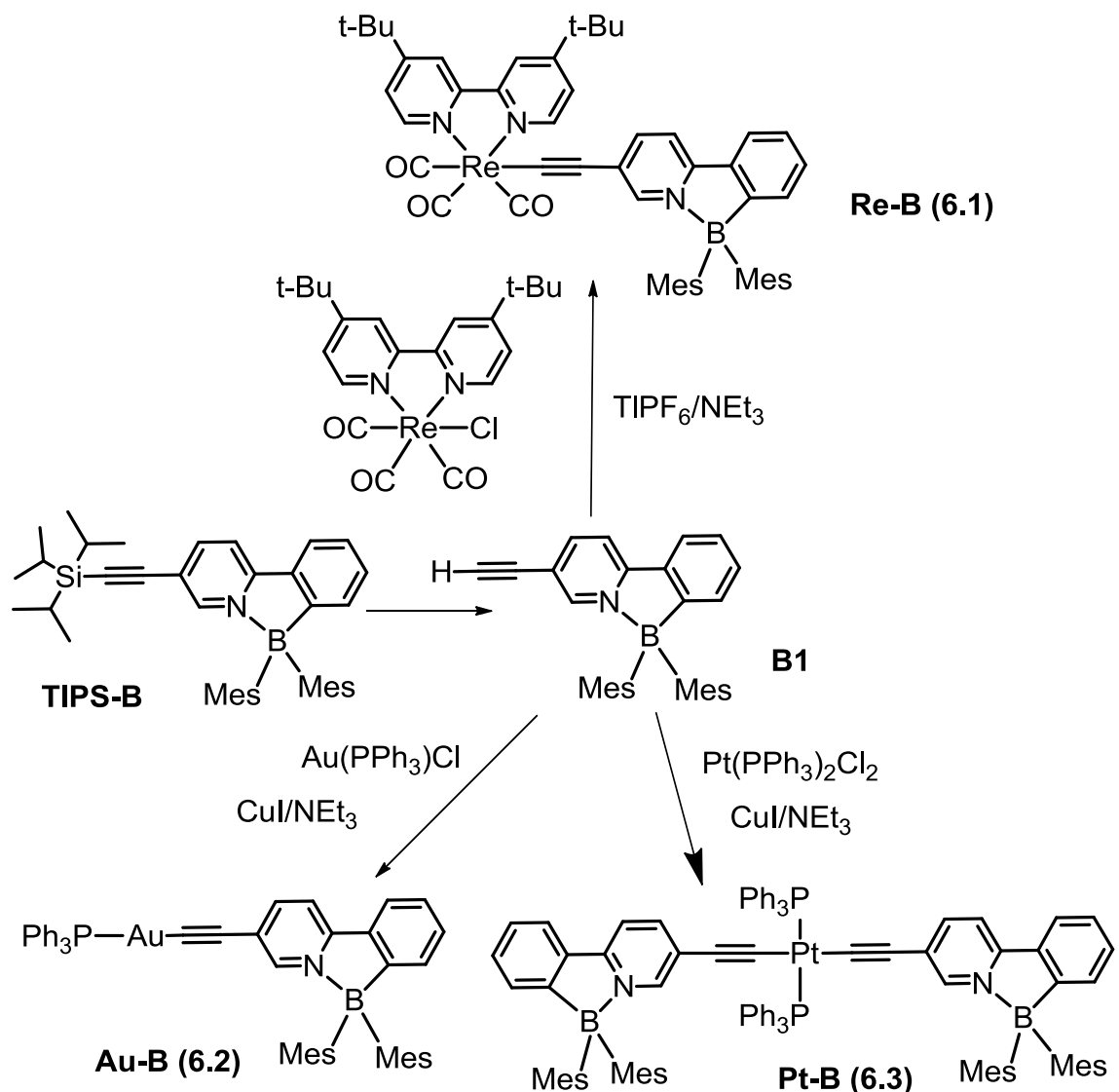


Figure 6-1. Reaction scheme for the syntheses of boron complexes.

6.2.2 Synthesis of Re-B (6.1)

A mixture of $[\text{Re}(\text{t-Bu}_2\text{bipy})(\text{CO})_3\text{Cl}]$ (140 mg, 0.24 mmol), TIPF_6 (100 mg, 0.28 mmol), Et_3N (5 mL) and **B1** (150 mg, 0.35 mmol) in 100 mL THF was refluxed under nitrogen for 2 days. Then the insoluble inorganic salt was removed through filtration and

the yellow filtrate was concentrated under vacuum. The residue is then purified by column chromatography using hexane- CH_2Cl_2 (1:1) as eluent to give analytically pure material. Recrystallization of the yellow product in CHCl_3 -hexane afforded **6.1** as yellow crystals (yield 25%). ^1H NMR (400 MHz, CDCl_3 , 298.0 K, δ , ppm): 8.96 (d, 2H, $J = 5.9$ Hz), 8.10 (s, 1H), 8.08 (d, 2H, $J = 1.7$ Hz), 7.66-7.61 (m, 4H), 7.47 (dd, 2H, $J = 5.9$ Hz, 1.9 Hz), 7.20-7.13 (m, 2H), 6.56 (s, 4H), 2.15 (s, 6H), 1.63 (s, 12H), 1.46 (s, 18H); $^{13}\text{C}\{^1\text{H}\}$ NMR (100 MHz, CDCl_3 , δ , ppm): 197.7, 192.4, 164.6, 162.9, 155.6, 154.4, 152.8, 148.1, 145.9, 143.1, 140.2, 135.3, 134.7, 133.4, 130.8, 130.4, 129.5, 124.9, 124.2, 123.0, 120.8, 119.2, 116.3, 101.2, 35.5, 30.3, 24.7, 20.6. Anal. for $\text{C}_{52}\text{H}_{53}\text{BN}_3\text{O}_3\text{Re}$: found C 64.58, H 6.17, N 3.99, calcd C 64.72, H 5.54, N 4.35.

6.2.3 Synthesis of Au-B (6.2)

A mixture of $\text{Au}(\text{PPh}_3)\text{Cl}$ (112 mg, 0.23 mmol), **B1** (100 mg, 0.23 mmol), CuI (2 mg) and Et_3N (6 mL) in 30 mL degassed CH_2Cl_2 was stirred under nitrogen in dark for 2 days. Then the mixture was concentrated in vacuum and partitioned between CH_2Cl_2 and water. The aqueous layer was further extracted with 2×20 mL of CH_2Cl_2 , dried with MgSO_4 . This was then further purified by column chromatography on silica using hexane- CH_2Cl_2 (4:1) as eluent to give this gold(I) compound as light yellow powder (yield 65%). ^1H NMR (400 MHz, CD_2Cl_2 , 298.0 K, δ , ppm): 8.48 (s, 1H), 7.99 (dd, 1H, $J = 8.3$ Hz, 1.6 Hz), 7.89 (d, 1H, $J = 8.3$ Hz), 7.83 (dd, 1H, $J = 6.5$ Hz, 2.8 Hz), 7.71 (dd, 1H, $J = 5.8$ Hz, 1.6 Hz), 7.57-7.46 (m, 15H), 7.29-7.22 (m, 2H), 6.62 (s, 4H), 2.16 (s, 6H), 1.77 (s, 12H). Anal. for $\text{C}_{49}\text{H}_{44}\text{AuBNP}$: found C 66.37, H 4.98, N 1.55, calcd C 66.45, H 5.01, N 1.58. Due to the gradual degradation of **6.2** and limited solubility issue, ^{13}C NMR spectrum is not obtained.

6.2.4 Synthesis of Pt-B (6.3)

This Pt(II) compound was prepared similarly to **6.2**, using *trans*-Pt(PPh₃)₂Cl₂ (108 mg, 0.14 mmol), **B1** (122 mg, 0.28 mmol), CuI (2 mg) and Et₃N (6 mL) in 30 mL degassed CH₂Cl₂. The mixture was purified by column chromatography on silica using hexane-CH₂Cl₂ (4:1) as eluent to give **6.3** as light yellow powder (yield 62%). ¹H NMR (400 MHz, C₆D₆, 298.0 K, δ, ppm): 8.22 (s, 1H), 8.00 (d, 1H, J = 7.4 Hz), 7.85 (dd, 6H, J = 12.8 Hz, 6.8 Hz), 7.41 (d, 1H, J = 7.4 Hz), 7.11-6.93 (m, 11H), 6.88 (d, 1H, J = 8.3 Hz), 6.77 (s, 4H), 6.66 (dd, 1H, J = 8.3 Hz, 1.5 Hz), 2.23 (s, 6H), 1.94 (s, 12H); ¹³C{¹H} NMR (100 MHz, CDCl₃, δ, ppm): 155.4, 147.2, 146.2, 142.8, 140.5, 135.7, 135.4, 135.3, 135.2, 134.1, 131.3, 131.1, 131.0, 130.7, 130.3, 128.6, 128.5, 128.4, 125.6, 121.7, 117.0, 25.2, 20.9. Anal. for C₉₈H₈₈PtB₂N₂P₂: found C 74.01, H 6.25, N 1.87, calcd C 74.86, H 5.64, N 1.78.

6.2.5 X-Ray Diffraction Analysis

Single crystal of **6.1**, **6.2**, and **6.3** were mounted on glass fibers and were collected on a Bruker Apex II single-crystal X-ray diffractometer with graphite-monochromated Mo K_α radiation, operating at 50 kV and 30 mA and at 180 K. Data were processed on a PC with the aid of the Bruker SHELXTL software package (version 5.10)⁸ and corrected for absorption effects. The structures were solved by direct methods. All non-hydrogen atoms were refined anisotropically. Disordered CH₂Cl₂ solvent molecules were located in the crystal lattice of **6.2** and modeled and refined successfully. CHCl₃ solvent molecules were located in the crystal lattice of **6.1** and were refined successfully. The positions of all hydrogen atoms were calculated and their contributions were included in structural

factor calculations. The crystal data are reported in Table 6-1. The selected bond angles and lengths are given in Table 6-2.

6.3 Results and Discussion

6.3.1 Synthesis and Structures of Metal Complexes

The new metal-functionalized B(ppy)Mes₂ compounds were synthesized according to Figure 6-1. The metal moiety was connected to the boron unit *via* an alkyne linker using procedures well established for related metal acetylide compounds.⁷ The boron parent molecule **B1** was obtained by synthesizing the **TIPS-B** compound first, then removing the TIPS group according to literature methods⁶ shown in Figure 6-1. By refluxing [Re(^tBu₂bipy)(CO)₃Cl], **B1**, TlPF₆ and Et₃N in THF, compound **6.1** was obtained in moderate yield. Compounds **6.2** and **6.3** were prepared by a copper(I)-catalyzed transmetalation reaction using **B1** with the corresponding Au(I) and Pt(II) precursors, respectively. These complexes can be purified by column chromatography. The Re(I) and Pt(II) complexes are air-stable, while the Au(I) compound undergoes gradual degradation in air. All the metal compounds are fully characterized by NMR, single-crystal X-ray diffraction, and elemental analyses.

The crystal structures of the three metal complexes are shown in Figure 6-2, Figure 6-3 and Figure 6-4, respectively. The metal ions in all three compounds display the expected geometry, i.e. octahedral for Re(I), linear for Au(I) and square planar for Pt(II). The metal-P, metal-C, B-C and B-N bond lengths in **6.2** and **6.3** are very similar. Although the B-C_{Mes} bond lengths in all three compounds are similar, the B-N bond (1.634(4) Å) in **6.1** is shorter than that in **6.2** (1.652(5) Å) and **6.3** (1.663(3) Å). This can be explained by the 18e Re(I) unit that takes less electron density away from the pyridyl

ring of the N[^]C-chelate, compared to the electron-deficient 14e Au(I) unit and the 16e Pt(II) unit. The other important feature revealed by the crystal structure is that in **6.3** compound, the two N[^]C-chelate units are coplanar and the π -conjugation is extended to the two alkyne linkers and the Pt(II) atom. In compound **6.1**, the three carbonyl ligands adopt a *facial* geometry, commonly observed for the Re(CO)₃(bipy)X units, to minimize the strong mutual *trans*-influence of the carbonyls. The Re-C(16) bond length (1.961(4) Å) is significantly longer than Re-C(14) and Re-C(15) (1.908(4) and 1.906(4) Å, respectively, which can be attributed to the greater *trans*-influence exerted by the alkyne ligand, compared to bipy. The M-C \equiv C bond angle in **6.1** and **6.2** is considerably out of linearity (167.6(3)° and 169.9(3)°, respectively). For **6.1**, the proton of the chloroform molecule forms H $\cdots\pi$ interaction with the alkyne bond with separation distances of ~2.50 Å while for **6.2**, the H atoms of the phenyl ring from PPh₃ and the mesityl ring form H $\cdots\pi$ interaction with the alkyne bond with separation distances of ~2.90-3.00 Å, as shown in Figures 6-5 and Figure 6-6. Such interactions may be responsible for the bending of the M-C \equiv C bond angle in these two compounds. The chlorine atoms of the chloroform solvent molecules also form H-bonds with protons of the mesityls in the **6.1** lattice. For **6.3**, the most significant intermolecular interactions are π -stacking between the ppy chelate units with the shortest separation distance being 3.74 Å. As a result, molecules of **6.3** all orient along one direction, forming extended π -stacked lattice as shown in Figure 6-7.

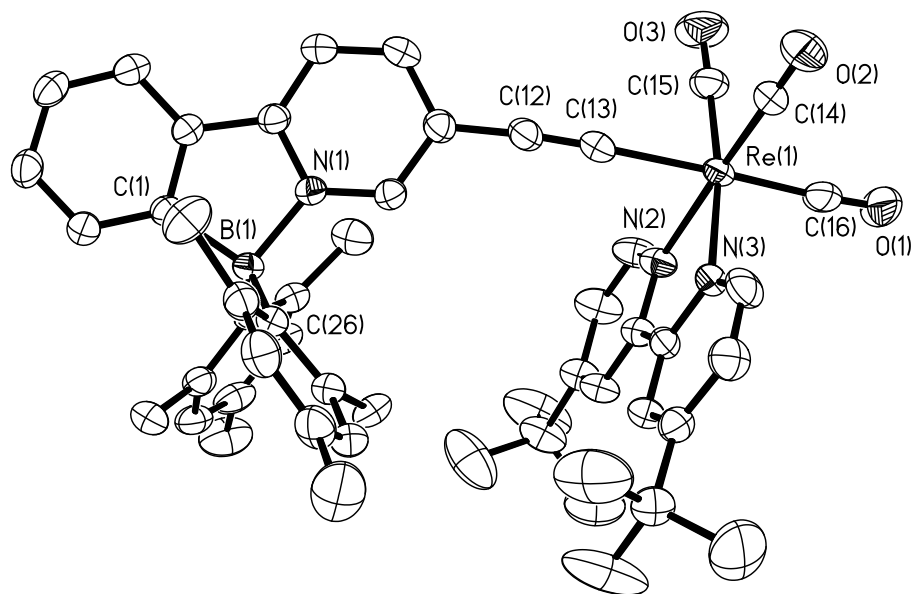


Figure 6-2. Crystal structure of **6.1** with labeling schemes for selected atoms and 50% thermal ellipsoids. Hydrogen atoms are omitted for clarity.

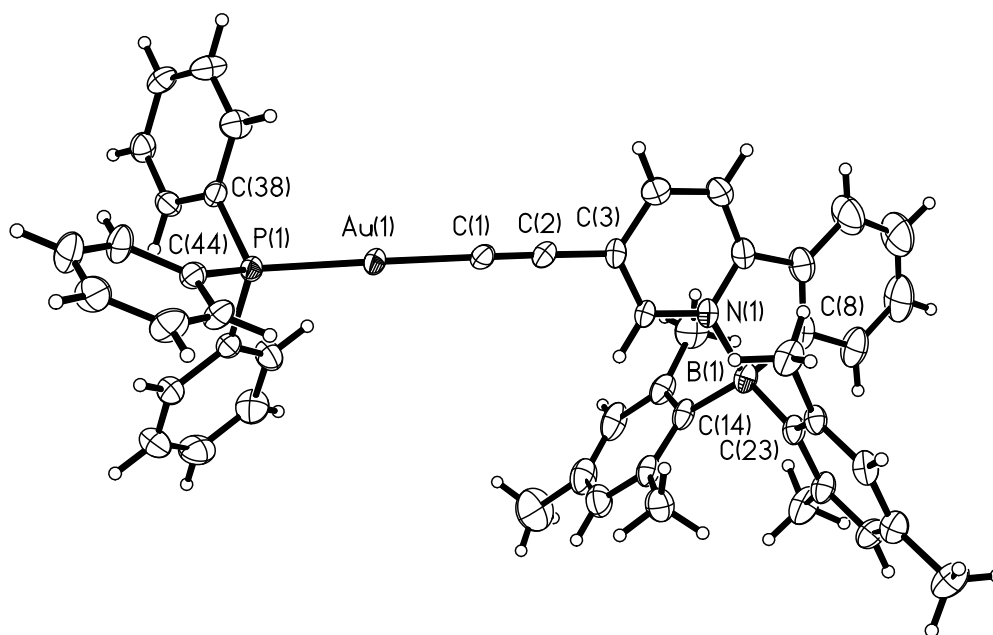


Figure 6-3. Crystal structure of **6.2** with labeling schemes for selected atoms and 50% thermal ellipsoids.

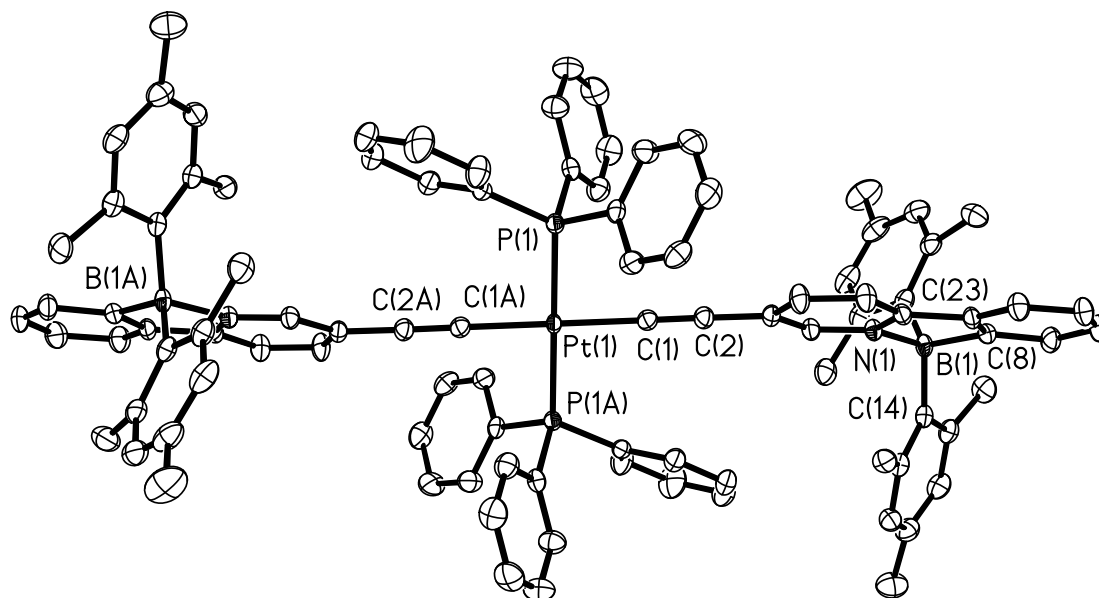


Figure 6-4. Crystal structure of **6.3** with labeling schemes for selected atoms and 50% thermal ellipsoids. Hydrogen atoms are omitted for clarity.

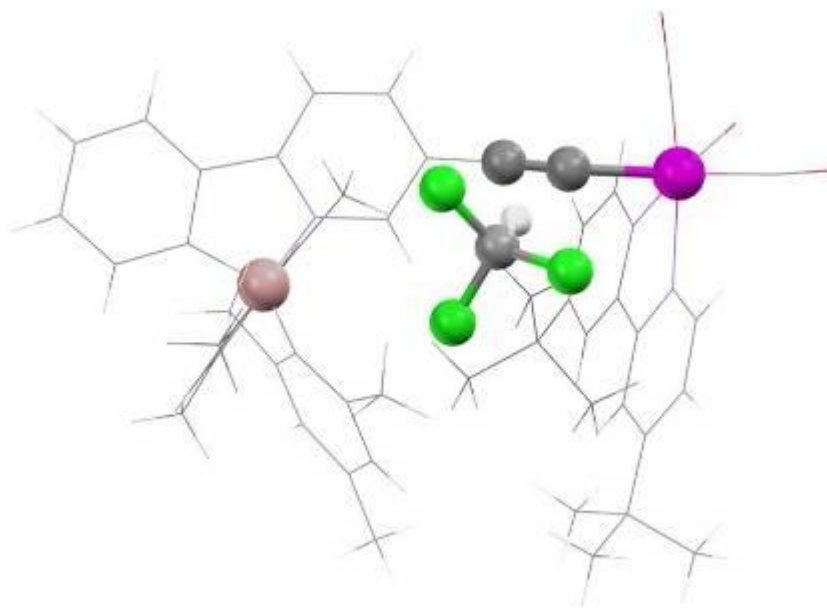


Figure 6-5. A diagram showing the H \cdots C interactions (~ 2.50 Å) between CHCl₃ and the alkyne bond in **6.1**.

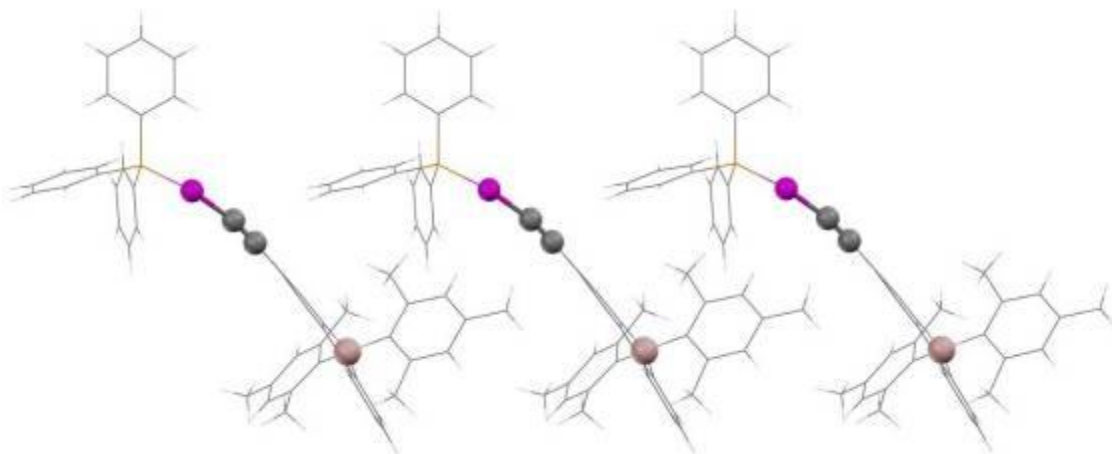


Figure 6-6. A diagram showing the relative orientation of the **6.2** molecules and the H...C interactions ($\sim 2.90 - 3.0 \text{ \AA}$) in the crystal lattice.

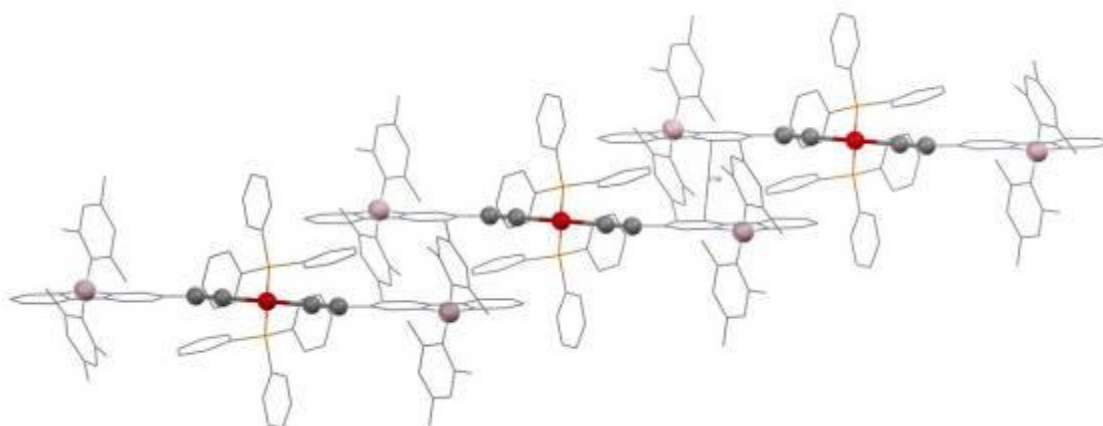


Figure 6-7. A diagram showing the π -stacking (the shortest C...C separation distance is 3.74 \AA) of **6.3** molecules in the crystal lattice.

Table 6-1. Crystallographic data for metal-boron complexes.

	6.1	6.2	6.3
Empirical formula	C52H53BN3O3Re/ 2CHCl ₃	C49H44AuBNP/1.5 CH ₂ Cl ₂	C98H88B2N2P2Pt 1962.89
Formula weight	1203.72	1009.96	1962.89
Space group	P2 ₁ /n	P-1	P-1
a, Å	13.273(16)	10.590(8)	13.703(8)
b, Å	25.084(3)	12.401(13)	14.389(8)
c, Å	16.645(2)	19.483(15)	14.591(8)
α, deg	90	80.398(10)	108.632(10)
β, deg	97.898(10)	79.707(10)	92.900(10)
γ, deg	90	70.053(10)	111.182(10)
V, Å ³	5489.2(12)	2350.8(4)	2496.6(2)
Z	4	2	1
Density (calculated), gcm ⁻³	1.457	1.427	1.306
μ, mm ⁻¹	2.549	3.367	1.491
2θ _{max} , deg	52.00	53.00	54.28
Reflns meads	53945	25215	27253
Reflns used	10783	9695	10911
(R _{int})	(0.0343)	(0.0325)	(0.0312)
Final R[I > 2σ(I)]			
R1 ^a	0.0315	0.0299	0.0284
wR2 ^b	0.0772	0.0756	0.0563
R(all data)			
R1 ^a	0.0384	0.0373	0.0297
wR2 ^b	0.0820	0.0787	0.0569
GOF on F ²	1.008	1.073	1.067

^a $R1 = \sum[|F_o| - |F_c|]/\sum|F_o|$. ^b $wR2 = \{\sum[w(F_o^2 - F_c^2)]/\sum(wF_o^2)\}^{1/2}$. $\omega = 1/[\sigma^2(F_o^2) + (0.075P)^2]$, where $P = [\max.(F_o^2, 0) + 2F_c^2]/3$.

Table 6-2. Selected bond lengths (Å) and angles (°) of metal containing boron complexes

6.1			
Re(1)-C(15)	1.906(4)	C(15)-Re(1)-C(14)	86.57(17)
Re(1)-C(14)	1.908(4)	C(15)-Re(1)-C(16)	90.44(16)
Re(1)-C(16)	1.961(4)	C(14)-Re(1)-C(16)	90.24(17)
Re(1)-C(13)	2.118(3)	C(15)-Re(1)-C(13)	86.02(15)
Re(1)-N(3)	2.178(3)	C(14)-Re(1)-C(13)	95.99(14)
Re(1)-N(2)	2.187(3)	C(16)-Re(1)-C(13)	172.63(16)
B(1)-N(1)	1.634(4)	C(15)-Re(1)-N(3)	171.85(13)
B(1)-C(1)	1.642(5)	C(14)-Re(1)-N(3)	97.29(14)
B(1)-C(26)	1.643(5)	C(16)-Re(1)-N(3)	96.70(13)
B(1)-C(17)	1.657(5)	C(13)-Re(1)-N(3)	86.43(11)
C(1)-C(2)	1.400(5)	C(15)-Re(1)-N(2)	101.79(14)
C(7)-N(1)	1.363(4)	C(14)-Re(1)-N(2)	170.88(14)
C(11)-N(1)	1.340(4)	C(16)-Re(1)-N(2)	93.31(14)
		C(15)-Re(1)-N(2)	101.79(14)
		N(1)-B(1)-C(1)	95.3(2)
		N(1)-B(1)-C(26)	103.3(2)
		C(1)-B(1)-C(26)	123.3(3)
		N(1)-B(1)-C(17)	114.5(3)
		C(1)-B(1)-C(17)	104.0(2)
		C(26)-B(1)-C(17)	115.1(3)
		C(2)-C(1)-B(1)	133.5(3)
		C(6)-C(1)-B(1)	110.3(3)
		C(12)-C(13)-Re(1)	167.6(3)
		C(22)-C(17)-B(1)	127.5(3)

6.2

Au(1)-P(1)	2.2728(9)	C(1)-Au(1)-P(1)	171.86(11)
Au(1)-C(1)	2.000(4)	C(8)-B(1)-N(1)	95.3(3)
B(1)-C(14)	1.636(6)	C(14)-B(1)-C(23)	115.8(3)
B(1)-C(23)	1.655(6)	Au(1)-C(1)-C(2)	169.9(3)
B(1)-C(8)	1.638(6)	C(44)-P(1)-C(38)	104.94(17)
B(1)-N(1)	1.652(5)	C(44)-P(1)-Au(1)	118.06(12)
B(1)-C(23)	1.655(6)	C(14)-B(1)-C(8)	123.7(3)
N(1)-C(7)	1.339(4)	C(14)-B(1)-N(1)	103.6(3)
N(1)-C(6)	1.352(5)	N(1)-B(1)-C(23)	115.0(3)
P(1)-C(44)	1.811(4)		

6.3

Pt(1)-C(1)	2.002(2)	C(1')-Pt(1)-C(1)	180.0(9)
Pt(1)-P(1)	2.314(5)	C(1')-Pt(1)-P(1)	92.3(6)
P(1)-C(32)	1.823(2)	C(1)-Pt(1)-P(1)	87.7(6)
P(1)-C(44)	1.825(2)	C(1')-Pt(1)-P(1')	87.7(6)
P(1)-C(38)	1.831(2)	C(1)-Pt(1)-P(1')	92.3(6)
N(1)-C(7)	1.348(2)	P(1)-Pt(1)-P(1')	180.0(3)
N(1)-B(1)	1.663(3)	C(32)-P(1)-Pt(1)	112.8(7)
B(1)-C(8)	1.633(3)	C(44)-P(1)-Pt(1)	111.3(7)
B(1)-C(14)	1.646(3)	C(7)-N(1)-B(1)	128.1(17)
B(1)-C(23)	1.653(3)	C(6)-N(1)-B(1)	111.8(16)
C(1)-C(2)	1.205(3)	C(8)-B(1)-C(14)	107.5(17)
C(2)-C(3)	1.441(3)	C(8)-B(1)-C(23)	121.6(18)
C(14)-C(19)	1.421(3)	C(14)-B(1)-C(23)	113.8(17)
Pt(1)-C(1')	2.002(2)	C(8)-B(1)-N(1)	95.6(15)
		C(14)-B(1)-N(1)	113.0(16)
		C(23)-B(1)-N(1)	103.9(16)
		C(2)-C(1)-Pt(1)	176.8(19)
C(9)-C(8)-B(1)	110.9(17)	C(13)-C(8)-B(1)	132.7(2)

6.3.2 UV-Vis Absorption Spectra

All absorption spectra were measured in the degassed CH_2Cl_2 solvents at room temperature. The data are shown in Table 6-3 and Figure 6-8. For comparison, the spectrum of **TIPS-B** is also shown in Figure 6-8. The absorption spectrum of **6.1** complex can be assigned by comparing with previously known Re(I) α,α' -diimine complexes^{9,7b} and N^C chelate four coordinate boron complexes.^{3,6,10} The absorption band at 270-360 nm is attributed to a mixture of intraligand $\pi \rightarrow \pi^*$ transitions centered on the diimine and alkynyl ligands. The low energy absorptions at about 370-420 nm can be assigned to a mixture of charge transfer transition from the mesityl groups to the π -conjugated backbone and $[\text{d}\pi(\text{Re}) \rightarrow \pi^*(\text{diimine})]$ metal-to-ligand charge transfer (MLCT) transitions with strong intensity, which are not well resolved. This enhanced MLCT transition can be explained by the incorporation of acetylide ligand. As a strong σ -donating ligand, the d-n state energy of the rhenium(I) center can be raised by the acetylide moiety compared to the weak ligand, such as chloride, and thus the population of MLCT state can be improved.⁹ Additionally, some $[\pi(\text{C}\equiv\text{C}) \rightarrow \pi^*(\text{diimine})]$ alkynyl-to-diimine ligand to ligand charge transfer probably mixed with this MLCT transition and constituted the absorption tail covering the 420-460 nm.

As observed in many previously reported Pt(II) phosphine acetylide complexes, **6.3** displays no MLCT bands.¹¹ Instead, an intense absorption band at around 395 nm was observed which is assigned as a ligand-centered (LC) transition of the two conjugated acetylide-B(ppy)Mes₂ units with contributions from both mesityl to chelate charge transfer and $\pi \rightarrow \pi^*$ transition of the backbone. The strong absorption intensity and the red

shift of the absorption energy compared to **TIPS-B** and **6.2** are clearly caused by the extended conjugation of the backbone through the Pt(II) center.

The absorption spectrum of **6.2** shows absorptions at 270-325 nm and 330-455nm. By comparing to the absorption spectra of previously known Au(I) acetylide systems¹² and the boron unit^{3,6,10} the high energy absorptions are assigned as $\pi \rightarrow \pi^*$ transitions involving the alkyne and PPh₃, while the low energy bands are attributed to the charge transfer from the mesityl groups to the chelate backbone.

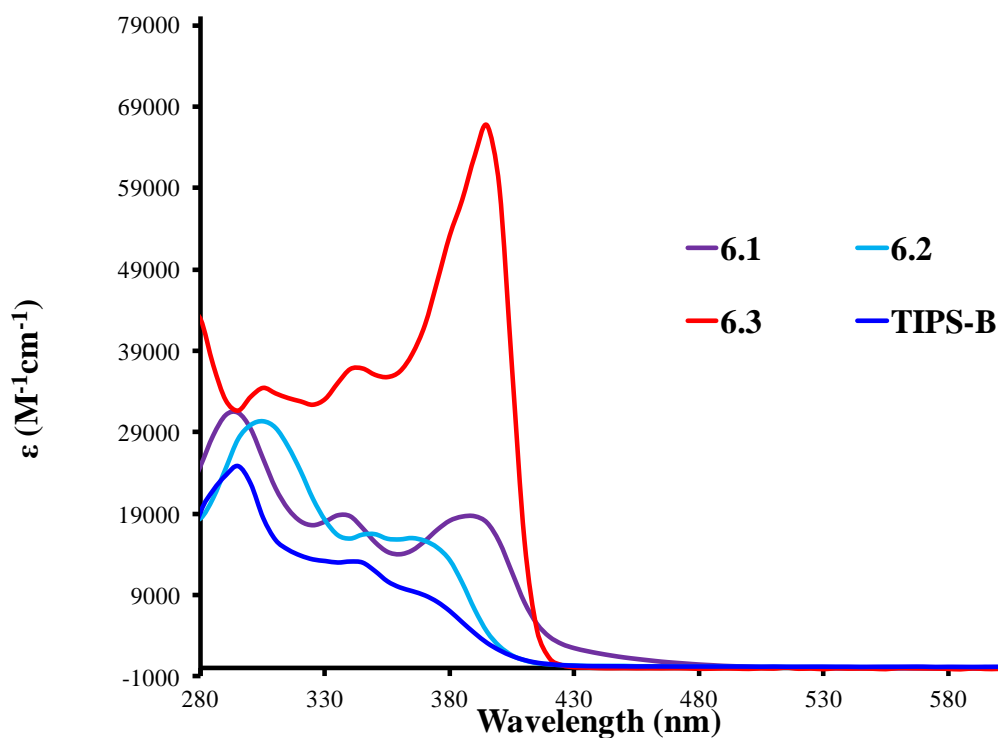


Figure 6-8. UV-Vis spectra of $\sim 1 \times 10^{-5}$ M solutions of boron complexes recorded in CH_2Cl_2 at ambient temperature.

6.3.3 Luminescence Spectra

Luminescence spectra at room temperature and 77 K were recorded for all complexes in degassed toluene solvents and shown in Figure 6-9 and Figure 6-10, respectively.

Upon excitation at 388 nm, the **6.1** displays a featureless broad emission peak with λ_{max}

at 615 nm at room temperature. With reference to other rhenium(I) acetylide complexes,⁹ this orange-red emission is assigned as a $^3\text{MLCT} [d\pi(\text{Re})\rightarrow\pi^*(\text{diimine})]$ transition, which can be also confirmed by its oxygen-sensitive property as shown in Figure 6-11. At 77K, the **6.1** complex shows bright luminescence with λ_{max} at 520 nm. Because the emission spectrum has a very long decay lifetime with well resolved vibrational feature and resembles the 77 K fluorescence spectrum of **TIPS-B**³ (The phosphorescence of **TIPS-B** could not be recorded at 77 K.) it can be assigned phosphorescence localized on the boron unit.

At room temperature the **6.3** compound displays a dual emission upon excitation at 390 nm. It is known that in platinum(II)-containing phenyl-ethynyl oligomers the spin-orbital coupling constant highly depends on the ligand length.¹³ With the increasing of the ligand length, the spin-orbit coupling decreases, since the S_0 - S_1 transition is more localized on the conjugated ligand and correspondingly further away from the metal center. Based on this consideration, both emission bands are assigned as ligand-centered transitions. The high-energy fluorescence emission band at $\lambda_{\text{max}} = 480$ nm is attributed to the mesityl to the chelate backbone charge transfer transition of the boron unit, while the low-energy band located at 520 nm is assigned as phosphorescence of the chelate backbone due to its sensitivity toward oxygen (as shown in Figure 6-12). This triplet state emission nature can be also confirmed by the time-resolved phosphorescence spectra as shown in Figure 6-13 at ambient temperature. At 77K, this Pt(II) compound displays a phosphorescent emission peak that resembles that of **6.1** as shown in Figure 6-10, with energy similar to the phosphorescent peak at ambient temperature, thus further confirming its $^3\pi\rightarrow\pi^*$ transition nature, localized on the conjugated backbone.

Table 6-3. Photophysical data for boron compounds.

Compounds	Absorption λ_{\max}/nm ($\epsilon/\text{M}^{-1}\text{cm}^{-1}$) ^a	Emission		τ (μs) ^e	
		$\lambda_{\max}/\text{nm}, \Phi_{\text{phos}}^{\text{d}}$		298 K ^b	77 K ^c
6.1	290(31100)	615	520	< 1	2500 (1)
	335 (18800)	(0.015)			
	390 (18700)				
6.2	305 (30400)	493	493	<1	1428 (1)
	345 (16500)	(0.082)			
	370 (15700)				
6.3	305 (34400)	452	516	<1	294 (1)
	345 (36700)	520 sh	556 sh		
	395 (66600)	(0.015)			
TIPS-B	295 (24800)	495	482		0.48(1)
	345 (12900)	(0.42) ^f			
	375 (8090)				

Conditions: ^a All the spectra of $\sim 1 \times 10^{-5}$ M solutions of metal complexes were recorded in degassed CH_2Cl_2 at ambient temperature. ^b All the spectra of $\sim 1 \times 10^{-5}$ M solutions of metal complexes were recorded in degassed toluene at room temperature. ^c All the spectra of $\sim 1 \times 10^{-5}$ M solutions of metal complexes were recorded in 2-methyltetrahydrofuran at 77K. ^d Degassed *fac*-Ir(*ppy*)₃ in 2-methyltetrahydrofuran ($\Phi = 0.97$)¹⁴ was used as a reference for quantum efficiency measurements. ^e The decay lifetimes were obtained by fitting the decay curve with a single exponential function.

Upon excitation at 365 nm, **6.2** displays a broad emission band with maximum peak at 490 nm at ambient temperature. By comparing to previously reported Au(I) acetylide complexes¹⁵ and **TIPS-B** and related boron compounds,^{3,6} this broad band is assigned to a mesityl to the chelate backbone CT transition mixed with phosphorescence of the Au(I) unit, as supported by the time-resolved phosphorescence spectrum at ambient

temperature (Figure 6-13). At 77K, the emission spectrum of **6.2** resembles those of **6.1** and **6.3** with a very long decay lifetime, which is also assigned as a $^3\pi\rightarrow\pi^*$ transition localized on the conjugated backbone.

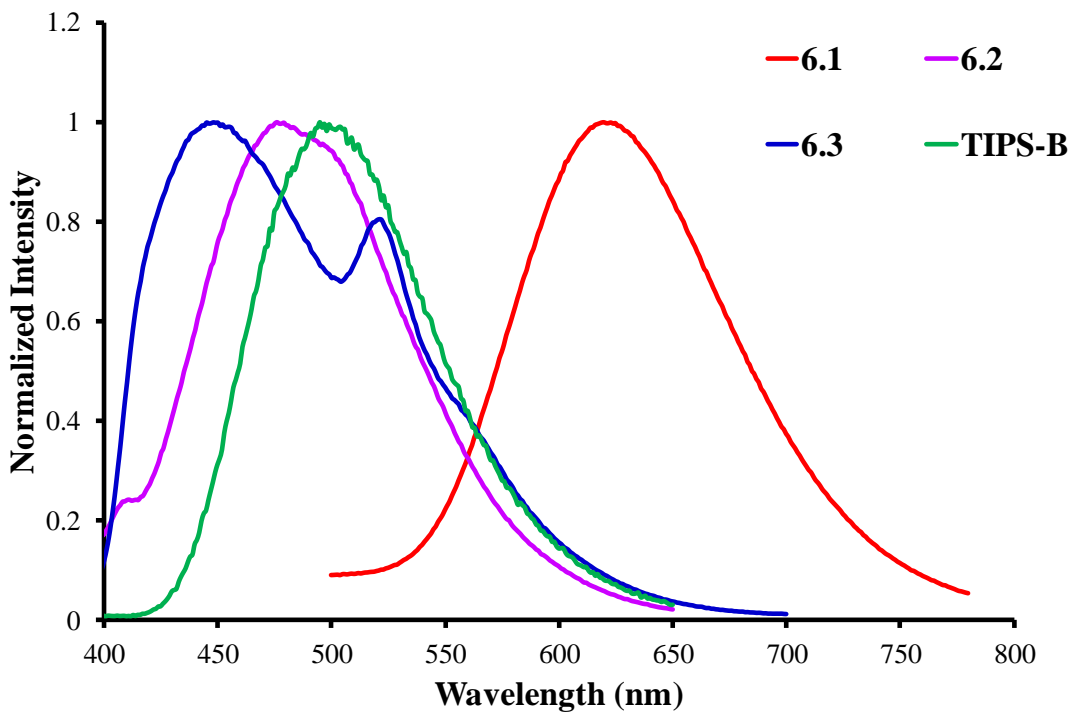


Figure 6-9. Emission spectra of $\sim 1 \times 10^{-5}$ M solutions of compounds recorded in toluene at ambient temperature under nitrogen.

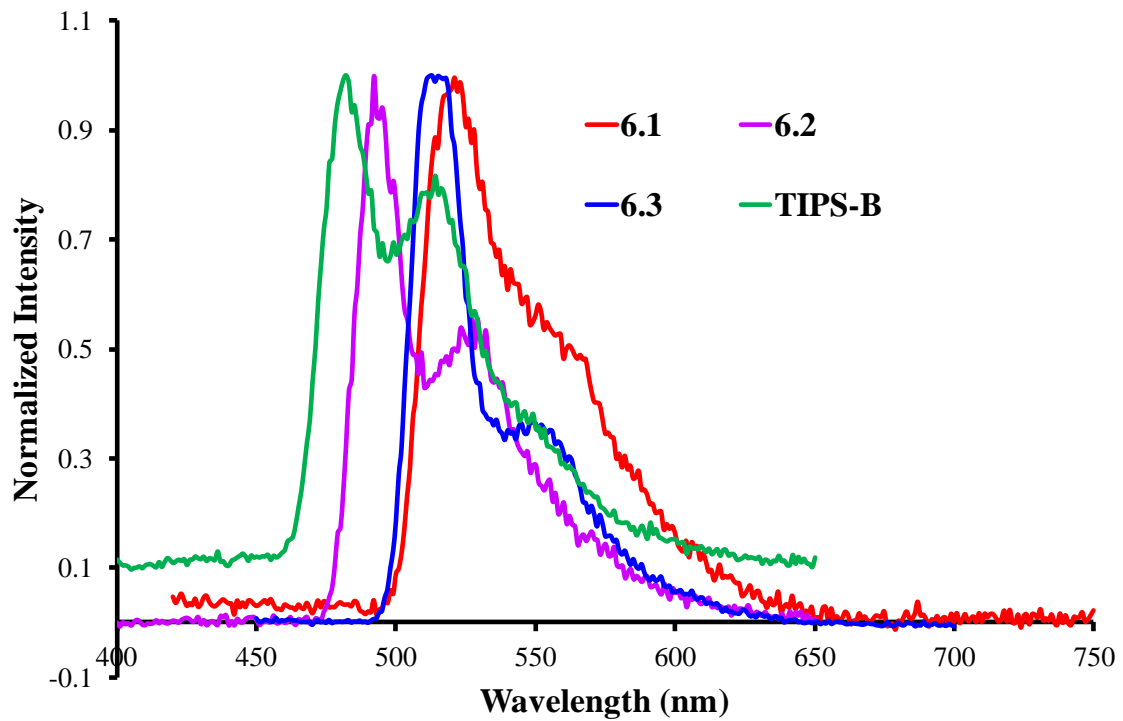


Figure 6-10. Time-resolved phosphorescence spectra of metal complexes and fluorescence spectrum of **TIPS-B** in 2-methyltetrahydrofuran at 77K.

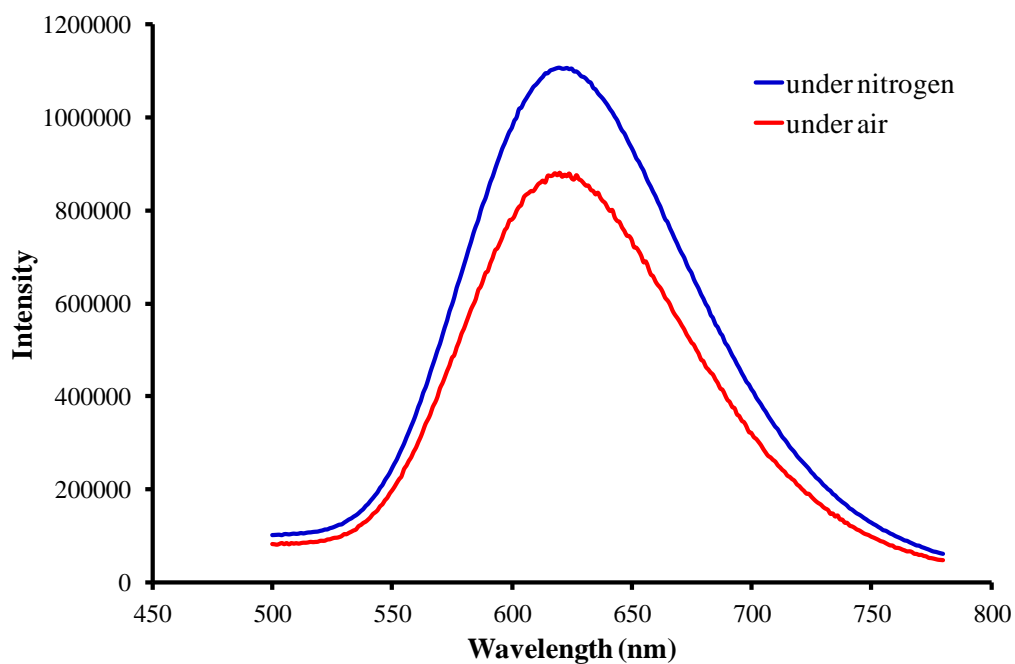


Figure 6-11. Phosphorescent spectral change of **6.1** before and after exposure to O_2 .

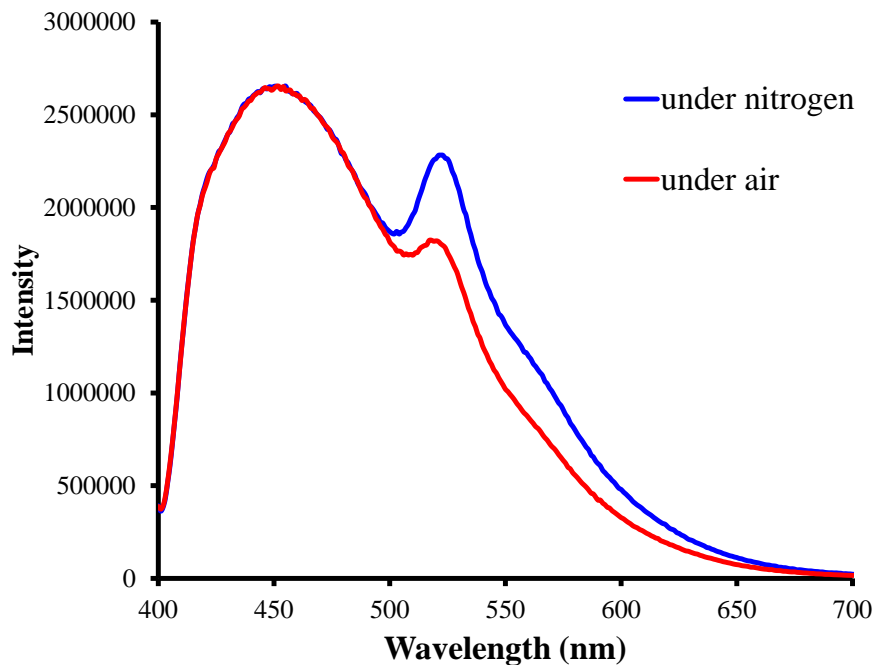


Figure 6-12. Phosphorescent spectral change of 6.3 before and after exposure to O₂.

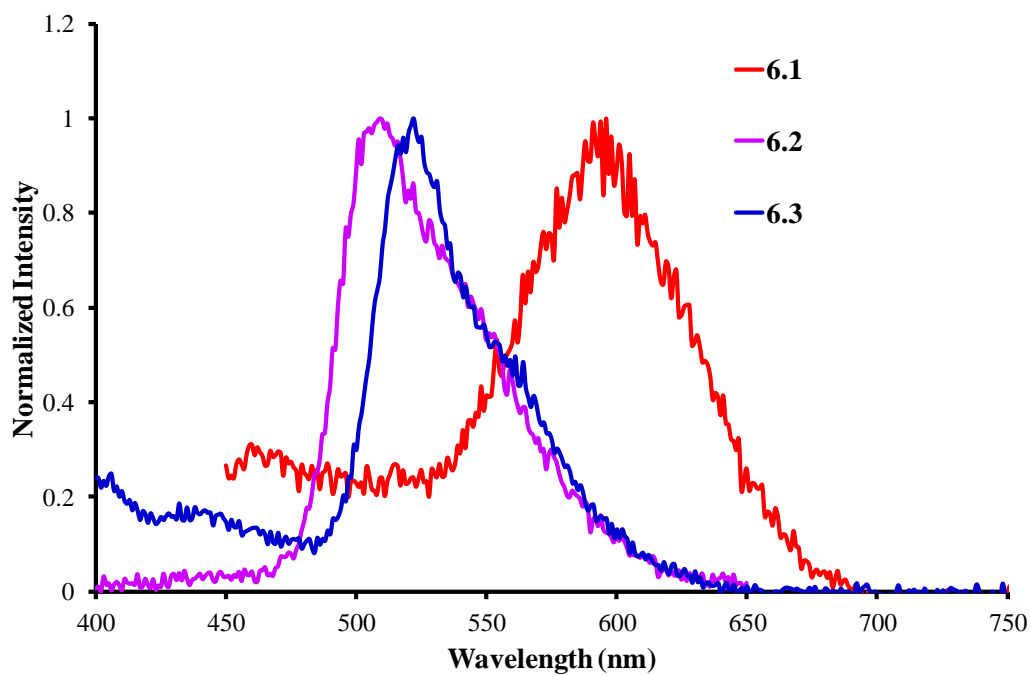


Figure 6-13. Time-resolved phosphorescence spectra of metal compounds in toluene at ambient temperature under nitrogen.

6.3.4 Photoisomerization

Upon excitation at 365 nm in toluene, **6.2** undergoes structural and color changes to isomer **Au-B'** as shown in Figure 6-14. The color of this Au(I) compound in toluene solution changes from colorless to dark blue-green. This photoisomerization process was monitored by ^1H NMR, ^{31}P NMR and UV-Vis spectroscopy. As shown in Figure 6-15, in the UV-Vis spectra, a broad band appears at about 620 nm and grows with irradiation time. This result was further confirmed by ^1H NMR and ^{31}P NMR studies. The ^{31}P NMR studies show that the chemical shift for the phosphorus move upfield as the formation of **Au-B'**, indicating the decreased donation of electron density from the phosphine to Au in the case of the ^{31}P signals and qualitatively indicating the formation of the new species (as shown in Figure 6-16). The ^1H NMR spectrum in C_6D_6 also displays a new set of well-resolved peaks as shown in Figure 6-17. The characteristic chemical shifts of the pyridyl and mesityl protons in the ^1H NMR spectrum show excellent agreement with those of the dark isomers in related systems as reported previously,^{1, 2, 3, 6, 10} confirming the dark isomer has a structure similar to those of previously reported dark isomers of N,C-chelate BMes_2 compound.

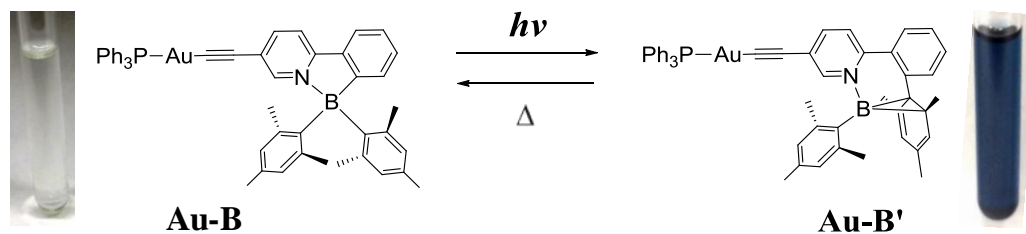


Figure 6-14. Photoisomerization of **6.2**. Inset: Photographs showing the color of the compounds before and after irradiation.

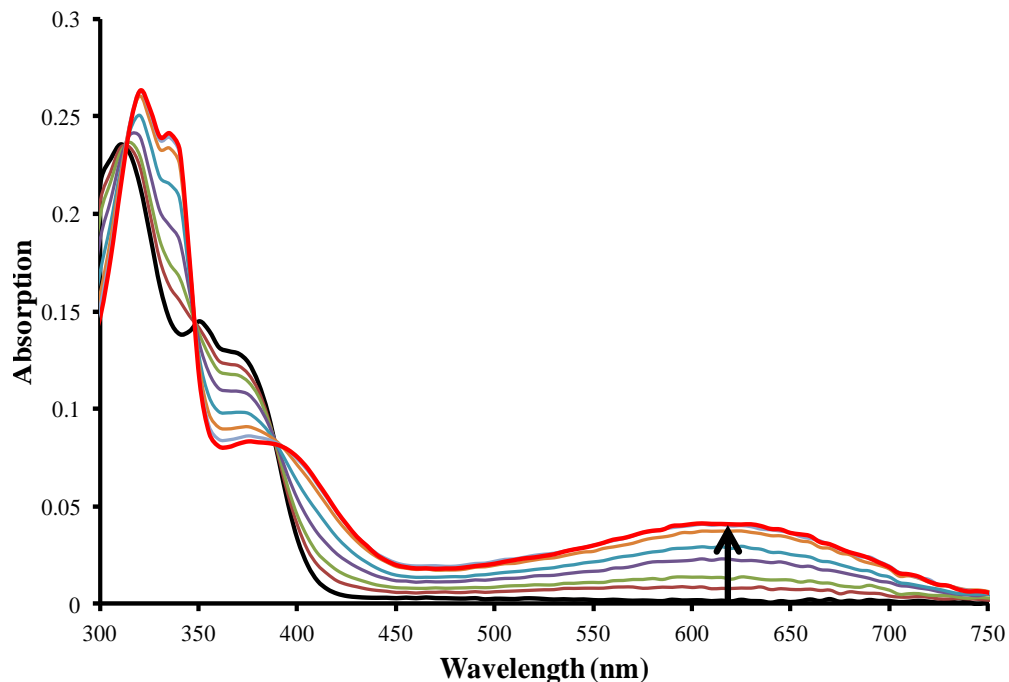


Figure 6-15. UV-Vis spectral change of **6.2** in toluene upon irradiation at 365 nm with a hand-held UV lamp.

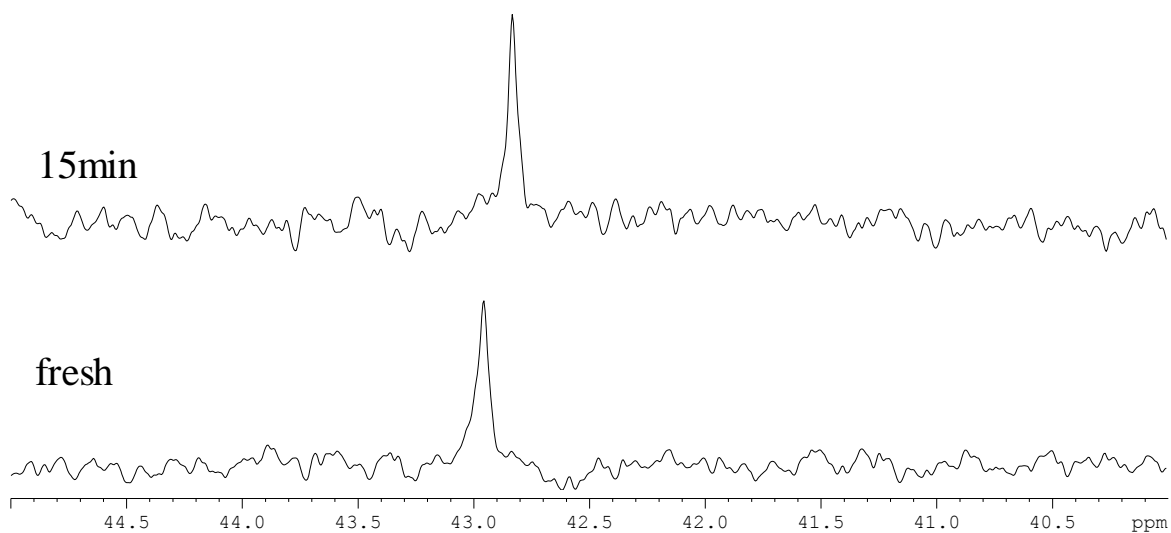


Figure 6-16. Stacked ^{31}P NMR spectra of **6.2** upon UV irradiation, under N_2 , in C_6D_6 .

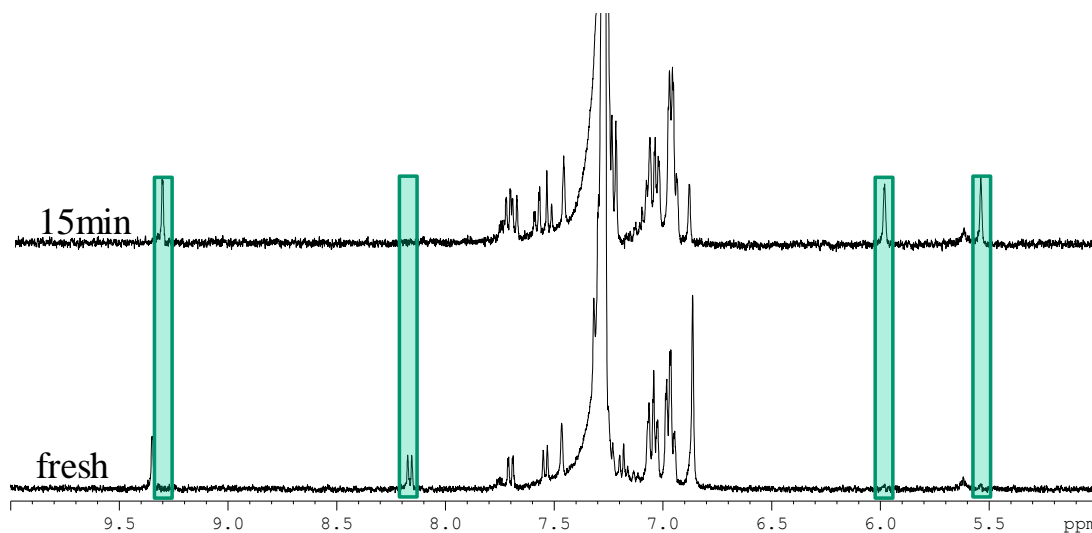


Figure 6-17. Stacked ^1H NMR spectra of **6.2** upon UV irradiation, under N_2 , in C_6D_6 (aromatic region).

The quantum yield for the photoisomerization of **6.2** at 298K was determined to be ~ 0.46 at 365 nm excitation, which is less than that of $\text{B}(\text{ppy})\text{Mes}_2$ ($\Phi_{\text{PI}} = 0.85$),^{2a, 10} but higher than that of $(\text{ph-C}\equiv\text{C-ppy})\text{BMes}_2$ ($\Phi_{\text{PI}} = 0.33$)^{2a} and the cyclometalated Pt(II) containing N $^{\wedge}$ C-chelate organoboron compounds (less than 0.01).³ The previous work has already demonstrated that the CT transition from a mesityl to the chelate backbone is a key driving force for the $\text{B}(\text{ppy})\text{Mes}_2$ chromophore photoisomerization. Since this Au(I) compound has no low-lying ^3LC or MLCT state, there is no alternative pathway for energy dissipation, and the photoisomerization of the boryl chromophore is still active. Similar as previously reported boryl compounds,^{1,2} photoisomerization process of compound **6.2** is also thermally reversible, similar to that observed for $\text{B}(\text{ppy})\text{Mes}_2$. The thermal conversion was studied using ^1H NMR at different temperatures as shown in Table 6-4, and the activation energy (120 kJ/mol) was estimated using an Arrhenius plot as shown in Figure 6-18. This activation energy is slightly higher than the non-metal attached N $^{\wedge}$ C-chelate boron system (110 kJ/mol).^{1a}

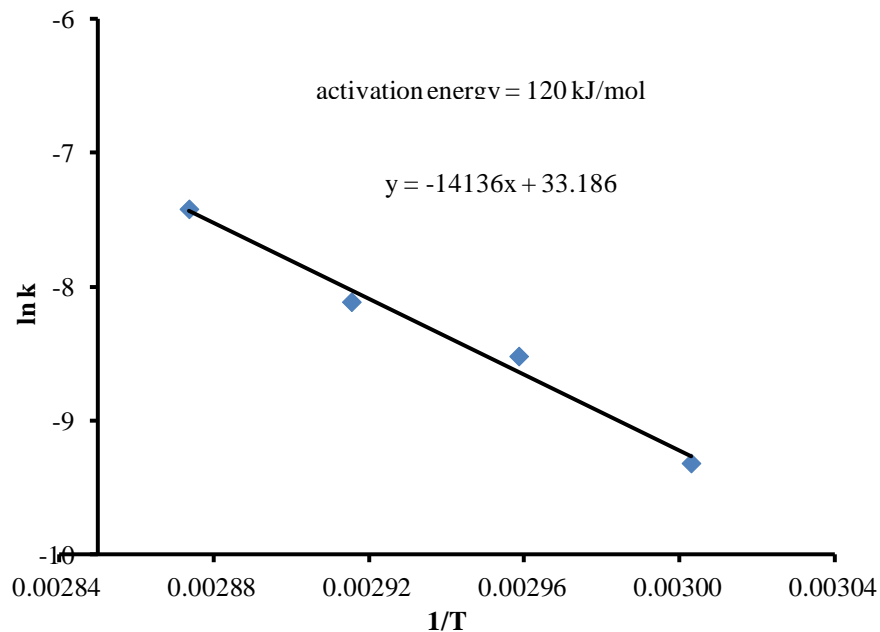


Figure 6-18. Activation energy of the thermal conversion of Au-B' to **6.2** using Arrhenius plot.

Table 6-4. Activation energy data of the thermal conversion of dark isomer Au-B' to **6.2** using ^1H NMR.

T (K)	1/T	k (s ⁻¹)	ln(k)
333	0.003003	0.00009	-9.3
338	0.002959	0.0002	-8.5
343	0.002915	0.0003	-8.1
348	0.002874	0.0006	-7.4

Upon irradiation with UV light (390 nm), the same photoisomerization phenomenon was also observed for **6.3** toluene solution. However, as shown in Figure 6-19, the spectral and color change is much less dramatic, compared to **6.2** with a weak broad peak appearing at $\lambda_{\text{max}} = \sim 600$ nm. Because of the presence of two boron chromophores in **6.3**, to establish whether both boron units are involved in the photoisomerization, we used ^1H

NMR spectra to monitor the process. As shown in Figure 6-20, after sufficient irradiation, the singlet proton H_A at ~ 8.35 ppm is replaced with two new peaks H_B and H_B' that maintain a 1:1 ratio, which can be assigned to the isomerized and the non-isomerized boron chromophore, respectively. The fact that only one boron unit undergoes photoisomerization can be explained by a fast intramolecular energy transfer process in which the excited state energy is absorbed by the dark isomer due to its low energy absorption band, thus quenching the isomerization of the 2nd boron unit. The same phenomenon has also been observed in polyboron compounds we reported earlier.⁶

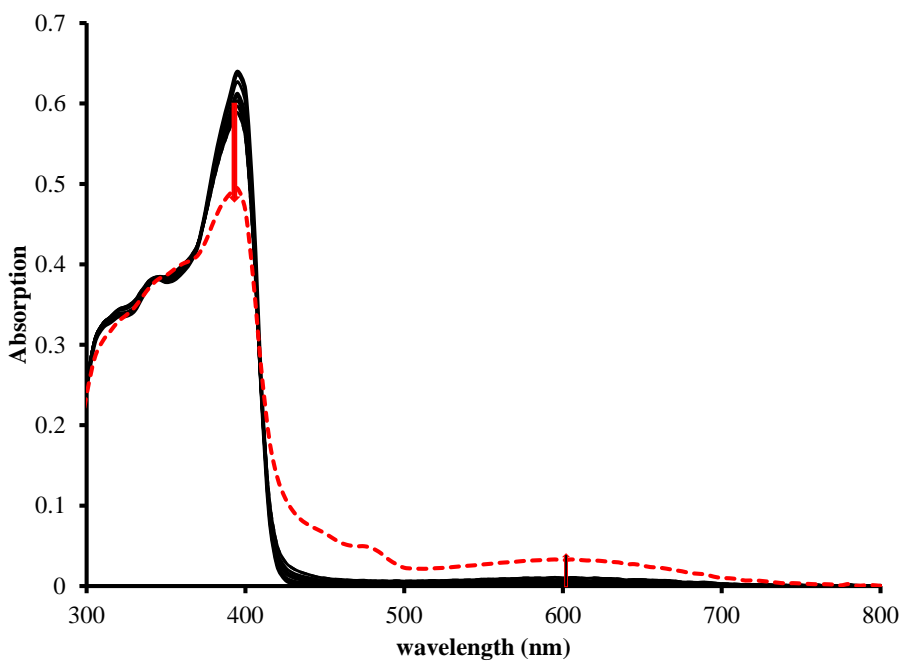


Figure 6-19. UV-Vis spectral change of **6.3** in toluene upon irradiation at 390 nm.

The photoisomerization of compound **6.3** was also monitored by ^{31}P NMR spectra as shown in Figure 6-21. During entire irradiation process only two phosphorus signals or a mixture of these two signals were detected, showing that only one boron chromophore moiety undergoes photoisomerization. The quantum yield for **6.3** photoisomerization at

390 nm was determined to be ~ 0.001 . This low photoisomerization quantum efficiency may be attributed to the low-lying $\pi \rightarrow \pi^*$ state of the chelate backbone that contributes significantly to the lowest excited state.

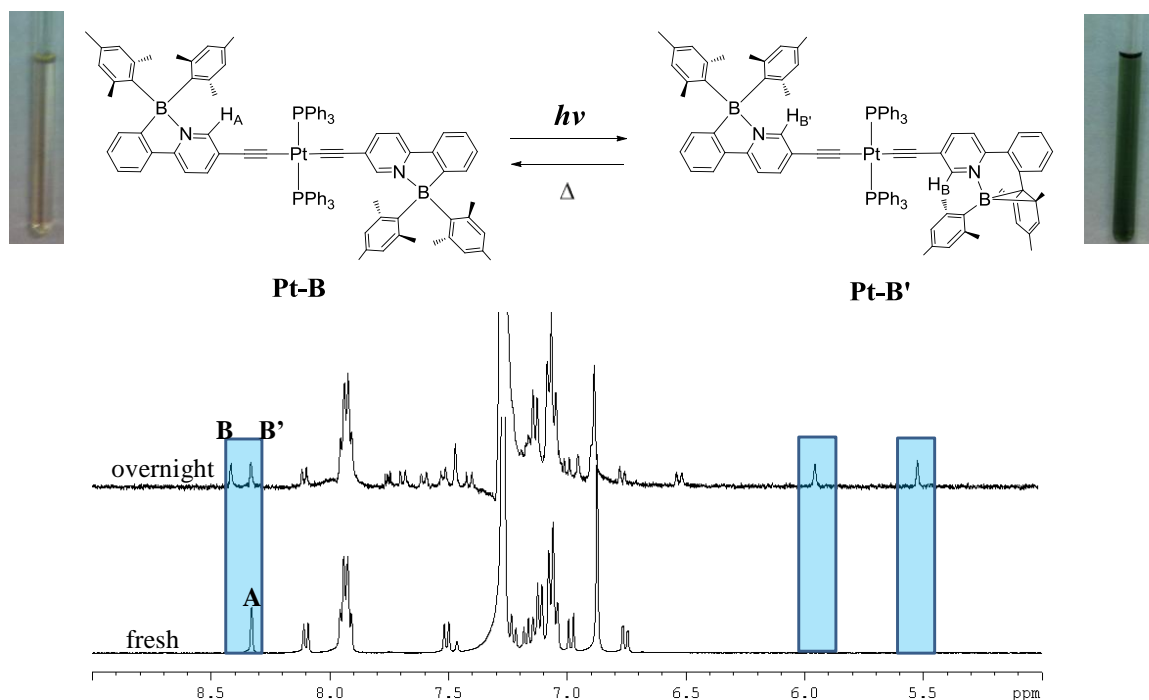


Figure 6-20. Stacked ¹H NMR spectra (aromatic region) of **6.3** upon UV irradiation, under N₂, in C₆D₆. Inset: Photographs showing the color of the compounds before and after irradiation.

In contrast to the behavior of **6.2** and **6.3**, compound **6.1** does not show any photoisomerization at all and remains intact after being irradiated for nearly 2 hours at 360 nm as shown in Figure 6-22. The high photostability of **6.1** can be attributed to the low lying MLCT state that dominates the lowest excited state, as indicated by the absorption spectrum.

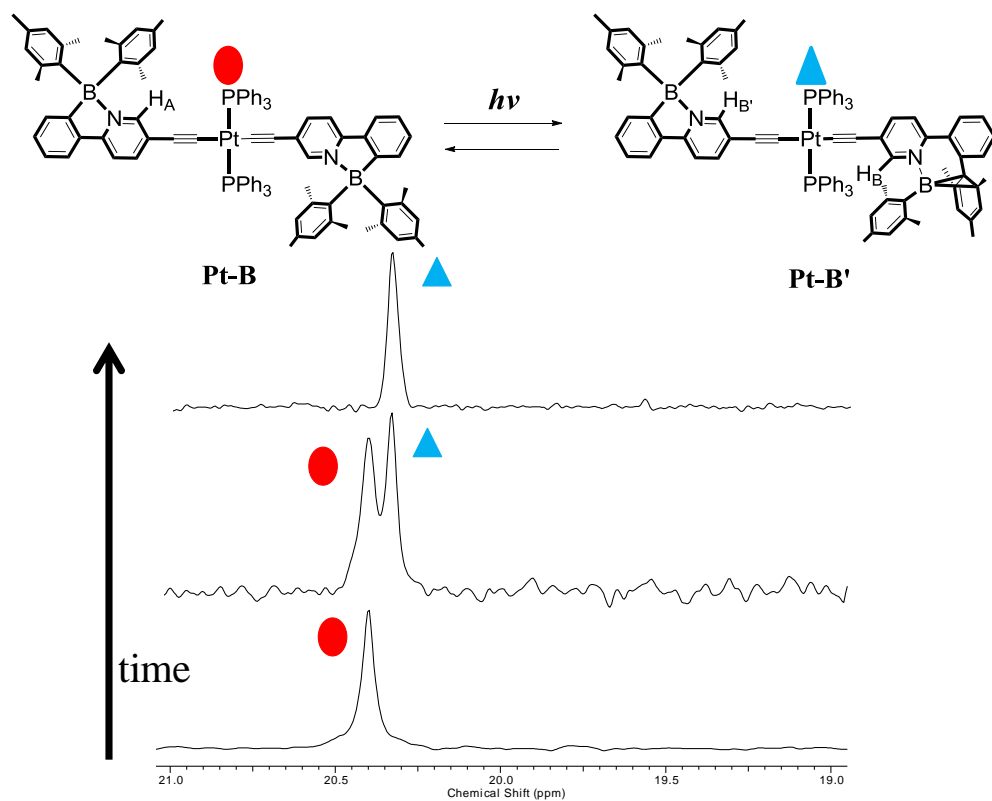


Figure 6-21. Stacked ^{31}P NMR spectra showing the conversion of **6.3** to **Pt-B'** upon UV irradiation with time, under N_2 , in C_6D_6 .

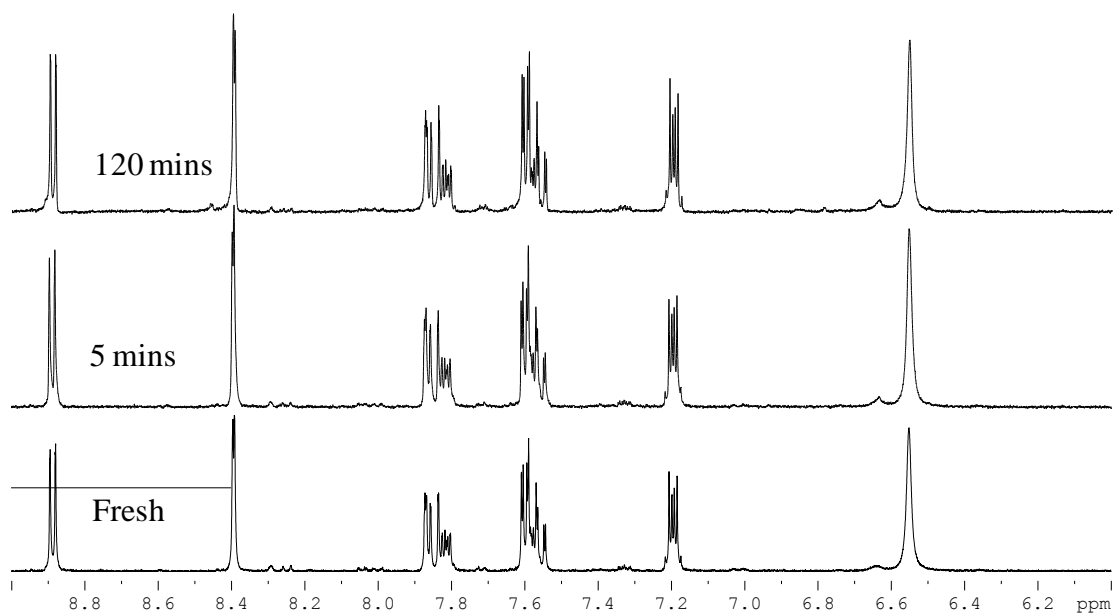


Figure 6-22. Stacked ^1H NMR spectra (aromatic region) of **6.1** upon UV irradiation, under N_2 , in CD_3CN .

To further examine the impact of the Au-PPh₃ unit on photoisomerization of **B1**, we measured the relative photoisomerization quantum efficiency of **TIPS-B** with **6.2**. (**B1** is unstable toward photolysis, thus cannot be used as a control compound for photoisomerization study.), using UV-Vis spectroscopy, employing a modified Hatchard-Parker method.¹⁶ The toluene solutions (10⁻⁵ M) of both compounds were prepared in a glove box and irradiated using two different wavelengths, 362 and 310 nm, respectively, at which both compounds have a similar absorbance (as shown in Figure 6-23). The absorbance of **Au-B'** was monitored at 615 nm, while the absorbance of the dark isomer of **TIPS-B** was monitored at 650 nm (as shown in Figure 6-24). Figure 6-25 shows the number of moles of dark isomer produced over time for each compound. By comparing the slopes of each graph (the initial rates), the relative photoisomerization quantum yield ratio can be obtained. At 362 nm excitation, the photoisomerization quantum yield ratio between **6.2** and **TIPS-B** was found to be 0.64:1. The lower isomerization quantum efficiency of **6.2** at 362 nm excitation could be attributed to the contribution of the Au(PPh₃)(C≡C) unit to the lowest excited state. When excited at 310 nm, the photoisomerization quantum efficiency of **6.2** is greatly increased, compared to **TIPS-B** with the relative quantum efficiency ratio being ~1:1. This could be caused by greater triplet energy transfer from the Au(I) unit to the boron unit at the higher excitation energy, that partially compensates the loss of efficiency due to the Au(I) centered low-lying excited state.

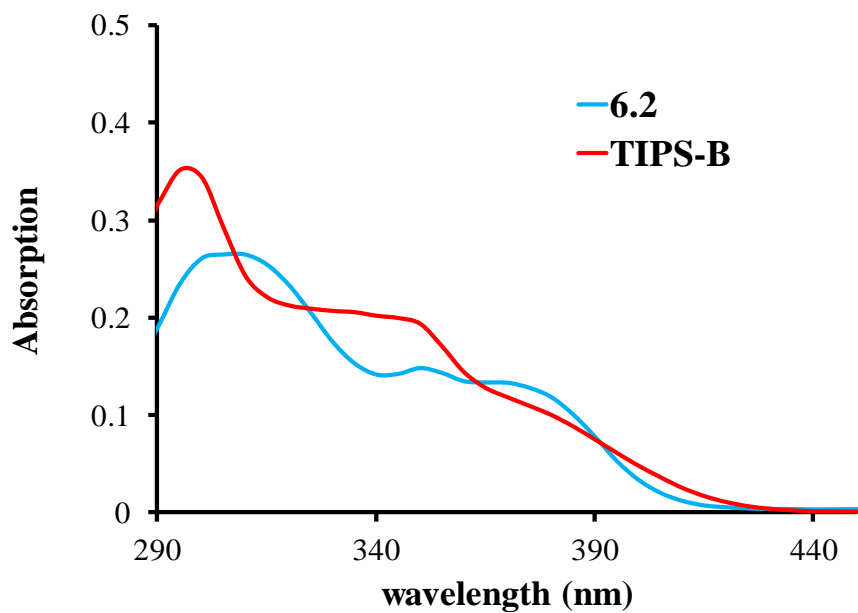


Figure 6-23. UV-Vis spectra of $\sim 1 \times 10^{-5}$ M **6.2** and **TIPS-B** recorded in degassed toluene at ambient temperature used for photoisomerization quantum efficiency comparison measurement.

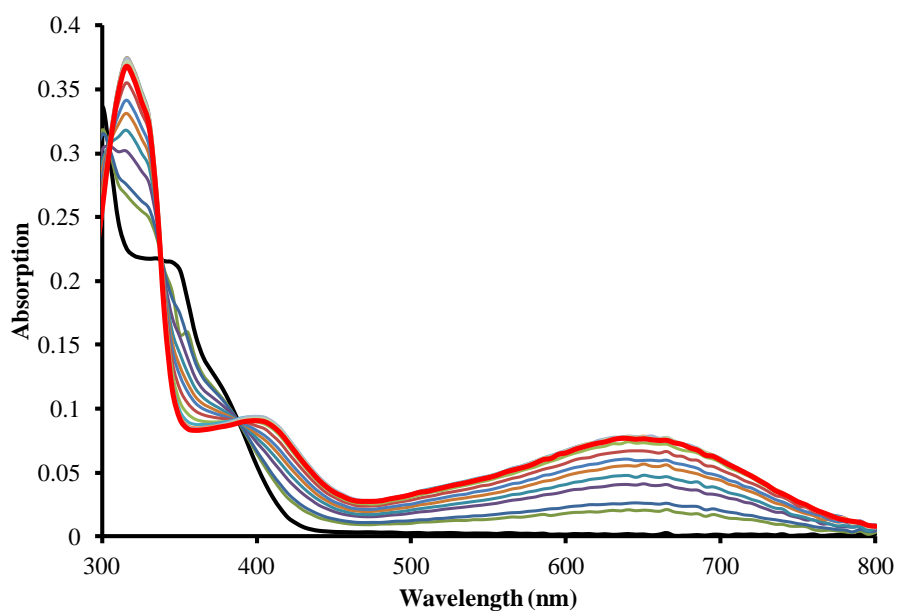


Figure 6-24. UV-Vis spectral change of **TIPS-B** in toluene upon irradiation at 362 nm.

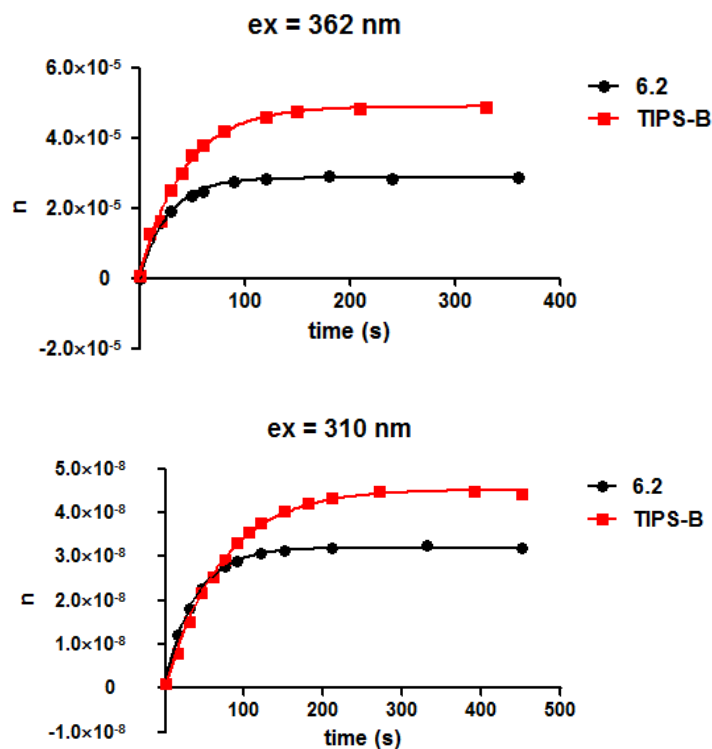


Figure 6-25. Number of moles of dark isomer produced over time. (top) Ex = 362 nm; (bottom) Ex = 310 nm.

6.3.5 TD-DFT Calculations

To further understand the electronic structures and the factors that influence the photochromic behaviors of these metal containing boron compounds, both DFT and TD-DFT calculations were performed on all the metal complexes and control precursors. The structures of control compounds are shown in Chart 6-1.

Using TD-DFT calculations, the lowest triplet state for control precursor **B1** was found to lie at 2.75 eV (as shown in Figure 6-26 and Table 6-5), while the triplet energies of the metal compounds **PAu1** (Figure 6-27 and Table 6-6) and **PPt1** (Figure 6-28 and Table 6-7) were calculated at 3.66 eV and 3.50 eV, respectively. Since the lowest triplet state of the independent heavy metal units are both higher than that of the boryl unit **B1**, it was likely that **PAu1** and **PPt1** fragments in **6.2** and **6.3** would sensitize

photoisomerization reactions. But in fact, the covalent attachment of the metal fragments to the photoactive boryl units didn't significantly enhance the isomerization efficiency as expectation, which may be due to the conjugated linker used which connected the metal and boron unit together, as the energies of the excited states on the metal fragments and the boron unit in compounds **6.2** and **6.3** may be different to those for the independent chromophores. Furthermore, the increased extent of π -conjugation about the boron chromophore can slow or even inhibit the photoreaction, which can explain the low isomerization quantum efficiency of **6.3**.^{4,6}

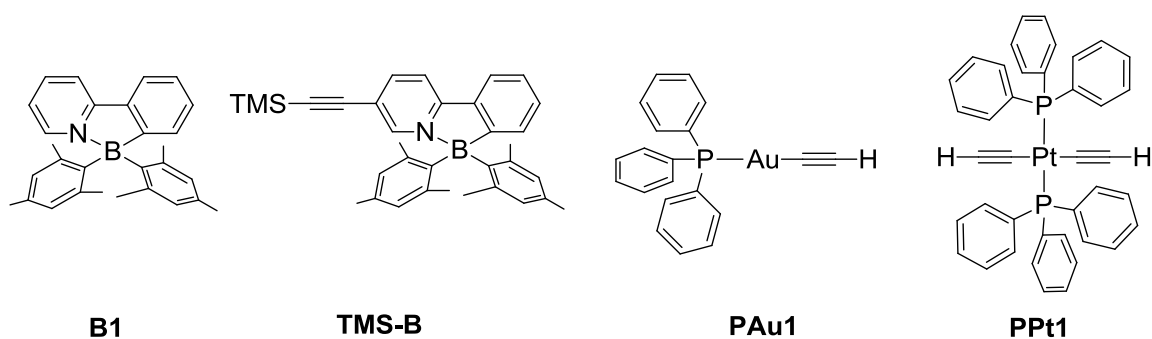


Chart 6-1

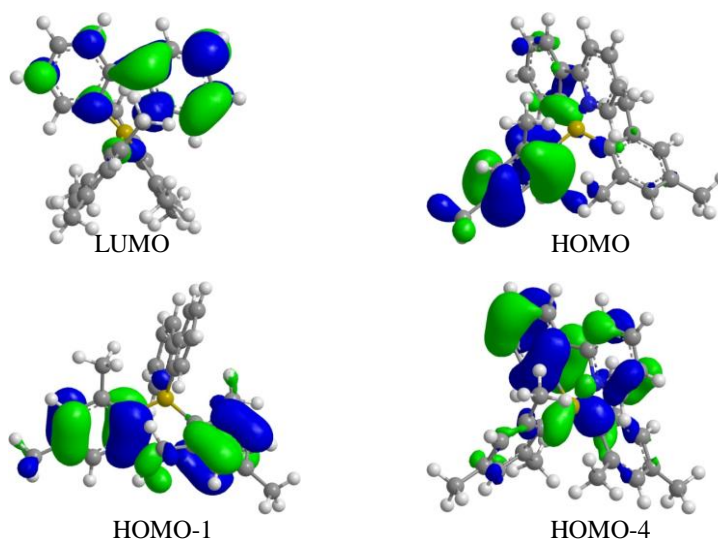


Figure 6-26. Molecular orbitals of **B1** with a surface isocontour value of 0.03.

Table 6-5. TD-DFT transition energies (E_{ex}) and oscillator strengths (f) for **B1**.

Transition	E_{ex} (nm)	f	Transition Weights		Energy (eV)
			Configuration	Composition (%)	
T1	450.1	--	H-4→L	10	2.75
			H→L	83	
S1	429.7	0.0129	H→L	98	2.89
S2	393.8	0.0067	H-1→L	79	3.15

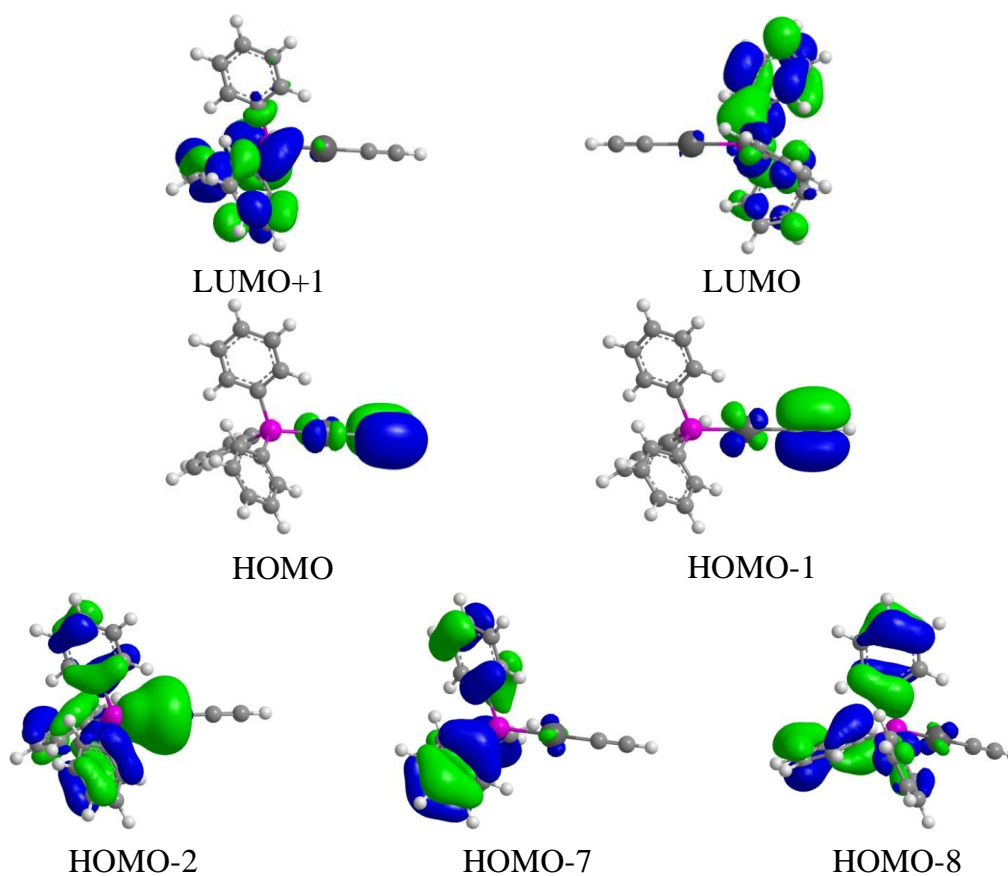


Figure 6-27. Molecular orbitals of **PAu1** with a surface isocontour value of 0.03.

Table 6-6. TD-DFT transition energies (E_{ex}) and oscillator strengths (f) for **PAu1**.

Transition	E_{ex} (nm)	f	Transition Weights		Energy (eV)
			Configuration	Composition (%)	
T1	339.2	--	H-8→L+1	10	3.66
			H-7→L	10	
			H-2→L	10	
			H-2→L+1	19	
S1	297.0	0.0001	H-1→L	56	4.18
			H→L	25	
			H→L+1	10	
S2	296.1	0.0009	H-1→L+1	31	4.19
			H→L	40	

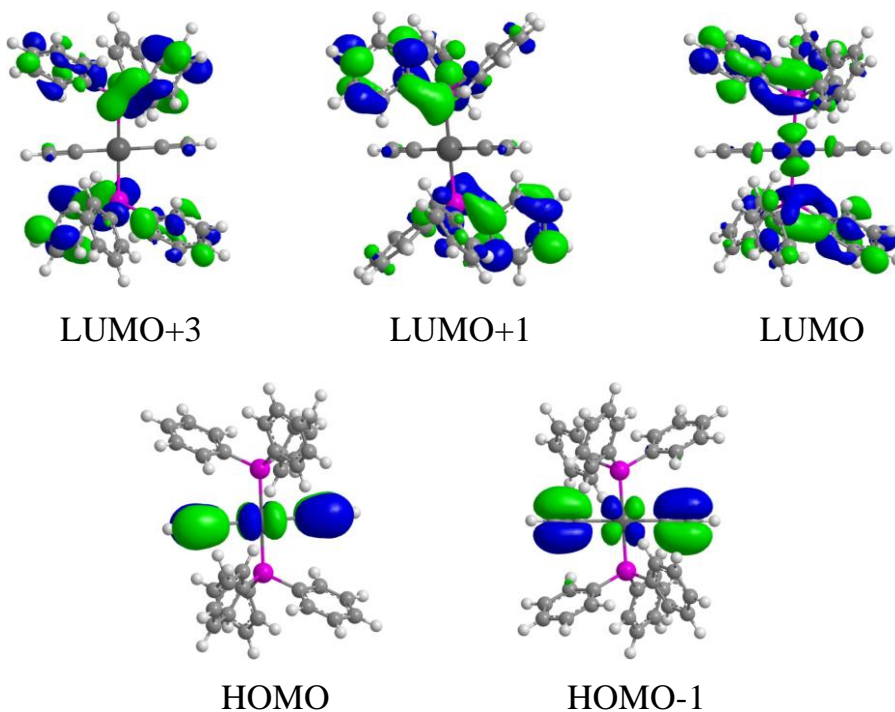
**Figure 6-28.** Molecular orbitals of **PPt1** with a surface isocontour value of 0.03.

Table 6-7. TD-DFT transition energies (E_{ex}) and oscillator strengths (f) for **Ppt1**.

Transition	E_{ex} (nm)	f	Transition Weights		Energy (eV)
			Configuration	Composition (%)	
T1	354.6	--	H→L+1	61	3.50
			H→L+3	16	
S1	357.4	--	H→L	95	3.47
S2	333.9	--	H-1→L	95	3.71
S3	330.9	0.0154	H→L+1	96	3.75

The key finding from TD-DFT for **6.1** is that the first few singlet states and the lowest triplet state are all charge transfer transitions from π (alkyne-chelate back bone, a CO ligand and the Re atom) to π^* (bipy), which is much lower in energy than the mesityl to chelate charge transfer (singlet and triplet), thus quenches the isomerization. The molecular orbitals and TD-DFT calculation results are shown in Figure 6-29 and Table 6-8.

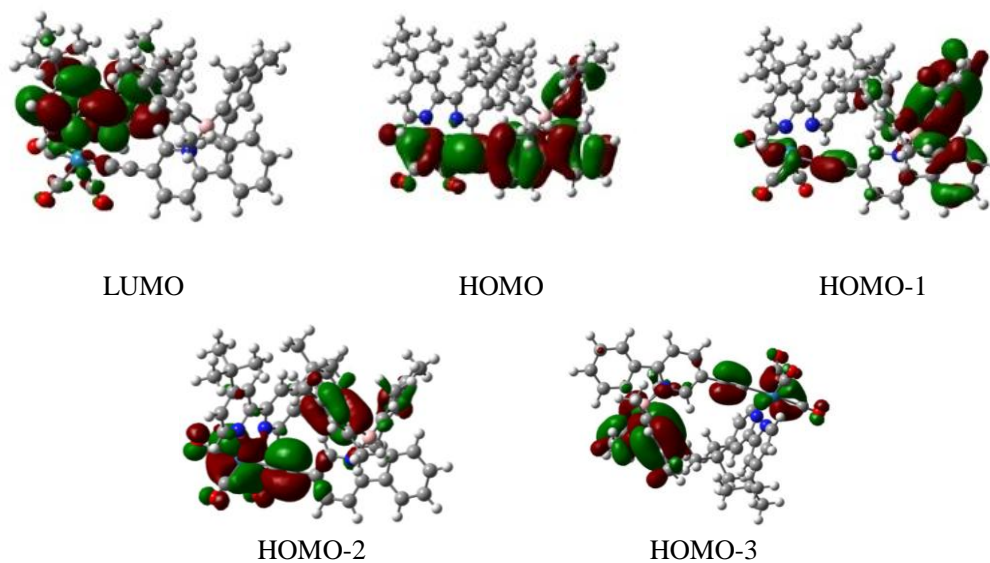
**Figure 6-29.** Molecular orbitals of **6.1** with a surface isocontour value of 0.03.

Table 6-8. TD-DFT transition energies (E_{ex}) and oscillator strengths (f) for **6.1**.

Transition	E_{ex} (nm)	f	Transition Weights		Energy (eV)
			Configuration	Composition (%)	
T1	617.2	--	H-1→L	5	2.01
			H→L	92	
S1	608.2	0.0017	H-1→L	5	2.04
			H→L	94	
S2	504.7	0.0328	H-3→L	15	2.46
			H-2→L	74	
			H-1→L	9	

Table 6-9. TD-DFT transition energies (E_{ex}) and oscillator strengths (f) for **6.2**

Transition	E_{ex} (nm)	f	Transition Weights		Energy (eV)
			Configuration	Composition (%)	
T1	474.3	--	H-4→L	50	2.61
			H-4→L+4	5	
			H→L	34	
S1	428.5	0.0409	H→L	92	2.89
			H→L+1	2	
			H→L+2	3	
S2	384.6	0.0041	H-2→L	7	3.22
			H-1→L	87	
			H-1→L+2	2	

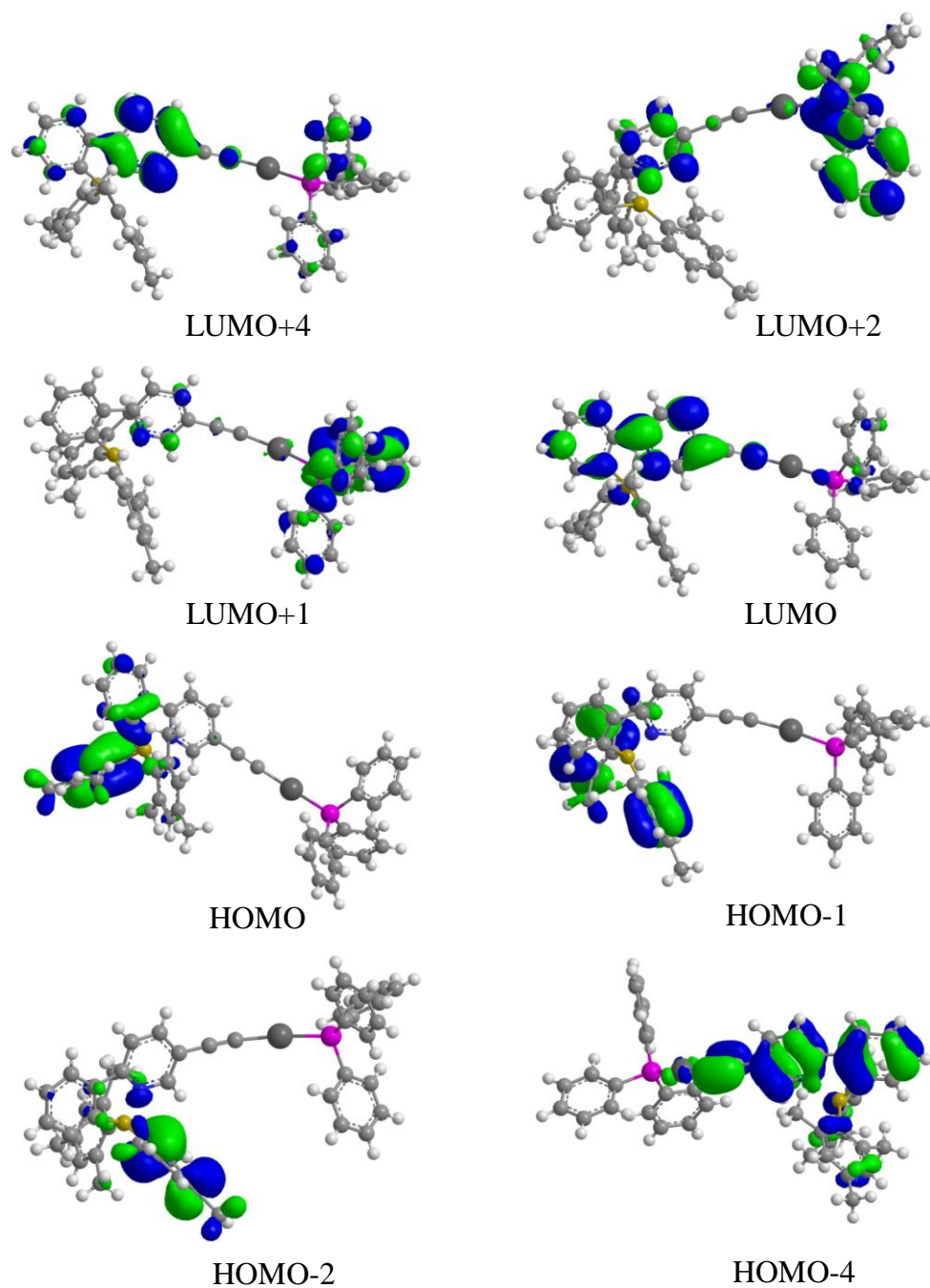


Figure 6-30. Molecular orbitals of **6.2** with a surface isocontour value of 0.03

For **6.2**, the S_1 is a typical mesityl to chelate charge transfer transition with moderate oscillator strength. The T_1 , however, is dominated by $\pi \rightarrow \pi^*$ transition (50%) of the alkyne-chelate backbone (the phosphorescent peak in luminescent spectrum), with about

34% mesityl to chelate charge transfer (as shown in Figure 6-30 and Table 6-9). Although the same pattern is also observed for **TMS-B** (to simplify the computation, we calculated **TMS-B** instead of **TIPS-B**), the mesityl to chelate charge transition contribution to the T_1 state is much greater (51%), compared to the $\pi \rightarrow \pi^*$ transition (40%) as shown in Figure 6-31 and Table 6-10. This may explain why at 362 nm excitation, the quantum efficiency of **6.2** is lower than that of **TIPS-B**.

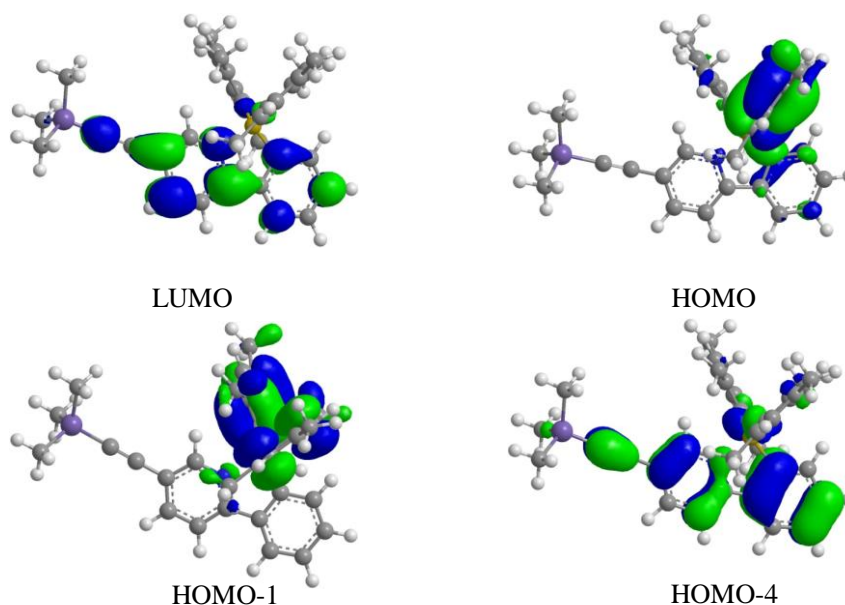


Figure 6-31. Molecular orbitals of **TMS-B** with a surface isocontour value of 0.03.

Table 6-10. TD-DFT transition energies (E_{ex}) and oscillator strengths (f) for **TMS-B**.

Transition	E_{ex} (nm)	f	Transition Weights		Energy (eV)
			Configuration	Composition (%)	
T1	488.3	--	H-4 \rightarrow L	40	2.54
			H \rightarrow L	51	
S1	453.0	0.0253	H \rightarrow L	97	2.74
S2	414.7	0.0081	H-1 \rightarrow L	80	2.99

For **6.3**, S_1 is dominated by mesityl to backbone charge transfer with strong oscillator strength. However, T_1 is dominated by $\pi \rightarrow \pi^*$ transitions of the conjugated backbone, which explains the low quantum isomerization efficiency of **6.3** (Figure 6-32 and Table 6-11).

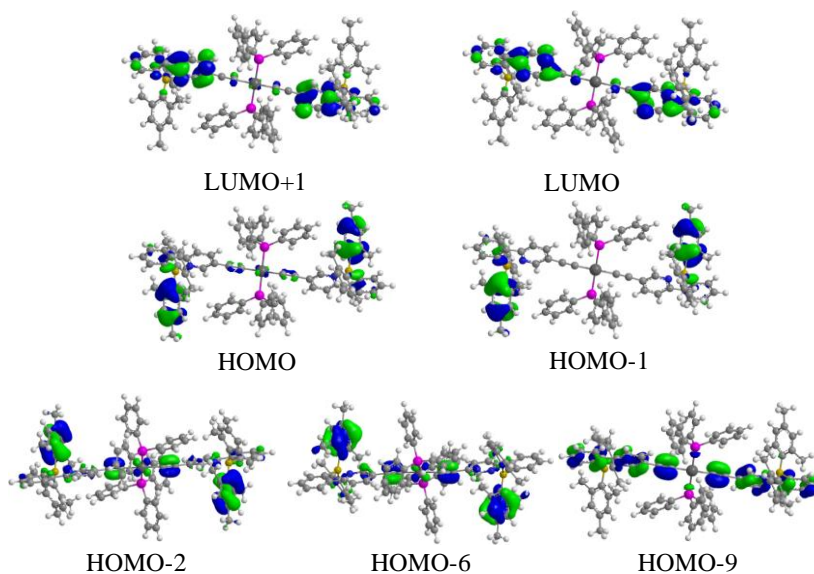


Figure 6-32. Molecular orbitals of **6.3** with a surface isocontour value of 0.03.

Table 6-11. TD-DFT transition energies (E_{ex}) and oscillator strengths (f) for **6.3**.

Transition	E_{ex} (nm)	f	Transition Weights		Energy (eV)
			Configuration	Composition (%)	
T1	471.7	--	H-9→L+1	17	2.63
			H-6→L	13	
			H-2→L	25	
			H→L	18	
S1	412.5	0.1180	H-1→L+1	36	3.01
			H→L	62	
S2	411.0	--	H-1→L	57	3.02
			H→L+1	40	

6.4 Conclusions

In summary, choosing Au(I), Pt(II) and Re(I) three metal acetylides containing photo active B(ppy)Mes₂ chromophores have been synthesized and fully characterized. We have shown that by taking advantage of different heavy metals the photoisomerization quantum efficiency of the chromophores can be tuned through the adjustment of ³LC state localized on the chelate backbone or the involvement of MLCT state in the lowest electronic transition. Among three metal complexes, compound **6.2** shows the highest photoisomerization quantum efficiency due to its high mesityl to chelate charge transition contribution to the T1 state. When irradiated using higher excitation energy, the photoisomerization quantum efficiency of **6.2** can be further enhanced, which may be due to the triplet state energy transfer from the metal center to the boron unit. On the contrary, if there is efficient involvement of MLCT state in the lowest excited state (such as compound **6.1**), complexes will show high photostability, making them potential useful as high emissive triplet emitter.

Appendix: Photoisomerization Quantum Yield Measurement

The absorption of 3 mL of a 0.012 M solution of ferrioxalate in a spectrophotometric cell is measured as the original point. Then 0.5 mL of buffered phenanthroline solution is added in the cell and the absorbance at 510 nm measured immediately. The solution is then irradiated at 365 nm (or the selected wavelength used for the sample solution between 254 nm and 436 nm) and the absorption spectra are measured every 15 seconds. The same procedure was used for the measurement of the sample solution. The moles of photons absorbed by the irradiated solution per time unit ($Nh\nu/t$) are calculated using the equation: $Nh\nu/t = (\text{moles of solutes})/(\Phi_\lambda \times t \times F)$ where Φ_λ is the quantum yield at the

irradiation wavelength, t is the irradiation time, and F is the mean fraction of light absorbed by the solution. ($F = 1 - 10^{-A}$)

Preparation of standard solutions: Ferrioxalate 0.012 M: 6 g of potassium ferrioxalate in 1 liter of H_2SO_4 0.05 M. Buffered phenanthroline 0.1%: 225 g $\text{CH}_3\text{COONa} \cdot 3\text{H}_2\text{O}$, 1 g of phenanthroline in 1 liter of H_2SO_4 0.5 M. Both solutions should be kept in dark.

6.5 References

1. (a) Y. L. Rao, H. Amarne, S. B. Zhao, T. M. McCormick, S. Martic, Y. Sun, R. Y. Wang, S. Wang, *J. Am. Chem. Soc.* 2008, **130**, 12898; (b) H. Amarne, C. Baik, R. Y. Wang, S. Wang, *Organometallics* 2011, **30**, 665.
2. (a) H. Amarne, C. Baik, S. K. Murphy, S. Wang, *Chem. Eur. J.* 2010, **16**, 4750; (b) S. K. Murphy, C. Baik, J. S. Lu, S. Wang, *Org. Lett.* 2010, **12**, 5266.
3. Y. L. Rao, S. Wang, *Organometallics* 2011, **30**, 4453.
4. Z. M. Hudson, S.-B. Ko, S. Yamaguchi, S. Wang, *Org. Lett.* 2012, **14**, 5610.
5. (a) N. Tamai, H. Miyasaka, *Chem. Rev.* 2000, **100**, 1875 and references therein; (b) E. D. M. Battal, J. Cusido, S. Sortino, F. M. Raymo, *Phys. Chem. Chem. Phys.* 2012, **14**, 10300.
6. C. Baik, S. K. Murphy, S. Wang, *Angew. Chem. Int. Ed.* 2010, **49**, 8224.
7. (a) V. W.-W. Yam, V. C.-Y. Lau, K.-K. Cheung, *Organometallics* 1995, **14**, 2749; (b) S.-T. Lam, N. Zhu, V. W.-W. Yam, *Inorg. Chem.* 2009, **48**, 9664; (c) M. N. Roberts, C.-J. Carling, J. K. Nagle, N. R. Branda, M. O. Wolf, *J. Am. Chem. Soc.* 2009, **131**, 16644.
8. SHELXTL Version 6.14, Bruker AXS, 2000–2003.
9. (a) V. W.-W. Yam, *Chem. Comm.* 2001, 789; (b) M. Wrighton, D. L. Morse, *J. Am. Chem. Soc.* 1974, **96**, 998; (c) A. S. Polo, M. K. Itokazu, K. M. Frin, A. O. de T. Patrocínio, N. Y. M. Iha, *Coord. Chem. Rev.* 2006, **250**, 1669; (d) V. W.-W. Yam, Y. Yang, J. Zhang, B. W. K. Chu, N. Zhu, *Organometallics* 2001, **20**, 4911; (e) V. W.-W. Yam, V. C.-Y. Lau, K.-K. Cheung, *Organometallics* 1995, **14**, 2749; (f) M. K. Itokazu, A. S. Polo, N. Y. M. Iha, *J. Photochem. Photobio.* 2003, **160**, 27.
10. C. Baik, Z. M. Hudson, H. Amarne, S. Wang, *J. Am. Chem. Soc.* 2009, **131**, 14549.
11. (a) M. L. Muro, S. Diring, X. Wang, R. Ziessel, F. N. Castellano, *Inorg. Chem.* 2009, **48**, 11533; (b) Z. M. Hudson, C. Sun, K. J. Harris, B. E. G. Lucier, R. W. Schurko, S. Wang, *Inorg. Chem.* 2011, **50**, 3447.

12. (a) V. W.-W. Yam, S. W. K. Choi, *J. Chem. Soc., Dalton Trans.* 1996, 4227; (b) V. W.-W. Yam, S. W. K. Choi, K.-K. Cheung, *J. Chem. Soc., Dalton Trans.* 1996, 3411; (c) V. W.-W. Yam, K. L. Cheung, S. K. Yip, K.-K. Cheung, *J. Organomet. Chem.* 2003, **681**, 196.
13. J. E. Rogers, T. M. Cooper, P. A. Fleitz, D. J. Glass, D. G. McLean, *J. Phys. Chem. A* 2002, **106**, 10108.
14. (a) T. Sajoto, P. I. Djurovich, A. B. Tamayo, J. Oxgaard, W. A. Goddard, M. E. Thompson, *J. Am. Chem. Soc.* 2009, **131**, 9813; (b) N. J. Demas, G. A. Crosby, *J. Am. Chem. Soc.* 1970, **92**, 7262.
15. (a) K.-L. Cheung, S.-K. Yip, V. W.-W. Yam, *J. Organometallic Chem.* 2004, **689**, 4451; (b) V. W.-W. Yam, K.-L. Cheung, S.-K. Yip, K.-K. Cheung, *J. Organometallic Chem.* 2003, **681**, 196; (c) M. J. Irwin, J. J. Vittal, R. J. Puddephatt, *Organometallics* 1997, **16**, 3541; (d) V. W.-W. Yam, K.-L. Cheung, E. C.-C. Cheng, N. Zhu, K.-K. Cheung, *Dalton Trans.* 2003, 1830.
16. (a) D. Abdallah, J. Whelan, J. M. Dust, S. Hoz, E. Buncel, *J. Phys. Chem. A* 2009, **113**, 6640; (b) C. A. Parker, *Proc. R. Soc. London A* 1953, **220**, 104.

Chapter 7

Summary and Perspectives

7.1 Summary and Conclusions

This thesis started with the syntheses of the polypyridyl ligand L1 containing both py-in and py-im units. Due to the different binding modes and reactivity, L1 shows different affinity toward metal ions, which makes it useful in the synthesis of heterobimetallic complexes and supramolecular architectures. Ligand L2 and L3 were also isolated as by-products from the reaction mixture for L1. The polypyridyl ligand L2 and L3 were the result of C-N and C-C coupling in a one-pot reaction. The photophysical properties of these ligands were examined in CH₂Cl₂ at ambient temperature. The intramolecular excimer emission has been observed for both L2 and L3.

Based on ligand L1, two Ru(II) based bimetallic complexes, **3.3** and **3.4** were prepared with good yields. It is was found that little electronic communication between the two different centers bridged by L1 was existed due to the lack of conjugation of the two chelating units with the central benzene ring. The quantum yield measurements revealed that Pt(II) unit enhanced phosphorescence efficiency of the Ru(II) unit *via* intramolecular energy transfer.

An interesting dual emission phenomenon was also observed during the study of the control mononuclear Pt(II) complex **3.5**. At ambient temperature, complex **3.5** shows two emission peaks at 507 nm and 633 nm, respectively. The high energy emission band is assigned to a ligand-centered fluorescence state, while the low energy emission band is sensitive toward oxygen and thus attributed to phosphorescent nature. The relative

intensity of the two emission bands can be modulated reversibly by using nitrogen and oxygen, which enables it as a potential oxygen sensor.

Ligand L1 was further used to synthesize Re(I)-Pt(II) and Re(I)-Pd(II) bimetallic complexes **4.2**, **4.3**, **4.4**, and **4.5**. Single crystals of Re(I)-Pt(II) complexes **4.2** and **4.4** were obtained, even though the quality of both was poor and displayed some degree of twinning and disordering. The Re and Pt units showed typical octahedral and square-planar geometry, respectively. All the Re(I)-Pt(II) complexes displayed solution luminescence at ambient temperature. The Re(I) unit was found to enhance phosphorescence efficiency of Pt(II) unit *via* efficient intramolecular energy transfer. TD-DFT data also confirm that the observed phosphorescence of **4.3** is indeed from the Pt chelate unit. Due to the low-lying d-d state of the Pd(II) center, mono-nuclear Pd(II) complex **3.6** is non-emissive in solution. Efficient intramolecular energy transfer from the Re(I) unit to the non-emissive Pd(II) results in the lacking of luminescence for bimetallic complex **4.5**.

The preliminary electrochemistry study also indicated that complex **4.1** is a promising candidate for the electrocatalytic CO₂ reduction. Under the same conditions, complex **4.1** showed better performance than Re(bipy-tBu)(CO)₃Cl, a literature known good catalyst in CO₂ reduction. The activity of **4.1** may be attributed to the electron rich property of py-im chelating ligand that making the Re(I) center more nucleophilic toward CO₂ reduction.

The synthesis of ligand L4 and its Pt(II) (**5.1**) and Pd(II) (**5.2**) complexes was reported by our group previously.¹ This ligand was isolated as by-products from the reaction mixture for pib. Previous literature showed that ligand L4 was chelated to Pd(II) and Pt(II) in a rare *trans* geometry, forming a large 9-membered chelate ring. To further

explore the impact of the *trans*-chelating ligand L4 on catalytic properties of Pd(II) compounds, acetoxylation of benzene, chlorobenzene and toluene by $\text{PhI}(\text{OAc})_2$ using $\text{Pd}(\text{OAc})_2/\text{L4}$ (2:1) as the catalyst was examined and compared to the *cis*-chelating system $\text{Pd}(\text{OAc})_2/2,2'$ -bipyridine. The preliminary results indicated that L4 significantly accelerated the reaction rate for the three substrates, especially for chlorobenzene in the first 6 hours. The product distribution study for the $\text{Pd}(\text{OAc})_2/\text{L4}$ system showed that the *p*-isomer is somewhat favored compared to *o*- and *m*-isomer. However, the yield is low for toluene and chlorobenzene substrates, which might be attributed to the relatively low stability of the *trans*-L4 Pd complex, causing irreversible decomposition of the catalyst and side reactions.

To explore the heavy metal effects on the 4-coordinate boron photochromic behaviors, Re(I), Pt(II) and Au(I) were employed to synthesize three metal containing boron complexes **6.1**, **6.2**, and **6.3**. Through metal ion tuning, the photoisomerization quantum efficiency of the same N[^]C-chelate boron chromophore can be tuned.

7.2 Future Directions

Future directions of this work should focus on synthesizing transition metal complexes of ligand L2 and L3. Through choosing suitable metal centers, such as tetrahedral Cu(I) ion, metal-assembled bowl-shaped molecules that are structural analogues of calixarenes based on ligand L3 can be prepared as shown in Figure 7-1.

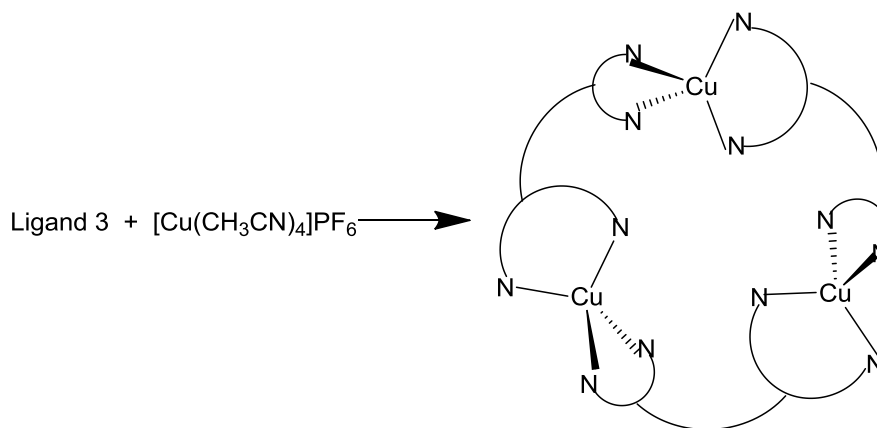


Figure 7-1. Synthesis of supramolecular Cu(I)-L4 compounds.

Ligand L2 discussed in Chapter 2 also has two different binding sites. As a result, it can be used to prepare N^N-chelate boron containing metal complexes, which might be used as phosphorescent emitters. One example is shown in Figure 7.2, but many combinations, such as Cu(I)-boron and Pt(II)-boron can also be achieved with L2.

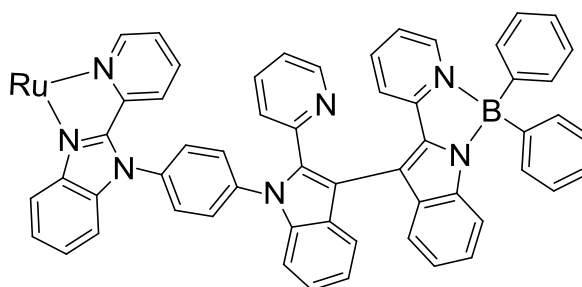


Figure 7-2. Structure of possible Ru(II) containing boron complex.

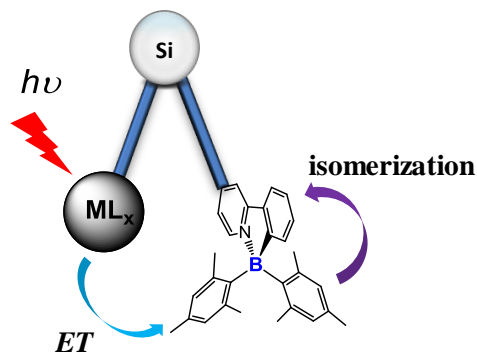


Figure 7-3. Structure of non-conjugated metal containing N^C-chelate boron compound.

Another direction is the development of non-conjugated metal compounds that contain a photo-active N[^]C-chelate BMes₂ unit (B(ppy)Mes₂) (as shown in Figure 7-3). By using a non-conjugated linker, the heavy metal may effectively sensitize photoisomerization reactions. As a result, 4-coordinated boron containing metal complexes with high isomerization quantum efficiency will be achieved.

7.3 Reference

1. T. M. McCormick, **2008**. *Luminescent transition metal complexes of 2-(2'-pyridyl)benzimidazolyl and 2-(2'-pyridyl)indolyl based ligands and their applications* Ph.D. Thesis, Queen's University.